Structural changes of the amygdala subnuclei and limbic white matter tracts in healthy aging and major depressive disorder

by

Arash Aghamohammadi Sereshki

A thesis submitted in partial fulfillment of the requirements for the degree of

Doctor of Philosophy

Neuroscience

University of Alberta

© Arash Aghamohammadi Sereshki, 2019

Abstract

The world population is dramatically aging. Several factors affect brain in healthy aging. The apolipoprotein E (APOE), brain-derived neurotrophic factor (BDNF) and catechol-O-methyl transferase (COMT) might be involved in neurodegenerative diseases, depression and cognitive decline in healthy aging. Also, it has been suggested that depression can increase the risk of dementia and cognitive decline. Furthermore, exposure to childhood maltreatment and chronic stress increase risks of developing neuropsychiatric disorders, and changes in cognitive functions.

However, our knowledge is limited in first, how the brain changes in healthy aging differ from pathological aging; second, the effects of APOE, BDNF and COMT polymorphisms on the brain structures; and third, the underlying mechanisms of major depressive disorder (MDD) and detrimental effects of early adverse environment.

Amygdala is a group of subnuclei with different connectivity profiles and functions in the limbic system. Previously, amygdala volumetric changes in both healthy aging and MDD were reported. However, most of the previous *in vivo* studies of the human amygdala were at the level of the total structure and not its subnuclei. Uncinate fasciculus is one of the major limbic tracts which connects the amygdala to the orbitofrontal cortex. Cingulum bundle is another major tract of the limbic system which connects the cingulate cortex to its neighboring structures. Healthy aging studies of limbic white matter tracts can improve our understanding of healthy cognitive aging which might be related to cognitive decline with advanced age. Also, our knowledge is very limited regarding the effects of APOE, BDNF and COMT on the limbic tracts.

MDD is one of the major causes of disability worldwide. Reduction in hippocampal volume is one of the most replicated findings of MDD and childhood maltreatment studies. However, similar to

the amygdala, the hippocampus consists of different subregions and subfields, and findings regarding the effects of MDD and childhood maltreatment on the amygdala are inconsistent. All these studies investigated the total amygdala and not the amygdala subnuclei. Currently, there is a gap in literature about the effects of MDD and childhood maltreatment on the amygdala subnuclei and hippocampal subregions/subfields.

The first aim of this thesis was developing a novel segmentation method using ultra-high-resolution magnetic resonance imaging (MRI) to study five major amygdala subnuclei (basolateral (i.e. lateral, basal, accessory basal nuclei), cortical and centromedial groups). The results demonstrated the feasibility of reliable studying of the human amygdala subnuclei groups *in vivo* which approximately correspond to the amygdala subnuclei location and orientation in histological references.

The second aim was investigating the effects of healthy aging, APOE and BDNF polymorphisms on volumes of amygdala subnuclei in a large cohort of healthy individuals using our new amygdala segmenting method. We found that amygdala subnuclei were nonuniformly affected by aging and that age-related associations were sex specific. We also did not find any significant effects of APOE and BDNF polymorphisms on the amygdala subnuclei volumes.

The third aim was investigating the effects of MDD and childhood adversity on volumes of amygdala subnuclei and hippocampal subregions/subfields using ultra-high-resolution MRI. We did not find significant effects of MDD on volumes of the amygdala subnuclei. However, history of childhood adversity was negatively associated with the anterior hippocampus in both hemispheres limited to the CA1-3 subfield, while these effects were limited to the basolateral group of the amygdala in the right hemisphere.

The fourth aim was investigating the effects of healthy aging, APOE, BDNF and COMT on the uncinate fasciculus, rostral, dorsal and parahippocampal cingulum in a large cohort of healthy individuals. We found that while microstructural integrity of the uncinate fasciculus, rostral cingulum and dorsal cingulum were reduced with age, the parahippocampal cingulum microstructural integrity did not associate with age. Moreover, the COMT Met/Met genotype was associated with better microstructural integrity of the right rostral cingulum compared to the Val/+ genotype across life span.

In summary, our experiments revealed: first, susceptibility of the basolateral group to both healthy aging and childhood maltreatment; second, vulnerability of the CA1-3 and the anterior hippocampus to childhood maltreatment; third, relative resiliency of the parahippocampal cingulum, but not uncinate fasciculus, rostral and dorsal cingulum in aging; and finally, the advantage of the COMT Met/Met over the valine carriers in microstructural integrity of the right rostral cingulum.

Preface

This thesis is an original work by Arash Aghamohammadi Sereshki. The research project, that this thesis is a part of, received research ethics approval from the University of Alberta Health Research Ethics Board.

Chapter 4 of this thesis has been published as: Aghamohammadi-Sereshki, A., Huang, Y., Olsen, F., Malykhin, N.V., (2018): **In vivo quantification of amygdala subnuclei using 4.7 T fast spin echo imaging**. Neuroimage. 170:151-163. Doi: 10.1016/j.neuroimage.2017.03.016.

I was responsible for the development of the volumetric protocol, data analysis, and writing, reviewing and editing of the manuscript. Yushan Huang was involved in data analysis. Fraser Olsen was involved in data collection. Nikolai V. Malykhin was the supervisory author and was involved in protocol development, data analysis, and reviewing and editing the manuscript.

Chapter 5 of this thesis has been published as: Aghamohammadi-Sereshki, A., Hrybouski, S., Travis, S., Huang, Y., Olsen, F., Carter, R., Camicioli, R., Malykhin, N.V., (2019): **Amygdala subnuclei and healthy cognitive aging**. Hum Brain Mapp. 40(1):34-52. doi: 10.1002/hbm.24353.

I was responsible for the data analysis, writing, reviewing and editing the manuscript. Stanislau Hrybouski was involved in data analysis, and writing, reviewing and editing of the manuscript. Scott Travis was involved in data analysis. Yushan Huang was involved in data analysis. Fraser Olsen and Rawle Carter were involved in data collection. Richard Camicioli was involved in study design and reviewing and editing the manuscript. Nikolai V. Malykhin was the supervisory author and involved in study design and reviewing and editing the manuscript.

Chapter 6 of this thesis has been submitted to the Journal of Human Brain Mapping as: Aghamohammadi-Sereshki, A., Coupland, N.J., Silverstone, P.H., Huang, Y., Hegadoren, K.M., Carter, R., Seres, P., Malykhin, N.V., **Effects of childhood adversity on the volumes of the amygdala subnuclei and hippocampal subfields in major depressive disorder.**

I was responsible for the data analysis, and writing, reviewing and editing of the manuscript. Nicholas J. Coupland was involved in study design, data collection, data analysis, and reviewing and editing of the manuscript. Peter H. Silverstone was involved in data collection and reviewing and editing of the manuscript. Yushan Huang was involved in data analysis. Kathleen M. Hegadoren was involved in reviewing and editing of the manuscript. Rawle Carter and Peter Seres were involved in data collection. Nikolai V. Malykhin was the supervisory author and involved in study design, data collection, data analysis, and reviewing and editing of the manuscript.

Chapter 7 of this thesis is a manuscript prepared for submission: Aghamohammadi-Sereshki, A., Olsen, F., Carter, R., Camicioli, R., Malykhin, N.V., **Healthy cognitive aging and limbic white matter tracts**.

I was responsible for the data analysis, and writing, reviewing and editing of the manuscript. Fraser Olsen was involved in data collection. Richard Camicioli was involved in study design and reviewing and editing of the manuscript. Nikolai V. Malykhin was the supervisory author and involved in study design and reviewing and editing of the manuscript.

To my dearest parents and sister

Acknowledgement

I wholeheartedly thank my parents, Hamid and Chitra, for their teachings, sacrifice, and continued support to this day.

I would like to thank my supervisor, Dr. Nikolai Malykhin, for the opportunity that he gave me to join his lab, for his scientific guidance and patience over the last several years. My approach towards scientific problems, data analysis, and manuscript writing has improved during my PhD program.

I am thankful to my supervisory committee, Dr. Richard Camicioli and Dr. Nicholas Coupland for their constructive comments, feedback and scientific guidance regarding my research projects.

I would like to thank all past and current members of our lab, Stanislau Hrybouski, Scott Travis, Melanie MacGillivray, Wojciech Pietrasik, Fraser Olsen, Rawle Carter, and Yushan Huang for their help and support.

I am thankful to the department of biomedical engineering, Maisie Goh and Catherine Leung for being great sources of support throughout my PhD program.

I would also like to express my gratitudes to Peter Seres and Shahnaz Shahtoosi for their helps in setting up and scanning participants for the project and assisting with editing the manuscripts.

Finally, a special thank goes to Amber Lapointe, Megan Airmet, Dr. Clayton Dickson, Dr. Bradley Kerr, and the Neuroscience and Mental Health Institute for being great sources of support throughout my PhD program.

Table of Contents

I. Introduction 1

Chapter 1: General Overview

Statement of the problems 2

1.2 Objectives 6

1.3 Thesis Outline 7

Chapter 2: Literature Review

2.1. Limbic system 9

2.2. Amygdala 10

2.3. *In vivo* studies of the human amygdala 14

2.4. Amygdala in healthy aging 17

2.5. Amygdala and major depressive disorder 17

2.6. The effects of the early adverse environment on the volumes of the amygdala and the hippocampus 18

2.7. Limbic white matter tracts and healthy aging 20

2.8. APOE, BDNF and COMT in healthy aging 22

Chapter 3: Hypothesis 27

II. Experiments 28

Chapter 4: *In vivo* quantification of amygdala subnuclei using 4.7 T fast spin echo imaging 29

4.1. Introduction 31
4.2. Material and methods 34
4.3. Results 48
4.4. Discussion 54

Chapter 5: Amygdala subnuclei and healthy cognitive aging 65

5.1. Introduction 67
5.2. Material and methods 70
5.3. Results 84
5.4. Discussion 95

Chapter 6: Effects of childhood adversity on the volumes of the amygdala subnuclei and hippocampal subfields in major depressive disorder 107

6.1. Introduction 109
6.2. Material and method 112
6.3. Results 116
6.4. Discussion 123

Chapter 7: Healthy cognitive aging and limbic white matter tracts ... 131

7.1. Introduction 133
7.2. Material and methods 136
7.3. Results 146
7.4. Discussion 160

III. Discussion 168

Chapter 8: Conclusion 169

8.1. *In vivo* study of the human amygdala (chapter 4) 169

8.2. Healthy aging study of the human amygdala: Imaging-genetics (chapter5) 171

8.3. Effects of childhood adversity on the volumes of the amygdala subnuclei and hippocampal subfields in major depressive disorder (chapter 6) 173

8.4. Healthy cognitive aging and limbic white matter tracts (chapter 7) 176

8.5. Conclusion 179

List of Tables

Table 4.1. Summary of the landmarks lines and reference points of the AG segmentation protocol. 41

Table 4.2. Reliability results. 48

Table 4.3. Raw (before ICV correction) and ICV adjusted volumes of the AG and its subnuclei. 50

Table 4.4. Relative volume of the AG subnuclei reported from *ex vivo* and *in vivo* human studies. 52

Table 5.1. Reliability results. 76

Table 5.2. Demographic information. 85

Table 5.3. ICV-adjusted AG and its subnuclei volumes (mean ± SD) in young, middle-age, and older adults. 86

Table 5.4. Summary of all regression models-related R^2, *p*-values and likelihood ratios (LR). 90

Table 5.5. ICV-adjusted AG and its subnuclei volumes (mean ± SD) for the BDNF Met carrirs [met+/+; met+/-] and homozygous Val [+/+]) individuals. 93

Table 5.6. ICV-adjusted AG and its subnuclei volumes (mean ± SD) for the APOE ε2 [ε2/x], homozygote ε3 [ε3/ε3], and ε4 [ε4/x]) carriers. 94

Table 6.1. Reliability results. 115

Table 6.2. Demographic and clinical characteristics. 117

Table 6.3. Childhood Trauma Questionnaire (CTQ) scores. 118

Table 6.4. Analysis of covariance (ANCOVA) and descriptive statistics for the amygdala measurements. 119

Table 6.5. Summary of all *p*-values for relationships between CTQ factors scores and volumetric measurements in MDD participants. 122

Table 7.1. Inter/Intra-rater intra class correlation coefficients (ICC) and percent coefficient of variation (CV) for DTI-metrics. 141

Table 7.2. Demographic information (mean ± SD). 146

Table 7.3. DTI-measurements of the cingulum bundle and uncinate fasciculus (mean ± SD) for the COMT Val/+ [Val/Val; Val/Met] and homozygous Met [Met/Met]) individuals. 152

Table 7.4. Regression models of the age-, sex- and COMT effects on the DTI-metrics of the cingulum bundle and uncinate fasciculus and their R^2, Adj-R^2, and Standardized βs (*P values*). 154

List of Figures

Figure 2.1. Three-dimensional reconstructions of the major amygdala groups and their connectivity profiles and functions. 12

Figure 4.1. Sagittal view of the AG with references to coronal slices in figs 4.2, 4.3. 37

Figure 4.2. Coronal views of the AG and its subnuclei. 38

Figure 4.3. Coronal views of the AG and its subnuclei. 39

Figure 4.4. Relative distribution of AG subdivisions within the total AG volume for (a) the current study and (b) García-Amado and Prensa 2012. 53

Figure 4.5. Three-dimensional reconstruction of the amygdala subnuclei groups from a healthy volunteer. 53

Figure 5.1. Segmentation of the amygdala (AG) subnuclei on a sagittal (a), coronal (b-f) and axial (g and h) views is shown on T2-weighted FSE images with inverted contrast. 75

Figure 5.2. Flow chart depicting bootstrap methodology used to model the AG ROIs' relationship to age and their prediction R^2 values. 81

Figure 5.3. Flow chart depicting permutation methodology used to build null distributions to assess the statistical significance of the AG ROIs' (a) overall model significance, age and sex effects, as well as (b) age by sex interactions. LR: likelihood ratio. 84

Figure 5.4. Regression plot showing the relationship between age and the ICV-adjusted total AG volume. Model-averaged estimates for men (blue) and women (red) are

shown separately. Shaded areas represent the 95% bootstrap percentile confidence interval for each fit. 87

Figure 5.5. Regression plots showing the relationship between age and the ICV-adjusted volumes of the AG subnuclei groups: Basolateral (BLA) (a), Co (b) and CeM (c) subnuclei groups. Model-averaged estimates for men (blue) and women (red) are shown separately. Shaded areas represent the 95% bootstrap percentile confidence interval for each fit. *P*-values are corrected for multiple comparisons. 89

Figure 5.6. Regression plots showing the relationship between age and the ICV-adjusted volumes of BLA nuclei including La (a), B (b) and AB (c). Model-averaged estimates for men (blue) and women (red) are shown separately. Shaded areas represent the 95% bootstrap percentile confidence interval for each fit. *P*-values are corrected for multiple comparisons. 91

Figure 6.1. Three-dimensional reconstructions of the hippocampal subfields and subregions as well as the amygdala and its subnuclei from a healthy individual. 114

Figure 7.1. Three-dimensional reconstructions of the cingulum bundle and uncinate fasciculus. 140

Figure 7.2. Regression plots showing the relationship between age and fractional anisotropy (FA), mean diffusivity (MD) and radial diffusivity (RD) in the cingulum bundle. 157

Figure 7.3. Regression plots showing the relationship between age and axial diffusivity (AD), volume, linear tensor shape (C_L) and spherical tensor shape (C_S) in the cingulum bundle. 158

Figure 7.4. Regression plots showing the relationship between age and DTI-measurements in the uncinate fasciculus. 159

I. Introduction

Chapter 1: General Overview

1.1. Statement of the problems

Global population is dramatically aging (Broe 2003), and it is predicted that by 2050 more than 400 million people all around the world will be ≥ 80 years of age. There is a consensus that aging is a major risk factor for neurodegenerative disorders (Vanni et al., 2019). Therefore, it is estimated that in 21st century, neurodegenerative disorders will gradually become the major cause of death and morbidity (Broe 2003). Age-related studies have identified different risk factors which might increase the predisposition of developing dementia and cognitive decline later in life (Fjell and Walhovd, 2010). Studies demonstrated that apolipoprotein E (APOE), brain-derived neurotrophic factor (BDNF) and catechol-O-methyl transferase (COMT) are single nucleotide polymorphisms (SNPs) that might be involved in dementia, Alzheimer disease, Parkinson disease, depression, and cognitive decline in healthy aging (Dixon et al., 2014; Petrella et al., 2008; Pietzuch et al., 2019). Moreover, depression is regarded as one of the putative risk factors which can results in cognitive decline and dementia (Chen et al., 2019). Depression is estimated to have affected over 300 million people worldwide, and it is predicted that by 2030 it will be the major cause of disease burden (World Health Organization 2017). Furthermore, it has been demonstrated that chronic exposure to stressful life events, especially in the forms of childhood and adolescence adversity, not only is a risk factor for developing depression and other psychiatric disorders (Barzilay et al., 2019; Hammen et al., 2000; Hoyens et al., 2010; Lindert et al., 2014), but also has detrimental effects on executive functions, complex reasoning, social cognition and cell senescence (Barzilay et al., 2019; Epel et al., 2004).

Despite the surge in age- and depression-related research in recent decades, our current knowledge is limited in separating brain changes observed in healthy aging from the pathological age-related changes (Vanni et al., 2019). In addition, the underlying biological mechanisms of major depressive disorder (MDD) still remains uncertain (Schmaal et al., 2016).

Healthy aging does not uniformly affect brain structures. In general, aging is associated with more decline in cognitive-related functions (i.e. episodic memory, executive function, processing speed) and less decline in emotional-related ones (Fjell and Walhovd, 2010; Mather 2016; Rodrigue and Kennedy 2011). In contrast, neuroimaging studies in MDD demonstrated the involvement of the affective–salience circuit in MDD (Otte et al., 2016).

The limbic system is a group of cortical and subcortical structures (including orbitofrontal and cingulate cortices, as well as hippocampus, amygdala, hypothalamus, nucleus accumbens, ventral tegmental area, mammillary bodies and septal area) interconnected by white matter tracts (including cingulum bundle, uncinate fasciculus, fornix, mammillo-thalamic tract and anterior thalamic projections) involved in memory, spatial orientation, emotion and motivation, as well as goal-directed behaviours (Catani et al., 2013; Morgane et al., 2005; Rolls 2015). Neuroimaging studies of the limbic system in humans indicated the involvement of the limbic structures in both healthy aging (Fjell and Walhovd, 2010; Lebel et al., 2012; Malykhin et al., 2017; Michielse et al., 2010; Raz et al., 2005) and MDD (Campbell et al., 2004; Koolschijn et al., 2009; Lorenzetti et al., 2009; Malykhin and Coupland 2015; Schmaal et al., 2016).

The amygdala is a heterogeneous almond-shaped structure (Swanson and Petrovich 1998) of the limbic system which is well-known for its major role in mediation of the fear and other emotional-related functions (LeDoux, 2007). Amygdala involvement in different psychiatric and neurological disorders such as depression, anxiety, schizophrenia and autism (LeDoux, 2007; Otte et al., 2016),

as well as Alzheimer's and Parkinson's diseases (Braak et al., 1994; Scott et al., 1992) was reported. Also, similar to the hippocampus and entorhinal cortex, pathological age-related changes such as formation of neurofibrillary tangles and neuritic plaques were reported in the amygdala (for review, see Wright, 2009). However, the amygdala has been less the subject of healthy aging studies compared to the hippocampus and entorhinal cortex (Allen et al., 2005; Fjell and Walhovd, 2010). Moreover, there is not enough literature about the effects of SNPs' on the amygdala structure in healthy aging. Also, although adverse effects of the MDD and childhood maltreatment might uniformly affect the hippocampal subfields and subregions (Huang et al., 2013; Szeszko et al., 2006; Teicher et al., 2012), there is a general consensus on the total hippocampal volumetric reduction in MDD and childhood adversity (Koolschijn et al., 2009; Lorenzetti et al., 2009; Malykhin and Coupland 2015; Teicher and Samson 2016). However, structural magnetic resonance imaging (MRI) studies regarding the adverse effects of the MDD and early maltreatment on even the total amygdala volume have been inconsistent (Andersen et al., 2008; Calem et al., 2017; Campbell et al., 2004; Cohen et al., 2006; De Bellis et al., 2002; Hajek et al., 2009; Hamilton et al., 2008; Lupien et al., 2011; Mehta et al., 2009; Schmaal et al., 2016; Tottenham et al., 2010). Finally, despite the amygdala heterogeneity in terms of structure and function, the vast majority of previous *in vivo* studies of the human amygdala were at the level of the total amygdala and not the level of its subnuclei (LeDoux, 2007).

Amygdala is connected to other limbic structures through its afferents and efferents (Freese and Amaral, 2009). Uncinate fasciculus is one of the limbic white matter tracts which connects the rostral portion of the temporal lobe (i.e. temporal pole, uncus, parahippocampal gyrus, and amygdala) with the lateral and medial orbitofrontal cortex, as well as the frontal pole (BA 10) (Catani et al., 2002; Catani and Thiebaut de Schotten 2008; Von Der Heide et al., 2013). In addition

to the orbitofrontal cortex and the frontal pole (BA 10), amygdala is also reciprocally connected with the anterior part of the cingulate cortex (Freese and Amaral, 2009; Vogt and Palomero-Gallagher 2012). Cingulum bundle is the main white matter tract of the cingulate gyrus located around the corpus callosum and expands towards medial temporal lobe structures. It mediates attentional, emotional and memory-related functions (Catani and Thiebaut de Schotten 2008; Catani et al., 2013). Cingulate cortex is considered as a heterogenous structure due to the variety of the structural and functional properties, as well as the connectivity profile. Therefore, it has been suggested to subdivide the cingulate cortex into four subregions including the anterior cingulate, midcingulate, posterior cingulate and retrosplenial cortices (Vogt and Palomero-Gallagher 2012). Consequently, the cingulum bundle is also categorized into different subsections (Catani et al., 2013, Malykhin et al., 2008b) due to carrying afferents/efferents from/to different structural and functional cingulate cortex subregions. Nevertheless, most of the previous healthy aging studies of the cingulum bundle have considered the cingulum bundle either as one structure corresponding to (1) the dorsal cingulum (Lebel et al., 2012), (2) rostral + dorsal cingulum (Sala et al., 2012; Stadlbauer et al., 2008), (3) a whole cingulum bundle consisting of rostral + dorsal + parahippocampal cingulum (Voineskos et al., 2012) or as two separate structures that correspond to the rostral + dorsal cingulum and parahippocampal cingulum (Bennett et al., 2015; Cox et al., 2016; Westlye et al., 2010). Studies of the effect of healthy cognitive aging on limbic white matter tracts might help us understand first, the plausible underpinning age-related changes of cognitive functions; second, the association between the white and grey matter changes in aging; and third, pathological changes of the white matters in neuropsychiatric and neurological disorders (Yap et al., 2013). Finally, there is a huge gap in our knowledge about the effects of genes on the brain white matter tracts and their age-related changes (Kanchibhotla et al., 2013).

In summary, the current gaps in the literature are:

a. The effects of healthy cognitive aging, as well as the APOE and BDNF polymorphisms on the amygdala subnuclei;
b. The effects of MDD on the amygdala subnuclei;
c. The effects of childhood maltreatment on the amygdala subnuclei and hippocampal subregions and subfields in MDD;
d. The effects of healthy cognitive aging as well as APOE, BDNF and COMT polymorphisms of the cingulum subdivisions and the uncinate fasciculus.

1.2. Objectives

Considering the aforementioned, this research was conducted:

- ✓ First, to develop a reliable manual segmentation MRI method in order to study the five major amygdala subnuclei including lateral, basal, and accessory basal nuclei, as well as the cortical and centromedial groups *in vivo*;
- ✓ Second, to study the nature of the association between the amygdala subnuclei volumes and age in a large sample of cognitively healthy adults using an ultra-high-resolution MRI. In addition, we aimed to study the effects of the APOE and BDNF polymorphisms on the amygdala subnuclei in this cohort;
- ✓ Third, to study the effects of MDD on the amygdala and its subnuclei volumes;
- ✓ Fourth, to study the effects of early maltreatment on the amygdala subnuclei, as well as on hippocampal subregions/subfields volumes in MDD participants;
- ✓ Fifth, to study matter microstructural properties of the cingulum bundle and uncinate fasciculus in a large sample of cognitively healthy adults using deterministic DTI-

tractography methods. Moreover, we aimed to study the effects of the COMT, APOE and BDNF polymorphisms on the cingulum bundle and uncinate fasciculus in this cohort.

1.3. Thesis Outline

The present PhD thesis is structured as follows:

Introduction

- ✓ Chapter 1 provides a brief overview on the related literatures and describes the current gaps. In addition, goals of the current research are set in the chapter 1.
- ✓ Chapter 2 provides an overview of: first, the limbic system structures and their functions; second, amygdala neuroanatomy in both animals and humans; third, *in vivo* studies of the human amygdala; fourth, previous healthy aging studies of the amygdala; fifth, previous literature on the effects of MDD on the amygdala; sixth, the effects of early adverse environment on the human amygdala and the hippocampus, as well as the effects of chronic stress on the amygdala and the hippocampus in animal models; seventh, the anatomy of the uncinate fasciculus and cingulum bundle, as well as the effects of healthy aging on these structures; and finally, the APOE, BDNF and COMT polymorphism studies of the amygdala, cingulum bundle and uncinate fasciculus in healthy aging.
- ✓ Chapter 3 provides an overview of the proposed hypotheses based on reviewed literature.

Experiments

- ✓ Chapter 4 presents a novel MRI method to study the human amygdala subnuclei *in vivo*.
- ✓ Chapter 5 describes the method and results related to the effects of healthy aging, APOE and BDNF SNPs on the total amygdala and its subnuclei.

- ✓ Chapters 6 describes the method and results related to the effects of MDD and childhood maltreatment on the amygdala subnuclei, and hippocampal subregions/subfields.
- ✓ Chapter 7 explains the method and results related to the effects of healthy aging and the APOE, BDNF and COMT SNPs on the cingulum bundle and uncinate fasciculus.

Conclusion

- ✓ Chapter 8 summarizes the novelties and scientific contributions of the current research project.

Chapter 2: Literature Review

2.1. Limbic system

The limbic conception has evolved through years of research. The following paragraph gives a brief history of the conception of the limbic system. For more details, please see Catani et al. (2013), Rolls (2015), Roxo et al. (2011), and Nieuwenhuys et al. (2008).

In 1664, for the first time the term "limbic" was used by Thomas Willis to call the cortical border surrounding the brain stem (Catani et al., 2013). Later, in 1878, Paul Broca called cingulate and parahippocampal gyri the "Broca's Great Limbic Lobe". Although he mentioned that this term does not represent a homogeneous function, it was thought that it was mainly related to the olfactory functions since most of its structures received olfactory innervations (Catani et al., 2013; Nieuwenhuys et al., 2008; Roxo et al., 2011). In 1937, Papez introduced the "Circuit of Papez" involved in emotional mechanisms through the structural network between the hypothalamus and mesial cortex with hippocampus and cingulate cortex forming two centres for emotional processing (Nieuwenhuys et al., 2008). In 1939, the "Circuit of Papez" was supported by Klüver and Bucy whose work is known as the Klüver-Bucy syndrome. Klüver and Bucy provided the first evidence of the involvement of the limbic system in emotions (Nieuwenhuys et al., 2008; Roxo et al., 2011). In 1949 and 1952, Paul Donald MacLean redefined the concept of the limbic system and so far it has not dramatically changed. He stated that limbic cortex is reciprocally connected with subcortical structures and they form the limbic system involved mainly in emotions. He merged the amygdala, septum, and prefrontal cortex to the "Circuit of Papez" structures including the thalamus, hypothalamus, hippocampus, and cingulate cortex (Rolls, 2015; Roxo et al., 2011). In 1958 Walle Nauta added the septal and preoptic regions, the hypothalamus, the mesencephalic

central grey and the dorsal raphe nucleus to the telencephalic limbic structures (including the hippocampus and the amygdala) and proposed the "limbic system–midbrain circuit". The newly included structures were suggested to be associated with the regulation of the endocrine mechanisms related to emotions and behaviour (Nieuwenhuys et al., 2008; Roxo et al., 2011). Finally, it has been recently suggested that the single limbic system should be considered as the "emotional limbic system" and the "memory limbic system" (Rolls 2015). Rolls (2015) argued that rostral limbic structures (e.g. orbitofrontal cortex and the amygdala) are associated with emotions, reward valuation and reward-related decision-making. However, structures that located more caudally (e.g. hippocampus, posterior cingulate cortex, fornix-mammillary body-anterior thalamus-posterior cingulate circuit) are associated with episodic memory (Rolls 2015). However, it was acknowledged that emotional and reward-related inputs from the orbitofrontal cortex, the amygdala and the anterior cingulate cortex can be projected to the hippocampus and recalled back (Rolls 2015).

2.2. Amygdala

The amygdaloid complex is an almond-shape structure located in the medial temporal lobe (Sah et al., 2003). Amygdala is involved in different types of behaviours and functions such as motivation, maternal, sexual and feeding behaviours (LeDoux, 2007), as well as different cognitive-related functions such as goal-directed behaviours (Hampton et al., 2007), social behaviours (Adolphs, 2009; Bickart et al., 2011), attention, perception and explicit memory (LeDoux, 2007). However, the most important function of the amygdala is its involvement in processing of emotional-related behaviours and especially fear (LeDoux, 2007; Sah et al., 2003). Due to the important role of the amygdala in emotional processing, amygdala impairment is involved in different psychiatric disorders such as unipolar depression, bipolar disorder, anxiety

disorders and schizophrenia (Drevets et al., 2002; Drevets 2003; LeDoux, 2007). Amygdala is considered as a heterogenous region of the brain because of the various structural and functional features, as well as the developmental origins of its subnuclei groups (Freese and Amaral, 2009; Swanson and Petrovich 1998; Yilmazer-Hanke, 2012). The number of the amygdala subnuclei varies from 13 subnuclei in rodents to 36 subnuclei in humans (Yilmazer-Hanke, 2012). However, all of the subnuclei of the classic amygdala can be categorized either into two major groups based on the evolutionary features (Johnston 1923; LeDoux, 2007; Swanson and Petrovich 1998) or into three groups based on the developmental origin and connectivity features (Swanson and Petrovich 1998; Yilmazer-Hanke, 2012) of the amygdala subnuclei. Considering the phylogenetic features, amygdala is divided into an older evolutionary group called the cortico-medial group including cortical, medial and central subnuclei, as well as the nucleus of the lateral olfactory tract related to the olfactory system; and a newly formed group called basolateral complex (BLA) including lateral (La), basal (B) and accessory basal (AB) nuclei related to the neocortex (Johnston 1923; LeDoux, 2007; Swanson and Petrovich 1998). Considering the developmental and connectivity features, amygdala is divided into three groups: (1) BLA group including La, B and AB nuclei which is a ventromedial extension of the claustrum; (2) the superficial or cortical-like group which is caudal olfactory cortex; and (3) centromedial group (CeM) including central and medial nuclei which is a ventromedial part of the striatum (Swanson and Petrovich 1998) (Figure 1).

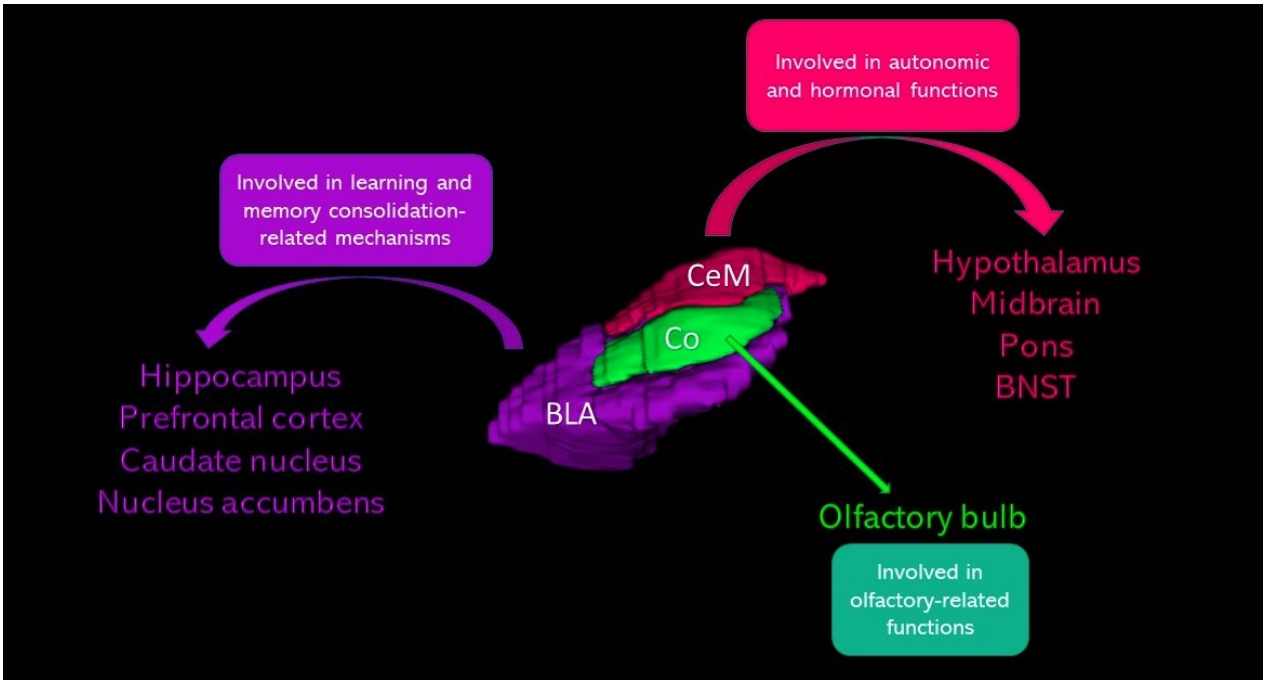

Figure 2.1. Three-dimensional reconstructions of the major amygdala groups and their connectivity profiles and functions.

Key: BLA group (including La, B and AB nuclei) is shown in purple, CeM group is shown in pink and Co group is shown in green. The figure is adapted from 'Stress, memory and amygdala' by Roozendaal et al., 2009, Nature Review Neuroscience. 10 (6): 423-33; and Yilmazer-Hanke, DM, (2012): Amygdala. In: Mai JK, Paxinos G, (Eds.), The Human Nervous System3rd ed. Elsevier Academic Press, London. Page: 759–834.

Each of the aforementioned nuclei of the amygdala has unique connectivity and function. The La nucleus is considered as the main region in the amygdala that receives sensory information (LeDoux and Schiller 2009). Considering the connectivity profile, B and AB nuclei have many common inputs and outputs. For example, both nuclei receive most of their inputs from the La nucleus and most of their projections terminate in the CeM group of the amygdala (Freese and Amaral, 2009). Furthermore, both nuclei send their projections to orbitofrontal, medial prefrontal

and entorhinal cortices, as well as hippocampus (Yilmazer-Hanke, 2012). However, they have some unique connections as well. The B nucleus is the connector of the amygdala to the rostral cingulate cortex (Yilmazer-Hanke, 2012) and stratial areas (LeDoux and Schiller, 2009), while AB nucleus generates one of the major amygdala projections to the perirhinal cortex (Yilmazer-Hanke, 2012). The central nucleus receives the intra-amygdala processed sensory information from the BLA group and sends its projections which mainly are GABAergic to the hypothalamus, bed nucleus of stria terminalis (BNST), pons and midbrain (Freese and Amaral, 2009; LeDoux and Schiller 2009; Roozendaal et al. 2009; Sah et al., 2003). These projections mediate behavioural response of emotional stimuli (Roozendaal et al., 2009). Medial nucleus is a heterogenous nucleus (Yilmazer-Hanke, 2012) in the amygdala which has common features with both central nucleus and the cortical group. Like central nucleus, medial nucleus is involved in the regulation of autonomic, behavioural and hormonal responses through its projections to the BNST and hypothalamus (Roozendaal et al., 2009). Also, both of the medial and central extrinsic outputs are mainly GABAergic (Swanson and Petrovich 1998). Moreover, animal behavioural studies showed that the medial nucleus is involved in food intake, sexual behaviour, aggression, and defensive behaviours (Yilmazer-Hanke, 2012). The common aspect of the medial nucleus and the cortical group (some parts of the cortical group including the anterior cortical nucleus, nucleus of the lateral olfactory tract, amygdala–piriform transition area and the rostral-superior ventral cortical nucleus receive the main olfactory bulb projections in primates) is that they both receive the olfactory bulb projections (Yilmazer-Hanke, 2012). Finally, studies of the cortical group which is often regarded as a secondary olfactory structure (Doty 2012) indicated that it might be involved in the olfactory related responses such as olfactory memory, response to pheromones, food-related behaviours and the sexual function (Yilmazer-Hanke, 2012).

Most of what we know about the amygdala comes from animal studies and especially rodents (Adolphs 2010). However, the amygdala has dramatically evolved from rodents to primates (Freese and Amaral, 2009). For example, Chareyron et al. (2011) indicated that in contrast to the CeM group which occupies almost the same proportion of the total amygdala in rats and monkeys, BLA group has evolved dramatically in both humans and non-human primates. While BLA group occupies only 28% volume of the total amygdala in rats, it occupies 62% and 69% of the total amygdala volume in monkeys and humans respectively (Chareyron et al., 2011). BLA evolutionary enlargement in primates is in parallel with the evolutionary enlargement of the prefrontal region (BA8 to 14 and BA44 to 47 as well as the anterior cingulate cortex) which has evolved more than the other parts of the cortex (Carlén 2017). As mentioned above, amygdala is reciprocally connected with the prefrontal region through its BLA group. Consequently, BLA volumetric increase in primates is in parallel with that of prefrontal region (Freese and Amaral, 2009). It suggested that complicated social life of primates is one of the forces for the amygdala evolution (Bickart et al., 2011). Therefore, like the concern expressed about the prefrontal region research regarding the translation of rodents' findings to primates (Carlén 2017), it might be a valid concern to ask how rodents' findings on BLA amygdala are transferable to the human amygdala.

2.3. *In vivo* studies of the human amygdala

In the past 3 decades, the advent of MRI has made a considerable improvement in the study of the human brain (Duyn, 2012). Overtime, there has been an improvement in the resolution of MRI from almost 4mm in the first years of MRI invention to a submillimeter size these days (Duyn, 2012). Despite the technological advances in high-field MRI, most previous structural MRI researches of the human amygdala have studied the amygdala at the level of the total structure and

not the subnuclei (Achten et al., 1998; Ancelin et al., 2019; Bickart et al., 2011; Bonilha et al., 2004; Convit et al., 1999; Makris et al., 1999; Makkinejad et al., 2019; Malykhin et al., 2007; Matsuoka et al., 2003; Pruessner et al., 2000; Siozopoulos et al., 2017; Watson et al., 1992; Zuo et al., 2019). The above-mentioned structural and functional heterogeneity of the amygdala subnuclei causes a concern about all studies that looked at the total amygdala. It might be a valid concern that the absence of the overall volumetric difference observed between different groups (e.g. patients vs healthy individuals) might be because different biological changes in the amygdala subnuclei results in no overall amygdala volumetric differences. Therefore, it is necessary to study the major amygdala subnuclei instead of measuring the total amygdala volume. In addition, different connectivity profiles of the amygdala subnuclei underline the functional difference between them (LeDoux, 2007). This important issue only recently started to get attention in neuroimaging literature with the implementation of the high-resolution functional MRI methods designed to measure functional activity in different amygdala subnuclei (for review see Hrybouski et al., 2016). Also considering the current technological advances, it is feasible to study the major amygdala subnuclei.

Some recent studies used different methods to segment the amygdala into 2 to 4 subdivisions (Amunts et al., 2005; Bach et al., 2011; Bzdok et al., 2013; Entis et al., 2012; Prévost et al., 2011; Saygin et al., 2011; Solano-Castiella et al., 2010; 2011). Probabilistic tractography-based segmentation method was harnessed in Bach et al. (2011) and Saygin et al. (2011) to segment amygdala into 2 groups (BLA group and the superficial group including central, medial and cortical nuclei) and 4 groups (La nucleus, Basal nucleus including B and AB nuclei, central nucleus and medial nucleus) respectively. Also, Bzdok et al. (2013) used ‘connectivity-derived parcellation based on whole-brain coactivation patterns to segment amygdala into BLA, CeM and Co groups.

Solano-Castiella et al. (2010) used diffusion-based segmentation approach to subdivide the amygdala into medial (i.e ventral, medial and cortical nuclei) and lateral (i.e. BLA group) regions. Nevertheless, Eickhoff et al. (2015) did a detail review on the major concerns of the connectivity-based parcellation such as, outlining the initial ROI (e.g. amygdala) for the subsequent segmentation process, the choice of clustering algorithm (e.g. K-means clustering, spectral clustering and hierarchical clustering), cluster validity-related issues, and finally, issues related to using the classical inferential statistics in connectivity-based parcellation. Cytoarchitectonic mapping-based approach was adopted by Amunts et al. (2005) in which probabilistic map of the amygdala subnuclei including BLA, CeM and superficial (i.e. Co) groups was developed using postmortem tissue with subsequent registration to the MNI space. Finally, Solano-Castiella et al. (2011) aimed to segment the amygdala into BLA, CeM and superficial based on correlations of the voxels' intensities within the amygdala acquired on different contrasts (T_1 MPRAGE, T_2-weighted TSE and a T2*-weighted GRE). However, the amygdala segmentation output of these methods does not correspond accurately to the histological references of the amygdala (Brabec et al., 2010; García-Amado and Prensa, 2012; Mai et al., 2008; Schumann and Amaral, 2005) which poses problems for a volumetric study of the amygdala.

Prévost et al. (2011) and Entis et al. (2012) both used manual segmentation method to subdivide the amygdala into three (BLA, CeM and Co groups) and four (La + B group, AB nucleus, CeM and Co groups) subdivisions respectively. The validity of the amygdala segmentation output of these two methods was better than the above-mentioned approaches. However, the development of our high-resolution MRI at 4.7T manual segmentation method enables us to reliably delineate all five major amygdala subnuclei.

2.4. Amygdala in healthy aging

In addition to the volumetric changes of the amygdala structure in healthy aging (Brierley et al., 2002; Fjell and Walhovd 2010; Mather 2016; Raz and Rodrigue 2006; Wright 2009), pathological age-related changes of the amygdala subnuclei in both Alzheimer's disease and Parkinson's disease have been reported (Braak et al., 1994; Harding et al., 2002; Wright, 2009). Therefore, it is important to differentiate healthy cognitive age-related changes from the pathological age-related changes. Majority of the previous healthy aging studies of the amygdala indicated smaller amygdala volume in elderly individuals compared to young individuals or a negative relationship between the age and the amygdala volume (Allen et al., 2005; Fjell et al., 2009; Grieve et al., 2011; Jäncke et al., 2015; Heckers et al., 1990; Malykhin et al., 2008a; Mu et al., 1999; Murphy et al., 1996; Sublette et al., 2008; Yang et al., 2016). However, a few studies did not report any effects of age on the amygdala volume (Brabec et al., 2010; Good et al., 2001; Jernigan et al., 2001). A meta-analysis study of the amygdala changes in healthy aging indicated a negative relationship between age and the amygdala volume (Brierley et al., 2002). All the above-mentioned studies were at the level of the total amygdala volume. Therefore, how individual amygdala subnuclei are affected by healthy aging is largely unknown.

2.5. Amygdala and major depressive disorder

The advances in neuroimaging method have improved our understanding of the structural and functional brain alterations in MDD (Malhi and Mann 2018). MRI studies of MDD demonstrated volumetric and functional changes in the anterior cingulate cortex, subgenual cingulate, prefrontal cortex, orbitofrontal cortex, ventral striatum, hypothalamus, pituitary, hippocampus and the amygdala (Aan het Rot et al., 2009; Koolschijn et al., 2009; Lorenzetti et al., 2009; Malykhin and

Coupland 2015; Malhi and Mann 2018; Murray et al., 2011; Otte et al., 2016). Regardless of some contradictory findings, volumetric reduction of the anterior cingulate cortex, subgenual cingulate, prefrontal cortex, orbitofrontal cortex, hippocampus, ventral striatum, putamen, caudate nucleus, as well as hyperactivity of the orbitofrontal cortex and the amygdala are more replicated in MRI studies of the MDD (Aan het Rot et al., 2009; Koolschijn et al., 2009; Lorenzetti et al., 2009; Malykhin and Coupland 2015; Malhi and Mann 2018; Murray et al., 2011; Otte et al., 2016). In contrast to the consistent findings on hyperactivity of the amygdala in MDD, structural studies of the amygdala have been contradictory (Campbell et al., 2004; Hajek et al., 2009; Hamilton et al., 2008; Schmaal et al., 2016). Previously, volumetric increase (Frodl et al., 2002; Malykhin et al., 2012; Vassilopoulou et al., 2013), decrease (Kronenberg et al., 2009) or no significant changes (Frodl et al., 2008; Koolschijn et al., 2009; Zavorotnyy et al., 2017) of the amygdala in MDD were reported. However, all the above-mentioned studies were at the level of the total amygdala volume and not the amygdala subnuclei. Therefore, it remains unknown if and how the amygdala subnuclei are affected in MDD.

2.6. The effects of the early adverse environment on the volumes of the amygdala and the hippocampus

The detrimental effects of chronic exposure to stressful life events on developing MDD were reviewed by Kessler (1997). However, a newer approach has focused on chronic exposure to early stressful life events (Malhi and Mann 2018; Otte et al., 2016). The theoretical concept of latent vulnerability argues that childhood maltreatment induces biological changes in neurocognition systems which lead to alter developmental trajectories of stress-related brain structures to maintain allostasis (i.e. ‘stability through changes’ [Danese and McEwen 2012]) in an early adverse environment. However, later in life the biological embedding might be maladaptive processes in

the normal environment, which makes the individual more vulnerable to psychiatric disorders in adolescence and adulthood (McCrory and Viding 2015). Despite some inconsistent findings, generally studies suggested that maltreatment histories are associated with smaller volumes of anterior cingulate, dorsolateral prefrontal and orbitofrontal cortices as well as the hippocampus (Danese and McEwen 2012; Teicher and Samson 2016). The amygdala structural studies are inconsistent, although most functional imaging studies of the amygdala reported overactivation of the amygdala in response to threatening stimuli in maltreated individuals in comparison with non-maltreated individuals (Hein and Monk 2017; McCrory et al., 2017; Teicher and Samson 2016). Amygdala volumetric increase (Lupien et al., 2011; Mehta et al., 2009; Tottenham et al., 2010), decrease (Lim et al., 2014; Paquola et al., 2016), or no significant difference (Andersen et al., 2008; Calem et al., 2017; Cohen et al., 2006; De Bellis et al., 2002) were reported when maltreated individuals were compared to non-maltreated individuals. Preclinical studies indicated that chronic stress mostly affected the BLA group (i.e. La, B and AB nuclei) (for review, see Qiao et al., 2016). For instance, Vyas et al. (2002; 2003; 2004) reported that while chronic immobilization stress (CIS) induced dendritic hypertrophy in the BLA amygdala, it did not change dendritic arborization, number of branch points and the total dendritic length in the central nucleus of the amygdala. Furthermore, the effects of chronic stress on the structural changes in the medial nucleus of the amygdala are not conclusive. This is because following chronic restraint stress (CRS), while Bennur et al. (2007) reported a reduction in medial nucleus spine density, Marcuzzo and colleagues (2007) did not show significant changes in dendritic spine density of the posterodorsal medial amygdala neurons. However, there has been no published study about the effects of chronic stress on the amygdala subnuclei volume in humans to date.

The hippocampus is an old evolutionary brain structure located in the medial temporal lobe involved in episodic memory, language and higher-order perception (Insausti et al., 2017; Lee et al., 2017). Similar to the amygdala, hippocampus is also a heterogenous structure (Lee et al., 2017). The hippocampus can be subdivided anatomically into three antero-posterior subregions including the hippocampal head, body and tail (Duvernoy, 2005; Insausti et al., 2017). Furthermore, each of the above-mentioned antero-posterior subregions can be further studied into different cross-sectional cellular subfields including dentate gyrus (DG), cornu ammonis (CA1-3) and subiculum (Insausti et al., 2017). These antero-posterior subregions and subfields can be visualized and reliably measured with high resolution structural MRI (Malykhin et al., 2007; 2010a; for review see Yushkevich et al., 2015). Previous MRI studies of early maltreatment reported negative association between early adverse environment and hippocampal volume (Danese and McEwen, 2012; Teicher and Samson, 2016). However, it has been suggested that the adverse effects of early maltreatment might affect hippocampus subregions and subfields differently (Szeszko et al., 2006; Teicher et al., 2012). Also, preclinical studies of the effects of chronic stress on rat hippocampus in adults showed that the CA3 subfield is the most affected structure and CA1 and DG are susceptible to more severe forms of chronic stress (Conrad et al., 2017).

Consequently, it is currently unknown what the nature (hypertrophy vs hypotrophy) of the effects of childhood adversity on the amygdala subnuclei in MDD are, and whether similar effects are observed in hippocampal subfields as it has been demonstrated in preclinical studies.

2.7. Limbic white matter tracts and healthy aging

The cingulum bundle is the white matter tract of the cingulate cortex consisting of both short and long association fibers (Catani and Thiebaut de Schotten 2008). The cingulum bundle interconnects structures in the frontal, parietal and medial temporal lobes located around the cingulate gyrus. It also connects different parts of the cingulate gyrus to the subcortical structures including amygdala, anterior thalamic nuclei and parahippocampal region (Bubb et al., 2018; Catani et al., 2013 et al., 2013; Vogt and Palomero-Gallagher 2012). Previous studies indicated the involvement of the cingulum bundle in executive functions, emotions, pain and memory (Bubb et al., 2018). It has been suggested to divide cingulum bundle into different subcomponents and studying these subcomponents separately (Bubb et al., 2018). However, except for two studies (Jang et al., 2013; Michielse et al., 2010), most healthy aging studies of the cingulum bundle analyzed it as either a single structure that corresponds to (1) the dorsal cingulum (Lebel et al., 2012), (2) rostral + dorsal cingulum (Sala et al., 2012; Stadlbauer et al., 2008), (3) a whole cingulum bundle consisting of rostral + dorsal + parahippocampal cingulum (Voineskos et al., 2012), or as two separate structures that correspond to the rostral + dorsal cingulum and parahippocampal cingulum (Bennett et al., 2015; Cox et al., 2016; Westlye et al., 2010).

Uncinate fasciculus is one the major white matter tracts of the limbic system whose development continues into the third decade of life (Lebel et al., 2012). Uncinate fasciculus is an association fiber tract that connects the anterior part of the temporal lobe including the amygdala, perirhinal cortex and the anterior part of the parahippocampal gyrus to the lateral orbitofrontal and the anterior prefrontal cortices (Olson et al., 2015). Considering the gray matter structures that are inter-connected by the uncinate fasciculus, it has been suggested that the uncinate fasciculus might

be involved in social–emotional processing, language and episodic memory (Olson et al., 2015; Von Der Heide et al., 2013).

Overall, previous DTI studies of healthy aging showed a curvilinear trajectory for both fractional anisotropy (FA) and mean diffusivity (MD) of the cingulum bundle and the uncinate fasciculus (Lebel et al., 2012; Westlye et al., 2010). In both uncinate fasciculus and cingulum, FA decreases and MD increases during mid- and late-adulthood (Lebel et al., 2012; Westlye et al., 2010). However, some previous studies indicated that the age trajectories of DTI measurements of the cingulum bundle might be different across its subsections, with more effects of age on the rostral and dorsal cingulum, but less effects on the parahippocampal cingulum (Bennet et al., 2015; Cox et al., 2016; Jang et al., 2016; Lebel et al., 2012; Michielse et al., 2010; Westlye et al., 2010).

Therefore, it is important to investigate the nature of age-related changes of the cingulum subdivisions and uncinate fasciculus in order to understand if they follow similar trajectory as cortical structures where these tracts originate from or terminate to.

2.8. APOE, BDNF and COMT in healthy aging

The combination of technological advancement in neuroimaging and genomics can explain the phenotypic effects of genes on brain structures (Petrella et al., 2008). Apolipoprotein E (APOE), Brain-derived neurotrophic factor (BDNF) and catechol-O-methyl transferase (COMT) are amongst genetic polymorphisms that have been subjects of imaging genetics due to their associations with Alzheimer's disease, neuronal repair, protection and proliferation, as well as synaptic growth, memory and cognitive functions (Deary et al., 2004; Petrella et al., 2008).

APOE polymorphism has three known allelic variants (ε2, ε3 and ε4), and it is the most widely studied example of imaging genetics (Petrella et al., 2008). Studies showed that these different

alleles have different effects on developing Alzheimer's disease (Kim et al., 2009). The ε3 allele is considered as the neutral allele (Spinney 2014). The ε4 allele increases the risk of developing Alzheimer's disease; individuals with one copy and two copies of the ε4 are four times and twelve times greater at risk, respectively (Spinney 2014). In contrast to the ε4, the ε2 allele is suggested to be the protective allele against developing Alzheimer's disease (Kim et al., 2009; Spinney 2014). The primary role of the APOE in the brain is lipoprotein transportation (Petrella et al., 2008). However, the structural effects of APOE on brain regions are still obscure in healthy populations (Fjell and Walhovd 2010). Most of the APOE studies have focused on the hippocampus (Fjell and Walhovd 2010), and data about the effects of APOE alleles on the amygdala volume in healthy aging is scarce. Previously, significantly smaller amygdala volume in ε4 carriers compared to individuals with ε3ε3 genotypes was reported (den Heijer et al., 2002). However, Hibar et al. (2015) and Soldan et al. (2015) did not find any effects of ε4 on the amygdala volume.

BDNF is a neuronal growth factor (Sublette et al., 2008) involved in neuronal survival, synaptogenesis, proliferation and development and brain aging (Petrella et al., 2008). A common BDNF polymorphism is an amino-acid substitution of valine (Val) to methionine (Met) at amino-acid residue 66 (Val66Met) (Petrella et al., 2008). Most neuroimaging-genetics studies of the BDNF focused on the hippocampus and prefrontal cortex due to high expression of the BDNF in these structures (Petrella et al., 2008). Therefore, like APOE, we do not know very well how BDNF affects the amygdala in normal aging. While Hibar et al. (2015) did not find any association between the total amygdala volume and BDNF, another neuroimaging-genetics study, with a small sample size, found an inverse correlation between the amygdala volume and age in BDNF val66met carriers but not in non-carriers (Sublette et al., 2008). Consequently, we do not know if

APOE and BDNF polymorphisms affect the total amygdala and amygdala subnuclei in healthy aging.

DTI-genetics may enhance our understanding of the underlying mechanisms of microstructural changes in white matter tracts associated with healthy and pathological aging. However, there is a gap in our knowledge about genetic effects on the healthy aging of the white matter tracts (Kanchibhotla et al., 2013). Similar to the studies of the associations between genetic polymorphism and brain gray matter, APOE is the most studied gene in genetic studies of white matter tracts. COMT and BDNF are also amongst the studied genes (Kanchibhotla et al., 2013).

APOE studies of the cingulum bundle and uncinate fasciculus showed that while some studies reported lower FA in the cingulum (Heise et al., 2011; Smith et al., 2010) or shorter fiber bundle lengths in uncinate fasciculus (Salminen et al., 2013), others did not find significant differences in FA and MD in rostral + dorsal cingulum, parahippocampal cingulum and uncinate fasciculus in ε4 carriers compared to the ε4 non-carriers (Laukka et al., 2015; Wang et al., 2017).

The effects of BDNF on the white matter integrity of cingulum bundle and uncinate fasciculus have been less studied compared to the APOE. Previously, Voineskos et al. (2011) reported that while homozygote Val individuals were more at risk than Met carriers for the detrimental effects of aging on the white matter integrity of the left cingulum bundle (i.e. rostral + dorsal + parahippocampal cingulum) in late life, BDNF genotype did not interact with uncinate fasciculus integrity.

The COMT is involved in the neurotransmission and degradation of dopamine and other catecholamines (Deary et al., 2004; Mier et al., 2009; Petrella et al., 2008). The protective effects of dopamine on oligodendrocytes (Rosin et al., 2005) and its involvement in oligodendrocytes

differentiation (Bongarzone et al., 1998) were previously reported. The Val158Met polymorphism (rs4680) is a common COMT polymorphism in which amino acid Valine (Val) is substituted with Methionine (Met) (Goldman et al., 2005). The Val allele has higher degrading activity than the Met allele which results in lower synaptic dopamine level. Also, it was showed that there is a dose-dependent fashion in COMT enzymatic activity so that Val/Val > Val/Met > Met/Met (Chen et al., 2004). COMT enzyme is widely distributed in the brain, but its enzyme and mRNA are mainly located in first, choroid plexus; second, frontal cortex; and third, cerebellum. However, its mRNA has low to moderate expression in the human amygdala and hippocampus (Myöhänen and Männisto 2010). Due to the low level of the presynaptic dopamine transporter in the prefrontal cortex, the COMT is the major regulator of dopamine level in the prefrontal cortex (Sambataro et al., 2012).

Due to the involvement of dopamine in psychiatric disorders like schizophrenia (Foley 2019), many of the imaging COMT studies have been related to the aforementioned disorders (for review see Witte and Flöel 2012; van Haren et al., 2008). Also, most healthy aging studies of COMT have been focused on cognition (for review see Sambataro et al., 2012; Witte and Flöel 2012). Overall, the effects of COMT on both grey and white matter and not brain function have been less studied so far. Papenberg et al. (2015) has been the only age-related study that investigated the effects of COMT polymorphism on the brain white matter tracts. Papenberg and colleagues (2015) harnessed TBSS method in old adults (60-87 years old) and reported higher FA and lower MD in the cingulum of the Met homozygous compared to Val carriers only in the oldest adult group (81-87 years old).

Therefore, we do not know if APOE, BDNF and COMT polymorphisms affect the cingulum bundle and the uncinate fasciculus in healthy aging. Interdisciplinary studies combining

neuroimaging with genetics may help both diagnosing and preventing the disease and enhancing brain longevity and mental health (Petrella et al., 2008).

Chapter 3: Hypotheses

Considering the above-mentioned studies, for the current research we hypothesized that:

- First, age demonstrates negative associations with the total amygdala and its subnuclei volumes. However, the associations between the age and individual amygdala subnuclei might be different.
- Second, APOE ε4 carriers shows smaller amygdala volume compared to non-ε4 carriers. However, due to our limited knowledge about the effects of the BDNF polymorphisms on the amygdala, we made no prior hypothesis regarding the effects of the BDNF polymorphisms on the amygdala subnuclei.
- Third, we made no prior hypothesis about the effects of MDD on the volumes of the amygdala and amygdala subnuclei.
- Fourth, childhood adversity is associated with volumetric reductions in the BLA amygdala and CA1-3 subfield.
- Fifth, healthy aging is associated with declining in white matter integrity in the uncinate fasciculus, rostral and dorsal cingulum, whilst the parahippocampal cingulum is relatively preserved.
- Sixth, ε4 allele is associated with the reduction of the white matter microstructural properties of the uncinate fasciculus and cingulum bundle. However, due to our limited knowledge about the effects of the COMT and BDNF polymorphisms on the brain white matter, we made no prior hypothesis related to the effects of COMT and BDNF polymorphisms on uncinated fasciculus and cingulum bundle.

II. Experiments

Chapter 4: *In vivo* quantification of amygdala subnuclei using 4.7 T fast spin echo imaging

Abstract

The amygdala (AG) is an almond-shaped heterogeneous structure located in the medial temporal lobe. The majority of previous structural Magnetic Resonance Imaging (MRI) volumetric methods for AG measurement have so far only been able to examine this region as a whole. In order to understand the role of the AG in different neuropsychiatric disorders, it is necessary to understand the functional role of its subnuclei. The main goal of the present study was to develop a reliable volumetric method to delineate major AG subnuclei groups using ultra-high resolution high field MRI.

38 healthy volunteers (15 males and 23 females, 21-60 years of age) without any history of medical or neuropsychiatric disorders were recruited for this study. Structural MRI datasets were acquired at 4.7 T Varian Inova MRI system using a fast spin echo (FSE) sequence.

The AG was manually segmented into its five major anatomical subdivisions: lateral (La), basal (B), accessory basal (AB) nuclei, and cortical (Co) and centromedial (CeM) groups. Inter-(intra-) rater reliability of our novel volumetric method was assessed using intra-class correlation coefficient (ICC) and Dice's Kappa.

Our results suggest that reliable measurements of the AG subnuclei can be obtained by image analysts with experience in AG anatomy. We provided a step-by-step segmentation protocol and reported absolute and relative volumes for the AG subnuclei. Our results showed that the basolateral (BLA) complex occupies seventy-eight percent of the total AG volume, while CeM

and Co groups occupy twenty-two percent of the total AG volume. Finally, we observed no hemispheric effects and no sex differences in the total AG volume and the volumes of its subnuclei.

Future applications of this method will help to understand the selective vulnerability of the AG subnuclei in neurological and psychiatric disorders.

Keywords: amygdala, nuclei, magnetic resonance imaging (MRI), basolateral amygdala, centromedial amygdala

A version of this Chapter was published in

Aghamohammadi-Sereshki A, Huang Y, Olsen F, Malykhin NV., (2018): In vivo quantification of amygdala subnuclei using 4.7 T fast spin echo imaging. Neuroimage. 170:151-163. doi: 10.1016/j.neuroimage.2017.03.016.

4.1. Introduction

The amygdala (AG) is an almond-shaped heterogeneous structure located in the medial temporal lobe (MTL). The AG is involved in neuronal circuits of fear and reward learning, as well as aggressive, maternal, sexual, and feeding behaviors (LeDoux, 2007). Moreover, through its extensive connections with cortical and subcortical areas, the AG plays an important role in stress response (Davis and Whalen, 2001), goal-directed behavior (Hampton et al., 2007), social behavior (Adolphs, 2009), attention and perception (Vuilleumier, 2009), processing of facial expression (Tottenham et al., 2009), motivation and explicit memory (LeDoux, 2007).

Alterations in the AG structure and function have been reported in different psychiatric and neurological disorders including affective disorders (Hajek et al., 2009), anxiety disorders (LeDoux, 2007), Alzheimer's disease (Kromer et al., 1990; Scott et al., 1991), and Parkinson's disease (Braak et al., 1994).

In human and animal studies the AG is subdivided into at least thirteen different subnuclei and cortical areas (Amaral et al., 1992; Pitkänen et al., 1997; Sah et al., 2003). These subnuclei are further grouped into two major divisions: (1) the cortico-medial region consisting of the cortical (Co), medial (Me), and central (Ce) nuclei; and (2) the basolateral complex (BLA) consisting of the lateral (La), basal (B), and accessory basal (AB) nuclei (LeDoux, 2007). Animal studies have demonstrated that these subnuclei – via their unique connectivity patterns – appear to have specialized roles in the expression of fear responses as well as the acquisition and storage of a memory for the conditioning experience (Phelps and LeDoux, 2005). In addition, patients with focal lesions to the BLA produce hypervigilance to subliminal fearful facial expressions (Terburg et al., 2012), while bilateral destruction of the entire AG impairs the processing of the fearful facial

expression as demonstrated by an insensitivity to the intensity of fear expressed by faces (Adolphs et al., 1995). Recent high-resolution functional Magnetic Resonance Imaging (fMRI) studies of the AG provide further support for functional specialization of AG subnuclei (Bach et al., 2011; Boll et al., 2013; Hrybouski et al., 2016; Prévost et al., 2013).

The majority of previous structural MRI volumetric methods for AG measurement have so far only been able to examine this region as a whole (Achten et al., 1998; Bonilha et al., 2004; Convit et al., 1999; Makris et al., 1999; Malykhin et al., 2007; Matsuoka et al., 2003; Pruessner et al., 2000; Watson et al., 1992). For a better understanding of AG subnuclei function, it is crucial to delineate and measure these structures using volumetric MRI. This could only be achieved by developing new methods for measuring the AG subnuclei in-vivo.

Improved spatial resolution and contrast of MRI images due to the continued increase in magnetic field strength have allowed researchers to study very small details of brain anatomy that previously were not visible on conventional MR images (Duyn et al., 2012). Different MRI techniques with high spatial resolution have been developed for high-field MRI magnets to visualize different MTL structures, particularly hippocampal subfields: 3 T (Bonnici et al., 2012; La Joie et al., 2010; Raz et al., 2014; Winterburn et al., 2013), 4 T (Mueller et al., 2007), 4.7 T (Malykhin et al., 2010), 7 T (Boutet et al., 2014; Henry et al., 2011; Goubran et al., 2014; Kerchner et al., 2012; Parekh et al., 2015, Wisse et al., 2014) and 9.4 T (Fatterpekar et al., 2002; Yushkevich et al., 2009). Since visualization of different cell types in-vivo at this resolution is impossible, all methods for segmentation of the hippocampal subfields are based on visibility of the white matter band called the stratum lacunosum-moleculare (SLM) (Duvernoy et al., 2005) and combination of known anatomical landmarks with different geometrical rules to define the boundaries between neighboring substructures (Yushkevich et al., 2015).

Unfortunately, since the AG has low myelin sheath content (Solano-Castiella et al., 2011), visualization of the intra-white matter borders between AG subnuclei using in-vivo MRI is problematic. As a result, various strategies and methods have been utilized to segment the AG as a whole structure or into different subnuclei: manual segmentation (Entis et al., 2012; Prévost et al., 2011), automated segmentation (Morey et al., 2009; Schoemaker et al., 2016), voxel intensity based segmentation (Solano-Castiella et al., 2011), spectral clustering algorithm of diffusion tensor based segmentation (Solano-Castiella et al., 2010), atlas based segmentation (Amunts et al., 2005), diffusion probabilistic tractography based segmentation (Bach et al., 2011; Saygin et al., 2011), and resting-state functional connectivity with cortical regions based segmentation (Bickart et al., 2012).

Despite some limitations of manual segmentation methods, it is still commonly considered the "gold standard" in neuroimaging research (Despotović et al., 2015). In contrast to a large number of protocols for segmentation of hippocampal subfields in-vivo (Yushkevich et al., 2015), there are only a few studies that aimed to delineate the AG subnuclei in humans and report their volumetric measurements. In the first study (Amunts et al., 2005) architectonic probabilistic maps for the BLA, centromedial (CeM) and superficial AG parcellation were developed using ex-vivo histological data from ten individuals. In a second study (Bach et al., 2011), AG was segmented into anterior/inferior/lateral and posterior/superior/medial clusters corresponding to the BLA and the cortico-medial regions respectively. AG subregions were outlined using clustering methods based on differences in the connectivity profile of the clusters. In a third study (Saygin et al., 2011) AG was segmented into La, BA (B and AB), superficial (Co and Me) and Ce nuclei using the differential connectivity patterns of the AG subregions. The last study used high-resolution T_1-weighted Magnetization Prepared Rapid Gradient-Echo (MPRAGE) MRI scans to manually

segment the BL group (consisting of the La and B nuclei), basomedial, CeM and Co AG using external landmarks and geometrical rules (Entis et al., 2012).

Ultra–high resolution T_2-weighted images have not been used so far for manual segmentation of the AG and its subnuclei despite the fact that they provide improved resolution and contrast to delineate MTL structures compared to T_1-weighted images (Malykhin et al., 2010; Wisse et al., 2014). Moreover, the accuracy of atlas-based methods crucially depends on the registration methods (Despotović et al., 2015) and atlases registration to the MNI reference space omits individual neuroanatomy differences (Saygin et al., 2011).

Therefore, the main goal of the present study was to develop a reliable volumetric method to delineate five major AG subnuclei groups using ultra-high resolution T_2-weighted images acquired with a high-field MRI magnet. The second goal was to provide in-vivo volumetric measurements from the larger cohort of healthy individuals in order to ensure consistency of our AG subnuclei methodology with histological measurements from post-mortem literature.

4.2. Material and methods

Study participants

Thirty-eight healthy volunteers without any history of medical or psychiatric disorders were recruited for this study. The sample consisted of 15 males and 23 females, 21-60 years of age, with a mean age of 34.7 years (SD: 12.4). Our participants were all right-handed. Handedness was assessed using a 20-item Edinburgh Handedness Inventory and individuals with laterality quotient $\geq +80$ were determined as right-handed (Oldfield 1971). Participants were excluded if they had any history of psychiatric, psychotic or mood disorders in first-degree relatives as assessed by a structured interview (Anxiety Disorders Interview Schedule-IV: Brown et al., 2001). They were

also screened against the use of medications that might affect brain structure. Medical exclusion criteria were defined as active and inactive medical conditions that may interfere with normal cognitive function: cerebrovascular pathology, tumors or congenital malformations of the nervous system, diabetes, multiple sclerosis, Parkinson's disease, epilepsy, dementia, organic psychosis (other than dementia), schizophrenia, and stroke. Medications that affect cognition, including alcohol, anti-cholinergic medications, benzodiazepines, antipsychotics, and antidepressants were also exclusionary. Written, informed consent was obtained from each participant. The study was approved by the University of Alberta Health Research Ethics Board.

MRI acquisitions and data analysis

Imaging was performed using a 4.7 T Varian Inova MRI system at the Peter Allen MR Research Centre (University of Alberta, Edmonton, AB). A T_2-weighted FSE technique (TE: 39 ms; TR: 11000 ms; FOV: 20×20 cm; native resolution: 0.52×0.68×1.0mm^3) was utilized with contiguous 1-mm-thick slices with no gap and a 90° excitation followed by a 160° and three 140° refocusing pulses. In total ninety slices were attained perpendicular to the anterior–posterior commissure (AC-PC) line in a total acquisition time of 13.5 min. Motion artifacts were checked while the subject was in the scanner and a second FSE image was acquired if necessary. In order to get intracranial volumes (ICV) a whole brain T_1-weighted 3D MPRAGE sequence was acquired (TR: 8.5 ms; TE: 4.5 ms; inversion time: 300 ms; flip angle: 10°; FOV: 256×200×180 mm^3; voxel size: 1×1×1 mm^3). Every tenth slice was manually traced in the sagittal plane, and the summed total volume was then multiplied by 10 in order to estimate the intracranial volume (ICV) for each subject (Eritaia et al., 2000). The inter-rater and intra-rater intraclass correlation coefficients (ICCs) for the ICV were 0.98 and 0.99, respectively.

The original (before creation of the DICOM files) FSE datasets were interpolated in-plane with *imresize* function in Matlab by a factor of 2 to yield a final resolution of 0.26×0.34×1.0 mm^3 and voxel volume of 0.09 µl. DISPLAY (Montreal Neurological Institute, QC, Canada) software was used to trace the ICV, AG and AG subnuclei. Also, ITK-SNAP (v. 3.2.0; Yushkevich et al., 2006) was utilized to construct 3D models of the AG and its subnuclei.

AG subnuclei tracing protocol

Nomenclature used for the AG subdivisions

The AG was segmented into its five major subdivisions: The La nucleus, B nucleus, AB nucleus, as well as the Co and CeM groups (Figs. 4.1, 4.2, 4.3). There are three classification systems related to the Co, Ce and Me nuclei. The first approach is to assign the Co and Me nuclei to the superficial nuclei and view the Ce as a separate nucleus (Freese and Amaral, 2009). The second classification system combines the Ce, Me and Co nuclei into the cortico-medial region (LeDoux, 2007). In the last approach, the Ce and Me nuclei are combined together as the CeM group and Co nucleus is viewed as part of superficial group (Price et al., 1987; Sah et al., 2003). In our method, the last approach was used since at this level of MRI resolution, combining the Ce and the Me nuclei into the CeM group was more accurate and reliable than tracing the Me and Co nuclei as a part of the superficial nuclei.

It is important to note that there are nomenclature inconsistencies in both human and animal studies of the AG, and this might lead to confusion. This issue is particularly pronounced when the term "BLA" is used to refer to both a specific nucleus (the basal or basolateral nucleus) and to the larger region that includes the lateral, basal and accessory basal nuclei (the basolateral complex) (LeDoux, 2007). For instance, some anatomical studies (Mai et al., 2008; Paxinos and Watson,

2005) used the term “basolateral nucleus” to refer to the B nucleus, while other studies (García-Amado and Prensa, 2012; Sah et al., 2003) used the term “basolateral complex” (BLA) to refer to a group of evolutionarily newer AG nuclei, consisting of the La, B and AB nuclei (LeDoux, 2007). Also, the term “basomedial nucleus” is used interchangeably with the term “AB nucleus” (LeDoux, 2007). In this study, we used classification which combined the La, B and AB nuclei into the BLA complex (LeDoux, 2007).

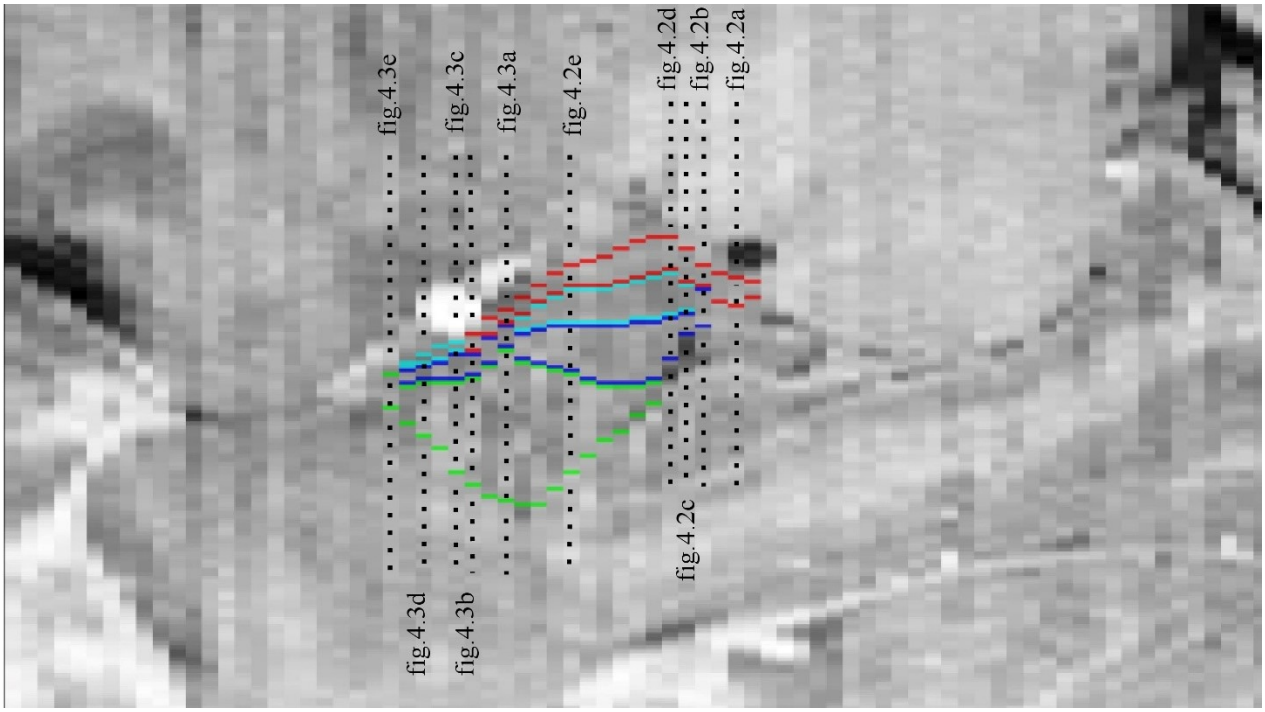

Figure 4.1. Sagittal view of the AG with references to coronal slices in figs 4.2, 4.3.
La nucleus is outlined in green; B nucleus is outlined in dark blue; AB nucleus is outlined in light blue and CeM group is outlined in red.

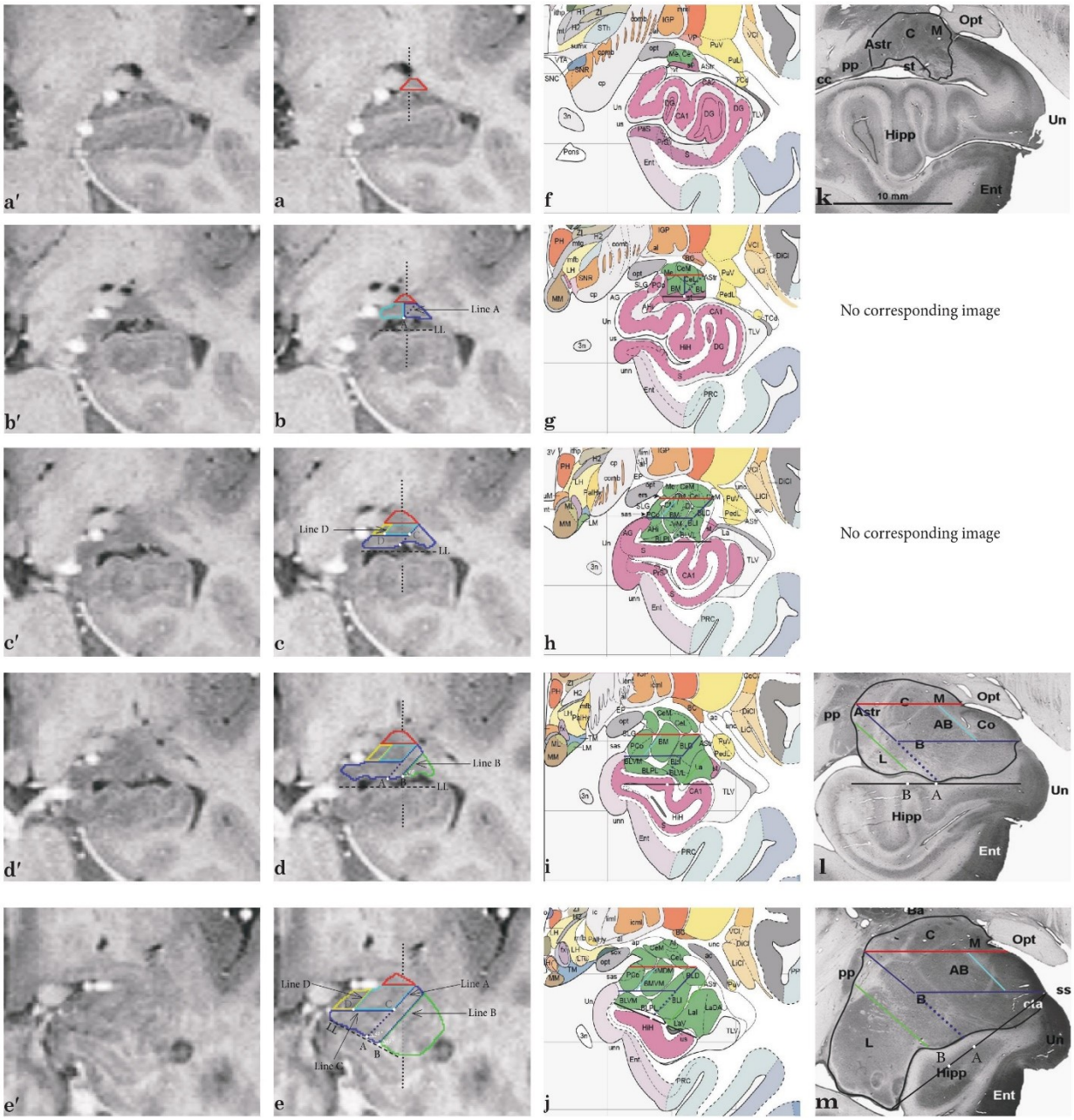

Figure 4.2. Coronal views of the AG and its subnuclei.

Figs a-e represent coronal views of the AG and its subnuclei on high resolution T_2-weighted structural FSE images. Figs a′-e′ represent the corresponding untouched MRI images of figs a-e. Figs f-j represent the corresponding coronal schematic views of the AG and its subnuclei from the Mai (et al. 2008) atlas. Figs k-m represent the corresponding coronal views of the AG and its subnuclei from the post-mortem study (Brabec et al. 2010). La nucleus is outlined in green, B

nucleus is outlined in dark blue, AB nucleus is outlined in light blue, Co group is outlined in yellow and CeM group is outlined in red.

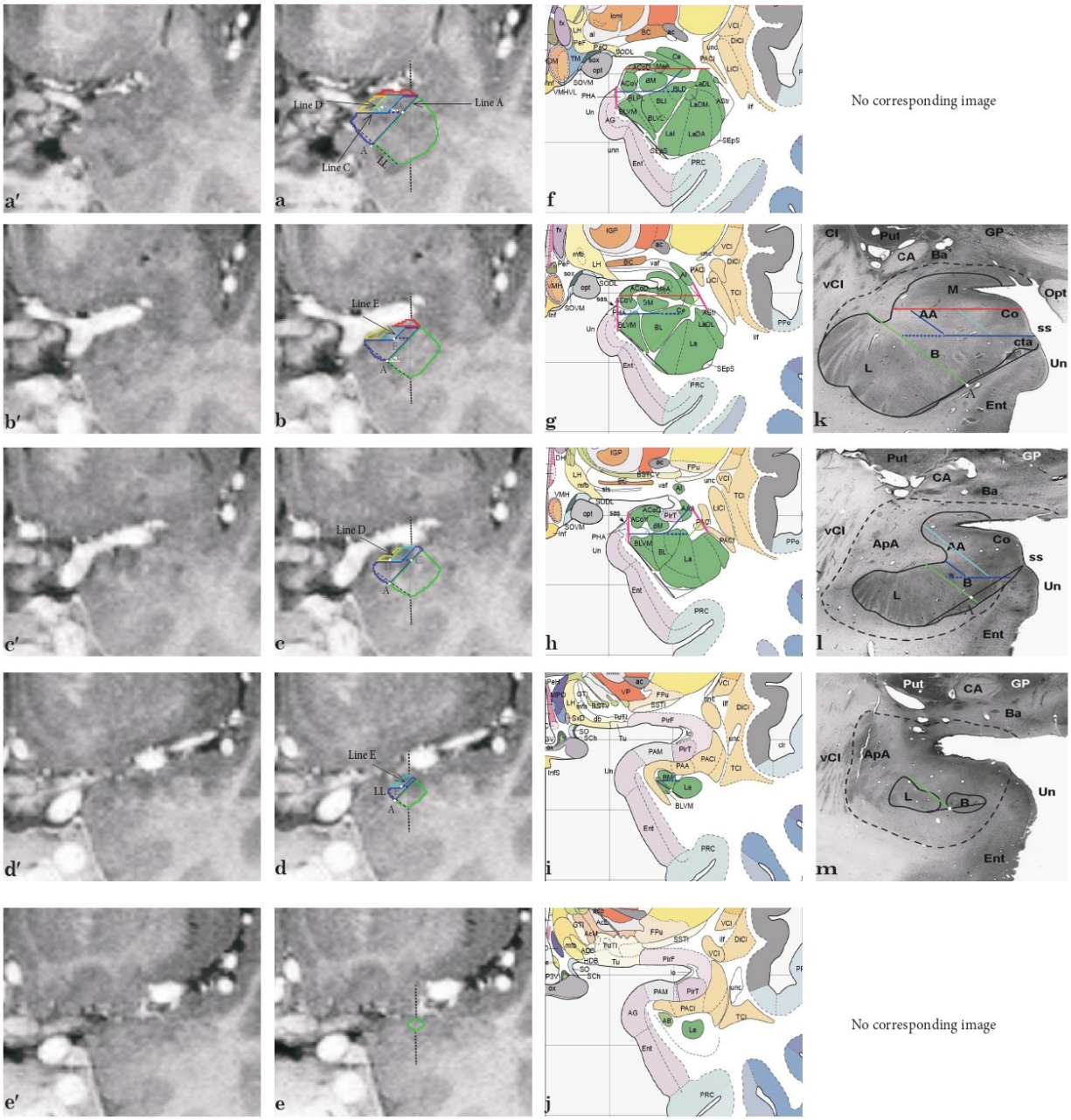

Figure 4.3. Coronal views of the AG and its subnuclei.

Figs a-e represent coronal views of the AG and its subnuclei on high resolution T_2-weighted structural FSE images. Figs a′-e′ represent the corresponding untouched MRI images of figs a-e. Figs f-j represent the corresponding coronal schematic views of the AG and its subnuclei from the

Mai (et al. 2008) atlas. Figs k-m represent the corresponding coronal views of the AG and its subnuclei from the post-mortem study (Brabec et al. 2010).

Overview of the geometrical AG segmentation protocol

Delineation of the AG nuclei in the current protocol was not based on the white matter boundaries between nuclei because myelin sheath inside the AG is too small (Solano-Castiella et al., 2011) to be visible even with high-field MRI methods. Therefore, we established a method that combines geometrical rules that approximately match the location and orientation of the AG subnuclei based on histological references (Brabec et al., 2010; García-Amado and Prensa, 2012; Mai et al., 2008; Schumann and Amaral, 2005).

The whole AG was manually traced using a method previously described in detail elsewhere (Malykhin et al., 2007). T_2-weighted images provide much better contrast and resolution for the AG and hippocampus compared to T_1-weighted images. Therefore, T_2-weighted images were used to segment AG into its five major subnuclei.

The measurements started from the most posterior slice of the AG (Fig. 4.2a) continued through slices where both the AG and the hippocampal head (HH) were present, and ended at the level of the lateral sulcus closure (Fig. 4.3e). Once the total AG boundaries were outlined, only the coronal plane was used to segment the AG into its 5 major subdivisions using a single internal landmark line (LL), defined on each coronal slice where the AG was present (Figs. 4.2b-e and 3a-d). This landmark line allowed us to separate the AG into nuclei and groups, approximately matching the intra-AG anatomy described in the Mai et al. (2008) atlas and postmortem histological studies (Brabec et al., 2010; García-Amado and Prensa, 2012; Schumann and Amaral, 2005). Segmenting the AG in the posterior part (coronal slices where HH is present) (Fig. 4.2) is slightly different from that of anterior part (coronal slices where HH is absent) (Fig. 4.3). The difference mainly

arises from splitting LL differently in in each part (Figs. 4.2, 4.3). The anatomical landmarks employed in the present segmentation protocol including reference points and lines are summarized in the Table 4.1.

Table 4.1. Summary of the landmarks lines and reference points of the AG segmentation protocol.

Landmark		**Begin**	**End**	**Description and role**
LL	Before the inferolateral expansion of the AG.	When the AG expands towards the ambient gyrus (Fig. 4.2b).	1mm posterior to the inferolateral expansion of the AG (Fig. 4.2d).	LL is the major landmark of the protocol and it defines other lines and points for AG subnuclei segmentation. Before inferolateral expansion of the AG in, LL is a horizontal line (Figs. 4.2b-d) that connects the most medial border of the AG to the most lateral border of the AG. After the inferolateral expansion of the AG, LL is a diagonal line that connects the most inferomedial border of the AG to the most medio-inferior border of the AG (Figs. 4.2e and 4.3a-d).
	After the inferolateral expansion of the AG.	When the AG expands inferolaterally (Fig. 4.2e)	The second most anterior slice of the AG (Fig. 4.3d).	
Point A		When the AG expands towards the ambient gyrus (Fig. 4.2b).	The second most anterior slice of the AG (Fig. 4.3d).	It divides LL into two equal parts and defines the beginning of the line A.
Point B		2 mm anterior to the AG expansion towards the ambient gyrus (Fig. 4.2d).	The most anterior slice of the HH (Fig. 4.2e).	It divides LL into the lateral 1/3 and the medial 2/3 and defines the beginning of the line B.
Point C	Presence of the HH	1 mm anterior to the AG expansion towards the ambient gyrus (Fig. 4.2c).	The second most anterior slice of the AG (Fig. 4.3d).	It is placed in the middle of the line A and it defines the beginning of the line C (Figs. 4.2c-e).
	Absence of the HH			It is placed on the superior 1/3 and the inferior 2/3 of line A. It defines the beginning of line C (Figs. 4.3a-d).

Point D		1 mm anterior to the AG expansion towards the ambient gyrus (Fig. 4.2c).	4 mm anterior to the most anterior slice of the HH (Fig. 4.3c).	Point D is placed on the medial 1/3 and the lateral 2/3 of the line C (Figs 4.2c-e, 4.3a-c). It defines the beginning of the line D.
Point E		1 mm anterior to the most anterior slice of the HH (Fig. 4.3a).	The second most anterior slice of the AG (Fig. 4.3d).	Point E is placed on the lateral 1/3 and the medial 2/3 of the line C (Figs 4.3a-d). It defines the beginning of the line E.
Line A	Presence of the HH	When the AG expands towards the ambient gyrus (Fig. 4.2b).	The second most anterior slice of the AG (Fig. 4.3d).	It is drawn at a 45° angle (from the horizontal plane) from the point A towards the lateral border of the AG. It defines the superomedial border of the B nucleus (consequently, the most lateral border of the AB nucleus) (Figs. 4.2c-e).
	Absence of the HH			It is drawn at a 45° angle (from the horizontal plane) from the point A towards the lateral border of the AG. It defines the superomedial border of the La nucleus (consequently, the most lateral border of the B nucleus) (Figs. 4.3a-d).
Line B		2 mm anterior to the AG expansion towards the ambient gyrus (Fig. 4.2d).	The most anterior slice of the HH (Fig. 4.2e).	It is drawn at a 45° angle (from the horizontal plane) from the point B towards the lateral border of the AG. It defines the superomedial border of the La nucleus prior to the disappearance of the HH (consequently, the most lateral border of the B nucleus) (Figs. 4.2d-e).
Line C		1 mm anterior to the AG extension towards the ambient gyrus (Fig. 4.2c).	The second most anterior slice of the AG (Fig. 4.3d).	Line C is a horizontal line drawn from the point C towards the medial border of the AG. It defines the most inferior border of AB nucleus and Co group (Figs 4.2c-e, 4.3a-d).
Line D		1 mm anterior to the AG extension	4 mm anterior to the most anterior	It is drawn at a 45° angle (from the horizontal plane) from the point D towards the most inferior border of the CeM group (Figs. 4.2c, 4.3a) or the superomedial border of the AG (Figs. 4.2e, 4.3c).

	towards the ambient gyrus (Fig. 4.2c).	slice of the HH (Fig. 4.3c).	It defines the most medial border of the AB nucleus (consequently the most lateral border of the Co group) (Figs 4.2c-e,4. 3a-c).
Line E	1 mm anterior to the most anterior slice of the HH (Fig. 4.3a).	The second most anterior slice of the AG (Fig. 4.3d).	It is drawn at a 45° angle (from the horizontal plane) from the point E towards the most inferior border of the CeM group (See fig. 4.3b) or the superior border of the AG (See fig. 4.3d). It defines the most lateral border of the AB nucleus (consequently, the most superomedial border of the B nucleus) (Figs. 4.3a-d).

Geometrical protocol's landmarks and segmentation description

Initially, the landmark line was horizontal and was drawn by connecting the most medial border of the AG to the most lateral border of the AG (Figs. 4.2b-d). As soon as the AG expanded in the inferolateral direction (Fig. 4.2e), the horizontal landmark was replaced by a diagonal landmark line, drawn by connecting the most inferomedial border of the AG to the most medio-inferior border of the AG (Figs. 4.2e and 4.3a-d). On each slice of the AG we placed point A exactly in the middle of the LL (Figs 4.2b-e and 4.3a-d). On posterior AG slices, where the HH was present the LL was also split into the lateral 1/3 and the medial 2/3 by point B (Figs. 4.2d, e). These two points were then used to define two secondary lines. The first line, subsequently called 'line A,' began on the AG border, directly above point A, and was drawn at a 45° angle (from the horizontal plane) towards the lateral border of the AG (See fig. 4.2e). The second line, subsequently called 'line B,' began on the AG border, directly above point B, and was also drawn at a 45° angle (from the horizontal plane) towards the lateral border of the AG (See fig. 4.2e). Point C was placed in the middle of line A prior to the disappearance of the HH (See fig. 4.2e) and when the HH is no longer

present it splits line A into the superior 1/3 and the inferior 2/3 (See fig. 4.3a). The AG and its subdivisions were traced in the posterior to anterior direction.

First, we delineated the CeM group. Next, the La nucleus was defined. Subsequently, the remaining AG tissue was further subdivided into the B, AB nuclei, and the Co group.

Centromedial group

Delineation of the CeM AG started at the first coronal slice, when the AG appears as a small grey matter structure superior to the uncal recess just above the HH (Malykhin et al., 2007) (Fig. 4.2a). The CeM group occupies the entirety of the AG tissue until the AG extends (completely or partially) towards the ambient gyrus (Fig. 4.2b). In subsequent slices, the CeM group occupies only the superior portion of the AG, separated from the rest of the AG by a horizontal line, drawn from the intersection of line A with the lateral border of the AG towards the medial border of the AG (Figs. 4.2b-e and 4.3a, b).

This rule was used to define the inferior border of the CeM group on all slices anterior to the AG extension towards the ambient gyrus. The last slice of the CeM group was 3 mm (3 MRI slices) anterior to the most anterior slice of the HH (Mai et al., 2008) (Figs. 4.3b, g).

Lateral nucleus

Delineation of the La nucleus started 2 mm (2 MRI slices) anterior to the AG extension towards the ambient gyrus (Fig. 4.2d). Since the La nucleus occupies the inferolateral portion of the AG (Figs. 4.2d, e and 4.3a-d), our goal was to establish its superomedial border, which separates the La nucleus from the rest of the AG. Prior to the disappearance of the HH, this was accomplished using line B (Figs. 4.2d, e). In the anterior part of the AG, where the HH is no longer present, the

La nucleus extends medially, and line A was used to define the superomedial boundary of the La nucleus (Figs. 4.3a-d). In the last (i.e. most anterior) slice, all of the AG tissue was assigned to the La nucleus (Fig. 4.3e).

Basal, accessory basal nuclei, and cortical group

Once the CeM group and the La nucleus were demarcated, the remaining AG tissue was segmented into the B nucleus, the AB nucleus and the Co group. Since the AB nucleus is situated between the B nucleus, the Co group and the CeM group, defining the AB nucleus boundaries also completes boundaries of the B nucleus and the Co group. The B and AB segmentation began on the slice in which the AG extends towards the ambient gyrus (Fig. 4.2b), and ended in the second most anterior slice of the AG (See fig. 4.3d). On the first MRI slice where the B and AB nuclei were present (Fig. 4.2b) they were separated from each other by drawing a vertical line from point A towards the most inferior border of the CeM group. The lateral part was assigned to the B nucleus and the medial part to the AB nucleus (Fig. 4.2b).

On the next slice (Fig. 4.2c) and all the remaining AG slices prior to the disappearance of the HH (Figs. 4.2d, e), line A established the most lateral border of the AB nucleus and consequently the superomedial border of the B nucleus.

The most inferior border of the AB nucleus (and the Co group) was formed by line C which is a horizontal line drawn from point C towards the medial border of the AG (See fig. 4.2e). Line C was divided into the medial 1/3 and lateral 2/3 by point D (See fig. 4.2e). A line at a 45° angle from the horizontal plane (line D) was drawn from point D towards the most inferior border of the CeM group (See fig. 4.2c) or the superomedial border of the AG (See fig. 4.2e) and formed the most medial border of the AB nucleus (consequently the most lateral border of the Co group).

Delineation of the Co group started 1 mm (one MRI slice) anterior to the AG extension towards the ambient gyrus (Fig. 4.2c) and ended 4 mm (4 MRI slices) anterior to the most anterior slice of the HH (Mai et al., 2008) (Fig. 4.3c, h).

These rules and lines (C and D) were used to define borders between the B nucleus, the AB nucleus and the Co group in slices prior to the disappearance of the HH (Figs. 4.2c-e).

In summary, on slices where the HH is present (except for the slice in which the AG extends towards the ambient gyrus (Fig. 4.2b)): 1) the AB nucleus was defined by lines A, C and D as well as the most inferior border of the CeM group; 2) the B nucleus was defined by lines A and C as well as the lateral, the inferior and the medial borders of the AG on slices where the La nucleus is absent (Fig. 4.2c) or by lines A, C and B as well as the inferior and the medial borders of the AG on slices where the La nucleus is present (Figs 4.2d, e); 3) the Co group was defined by lines C and D as well as the medial border of the AG (See fig. 4.2e).

Modifications of the segmentation landmarks for the anterior part of the AG

Anterior to the HH we employed similar rules and lines except for some minor modifications. As previously described, line C defined the most inferior borders of the AB nucleus and the Co group anterior to the HH (See fig. 4.3a) and line D defined the most medial border of the AB nucleus (consequently the most lateral border of the Co group) (See fig. 4.3a). The most lateral border of the AB nucleus (consequently the most superomedial border of the B nucleus) was not defined by line A anymore. Instead, an additional line (line E) at a 45° angle (from the horizontal plane) was drawn from the lateral 1/3 of line C (point E) towards the most inferior border of the CeM group (See fig. 4.3b) or superior border of the AG (See fig. 4.3c). On the remaining AG slices, anterior

to the most anterior slice of the Co group (Fig. 4.3c) and posterior to the most anterior slice of the AG (Fig. 4.3e) only three AG subnuclei (L, B and AB nuclei) were delineated (See fig. 4.3d).

Statistics

Inter (intra)-rater reliabilities were analyzed using ICCs for a one-way fixed-effects design (McGraw and Wong, 1996) and Dice's Kappa (Dice, 1945). ICC shows the correlation between the volumetric measurements of tracers while Dice's Kappa calculates the size of the voxel overlap of operator's tracings. Dice's Kappa values were calculated using the following formula: ([2×a]/[b+c]). Here, "a" represents the number of voxels overlapping between two tracings while "b + c" represents the sum of voxels in the two tracings. For assessing inter-rater reliability two raters (A.A.S and N.V.M; developers of the AG segmentation protocol) separately performed manual tracing of the AG in 5 subjects (10 amygdalae) and subdivided it into its subnuclei. Intra-rater reliability for the total AG and its subnuclei volume measures was assessed by retracing the images from the same five subjects at a 1-week interval by a single rater (A.A.S) (Table 4.2). The MRI datasets used to assess the intra/inter- rater reliability were different from the datasets used for training.

The AG and its subnuclei volumes in the left and the right hemispheres were compared using paired-samples t-tests. A one-way ANOVA was used to compare the demographic data, ICV and AG volumes between males and females. Individual raw volumes were normalized to the ICV by using the following formula: *normalized volume = raw volume/ICV×1000 mm*^{3} (Lehericy et al., 1994).

4.4. Results

Reliability tests

Both inter/intra-rater ICCs were high (> 0.84) (Table 4.2). The inter (intra)-rater Dice's Kappa values were above 0.81 for the total AG and the La nucleus which is the largest nucleus of the AG (Table 4.2). However, for the smaller subnuclei it was somewhat lower (0.71-0.81). The significance level for all ICCs was less than 0.0005.

Table 4.2. Reliability results.

ICCs and Dice's Kappa values				
	ICC		Dice Kappa	
	Intra-rater	Inter-rater	Intra-rater	Inter-rater
La	.95	.93	.86	.82
B	.94	.87	.81	.76
AB	.96	.95	.77	.71
Co	.97	.87	.72	.72
CeM	.86	.85	.79	.76
AG	.93	.95	.93	.91

AG subnuclei volumes

Raw (before ICV correction) and ICV adjusted volumes of the AG and its subnuclei are shown in Table 4.3, including volumes for the left and the right AG, together with the mean values for the AG average across hemispheres. Total AG and its subnuclei volumes did not differ between hemispheres: total AG, $t = 0.059$; $p = 0.55$; La, $t = -1.05$; $p = 0.29$; B, $t = 0.60$; $p = 0.55$; AB, $t=0.942$, $p=0.352$; Co, $t = -0.97$; $p = 0.33$; CeM, $t = -1.07$; $p = 0.29$.

AG subnuclei volumes within the left and the right hemispheres were correlated: La, $r = 0.46$; $p = 0.003$; B, $r = 0.68$; $p < 0.001$; AB, $r = 0.70$, $p < 0.001$; Co, $r = 0.58$; $p < 0.001$; CeM, $r = 0.51$; $p = 0.001$.

Males had larger ICVs ($F=29.73$, $p<0.001$) and raw left and right AG volumes (respectively $F=10.97$, $p=0.002$, and $F=17.88$, $p<0.001$) than females (Table 4.3), whilst males and females did not differ in age ($p=0.20$) or education ($p=0.87$). Males also had larger raw volumes of left and right La (respectively $F=7.23$, $p=0.01$ and $F=15.24$, $p<0.001$), left and right B ($F=10.74$, $p=0.002$ and $F=11.55$, $p=0.002$), left and right AB ($F=4.79$, $p=0.035$ and $F=14.41$, $p=0.001$), and left and right Co ($F=5.49$, $p=0.025$ and $F=7.56$, $p=0.009$). CeM volumes did not differ (left $p=0.144$ and right $p=0.315$) (Table 3).

After ICV normalization none of the AG subnuclei volumes or total AG volume differed between males and females (all $ps>0.19$).

Relative volume of the AG subnuclei (Table 4.4) and their distribution within the total AG volume is shown in figure 4.4. Furthermore, our analyses showed that the Pearson's correlation and the coefficient variation of the relative volume of the AG subnuclei between our study and a postmortem study of the amygdala subnuclei (García-Amado and Prensa 2012) were 0.963 and 17.4% respectively.

Three-dimensional reconstructions of the AG and its subnuclei from the left hemisphere of a single volunteer are shown in figure 4.5 to illustrate the structural relationship between subnuclei.

Table 4.3. Raw (before ICV correction) and ICV adjusted volumes of the AG and its subnuclei.

		Raw volumes			**ICV adjusted volumes**
Structure		Males (15) Mean ± SD (mm^3)	Females (23) Mean ± SD (mm^3)	Mean Values (38) [1] Mean ± SD (mm^3)	Mean Values (38) [1] Mean ± SD (mm^3)
La	Range	527.3 - 987.2	372.9 - 945.9	372.9 - 987.2	241.1- 632
	Left	729.5 ± 133.8	613.7 ± 127.2	659.4 ± 140.3	407.3 ± 77.4
	Right	723.4 ± 100	577.5 ± 120	635.1 ± 132.6	392.3 ± 72.7
	Average	726.5 ± 73.9	595.6 ± 111.2	647.2 ± 116.7	399.8 ± 62
B	Range	517.6 - 920.1	361.4 - 846.5	361.4 - 920.1	241.9 - 265.5
	Left	703.6 ± 117.2	571.8 ± 123.6	623.8 ± 136.2	385 ± 74.3
	Right	683.3 ± 107.7	568.7 ± 97.5	613.9 ± 115.2	380.4 ± 68.4
	Average	693.4 ± 95.6	570.2 ± 101.9	618.9 ± 115.5	382.7 ± 64.4
AB	Range	240 - 457.2	196 - 379.7	196 - 457.2	116.5 - 258.6
	Left	317.5 ± 51.3	279.2 ± 53.6	294.3 ± 55.4	181.8 ± 29.7
	Right	327 ± 56.9	261.6 ± 48.4	287.42 ± 60.5	177.7 ± 33.8
	Average	322.2 ± 48.8	270.4 ± 46.8	290.9 ± 53.5	179.8 ± 28.6
Co	Range	113.5 - 232.6	101.2 - 208.5	101.2 - 232.6	64.8 - 135.3
	Left	165.8 ± 39.4	141.7 ± 23.9	151.2 ± 32.7	93.5 ± 17.7
	Right	171.6 ± 28.6	145.6 ± 28.4	155.9 ± 30.9	96.3 ± 16.7
	Average	168.7 ± 30.1	143.7 ± 22.6	153.5 ± 28.3	94.9 ± 14.7
CeM	Range	126.1- 440	125.8 - 434.5	125.84 - 440	72.1- 303.7

	Left	293.9 ± 92.1	260.7 ± 43.8	273.8 ± 68	169.8 ± 39.4
	Right	300.1 ± 68.6	276.3 ± 71.1	285.7 ± 70.2	178.1 ± 48.2
	Average	297 ± 73.3	268.5 ± 48.1	279.7 ± 60.1	174 ± 38.3
AG	Range	1774.7 - 2789.1	1354.6 - 2583.7	1354.6 - 2789.1	886.9 - 1726.2
	Left	2210.2 ± 309	1867.5 ± 314	2002.5 ± 351.6	1237.5 ± 184.6
	Right	2205.3 ± 251.5	1829.7 ± 277.4	1978 ± 322.9	1224.8 ± 182.6
	Average	2207.7 ± 225.7	1848.4 ± 280.8	1990.2 ± 312.8	1231.1 ± 166.5

[1] Represents the information for both sexes.

Table 4.4. Relative volume of the AG subnuclei reported from *ex vivo* and *in vivo* human studies.

Studies		**AG subnuclei/total AG (%)**					**Total AG volume[1] Mean ± SD (mm^3)**	**Age mean± SD**
		BLA			**Co**	**CeM**		
Ex vivo								
Amunts et al. 2005		69.5 ***(La, B, AB)***			21.5	9	1521± 272	64.9±16.9
		La	**B**	**AB**				
Schumann and Amaral 2005		33.3	25.8	11	27.5 (+remaining nuclei)[1]	2.4 ***(Ce)***	44.54± 6.1	23.9± 9.6
García-Amado and Prensa 2012		39.4	29.2	15	7.2	9.2	956 ± 149	52.1±17.6
In vivo								
Bach et al. 2011	dataset 1	46.8 ***(La, B, AB)***			54.2 ***(Ce, Me, Co)***		1356± 209	29.4±5.8
	dataset 2	45 ***(La, B, AB)***			55 ***(Ce, Me, Co)***		1048± 217	23.8±3.7
Saygin et al. 2011		40	33.5 ***(B, AB)***		13 ***(Co and Medial nuclei)***	13.5 ***(Ce)***	-	25.7±0.2
Entis et al. 2012	Young subjects	64 (***La, B)***		18.2	8	9.7	1095± 181.1	23.8±1.3
	Elderly subjetcs	63.6 ***(La, B)***		18.8	7.95	9.6	1017± 147.5	74.8±2.6
Current study		32	31	15	8	14	1231± 166.4	34.7±12.4

[1] There are some methodological differences in postmortem studies such as definition of AG border, slice thickness, number of slice sections per case and distance between two measured sections.

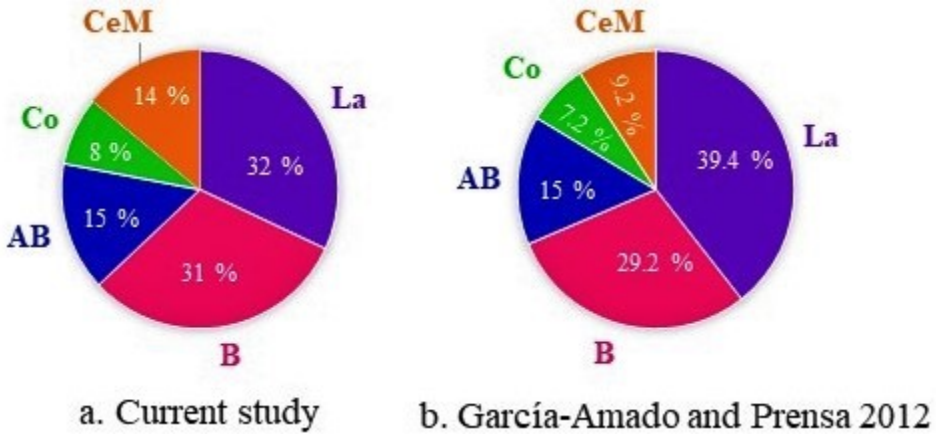

Figure 4.4. Relative distribution of AG subdivisions within total AG volume for (a) the current study and (b) García-Amado and Prensa 2012.

Abbreviations: La, lateral nucleus; B, basal nucleus; AB, accessory basal nucleus; Co, cortical nucleus; CeM, centromedial group.

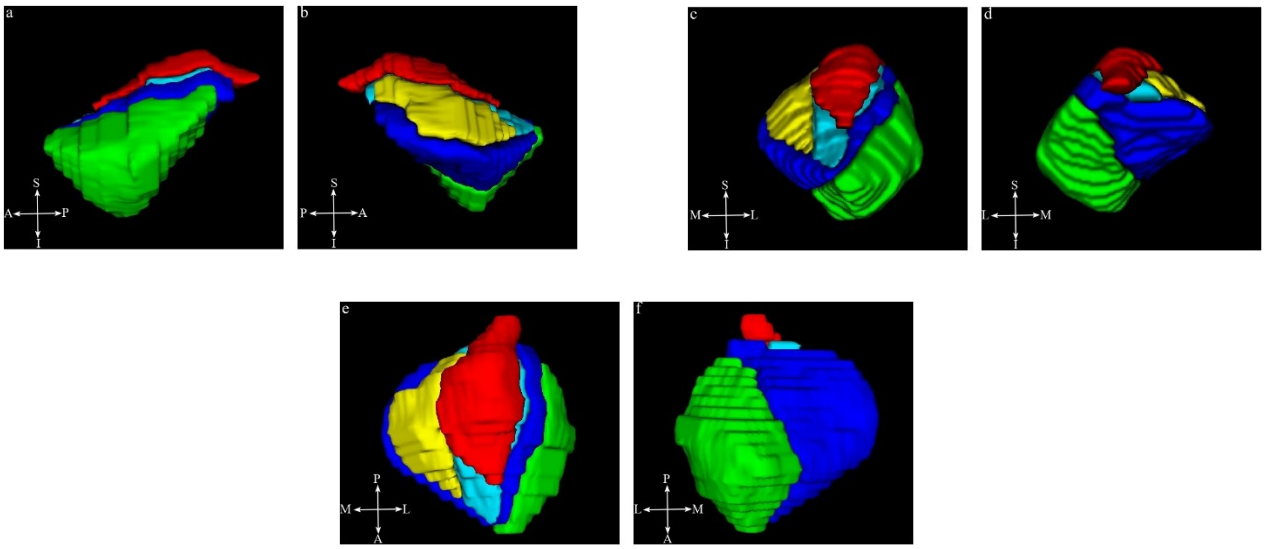

Figure 4.5. Three-dimensional reconstruction of the amygdala subnuclei groups from a healthy volunteer.

(a) lateral view; (b) Medial view; (c) Anterior view; (d) Posterior view; (e) Superior view; (f) Inferior view. La nucleus is in green, B nucleus is in dark blue, AB nucleus is in light blue, Co group is in yellow and CeM group is in red.

4.4. Discussion

Using ultra-high resolution structural T_2-weighted MR images, we developed a reliable segmentation method of the human AG into its five major subnuclei in-vivo for the first time. Our results suggest that consistent measurements of the AG subnuclei can be obtained by experienced MTL image analysts in 2 hours. The strength of our method is that it relies on the internal AG landmarks, not arbitrary boundaries, which are often insensitive to individual brain variations. Finally, we provided a step-by-step protocol, which explains the entire AG subnuclei tracing procedure, and it can be applied by other image analysts to segment the AG into its five major subnuclei with millimeter precision.

Previous methods for the AG segmentation were designed to measure the structure as a whole (Achten et al., 1998; Bonilha et al., 2004; Convit et al., 1999; Makris et al., 1999; Malykhin et al., 2008, 2007; Matsuoka et al., 2003; Pruessner et al., 2000; Watson et al., 1992). More recent studies aimed to segment the AG into its subnuclei and measured the volume of the AG subdivisions (Amunts et al., 2005; Bach et al., 2011; Entis et al., 2012; Saygin et al., 2011).

Amunts and colleagues (2005) provided for the first time cytoarchitectonically verified probabilistic maps for the laterobasal, CeM and superficial AG parcellation that were developed using postmortem histological data from ten human postmortem brains from elderly individuals (average age 65 years). Because structures in the MTL exhibit significant inter-individual variability, the signal-to-noise ratio in MNI transformed group analysis is substantially reduced (Insausti et al., 1998; Prévost et al., 2013). Therefore, the segmentation of the AG in native space can better account for such individual differences in the AG anatomy.

Bach et al. (2011) manually delineated the AG into anterior/inferior/lateral and posterior/superior/medial clusters corresponding to the BLA and the cortico-medial regions respectively. The AG subregion boundaries were not based on intra-AG anatomy. Instead, the authors used a clustering method and probabilistic tractography to segment the AG into the mentioned subregions based on their cortical connections. Volumetric data shown in Table 4.4 indicate that BLA was somewhat underestimated while cortico-medial region was overestimated.

Saygin and colleagues (2011) employed an automated segmentation for the segmentation of the total AG and then divided it into La, BA (B and AB), superficial (Co and Me) and Ce nuclei based on their differential connectivity patterns. Although a connectivity-based segmentation approach is getting popular amongst neuroimaging investigators, it is prone to potential pitfalls. For example, initial definition of the ROI, employing the best clustering algorithm, finding an optimal number of clusters in the defined ROI and assessing the significance of brain parcellation results by using classical inferential statistics in the absence of the null hypothesis to test against should be considered (Eickhoff et al., 2015). It is worth noting that tractography-based segmentation does not necessarily define a real neuroanatomical parcellation. In fact, it is utilized to demonstrate the best clustering explanation of the data (Eickhoff et al., 2015).

The last study used landmarks external to the AG and geometrical rules on high-resolution T_1-weighted anisotropic MPRAGE protocol with 380 μm in-plane resolution and slice thickness of 0.8 mm to manually segment the AG into BL (consists of lateral and basal nuclei), basomedial, CeM and Co subregions (Entis et al., 2012). Despite the fact that Entis et al. (2012) and the present study employed geometrical approaches to segment the AG into its subnuclei groups, there are several important differences between the two methods. First, our volumetric protocol employed T_2-weighted ultra-high resolution FSE images that allow much better visualization of the AG

boundaries, which is a crucial factor for accurate separation of the AG form other MTL structures, especially the hippocampus. Second, we used an acquisition plane perpendicular to the AC-PC line – a similar convention was used in the Mai et al. (2008) atlas – while Entis et al. (2012) acquired MRI data perpendicular to the long axis of the hippocampal formation. Third, our principal landmark line and different points used for geometrical rules were based on the internal AG landmarks (medial and lateral borders of the AG; the most inferomedial border and the most medio-inferior border of the AG), whilst Entis et al. (2012) employed landmarks external to the AG. In addition, the present method also allows the separation of the B from the La AG, while Etnis et al. (2012) analyzed these subnuclei as a single structure (BL).

We think that it is important to analyze these structures separately since all of the AG subnuclei have unique connectivity profile and functions. For instance, the La nucleus is considered the main region in the AG that receives sensory information from all modalities, whilst the B nucleus is generally considered the bridge between the La nucleus and CeM group and a connector of the AG to the orbitofrontal cortex, medial prefrontal cortex, rostral cingulate cortex, and stratial areas (Freese and Amaral, 2009; LeDoux and Schiller, 2009). Similar to the B nucleus, the AB nucleus receives most of its inputs from the La nucleus and most of its projections terminate in the Ce nucleus of the AG (Freese and Amaral, 2009). In addition, the AB nucleus generates one of the major AG projections to the hippocampal, entorhinal and perirhinal cortices. The AB nucleus also sends projections to the orbitofrontal/medial prefrontal cortices, but these are less numerous than projections from the B nucleus (Yilmazer-Hanke, 2012). Ce nucleus is the major site of the AG output and it mediates behavioral responses to emotional stimuli (Hrybouski et al., 2016) by sending its projections to the hypothalamus, the bed nucleus of stria terminalis (BNST), the pons, and the midbrain (Roozendaal et al., 2009). Both the Co and Me nuclei have reciprocal connections

with the olfactory cortex (LeDoux, 2007), which explains their similar functions. However, the Me nucleus also projects to the BNST and hypothalamus (Roozendaal et al., 2009). Most of the findings on AG function come from lesion and animal studies, partially because few patients with the focal AG lesions were reported (Sah et al., 2003), and partially because of resolution limitations in functional imaging (Hrybouski et al., 2016). Despite the fact that the current study did not investigate the function of AG subnuclei, future volumetric and fMRI studies will be able to address this topic directly.

It is important to emphasize that the design of acquisition protocols to image MTL structures depends on two major factors that are contingent on the choice of the magnetic field strength and the acquisition time. First, it depends on the in-plane resolution and whether it is adequate to visualize the structure of interest. For instance, the optimal in-plane resolution to image hippocampal subfields in-vivo is within the range of 0.22mm-0.7mm: 0.22mm×0.22mm (Kerchner et al., 2012), 0.25mm×0.25mm (Henry et al., 2011), 0.4mm×0.4mm (Mueller et al., 2007), 0.52mm×0.52mm (Bonnici et al., 2012), 0.68mm×0.52mm (Malykhin et al., 2010), 0.6mm×0.6mm (Winterburn et al., 2013), and 0.7mm×0.7mm (Wisse et al., 2012). This range of in-plane resolution is sufficient to visualize SLM in the hippocampal body and to delineate hippocampal subfields within it. The second parameter that has to be carefully considered is the slice thickness. Slice thickness also varies between the high-resolution MTL studies from 0.5mm to 2mm: 0.5mm (Bonnici et al., 2012), 0.6mm (Winterburn et al., 2013), 0.7mm (Wisse et al., 2012), 1mm (Malykhin et al., 2010), 1.2mm (Henry et al., 2011), 1.5mm (Kerchner et al., 2012), and 2mm (Mueller et al, 2007). Although all aforementioned studies were able to visualize the subfields within the hippocampal body, the delineation of subfields within the hippocampal tail and head so far was only possible on MRI images acquired with 1mm (and thinner) slices. The

major reason is that subfield transition based on the visualization of changes in the shape of SLM within the HH and tail occurs at least at 1mm scale and therefore can only be detected with these MRI protocols. Unfortunately, the MRI protocols that employed thicker slices are not able to detect such small changes in the SLM anatomy and as a result SLM is poorly visualized on MRI images. Similar imaging parameters for in-plane resolution (0.2-0.7) and slice thickness of 1mm would work for the delineation of the AG subnuclei based on the current volumetric method. In contrast to the hippocampus with visible white matter (SLM), contrast variations within the AG are low due to its low myelin sheath content (Solano-Castiella et al., 2011). The AG has fewer myelinated fibers which are visible on histological images (Brabec et al., 2010; Sims and Williams, 1990), especially separating the central and the lateral AG from the basal AG (Sims and Williams, 1990). However, myelinated fibers are not visible on high resolution structural MRI images to allow for reliable segmentation of the AG subnuclei. At least 1mm slice thickness is necessary for the accurate anterior-posterior transition of the AG subnuclei and the accurate delineation of the AG boundaries from the HH. It remains to be determined whether further improvements in MRI resolution would be able to differentiate myelin fibers within the AG in-vivo.

Although several previous volumetric MRI studies reported asymmetry in AG volume between hemispheres (Achten et al., 1998; Bogerts et al., 1993; Good et al., 2001; Szeszko et al., 1999; Watson et al., 1992), the majority of the studies did not find any differences in AG volume between hemispheres (Berretta et al., 2007; Brabec et al., 2010; Brierley et al., 2002; Bzdok et al., 2013; Chance et al., 2002; Filipek et al., 1997; Heckers et al., 1990; Malykhin et al., 2007; Prestia et al., 2011; Rogers et al., 2009; Sachdev et al., 2000). Our results are in agreement with the latter studies.

Findings on the effects of sex on the AG volume have been equivocal so far. Although some studies, both post-mortem (Heckers et al., 1990) and neuroimaging (Brierley et al., 2002; Goldstein

et al., 2001; Good et al., 2001; Mechelli et al., 2005), claimed that the AG volume is different between males and females, some other studies, both post-mortem (Berretta et al., 2007; Bogerts et al., 1985; Brabec et al., 2010; Chance et al., 2002) and neuroimaging (Giedd et al., 1997; Karchemskiy et al., 2011) did not observe any effect of sex on AG volume. In the present study, we found that males had larger absolute (i.e. raw) volumes for the total AG, and all its subnuclei except for the CeM group. However, these differences disappeared when the AG and its subnuclei volumes were corrected for individual ICVs, suggesting that the relative AG size is similar between males and females. It is important to mention that most of the studies that reported sex differences in the AG volume (Brierley et al., 2002; Goldstein et al., 2001; Good et al., 2001; Heckers et al., 1990), argued that males have larger AG than females. Interestingly, Mechelli and colleagues (2005) found that there were significant patterns of covariance consistent between men and women in the size of many structures in the brain except for the left AG. Therefore, in volumetric studies of AG, it is important to correct AG volume for variations in ICV or total brain volume.

Since the primary goal of volumetric MRI studies is to provide researchers with accurate structural measurements, we compared volumes from the present study to postmortem studies (García-Amado and Prensa, 2012; Schumann and Amaral, 2005) and to the in-vivo MRI study (Entis et al., 2012) (Table 4). According to human postmortem studies (García-Amado and Prensa, 2012; Schumann and Amaral, 2005) the La nucleus is the largest nucleus of the AG while the B and the AB nuclei were the second and third largest nuclei respectively. Our results are in agreement with these findings. Although García-Amado and Prensa (2012) showed that the Me nucleus is the smallest nucleus of the AG, we could not replicate this finding since the Me nucleus in our study was merged together with the Ce nucleus to form the CeM group. However, our results are in

agreement with the postmortem study by García-Amado and Prensa (2012) with respect to the Co nucleus, the smallest AG subdivision in our protocol. We were not able to compare volumes of the CeM and the Co groups in our study with those of the Schumann and Amaral (2005) postmortem study because they did not measure volumes of the Co and Me nuclei separately.

Our inter/intra-rater reliability results indicated that Dice's Kappa values were slightly lower than those of ICCs since they represented the actual overlap between labels and as a result affected the volume of the smaller AG subnuclei more than its larger subnuclei. However, even the inter-rater Dice's Kappa value for AB (.71, the lowest Dice's Kappa value in the current study) is in the range (0.61-0.8) of substantial agreement (Landis and Koch, 1977). Moreover, inter/intra-rater Dice's Kappa values for the total AG (.91/.93) and La nucleus (0.82/.86) exceed the "almost perfect" (> .81) level (Landis and Koch, 1977). This can be explained by relatively simple geometrical rules used in the present segmentation protocol, where all the landmark lines were either 45-degree angle or horizontal, and the reference points were placed at 1/2 or 1/3 of those lines. The inter (intra)-rater Dice's Kappa values for the smaller AG subnuclei were somewhat lower and gradually increased to the largest AG subnuclei (Table 4.2).

Voxel overlap for both inter and intra-rater Dice's Kappa reliabilities was usually larger in the posterior part of the AG where it is surrounded by the hippocampus and white matter and smaller in the anterior part of the AG where the AG is surrounded by the primary olfactory cortex (periform and periamygdaloid cortices), and the preamygdalar claustrum (Mai et al., 2008). Delineation of the anterior AG boundaries is still difficult on MRI images despite recent improvements in resolution, and it reflects the overall complex anatomy of the temporal pole. For instance, Brabec and colleagues (2010) used two neuroanatomical definitions for the AG due to the lack of consensus in measurement of the anterior pole of the AG (Please see figs 4.3 k-m). While our

geometrical rules are highly reproducible, our method also takes into account the inter-individual size differences in the AG shape. In particular, the location and the appearance of the landmark line that corresponds to the inferomedial boundary of the AG is highly consistent across individuals. The additional lines and landmarks are almost exclusively specific to a particular subject, since they are based on superomedial, superolateral and inferolateral boundaries of the AG that showed greater variability in our participants. Furthermore, the appearance and disappearance of individual AG subnuclei and the transition between subnuclei are also based on individual anatomy and take into account the size of the AG in all directions.

Conclusion

AG is a heterogeneous structure, which plays a critical role in the neuronal pathway of emotions, social behaviors and cognition. Unfortunately, detailed information about the function, structure and connection of each of the AG subnuclei and groups in human is very limited. In order to address this gap, we developed a reliable volumetric protocol to delineate five major AG subnuclei in vivo on high-resolution T_2-weighted MRI images. Our results suggest that reliable measurements of the AG subnuclei can be obtained by image analysts with experience in AG anatomy. We provided a step-by-step segmentation protocol and reported absolute and relative volumes for the AG subnuclei. Finally, we did not observe any hemispheric and sex effects on the volume of the AG and its subnuclei. Future applications of this method will help to reveal the selective vulnerability of the AG subnuclei in psychiatric and neurological disorders as well as functional roles of the AG subnuclei in humans.

Limitations

4.7 T FSE protocol can provide very high resolution images in relatively short time. However, it is very sensitive to head motion which causes imaging artefacts and therefore has very limited application in individuals with reduced cooperation. Current acquisition protocol was designed with the main goal of the visualization of hippocampal subfields in-vivo across the entire hippocampal formation regardless of the brain size (9 cm coverage) in a reasonable scan time (13.5 min). Achieving higher in-plane resolution or acquisition thinner slices would result in smaller coverage and larger acquisition times which was not feasible at the time of the current protocol design. Although our MRI protocol has an advantage in terms of short acquisition time and increased coverage, it employs anisotropic voxel which might be more prone to partial volume effects than isotropic voxel (Amaral et al., 2018). However, it is unlikely that the voxel dimensions used in the current study would significantly affect the visualization of the white matter boundaries between the AG subnuclei. For instance, Yushkevich and colleagues (2009) acquired ex-vivo high resolution images of the MTL structures at 9.4 T with either $0.2mm^3$ isotropic resolution (acquisition time to ~ 63 hours) or $0.3\times0.2\times0.3mm^3$ resolution (acquisition time to ~ 15 hours). Despite the fact that the SLM was perfectly visible across entire hippocampus, the white matter fibers within the AG were not visible. Therefore, it is not clear if it is feasible to visualize and segment AG subnuclei in-vivo based on its white matter boundaries with high resolution MR images acquired with isotropic voxel size (at the cost of much longer acquisition time).

Although the AG consists of at least 13 different subnuclei, because of resolution limitations of in-vivo MRI only the five major AG nuclei groups were delineated and other AG subnuclei and periamygdaloid cortical areas were included as parts of the major subnuclei groups. Furthermore, volumetric MRI methods that combine geometrical rules can only approximately match the

location and the orientation of the AG subnuclei based on histological references. The straight-lines used in the current manual segmentation protocol do not exactly represent curved borders of the AG subnuclei and consequently might not yield the perfect segmentation. In manual segmentation protocols, there is sometimes a trade-off between the accuracy of the protocol and the reliability of the protocol. We think that in the current study, the accuracy of the volumetric protocol was minimally sacrificed for the sake of achieving high inter (intra)-rater reliabilities by using straight-lines in outlining boundaries between AG subnuclei.

The current volumetric protocol divided the AG into five subnuclei groups by connecting several internal landmarks that were drawn from a single main landmark line (LL). Although this landmark might not represent a perfect boundary like the SLM for separation of hippocampal subfields, there are several reasons to choose it as the main landmark. First, this is a consistent landmark that can be visualized across the entire length of the AG and it has very little variability between subjects. Second, except for the first few MRI slices this inferomedial border of the AG for the entire length of the AG does not border CSF where usually the first signs of atrophy are visible for both the AG and the hippocampus. Instead, this border is consistently attached to the HH and the parahippocampal white matter, that both show preservation with age (Malykhin et al., 2007; Michelsie et al., 2011). As a result, dramatic age-related changes in the visibility of this LL are not likely to be expected. In addition, stability of this landmark allows detecting changes in AG structure in all other directions (superior and lateral), that have much more variability between subjects and most likely are more prone to shifts associated with age-related atrophy.

Since the current protocol relied on either horizontal landmarks or on lines drawn at a 45° angle from the horizontal plane, extra time and care is needed to trace cases with significant head rotations (>10 degrees). Finally, tracing and segmenting the AG subnuclei in both hemispheres

takes approximately 2 hours for a well-trained rater. However, it is less time consuming compared to the hippocampal subfield segmentation methods, which delineate the subfields within the entire hippocampal formation (3 hours plus).

Acknowledgments

This work was supported by the Canadian Institutes of Health Research (CIHR MOP 115011 and MOP 111049 to NM). We thank Stanislau Hrybouski for assisting with Dice's Kappa calculations and Melanie MacGillivray and Scott G. Travis for editing the manuscript.

Chapter 5: Amygdala subnuclei and healthy cognitive aging

Abstract

Amygdala is a group of nuclei involved in the neural circuits of fear, reward learning, and stress. The main goal of this Magnetic Resonance Imaging (MRI) study was to investigate the relationship between age and the amygdala subnuclei volumes in a large cohort of healthy individuals. Our second goal was to determine effects of the apolipoprotein E (APOE) and brain-derived neurotrophic factor (BDNF) polymorphisms on the amygdala structure.

126 healthy participants (18-85 years old) were recruited for this study. MRI datasets were acquired on a 4.7T system. Amygdala was manually segmented into five major subdivisions (lateral, basal, accessory basal nuclei, as well as cortical, and centromedial groups). The BDNF (methionine and homozygous valine) and APOE genotypes (ε2, homozygous ε3, and ε4) were obtained using single nucleotide polymorphisms.

We found significant nonlinear negative associations between age and the total amygdala and its lateral, basal and accessory basal nuclei volumes, while the cortical amygdala showed a trend. These age-related associations were found only in males but not in females. Centromedial amygdala did not show any relationship with age. We did not observe any statistically significant effects of APOE and BDNF polymorphisms on the amygdala subnuclei volumes. In contrast to APOE ε2 allele carriers, both older APOE ε4 and ε3 allele carriers had smaller lateral, basal, accessory basal nuclei volumes compared to their younger counterparts.

This study indicates that amygdala subnuclei might be non-uniformly affected by aging and that age-related association might be sex specific.

Keywords: amygdala subnuclei, aging, Magnetic Resonance Imaging, brain-derived neurotrophic factor (BDNF), apolipoprotein E (APOE).

A version of this Chapter was published in

Aghamohammadi-Sereshki A, Hrybouski S, Travis S, Huang Y, Olsen F, Carter R, Camicioli R, Malykhin NV., (2019): Amygdala subnuclei and healthy cognitive aging. Hum Brain Mapp. 40(1):34-52. doi: 10.1002/hbm.24353.

5.1. Introduction

The amygdala (AG), a medial temporal lobe brain structure consisting of at least 13 subnuclei (Freese and Amaral, 2009; Sah et al., 2003; Yilmazer-Hanke, 2012), has been considered as a heterogenous structure due to its various cytoarchitectonic and functional features as well as its diverse developmental origin (Freese and Amaral, 2009; LeDoux, 2007; Sah et al., 2003; Yilmazer-Hanke, 2012). The AG is involved in emotional, social (Adolphs, 2009), and goal-directed (Hampton et al., 2007) behaviors, as well as motivation, explicit memory (LeDoux, 2007), attention and perception (Vuilleumier, 2009).

Postmortem studies revealed that pathological age-related changes such as the formation of neurofibrillary tangles and neuritic plaques were present in the AG, as well as in the hippocampus and entorhinal cortex (Wright, 2009). However, age-related changes in the AG have been less studied compared to the hippocampus and entorhinal cortex (Allen et al., 2005; Fjell and Walhovd, 2010). Previous Magnetic Resonance Imaging (MRI) studies of healthy aging reported modest age-related AG atrophy (Brierley et al., 2002; Fjell and Walhovd, 2010; Mather, 2016; Raz and Rodrigue, 2006; Wright, 2009). Furthermore, several studies demonstrated that deleterious effects of aging on the AG volume might not be only cumulative, but also progressive, and become evident after the age of 60 (Grieve et al., 2011; Mu et al., 1999), suggesting a nonlinear association between the AG and age. However, the underlying neuroanatomical sources of this age-related atrophy are not clear (Wright, 2009), since most of the previous MRI studies measured the AG as a single structure (Bonilha et al., 2004; Malykhin et al., 2008; Matsuoka et al., 2003; Pruessner et al., 2001; Sublette et al., 2008). Recent technological advances in MRI, due to improvements in spatial resolution and tissue contrast (Duyn, 2012), made it possible to delineate the AG subnuclei in-vivo (Aghamohammadi-Sereshki et al., 2018; Entis et al., 2012; Saygin et al., 2017; Tyszka and Pauli,

2016). Despite the fact that the specific functions of the human AG subnuclei have not yet been identified (LeDoux and Schiller, 2009), differences in sensory input/output between the AG subnuclei may underlie their functional role (Freese and Amaral, 2009; LeDoux, 2007; Yilmazer-Hanke, 2012). Moreover, sexual hormone markers showed a wide distribution in most of the AG subnuclei in both human and non-human primates (Blurton-Jones et al., 1999; Österlund et al., 2000 a, 2000b; Roselli et al., 2001), suggesting possibility of sex-related differences in the effects of aging on the AG and its subnuclei. However, most of previous age-related studies of the AG did not investigate sexual dimorphism (Heckers et al., 1990; Laakso et al., 1995; Malykhin et al., 2008; Mu et al., 1999) or were limited by small sample sizes or narrow age range to find such an effect (Pruessner et al., 2001; Sublette et al., 2008).

Multiple factors, often called modifiers, including genetic, cardiovascular, lifestyle, physical and cognitive activities can contribute to the inter-individual variability observed in studies of healthy brain aging (Fjell and Walhovd, 2010; Raz et al., 2010; Raz and Rodrigue, 2006). Therefore, a better understanding of these modifiers and their effects on the human brain is critical (Fjell and Walhovd, 2010; Raz and Rodrigue, 2006). AG is one of the brain structures affected in Alzheimer's and Parkinson's diseases which are the two most common neurodegenerative diseases (Braak et al., 1994; Casey 2013; Harding et al., 2002; Krasuski et al., 1998; Scott et al., 1992). Moreover, the apolipoprotein E (APOE) and brain-derived neurotrophic factor (BDNF) are two most common genetic polymorphisms that have been investigated in a number of neuroimaging studies due to their associations with Alzheimer's disease, neuronal repair, protection and proliferation, as well as synaptic growth and memory function (Deary et al., 2004; Petrella et al., 2008). A better understanding of APOE and BDNF-related effects on healthy aging of the AG

might help us to understand protective and/or susceptible factors and mechanisms involved in neurodegenerative diseases.

APOE polymorphism has three known allelic variants (ε2, ε3, and ε4) (Petrella et al., 2008). Previous PET studies reported lower rates of glucose metabolism in posterior cingulate, parietal, temporal, and prefrontal cortex either in the late-middle-aged ε4 carriers (Reiman et al., 1996) or in relatively young adult ε4 carriers (Reiman et al., 2004). Moreover, volumetric MRI studies found ε4-related volumetric atrophy in the AG in Alzheimer's disease (Basso et al., 2006; Hashimoto et al., 2001) and in non-demented older adults (Honea et al., 2009).

The role of BDNF in healthy brain aging has also been a subject of many studies (Petrella et al., 2008). A common BDNF polymorphism is an amino-acid substitution of valine (Val) to methionine (Met) at amino-acid residue 66 (Val66Met). The BDNF is expressed throughout the brain and abundantly in the hippocampus and the prefrontal cortex (Petrella et al., 2008). Consequently, most of the previous MRI studies of the BDNF polymorphism focused on those two structures. However, the number of studies investigating effects of APOE and BDNF polymorphisms on the AG in healthy subjects is very limited (den Heijer et al., 2002; Hibar et al., 2015; Soldan et al., 2015, Sublette et al., 2008) and their effects on AG subnuclei have not been studied so far.

Therefore, the primary goal of the present study was to investigate nature of the AG subnuclei associations with age in a large sample of healthy individuals across the entire adult lifespan using recently developed ultra-high-resolution MRI volumetric method (Aghamohammadi-Sereshki et al., 2018). Our second goal was to determine effects of APOE and BDNF polymorphisms on the AG and its subnuclei volumes.

5.2. Material and methods

Participants

Originally 140 individuals (62 men, 78 women) were recruited through online, poster and local advertisements. However, fourteen participants were later excluded from the initial sample because of contraindications to the 4.7T scan or because of difficulty in remaining still during the scanning procedure. Therefore, the final sample consisted of 126 healthy volunteers (58 males, 68 females), between 18 and 85 years of age (mean: 47.6, SD: 18.9). Of those, 96 participants were Caucasian (76.2%), 23 Asian (18.2%), 7 Latin American (5.6%).

An initial phone interview was conducted to screen candidates for existing neuropsychiatric disorders, as well as MRI contraindications. Participants were excluded if they or their first-degree relatives had any history of psychiatric disorders, as assessed by the Anxiety Disorders Interview Schedule—IV (Brown et al., 2001). Therefore, healthy participants did not have any lifetime psychiatric disorders including schizophrenia, bipolar disorder, major depressive disorder and dysthymia, anxiety disorders, substance dependence, anorexia nervosa, antisocial or borderline personality disorder, panic disorder/agoraphobia, social phobia, specific phobia, and obsessive compulsive disorder. The exclusion criteria were active and inactive medical conditions that may interfere with normal cognitive function (cerebrovascular pathology, tumors or congenital malformations of the nervous system, diabetes, multiple sclerosis, neurodegenerative diseases, epilepsy, dementia, and stroke) and use of psychotropics medications and non-prescribed substances that could affect brain function. However, female participants were not controlled for receiving hormone replacement therapy. Most of the individuals were right-handed (R: 114; L: 12). Handedness was assessed using a 20-item Edinburgh Handedness Inventory and individuals with laterality quotient ≥ +80 were determined as right-handed (Oldfield, 1971).

A face-to-face interview was conducted in order to verify that our older volunteers retained healthy cognitive function. Older subjects (>50 years of age) with Mild Cognitive Impairment and dementia were excluded from the study. For exclusion, dementia was defined according to the DSM-IV criteria. Mild Cognitive Impairment was defined based on presence of cognitive complaints (documented on the AD-8, Galvin et al., 2007) with documented impairment on the Montreal Cognitive Assessment Test (MOCA) (all included subjects had MOCA score ≥ 26) (Nasreddine et al., 2005). Furthermore, older participants (>50 years of age) were assessed for vascular dementia with the Hachinski Ischemic Scale (HIS) (Hachinski et al., 1975). A score above 7 out of 18 has 89% sensitivity (Moroney et al., 1997). All elderly participants included in this study received a HIS score of 3 or lower.

The Clinical Dementia Rating scale (CDR) was used as an assessment of dementia symptom severity (Hughes et al., 1982), where subjects are assessed for functional performance in six areas: memory, orientation, judgment and problem solving, community affairs, home and hobbies, and personal care. We employed CDR as an additional screening measure for dementia in older participants. A composite score from 0 to 3 was calculated. All of our subjects met the cutoff score of < 0.5 for total CDR score. In order to screen older participants for depression, the Geriatric Depression Scale (GDS) was used (Yesavage et al., 1982). Designed to rate depression in the elderly, a score of > 5 is suggestive of depression and a score > 10 is indicative of depression. Our subjects met the cutoff score of 4 and below.

Written, informed consent was obtained from each participant. The study was approved by the University of Alberta Health Research Ethics Board.

MRI acquisition and data analysis

Imaging was performed on a 4.7T Varian Inova MRI system at the Peter Allen MR Research Centre (University of Alberta, Edmonton, AB). A T_2-weighted fast spin echo (FSE) sequence [TE: 39 ms; TR: 11000 ms; bandwidth: 34.97 kHz; echo spacing: 19.5 ms; echo train length: 4; FOV: 20×20 cm; native resolution: 0.52×0.68×1.0 mm^3] was utilized with contiguous 1-mm-thick slices and a 90° excitation followed by a 160° and three 140° refocusing pulses. In total ninety slices were attained perpendicular to the anterior-posterior commissure (AC-PC) line in a total acquisition time of 13.5 min. All high-resolution FSE images were reconstructed and inspected for motion artefacts while the subject was in the scanner, allowing a second or a third FSE dataset to be collected if required. A whole brain T_1-weighted 3D MPRAGE sequence [TR: 8.5 ms; TE: 4.5 ms; inversion time: 300 ms; flip angle: 10°; bandwidth: 80kHz; FOV: 256×200×180 mm^3; voxel size: 1×1×1 mm^3] was acquired for intracranial volume (ICV) estimation. FSE images were interpolated in-plane by a factor of 2 to yield a final resolution of 0.26×0.34×1.0 mm^3 and voxel volume of 0.09 µl. DISPLAY (Montreal Neurological Institute, QC, Canada) software was used to trace the ICV, and all AG ROIs. 3-dimensional models of the AG and its subnuclei were created using ITK-SNAP software (v. 3.6.0; Yushkevich et al., 2006).

Detailed reliable protocols for the manual tracing of the total AG (Malykhin et al., 2007) and AG subnuclei (Aghamohammadi-Sereshki et al., 2018) were previously reported in detail. The AG was manually segmented using geometrical rules that approximately match the location and orientation of the AG subnuclei based on histological references (Brabec et al., 2010; García-Amado and Prensa, 2012; Mai et al., 2008; Schumann and Amaral, 2005). Total AG was manually traced from the most posterior slice continued through slices where both the AG and hippocampal head were present and ended at the level of sulcus closure (Malykhin et al., 2007). Subsequently,

only the coronal plane was used to segment the AG into its 5 major subnuclei groups: The lateral (La) nucleus, the basal (B) nucleus, the accessory basal (AB) nucleus (these three nuclei form the basolateral group [BLA]), the cortical (Co) group and the centromedial (CeM) group (Fig. 5.1). A single internal landmark line which was either a horizontal line that connects the most medial border of the AG to the most lateral border of the AG, or a diagonal line that connects the most inferomedial border of the AG to the most medio-inferior border of the AG was used to segment AG into the aforementioned subnuclei groups (Aghamohammadi-Sereshki et al., 2018). Generally, consistent measurements of the AG subnuclei can be obtained by a person experienced in medial temporal lobe anatomy in 2 hours. All measurements were performed by a single rater (A.S.S) who was blind to all demographic and genotype information. Raw volumetric measurements were adjusted to the ICV by using the following formula: *ICV-adjusted volume = [raw ROI volume (mm^3)/ICV of the same individual (cm^3)] × sample average ICV (cm^3)* (Malykhin et al., 2017). Also, the normalization method used to compensate for the head size differences between individuals depends on the linear relationship between ICV and volumes of the amygdala and its subnuclei (Nordenskjöld et a., 2015). Therefore, in order to test the linear relationship between ICV and volumes of the AG, ROIs Pearson's correlations was used in individuals < 55 years old. Our analyses showed that the volumes of the total AG (r: 0.629, $p < 8.87E-10$), La (r: 0.530, $p < 7.05E-7$), B (r: 0.564, $p < 9.49E-8$), AB (r: 0.570, $p < 6.29E-8$), Co (r: 0.544, $p < 3.15E-7$) and the CeM (r: 0.504, $p < 2.94E-6$) had significant linear correlations with ICV.

Although both total brain volume (TBV) and ICV are frequently used to correct for individual differences in the head size (Mankiw et al., 2017; Nordenskjöld et al., 2015; Reardon et al., 2016; Tan et al., 2016), we used ICV to normalize the AG volumes because unlike the TBV, ICV does not change with age (Michielse et al., 2010, Raz et al., 2004; Shang et al., 2018; Ystad et al., 2009).

The inter-rater reliability was assessed by two raters (A.A.S and N.V.M; developers of the AG segmentation protocol), who independently traced the AG and its subnuclei in 5 subjects (10 amygdalae total). Intra-rater reliability for the total AG and its subnuclei volume measures was assessed by retracing the images from the same five subjects at 1-2 weeks interval by a single rater (A.A.S) who performed all manual measurements of the current study (Table 5.1). It is important to mention that the MRI scans used to assess the intra/inter- rater reliability were different from the datasets used for training.

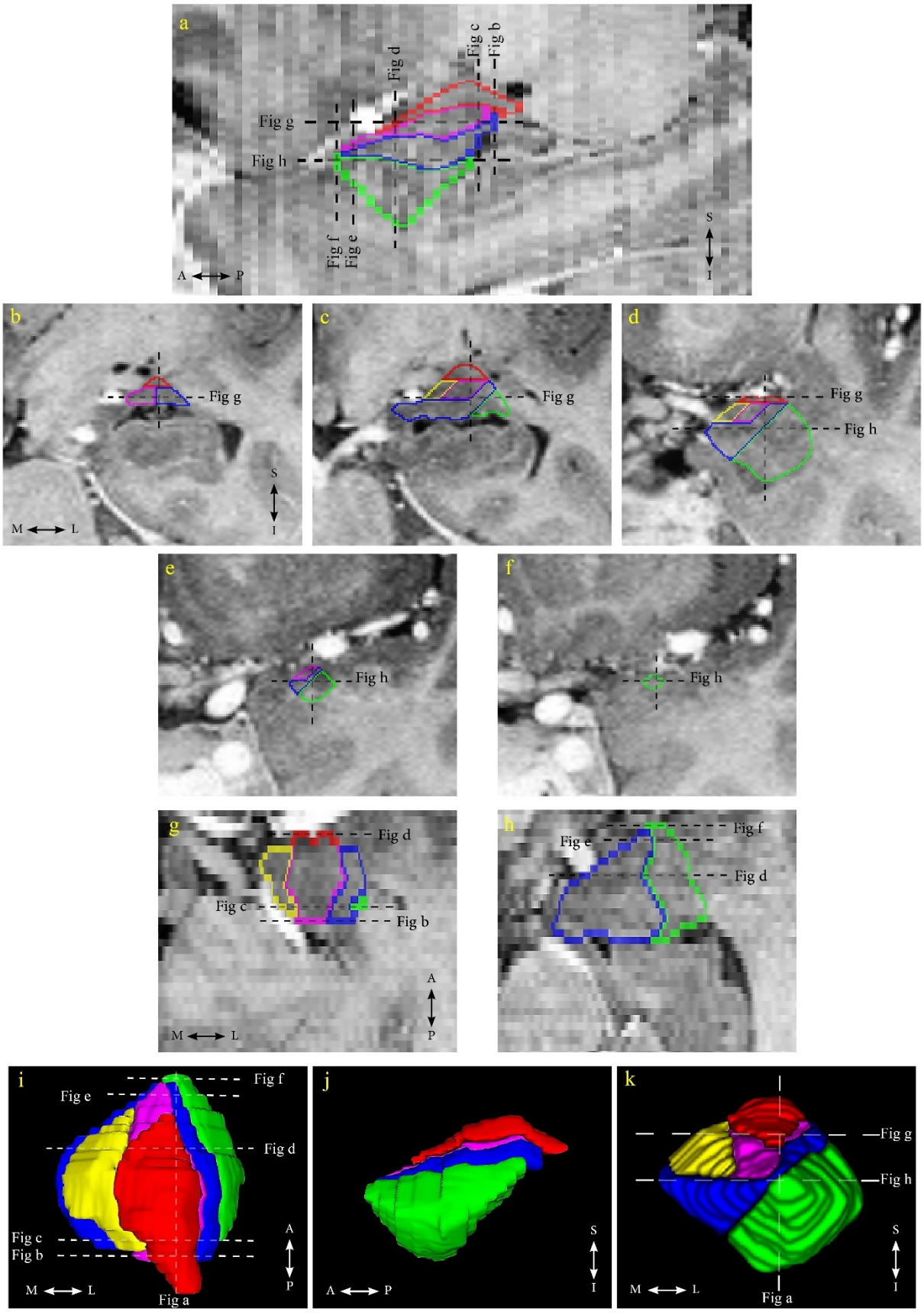
a
Fig d
Fig c
Fig b
Fig g
Fig h
Fig f
Fig e
A
P
S
I
b
Fig g
M
L
S
I
c
Fig g
d
Fig g
Fig h
e
Fig h
f
Fig h
g
Fig d
Fig c
Fig b
A
P
M
L
h
Fig f
Fig e
Fig d
i
Fig f
Fig e
Fig d
Fig c
Fig b
A
P
M
L
Fig a
j
S
I
A
P
k
Fig g
Fig h
S
I
M
L
Fig a

Figure 5.1. Segmentation of the amygdala (AG) subnuclei on a sagittal (a), coronal (b-f) and axial (g and h) views is shown on T_2-weighted FSE images with inverted contrast.
Three-dimensional reconstructions of the AG and its subnuclei from a healthy volunteer are shown from the superior (i), the lateral (j), and the anterior (k) views. Lateral (La) nucleus is outlined in green, basal (B) nucleus is outlined in dark blue, accessory basal (AB) nucleus is outlined in purple, cortical (Co) group is outlined in yellow and centromedial (CeM) group is outlined in red. Dashed lines indicate the corresponding slice locations.

Table 5.1. Reliability results.

ICCs and Dice's Kappa values				
	ICC		**Dice Kappa**	
	Intra-rater	**Inter-rater**	**Intra-rater**	**Inter-rater**
La	.95	.93	.86	.82
B	.94	.87	.81	.76
AB	.96	.95	.77	.71
Co	.97	.87	.72	.72
CeM	.86	.85	.79	.76
AG	.93	.95	.93	.91

Key: AB: accessory basal; AG: amygdala; B: basal; CeM: centromedial; Co: cortical; La: lateral.

Genetic analysis

The genotypes for our genes of interest were obtained using single nucleotide polymorphisms (SNPs) derived from cheek swabs from our participants. Primer3PLUS was used to generate primers using sequence data from dbSNP. Primers were positioned to generate a clean single PCR product with the variant in a position near the centre of the read to avoid common technical artifacts that can occur during the sequencing step. All primers were purchased from Integrated DNA Technologies (Coralville, IA). APOE polymorphisms were determined on the basis of two SNPs:

rs7412 (C; T), which ancestral nucleotide is C and rs429358(T; C) which ancestral nucleotide is T. The presence of rs7412-T and rs429358-T indicates an ε2 allele; the presence of rs7412-C and rs429358-T indicates an ε3 allele; and the presence of rs7412-C and rs429358-C indicates an ε4 allele. BDNF polymorphisms were obtained using rs6265(G; A), where the G allele encodes Val, and the A allele encodes Met. The BDNF Met zygosity was collapsed into a single group due to few homozygous Met/Met genotypes (n=4). For our final analysis, we, therefore, created two groups: Met carriers or "Met/*x*" (i.e. Met/Val and Met/Met) and homozygous "Val/Val". APOE genotype groups were created according to the presence of either the ε2 or ε4 alleles to test for preservative or deleterious effects. As such, three groups were created for the final analysis: "ε2/*x*" (ε2 carriers), homozygous "ε3/ε3", and "ε4/*x*" (ε4 carriers). Participants who possessed both ε2 and ε4 alleles were excluded from the analysis since we observed no statistically significant differences between their inclusion and exclusion, and their frequency was small (n=3). All genotype frequencies are reported in the results section.

Statistics

Demographic information and descriptive AG volumes analyses

All descriptive and inferential statistics other than regression models for age effects were calculated using IBM SPSS Statistics (Version 24.0 for Windows). Group characteristics such as age, education, and ICV were analyzed by a one-way analysis of variance (ANOVA) and with sex as the independent variable. Moreover, demographic information (sex, age, education) of BDNF (Methionine [met+/+; met+/-] and homozygous Valine [+/+] carriers) and APOE (ε2 [ε2/x], homozygous ε3 [ε3/ε3], and ε4 [ε4/x] carriers) polymorphisms were analyzed using a one-way ANOVA. In addition, the chi-squared test was used to evaluate deviation from the Hardy–Weinberg equilibrium. To analyze the effects of genetic polymorphism on the AG volumes, we

used a one-way ANOVA with polymorphism as the between-subject factor and the AG ROI volumes as the dependent variables. To avoid independence assumptions inherent to simple Bonferroni-related correction techniques (i.e., absence of any relationship among AG subdivisions' volumes), permutation tests (100,000 shuffles) were used to generate Holm-Bonferroni corrected null distributions when correcting for multiple comparisons [1 test for total AG; 3 tests for CeM, Co, and BLA groups; 3 tests subnuclei groups within the BLA group (i.e. La, B, and AB nuclei)].

Hemispheric effects analysis

A general linear model (GLM) was used to assess the main effect of age and age × sex interaction on asymmetry indices [({(Right volume) / (Left volume)} × 100) -100] as well as the hemispheric effects on the AG ROIs' volumes (within-subjects factor) in males and females (between-subjects factor). Since our statistical analyses did not reveal any significant effects of age (all *p*s > .05) and age × sex interaction (all *p*s > .14) on AG ROIs' asymmetry indices as well as significant effect of hemisphere on AG ROIs' volumes (all *p*s > .29), left and right AG volumetric data were averaged for analyses.

Modeling age relationships for the AG ROIs

Low-order regressions impose severe shape restrictions (e.g. straight line for linear models and a parabola for quadratic models), while higher-order functions may lead to overfitting and poor generalizability. Here, we relied on multi-model inference to overcome those limitations. Multi-model inference does not assume that a single model is the 'optimal' or 'true' fit to the dataset. Instead, each model receives a likelihood estimate and models are subsequently averaged, based

on their likelihoods (Burnham and Anderson, 2002; Ziegler et al., 2012). All of the ensuing computations were performed using in-house custom-written MATLAB (v. 2016b) programs.

Constructing models that explain the AG ROIs' age relationships

In order to estimate the relationship between age and the volumetric variations of the total AG and the AG subnuclei in males and females we first generated a complete set of 16 parameters incorporating age, sex, and age by sex interactions up to polynomial order 5 (1. Sex 2. Age 3. Age by sex [male] 4. Age by sex [female] 5. Age^2 6. Age^2 by sex [male] 7. Age^2 by sex [female] 8. Age^3 9. Age^3 by sex [male] 10. Age^3 by sex [female] 11. Age^4 12. Age^4 by sex [male] 13. Age^4 by sex [female] 14. Age^5 15. Age^5 by sex [male] 16. Age^5 by sex [female]). Second, all possible combinations of these parameters were computed to build a complete set of all possible models containing at least one of the aforementioned parameters. Third, models with severe multicollinearity (i.e. containing parameters with Variance Inflation Factor [VIF > 10]) were excluded, since severe multicollinearity can result in complex and unstable regression solutions (Ziegler et al., 2012), and the intercept terms was added to all remaining models. Finally, a single model containing only the intercept term was added to the trimmed model set, to reduce the risk of overfitting in case our data contained no evidence for age- or sex-related effects. The entire model generation produce produced 456 potential polynomial regression models, up to 5^{th} polynomial order, with various combinations of sex, age, and interactions terms (Fig. 5.2).

Next, we used non-parametric bootstrap to estimate relative model likelihoods for each of the aforementioned 456 models (Burnham and Anderson, 2002). Model likelihoods were estimated separately for each AG ROI. First, we generated a total of 10,000 paired (i.e., keeping age and volume together) bootstrap samples[1] from the original dataset. For each bootstrap sample the model with the lowest small-sample Akaike Information Criterion (AICc) score was selected.

[1]*Bootstrapping*: randomly sampling data, with replacement, from the original dataset (i.e., a data point is put back into the original dataset before drawing another data point). Therefore, each data point can be sampled several times or not at all. Each bootstrap sample had the same sample size as the original dataset (see Hesterberg et al., 2009 for further details).

Since males and females were modeled simultaneously, any sex differences or age × sex interactions were detected automatically by the AICc algorithm. From each bootstrap sample we built a list of model selection frequencies, which were used as estimates model likelihoods to compute model-averaged fits for relationships between age and AG ROI volumes in males and in females. Furthermore, since each bootstrap sample generated estimates of AG ROI volumes for the entire age range, we were able to construct 95% percentile intervals around our model-averaged fits. Next, we computed R^2 values for our model-averaged fits, as well as 'Prediction R^2' using .632+ bootstrap technique (Efron and Tibshirani, 1997) (Fig. 5.2). These 'Prediction R^2' values represent how much of variation in the volumes of the AG ROIs we expect to explain in new data by our model-averaged fits. Traditionally cross-validation techniques have been used for estimating model performance on new data. Although prediction error acquired by k-fold cross-validation is fairly accurate, it can be quite variable, requiring repeated random partitioning of the data into different folds, leading to computation constraints for computationally-heavy model fitting procedures like ours. The .632+ bootstrap is competitive and can even outperform cross-validation techniques (Efron and Tibshirani, 1997) when estimating out-of-sample Residual Sum of Squares (RSS), but is less computationally demanding than repeated cross-validation.

Finally, age at which AG ROIs' volumes reach maximum volume was estimated for each bootstrap sample. From these, percentile intervals for age at which the AG and the AG subnuclei volumes are at their peak were constructed (Fig. 5.2). The 99% two-tailed thresholds from these percentile

intervals were used to partition the data into two groups: (1) prior to age-related volumetric decline, and (2) after the onset of age-related volumetric decline.

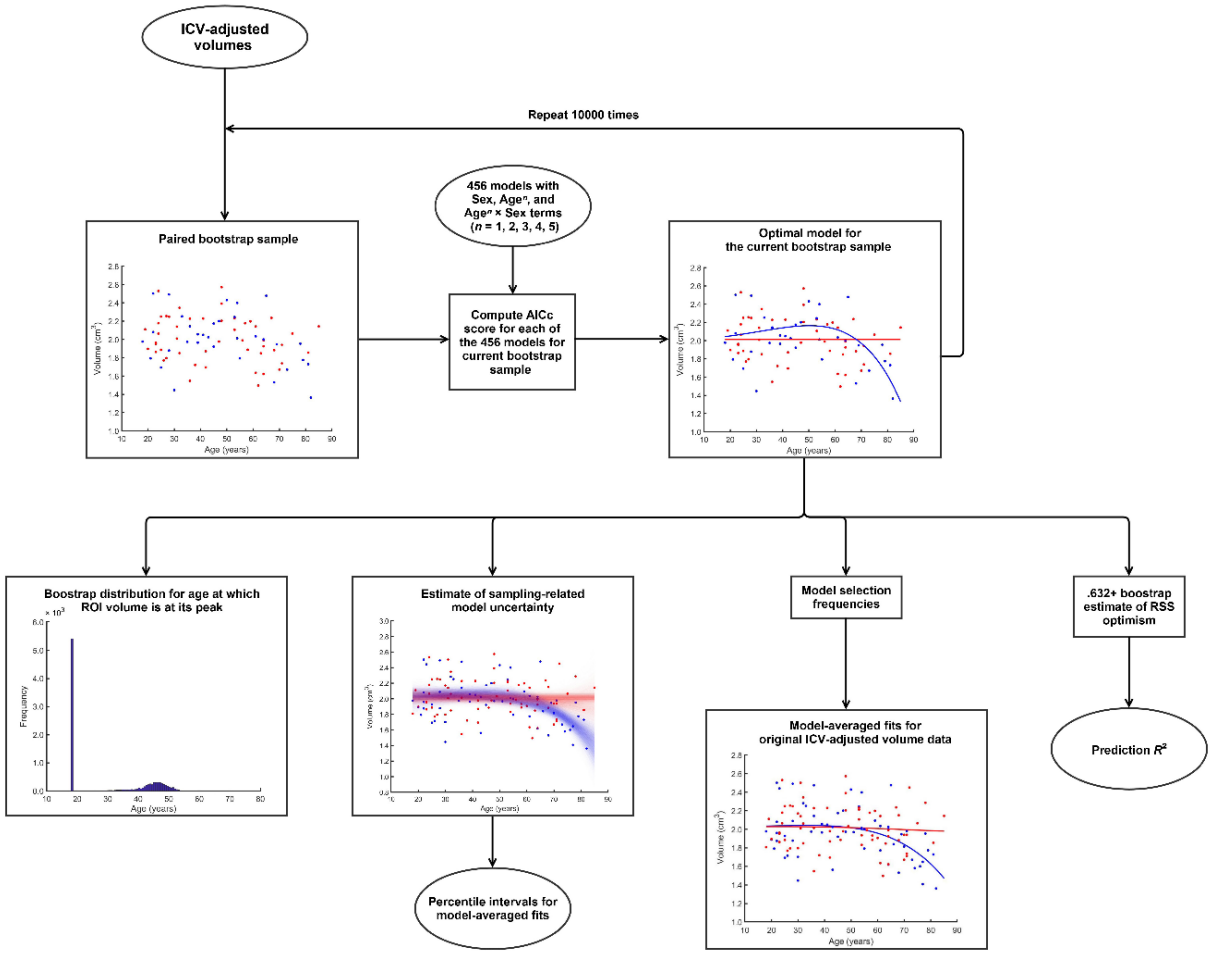

Figure 5.2. Flow chart depicting bootstrap methodology used to model the AG ROIs' relationship to age and their prediction R^2 values.

Assessing the statistical significance of the AG ROIs' model-averaged regression fits.

To evaluate the statistical significance of our model-averaged regression fits, Monte Carlo permutation tests[2] (25,000 simulations) were used to construct 'R^2' distributions under the null hypothesis (Fig. 5.3a). It should be noted that due to computational constraints, we were unable to employ resampling techniques to estimate model likelihoods for each of the 25,000 shuffled

datasets (it would result in 25,000 × 10,000 × 456 GLM estimations per each AG ROI). Instead, we used a theoretical framework (i.e., Akaike weights), which generally produces similar model likelihoods as bootstrap-based resampling techniques (Burnham and Anderson, 2002). Because the number of effective degrees of freedom is ambiguous when employing model averaging, we used R^2 distributions under the null hypothesis to conduct significance tests. Because the ratio of $R^2/ (1- R^2)$ is proportional to *F*-statistic scores, *p*-values estimated from R^2 distributions under the null hypothesis are mathematically equivalent to *p*-values from *F*-statistic distributions (Moore et al., 2009). In total, we simulated five R^2 distributions under the null hypothesis aimed at evaluating the statistical significance of (1) the entire regression model; (2) presence of any relationship between the AG ROI volumes and age, regardless of sex; (3) significance of main sex effects; significance of age relationships in (4) males and (5) females separately (Fig. 5.3a).

Finally, to assess the statistical significance of age × sex interactions, ROI volume shuffling was restricted to individuals of similar age (age difference < 3 years). Subsequently, AICc model selection with model averaging based on Akaike weights was performed under two sets of criteria: (1) from the entire set of 456 models, and (2) from a reduced set of 17 models, containing only main effect terms. For each randomized dataset, the likelihood ratio (LR) for the reduced over full model was computed. These LRs were converted to conventional -2log (LR) test statistic scores, which, in turn, were used to build the -2log (LR) distribution under the null hypothesis for age × sex interaction (Fig. 5.3b).

[2] *Permutation test*: assessing statistical significance using data randomization. Typically, this involves decoupling of the dependent variable from the independent variable by, for example, randomly assigning data points from the former to the data points of the latter [25,000 shuffles for each ROI in our pipeline]. This generates data samples of any possible association [positive, negative or neutral] between the dependent and independent variables.

Similar to conventional GLM procedures, we tested for the overall regression significance (i.e., significance of at least one of the following: main age effect, main sex effect, sex-specific age effect) first. These tests revealed the probability that variance explained by age or sex-related effects in the AG ROIs could have arisen due to chance. Next, we tested for significance of age, sex, and interaction effects. Last, we tested whether associations with age were statistically significant in each sex. We applied the Holm-Bonferroni procedure to correct for type I error inflation due to multiple hypothesis testing at the level of regression significance [1 test for total AG; 3 tests for CeM, Co, and BLA groups; 3 tests subnuclei groups within the BLA group (i.e. La, B, and AB nuclei)]. Similar to factorial designs, no correction for multiple comparisons was used when evaluating the significance of main effects or interactions within each AG ROI. However, a second Holm-Bonferroni correction for multiple comparisons was applied when examining age relationships in each sex separately (2 tests for each AG ROI). Finally, we also calculated Likelihood Ratios (LRs) for model-averaged relative to linear regression fits.

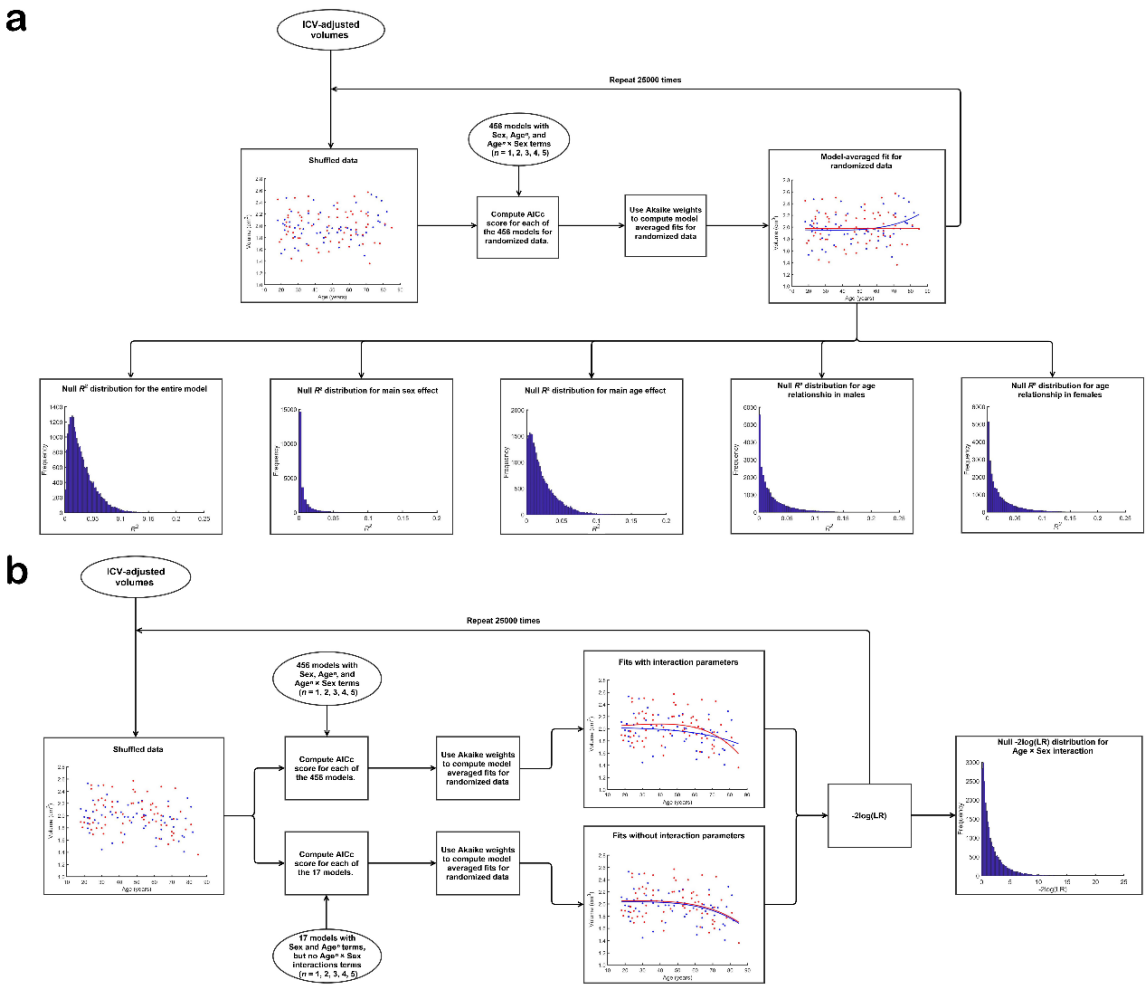

Figure 5.3. Flow chart depicting permutation methodology used to build null distributions to assess the statistical significance of the AG ROIs' (a) overall model significance, age and sex effects, as well as (b) age by sex interactions. LR: likelihood ratio.

5.3. Results

Demographics and descriptive statistics

Participants' characteristics for the entire sample is shown in the Table II. Males had larger ICVs [F (1, 124) = 99.5, $p < .0001$] than females whilst males and females did not differ in age, and education (all ps > .18) (Table 5.2). Furthermore, demographic characteristics were not different

between carriers of the BDNF genotypes (all *p*s > .23), and between carriers of the APOE genotypes (all *p*s > .08) either in the younger (< 55 years old) or in the older (≥ 55 years old) participants. ICV-adjusted AG and AG subnuclei volumes for the left hemisphere, the right hemisphere, and the average, as well as ICV for the young adults (18-39 years old), the middle age (40- 59 years old) and the old adults (≥ 60 years old), are shown in the Table 5.3.

Table 5.2. Demographic information.

Variable	**Male**	**Female**	**Total**	**F-Value**	***p*-value**
Number	58	68	126	-	-
Age in years (mean ± SD)	48.33± 19.7	47.13± 18.34	47.68± 18.91	0.124	0.73
Education in years (mean ± SD)	16.26± 2.44	15.68± 2.44	15.94± 2.45	1.782	0.18
ICV volume mean ± SD (cm^3)	1740.36± 136.88	1520.26± 110.75	1621.57± 165.07	99.5	0.000

Key: ICV: intracranial volume.

Table 5.3. ICV-adjusted AG and its subnuclei volumes (mean ± SD) in young, middle-age, and older adults.

AG ROIs (mm^3)		**Young adults (18-39 years, n=50)**		**Middle age (40-59 years, n=35)**		**Older adults (60-85 years, n=41)**	
		Male (n=23)	Female (n=27)	Male (n=15)	Female (n=20)	Male (n=20)	Female (n=21)
La	Left	656.8 ± 100.1	632 ± 116.1	669.8 ± 107.4	652.2 ± 91.6	590.8 ± 113.4	639.3 ± 117.8
	Right	641.2 ± 143.6	669.1 ± 138.7	659.6 ± 91.4	650.6 ± 102.4	556.4 ± 141.9	587.9 ± 101.7
	Average	648.9 ± 107.3	650.5 ± 108.7	664.7 ± 82.1	651.4 ± 78.8	573.6 ± 101.3	613.6 ± 92.4
B	Left	622.1 ± 99.4	612.4 ± 104.2	614 ± 62.1	641.3 ± 98.1	521.5 ± 89.5	593.6 ± 112.6
	Right	635.4 ± 147.5	630.8 ± 98.7	617.4 ± 85.6	618.1 ± 91.9	512.9 ± 98.5	578.9 ± 86.6
	Average	628.8 ± 113.7	621.6 ± 94.5	615.7 ± 64.9	629.7 ± 83.3	517.2 ± 85	586.3 ± 92.6
AB	Left	285.6 ± 44.5	278.8 ± 46	285.8 ± 39.6	291.5 ± 43.3	248.8 ± 46.3	269.4 ± 54.1
	Right	280.3 ± 59.2	284.2 ± 40	283.3 ± 44.6	282.8 ± 34.2	245 ± 53.6	259.5 ± 37.2
	Average	282.9 ± 48.4	281.5 ± 37.6	284.5 ± 38.2	287.1 ± 31.5	246.9 ± 44.4	264.4 ± 38.2
Co	Left	165.7 ± 22.2	163.8 ± 29.6	176.1 ± 39.9	174.6 ± 31.5	153.6 ± 30.6	159.8 ± 30.7
	Right	159.4 ± 33.8	163.3 ± 24.3	159.6 ± 31.8	168.2 ± 23	143.3 ± 23.9	153.4 ± 24.7
	Average	162.6 ± 24.7	163.5 ± 21.4	167.8 ± 30.1	171.4 ± 21.6	148.4 ± 22.3	156.6 ± 21.8
CeM	Left	282 ± 44.1	292.5 ± 70.4	319.2 ± 90.2	308.9 ± 61.3	291.5 ± 62.3	302.5 ± 67.9
	Right	299.9 ± 66.6	319.2 ± 43.7	303.1 ± 56.8	320.5 ± 56.5	290.9 ± 55.5	301.9 ± 54.3
	Average	291 ± 40.3	305.9 ± 47.1	311.1 ± 59.9	314.7 ± 46.6	291.2 ± 40.5	302.2 ± 52
Total AG	Left	2012.2 ± 227.1	1979.5 ± 253.9	2065.1 ± 212.6	2068.6 ± 251.1	1806.3 ± 268.8	1964.6 ± 292.2
	Right	2016.4 ± 376.7	2066.7 ± 253.8	2023.5 ± 262.3	2040.4 ± 242.1	1748.7 ± 301	1881.8 ± 242.6
	Average	2014.3 ± 279.8	2023.1 ± 237.6	2044.1 ± 219.1	2054.5 ± 209.1	1777.5 ± 256.5	1923.2± 242.4
ICV (cm^3)	Average	1771.9 ± 142	1514.1 ± 126.2	1752.8 ± 134.6	1522.2 ± 95.8	1694.7 ± 126.4	1526.4 ± 107.5

Key: AB: accessory basal; AG: amygdala; B: basal; CeM: centromedial; Co: cortical; ICV: intracranial volume; La: lateral; n: number of individuals; ROIs: regions of interest.

Age and sex effects on the AG ROIs

Age and sex effects on the total AG

The total AG volume showed a statistically significant relationship to age [R^2 = .15, p < .002; Prediction R^2 = .06] (Fig. 5.4), as was the age × sex interaction [p < .024]. Consequently, we examined age relationships in males and females separately, which revealed a significant association between the total AG volume and age in males [R^2 = .25, p < .001; Prediction R^2 = .13], but not in females [p > .57]. However, after controlling for age, males and females had similar ICV-adjusted total AG volume [p > .60].

Lastly, non-linearity LR for the relationship between total AG volume and age in males was 55.44, indicating that the association between age and total AG volume is likely to be nonlinear.

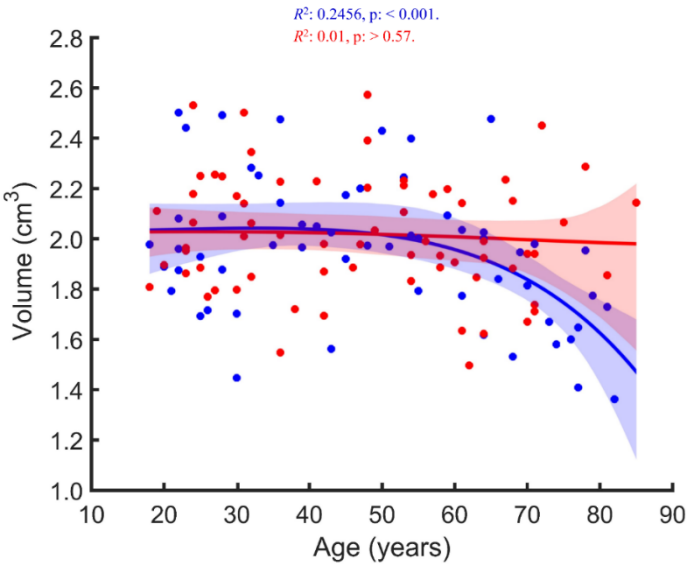

Figure 5.4. Regression plot showing the relationship between age and the ICV-adjusted total AG volume. Model-averaged estimates for men (blue) and women (red) are shown separately. Shaded areas represent the 95% bootstrap percentile confidence interval for each fit.

Age and sex effects on the AG subnuclei groups

Next, we investigated how age and sex related to the three major AG subnuclei groups: BLA, Co, and CeM. We found significant association between age and volume of the BLA group [R^2 = .16, p < .001; Prediction R^2 = .05], while the Co group showed a trend towards significance for age association [R^2 = .08, p < .092; Prediction R^2 = -.02]. However, the CeM group did not show any age- or sex-related effects [p > .48] (Fig. 5.5). Consequently, the CeM results were not investigated further. Both the BLA and the Co groups showed significant age × sex interaction effects (both ps < .050). Analysis of age-related effects in each sex separately revealed that both AG subnuclei groups displayed significant relationships to age in males [BLA: R^2 = .26, p < .001, Prediction R^2 = .14; Co: R^2 = .13, p < .021, Prediction R^2 = .03], but not in females (both ps > .40). No global sex differences, after accounting for age-related effects, were present in any of the AG groups (i.e. BLA, Co, and CeM; all ps > 0.50). Non-linearity LRs for age relationship in males were 35.53 for the BLA group and 10.86 for the Co group.

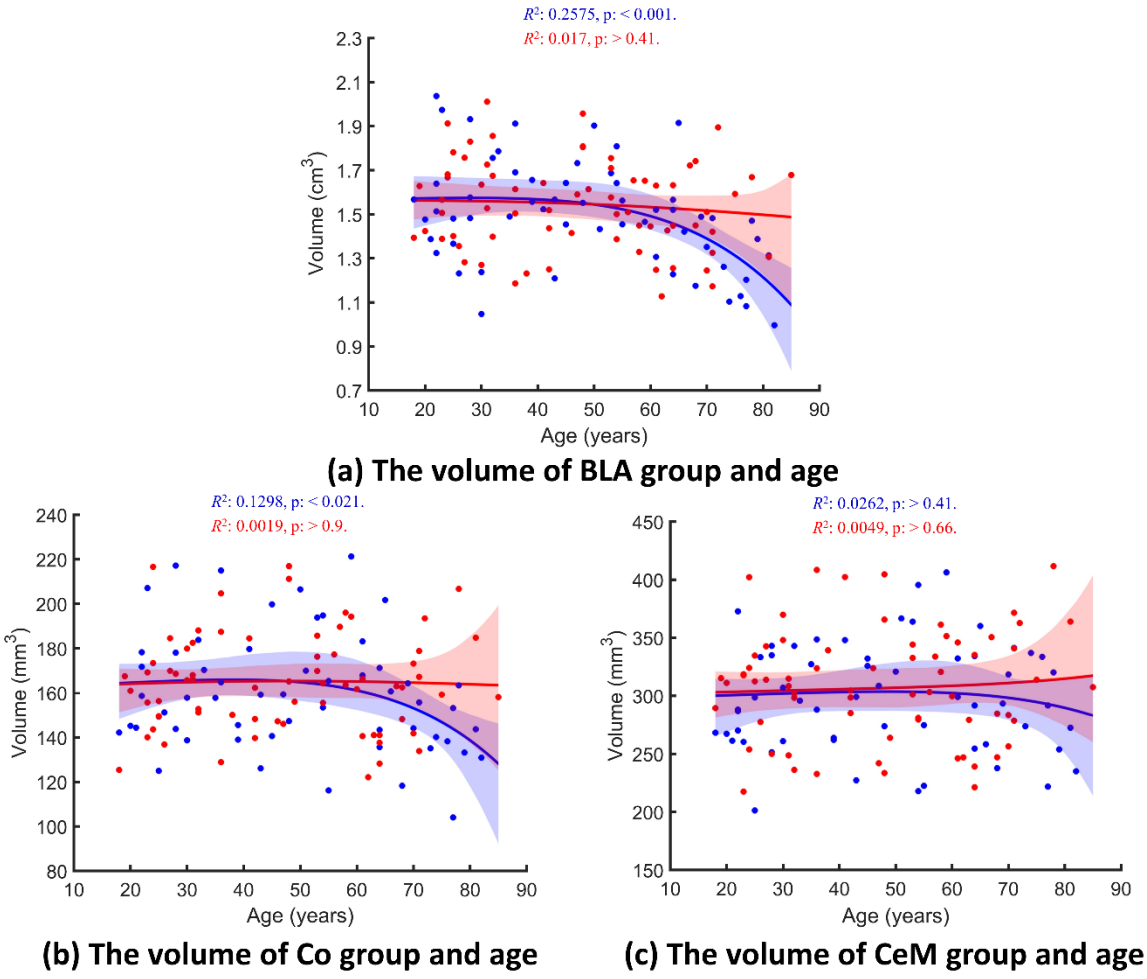

Figure 5.5. Regression plots showing the relationship between age and the ICV-adjusted volumes of the AG subnuclei groups: Basolateral (BLA) (a), Co (b) and CeM (c) subnuclei groups. Model-averaged estimates for men (blue) and women (red) are shown separately. Shaded areas represent the 95% bootstrap percentile confidence interval for each fit. *P*-values are corrected for multiple comparisons.

Age and sex effects on the BLA AG

Our multi-model regressions between age and BLA nuclei volumes were statistically significant for the La [$R^2 = .12$, $p < .006$; Prediction $R^2 = .01$], B [$R^2 = .16$, $p < .002$; Prediction $R^2 = .07$] and AB [$R^2 = .12$, $p < .007$; Prediction $R^2 = .02$] nuclei (Fig. 5.6). Age × sex interactions were

statistically significant for the B and the AB nuclei (both *p*s < .035) and showed a trend towards significance for the La nucleus ($p < .076$). Analyses of age-related effects for each sex separately demonstrated significant associations between age and each of the BLA nuclei in males [La: $R^2 = .22$, $p < .003$, Prediction $R^2 = .12$; B: $R^2 = .26$, $p < .001$, Prediction $R^2 = .16$; AB: $R^2 = .19$ $p < .003$, Prediction $R^2 = .06$,], but not in females (all *p*s > .44). After statistically controlling for age-related effects, ICV-adjusted La, B, and AB nuclei showed no volumetric differences between males and females (all *p*s > .46). Non-linearity LRs for age relationship in males were 75.85 for the La, 6.94 for the B, and 19.04 for the AB nuclei.

All regression-related results and linear vs. non-linear likelihood ratio estimations are presented in table 5.4.

Table 5.4. Summary of all regression models-related R^2, *p*-values and likelihood ratios (LR).

ROIs	Entire model*				Men				Women				Age × Sex
	R^2	Prediction R^2	*p*-value**	Model LR	R^2	Prediction R^2	*p*-value**	Model LR	R^2	Prediction R^2	*p*-value**	Model LR	*p*-value**
Total AG	0.15	0.06	< 0.002	71.90	0.25	0.13	< 0.001	55.44	0.010	0	> 0.57	0.93	< 0.024
CeM	0.03	0	> 0.48	2.24	0.03	0	> 0.41	2.16	0.005	0	> 0.66	1.08	> 0.233
Co	0.08	0	< 0.092	15.75	0.13	0.03	< 0.021	10.86	0.002	0	> 0.90	1.06	< 0.05
BLA	0.16	0.05	< 0.001	39.56	0.26	0.14	< 0.001	35.53	0.017	0	> 0.40	0.91	< 0.03
La	0.12	0.01	< 0.006	65.77	0.22	0.12	< 0.003	75.85	0.014	0	> 0.46	0.82	< 0.076
B	0.16	0.07	< 0.002	7.09	0.26	0.16	< 0.001	6.94	0.016	0	> 0.44	0.99	< 0.024
AB	0.12	0.02	< 0.007	34.95	0.19	0.06	< 0.003	19.04	0.01	0	> 0.57	1.05	< 0.035

Key: *Entire regression model represents significance of at least one of the followings: main age effect, main sex effect, sex-specific age effect. ** *p*-values are corrected for multiple comparisons.

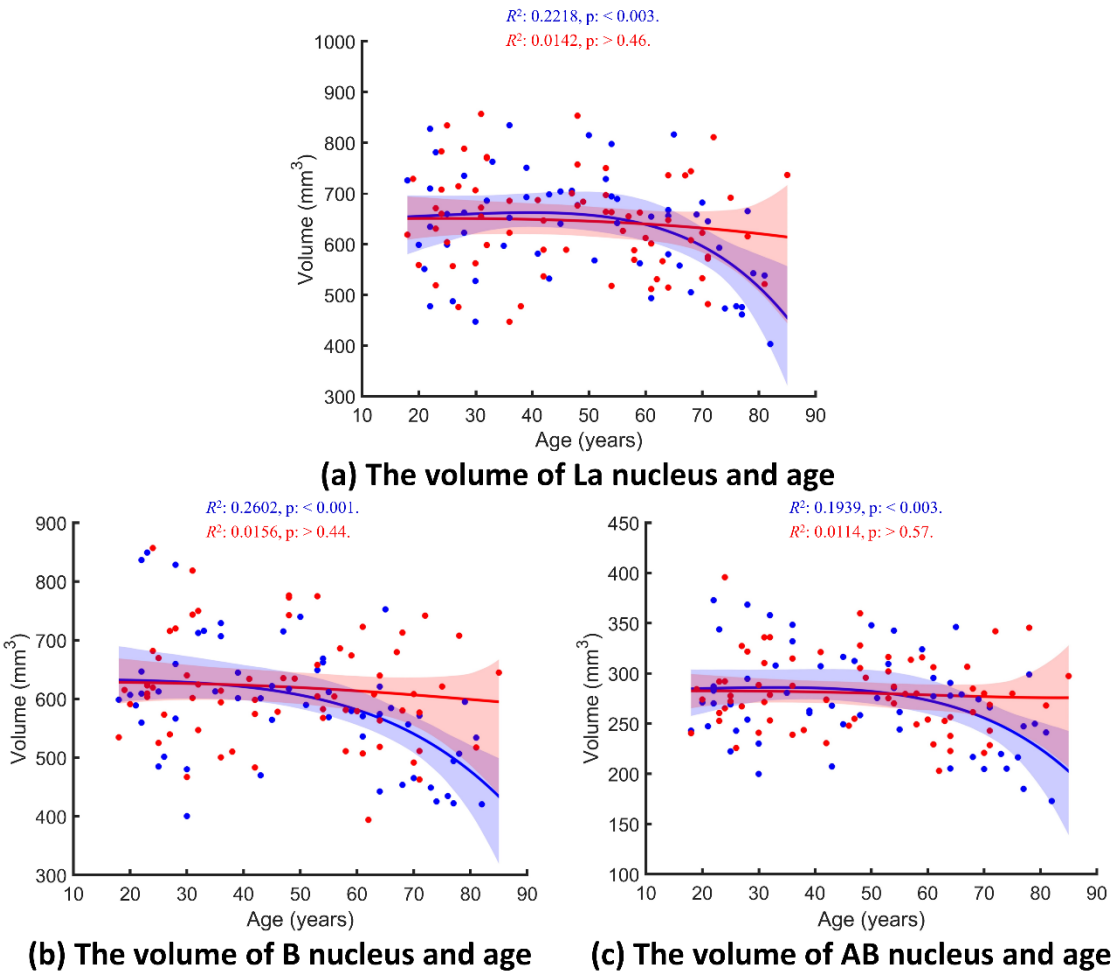

Figure 5.6. Regression plots showing the relationship between age and the ICV-adjusted volumes of BLA nuclei including La (a), B (b) and AB (c). Model-averaged estimates for men (blue) and women (red) are shown separately. Shaded areas represent the 95% bootstrap percentile confidence interval for each fit. *P*-values are corrected for multiple comparisons.

Effects of BDNF and APOE genetic polymorphism on the AG

The chi-squared test showed that our sample for both APOE (χ^2: 5.39, *p*: .37) and BDNF (χ^2: 0.07, *p*: .97) was in Hardy-Weinberg equilibrium. Also, we observed with a 99% confidence that in all AG subnuclei, which demonstrated significant relationship to age, most of age-related atrophy

occurs after the age of 55. Therefore, we divided our sample into two separate groups: prior to age-related volumetric decline (18-54 years), and (2) post-age-related volumetric decline (≥ 55 years). This categorization allowed us to investigate whether effects of genetic polymorphisms were different in younger or older individuals. The AG ROIs' volumetric analyses did not show any significant statistical differences in any of the AG ROIs' volumes between the carriers of BDNF and between the APOE allelic variants neither in the younger nor in the older groups (all uncorrected *p*s >.08) (Tables 5.5 and 5.6). However, volume of the total AG ($p = .09$) in older Met carriers showed a trend towards larger volumes compared to older homozygous Val carriers. Since previous literature indicated that the APOE ε2 allele was associated with positive survival and longevity effects in elderly individuals (Corder et al., 1996; Schächter et al., 1994; Wisdom et al., 2011), while APOE ε4 allele carriers are more likely to develop the late onset Alzheimer's disease (Farrer et al., 1997) we also compared AG subnuclei volumes between younger and older carriers of the same allele to determine if age-related volumetric atrophy was present in all APOE allele carriers. Younger and older individuals within each APOE allele did not differ in ICV (all *p*s >.18) or sex (all *p*s >.1). We found that older APOE ε2 allele carriers did not differ in any AG subnuclei volumes from younger counterparts, whilst both older APOE ε4 allele carriers and older APOE ε3 allele carriers had smaller BLA volumes (with the difference driven by all of its subnuclei; i.e., La, B, AB), which in turn translated to relatively smaller total AG volumes among older APOE ε4 and APOE ε3 allele carriers compared to their younger counterparts. Furthermore, the effects size of age-related volumetric differences was largest among the APOE ε4 carriers.

Table 5.5. ICV-adjusted AG and its subnuclei volumes (mean ± SD) for the BDNF Met carrirs [met+/+; met+/-] and homozygous Val [+/+]) individuals.

Alleles' frequency in the total sample			
	Met ≃ 0.19		**Val** ≃ 0.81
Number of different BDNF genotypes carriers within the total sample (n=126)			
	Met/ Met	**Met/ Val**	**Val/ Val**
Observed genotypes (n)[1]	4	39	83
Expected genotypes (n)[2]	4.55	38.78	82.67

Younger individuals (< 55 years old)					
	BDNF phenotypes				**Effect Size (Cohen's d)**
AG ROIs (mm^3)	**Met (n = 26)**	**Val (n = 51)**	**F-value**	***p*-value**	
La	662.1 ± 88.96	653.22 ± 105.09	.136	.71	0.091
B	643.92 ± 91.10	618.61 ± 96.23	1.234	.27	0.27
AB	284.91 ± 40.46	283.52 ± 40.12	.021	.88	0.035
BLA	1590.93 ± 190.52	1555.35 ± 225.94	0.47	.49	0.17
Co	164.47 ± 21.28	164.93 ± 24.05	.007	.93	0.02
CeM	303.14 ± 41.75	303.44 ± 49.95	.001	.97	0.007
Total AG	2058.54 ± 210.71	2023.71 ± 262.15	.345	.55	0.15

Older individuals (≥ 55 years old)					
	BDNF phenotypes				**Effect Size (Cohen's d)**
AG ROIs (mm^3)	**Met (n = 17)**	**Val (n = 32)**	**F-value**	***p*-value**	
La	623.58 ± 103.99	585.02 ± 82.78	2.013	.16	0.41
B	589.37 ± 92.27	544.50 ± 87.17	2.825	.09	0.5
AB	270.02 ± 42.56	254.86 ± 39.96	1.528	.22	0.37
BLA	1482.96 ± 226.47	1384.38 ± 188.51	2.64	.11	0.47
Co	160.58 ± 20.18	154.48 ± 27.48	.649	.42	0.25
CeM	313.37 ± 37.9	293.83 ± 52.29	1.848	.18	0.43
Total AG	1956.92 ± 270.29	1832.7 ± 225.84	2.928	.09	0.5

Key: [1] Observed genotypes represent the number of carriers for each genotype in the current sample. [2] Expected genotypes represent the number of carriers for each genotype calculated using Met and Val frequencies.

Table 5.6. ICV-adjusted AG and its subnuclei volumes (mean ± SD) for the APOE ε2 [ε2/x], homozygote ε3 [ε3/ε3], and ε4 [ε4/x]) carriers.

Alleles' frequencies in the total sample						
	ε2 ≃ 0.09			**ε3** ≃ 0.80	**ε4** ≃ 0.11	
Number of different APOE genotypes carriers within the total sample (n=126)						
	ε2/ ε2	**ε2/ ε3**	**ε2/ ε4**	**ε3/ε3**	**ε3/ ε4**	**ε4/ ε4**
Observed genotypes (n)[1]	3	14	3	84	20	2
Expected genotypes (n)[2]	1.02	18.14	2.49	80.44	22.18	1.52
Younger individuals (< 55 years old)						
	APOE phenotypes[3]					Effect size (η^2)
AG ROIs (mm3)	**ε2 (n =11)**	**ε3 (n =53)**	**ε4 (n =13)**	**F-value**	***p*-value**	
La	624.54 ± 99.54	662.21 ± 100.64	658.6 ± 96.85	.652	.52	0.017
B	628.14 ± 84.96	629.22 ± 99.83	617.9 ± 86.5	.073	.93	0.002
AB	282.31 ± 30.35	284.6 ± 43.4	282.95 ± 34.41	.02	.98	0.001
BLA	1534.99 ± 201.43	1576.02 ± 222.71	1559.44 ± 200.11	.174	.84	.005
Co	167.49 ± 18.97	162.97 ± 24.5	169.84 ± 20.12	.548	.58	0.015
CeM	322.15 ± 26.79	295.1 ± 48.34	321.01 ± 48.36	2.727	.07*	0.69
Total AG	2024.64 ± 219.19	2034.09 ± 259.02	2050.29 ± 222.42	.034	.97	0.001
Older individuals (≥ 55 years old)						
	APOE phenotypes[3]					Effect size (η^2)
AG ROIs (mm3)	**ε2 (n =6)**	**ε3 (n =31)**	**ε4 (n =9)**	**F-value**	***p*-value**	
La	662.01 ± 82.98	594.05 ± 93.03	560.69 ± 88.12	2.26	.12	0.095
B	606.79 ± 71.97	558.55 ± 97.04	521.97 ± 82.82	1.54	.23	0.067
AB	278.59 ± 37.76	258.25 ± 42.45	250.23 ± 44.93	.86	.44	0.037
BLA	1547.39 ± 185.19	1410.84 ± 215.6	1332.89 ± 184.19	1.95	.16	.083
Co	169.89 ± 21.21	152.67 ± 27.4	158.04 ± 21.4	1.16	.32	0.051
CeM	328.3 ± 21.04	292.08 ± 50.52	317.67 ± 50.64	2.04	.14	0.087
Total AG	2045.58 ± 213.41	1855.59 ± 260.56	1808.6 ± 227.16	1.81	.18	0.078
Young vs Old[4]						
	ε2 (n =17)		**ε3 (n =84)**		**ε4 (n =22)**	
AG ROIs (mm3)	***p*-value**	**Effect Size (Cohen's d)**	***p*-value**	**Effect Size (Cohen's d)**	***p*-value**	**Effect Size (Cohen's d)**
La	.679	0.41	.005	0.7	.047	1.06
B	.762	0.27	.005	0.72	.039	1.13
AB	.826	0.11	.009	0.61	.067	0.82
BLA	.902	0.06	.004	0.75	.039	1.18
Co	.943	0.12	.0127	0.4	.321	0.57

CeM	.923	0.26	.785	0.06	.88	0.07
Total AG	.85	0.1	.003	0.69	.022	1.08

Key: [1] Observed genotypes represent the number of carriers for each genotype in the current sample. [2] Expected genotypes represent the number of carriers for each genotype calculated using ε2, ε3 and ε4 frequencies. [3] ε2/ε4 (N= 3) genotype was excluded from the volumetric analysis. [4] All *p*-values are corrected for multiple comparisons. * A post hoc comparisons, using the LSD test did not show any significant difference in the volume of the CeM group between APOE polymorphism carriers.

5.4. Discussion

This is the first in-vivo study that examined the effects of healthy aging on the AG subnuclei. First, we found that volumes of the total AG, its BLA group, including the La, B and AB nuclei showed significant nonlinear negative relationships with age, while the Co group demonstrated a trend towards significance. In contrast, the CeM group volume was not associated with age. Second, these age-related associations were found only in males, but not in females. We did not find any statistically significant effects of APOE and BDNF polymorphisms on the total AG and its subnuclei neither in younger nor older adults. Nevertheless, both older APOE ε4 and ε3 allele carriers had smaller lateral, basal, accessory basal nuclei volumes compared to their younger counterparts. In contrast, older and younger APOE ε2 allele carriers did not differ in any AG subnuclei volumes.

Aging trajectory of the total AG

Previous in-vivo structural MRI (Allen et al., 2005; Laakso et al., 1995; Malykhin et al., 2008; Mu et al., 1999; Murphy et al., 1996; Sublette et al., 2008) and postmortem (Heckers et al., 1990) studies reported a negative relationship between the AG volume and age, or smaller AG volumes in older compared to younger participants with volumetric reduction becoming more pronounced in advanced age (Grieve et al., 2011; Mu et al., 1999). In contrast, several other studies, including

both in-vivo MRI, (Jernigan et al., 2001; Pruessner et al., 2001) and postmortem (Brabec et al., 2010) did not observe any effects of age on the AG structure. Some of the discrepancies between our findings and the after-mentioned studies are likely driven by methodological differences. For instance, Pruessner et al. (2001) investigated the effects of age and sex on the AG and hippocampal volumes in individuals who were between 18 and 42 years old; however, no association between the AG volume and age was reported separately for men and women. In contrast, the present study suggests that age-related volumetric reduction in the AG starts in mid-fifties. The most important difference between the present study and Jernigan and colleagues (2001) is the definition of the AG boundary. Jernigan and colleagues (2001), combined the AG tissue with adjacent entorhinal and perirhinal cortices and used this "amygdala +" volume in their analysis, whilst in the present study these cortices were excluded from AG ROIs.

Although a published meta-analysis by Brierley and colleagues (2002) and a recent review article (Fjell and Walhovd, 2010) both suggested that the relationship between the AG volume and age is linear, our results demonstrated nonlinear correlations between age and volumes of the total AG as well as the AG subnuclei. Such inconsistencies could have arisen by infrequent use of nonlinear regression fits by other research groups: the majority of previous age-related MRI studies of the AG tested for linear correlations only (Brabec et al., 2010; Laakso et al., 1995; Mu et al., 1999; Pruessner et al., 2001; Sublette et al., 2008). A few previous studies, which used a limited number of nonlinear regression models (Allen et al., 2005; Jernigan et al., 2001; Murphy et al., 1996), found no improvement in model fit by adding nonlinear terms to the model. However, two structural MRI studies, employing automated segmentation methods to estimate the AG volumes, showed that the rate of AG atrophy is not constant in advanced age (Fjell et al., 2009; Grieve et al., 2011). Therefore, future structural MRI studies of the relationship between the AG volume and

age would need to test non-linear models in addition to linear models in order to further address these discrepancies between studies.

It is important to mention that differences in MRI segmentation methods (e.g., manual versus automated) can lead to discrepancies in volumetric measures. Findings from studies that employed automated segmentation methods, such as the FreeSurfer and FSL-FIRST, need to be interpreted with caution because these software packages tend to overestimate both the AG and hippocampal volumes (Morey et al., 2009; Schoemaker et al., 2016). Discrepancies between manual segmentation and automated techniques are usually larger for the AG than for the hippocampal formation (Morey et al., 2009; Schoemaker et al., 2016). Furthermore, the accuracy of automatic segmentation methods might be further reduced in brains with noticeable atrophy (Sánchez-Benavides et al., 2010).

Aging patterns of the AG subnuclei

Results of the present study demonstrated a mosaic pattern of relationships between the AG subnuclei volumes and age. While the volumes of the La, B and AB nuclei showed significant negative nonlinear associations with age, the CeM group did not correlate with age and the Co group showed a trend towards significance. The exact underlying reasons for the observed non-uniform correlations between the AG subnuclei volumes and age are not known. We speculate that these differences in vulnerability of the AG subnuclei to aging might be related to their heterogeneous connectivity profiles and function as well as evolutionarily features and developmental origins.

The number of the AG subnuclei varies from 13 subnuclei in rodents to 36 subnuclei in humans (Yilmazer-Hanke, 2012). Each of the main AG subnuclei has specific functions through their unique anatomical connections (LeDoux, 2007).

The BLA group is connected to regions in the brain involved in learning and memory (Roozendaal et al., 2009) and these regions are vulnerable to the age-related changes (Fjell et al., 2013; Fjell and Walhovd, 2010; Jernigan et al., 2001; Looi and Sachdev, 2003; Malykhin et al., 2008; Malykhin et al., 2017; Raz and Kennedy, 2009; Walhovd et al., 2005). In contrast to the BLA, the CeM group is connected to the brain regions involved in regulation of autonomic functions and mediating intrinsic behaviors (Roozendaal et al., 2009) which are resilient to age-related adversity (Doraiswamy et al., 1992; Fjell and Walhovd, 2010; Luft et al., 1999; Raz, 2000; Roberts et al., 2012). Finally, age-related findings on the olfactory bulb which projects to the Co group remain inconsistent with both preservation and decrease in volume with age (Mobley et al., 2014).

The second possible explanation for differential effects of aging processes on the AG subnuclei might be due to the ontogenetic (an individual's development) and phylogenetic (evolutionary history) properties of various brain regions (Raz et al., 1997). All of the AG subnuclei can be categorized based on either their evolutionarily features (LeDoux, 2007; Swanson and Petrovich, 1998) or their developmental origins (Swanson and Petrovich, 1998; Yilmazer-Hanke, 2012).

According to phylogenetics, the AG is divided into two major groups: (1) the cortico-medial region including Co, medial (Me) and central (Ce) subnuclei which is a primitive division of the AG; and (2) the BLA group consists of the La, B and AB nuclei which is a phylogenetically newer division of the AG (LeDoux, 2007; Swanson and Petrovich, 1998). In the present study, the CeM group was the only sub-region in the AG that did not show any relationship with age. Chareyron et al. (2011) showed that the Me and Ce nuclei comprise a conservative group that exhibited relatively

a small size difference between rats and monkeys. In contrast, the BLA group (that showed significant negative correlations with age in the present study) is noticeably more developed in monkeys and humans than in rats. While the BLA group comprises 62% and 69% of the total AG volume in monkeys and humans respectively, it comprises only 28% of the total AG volume in rats (Chareyron et al., 2011). Therefore, it is likely that age-related susceptibility of the AG subnuclei might have phylogenetic underpinnings. In addition, the present finding on the preservation of the CeM group with age is consistent with the conservation of the autonomic AG [including Ce and Me nuclei that project to autonomically-related structures in the brain (Roozendaal et al., 2009)] during the evolution (Moreno and González, 2007). CeM group is critically important in mediating the behavioral response to environmental stimuli (Moreno and González, 2007). Furthermore, the previous behavioral study showed that elderly adults have similar responses in detecting potentially threatening stimuli as young adults (Mather and Knight, 2006).

The AG subnuclei can also be categorized according to their developmental origins and preferential connections into 3 major groups: (1) the BLA group; (2) the superficial or Co-like group; and (3) the CeM group which includes the Ce and Me nuclei (Yilmazer-Hanke, 2012). The development of the AG subnuclei and their aging patterns may follow the notion that the last regions in the brain to mature are among the first to show the signs of aging (Raz et al., 2005, 1997).

Amongst the AG subnuclei, the Co and Me nuclei develop first (Humphrey, 1968). However, the Ce nucleus develops considerably later than the Co and Me nuclei. The BLA group also differentiates into its constituent nuclei much later than the Co and Me nuclei (Humphrey, 1968). Therefore, developmental patterns of the AG subnuclei might explain their aging patterns to some

extent. Despite the developmental timing of the Co and Ce nuclei, the former showed a negative relationship with age and the latter did not correlate with age, which contrasts the "last in, first out" hypothesis (Fjell and Walhovd, 2010). It is important to mention that although we did not segment Ce and Me nuclei separately, due to the larger volume of the Ce compared to Me (almost 2 times) (García-Amado and Prensa, 2012); we think that if the Ce nucleus indeed underwent volumetric atrophy with age, the CeM group would also show such effect.

In summary, in our view, heterogeneous connectivity profiles and phylogenetic properties of the AG subnuclei might play a more important role in their differential vulnerability to aging than their ontogenetic properties.

Sexual dimorphism in the association of AG ROIs' volumes with age

In the present study, we found significant age × sex interaction in the total AG, the BLA and Co groups, as well as the B and AB nuclei, while the La nucleus showed a trend towards significance for this interaction ($p < .076$).

The existence of a sex bias (Jazin and Cahill, 2010) in brain structures and functions as well as a healthy behavior across the lifespan has been previously suggested (Cosgrove et al., 2007; Gur et al., 2010; Jazin and Cahill, 2010). The effects of aging on the global gray matter volume and on other brain structures were previously compared between men and women (Abe et al., 2010; Coffey et al., 1998; Cowell et al., 1994; Good et al., 2001; Murphy et al., 1996; Raz et al., 2004) and only few brain structures showed greater volumetric reduction in women compared to men (Li et al., 2014; Murphy et al., 1996). In general, studies that reported age-specific differences between the two sexes, claimed that the effects of aging were more pronounced in men compared to women (Allen et al., 2005). It is important to note that, in contrast to the observed sex bias in aging patterns

of the AG and its subnuclei, ICV-adjusted volumes of the AG and the AG subnuclei did not differ between men and women. This is in agreement with both postmortem (Brabec et al., 2010) and neuroimaging (Aghamohammadi-Sereshki et al., 2018; Giedd et al., 1997; Karchemskiy et al., 2011; Laakso et al., 1995; Mu et al., 1999; Murphy et al., 1996; Pruessner et al., 2001; Sublette et al., 2008) studies. Although Brabec et al. (2010) did not find any associations between the AG volumes and age in both males and females, a negative correlation between age and a portion of the AG volume that represented the difference between the AG with wider borders ("$V_{Class+ Add}$") (Brabec et al., 2010) and the classical definition of the AG ("V_{Class}") (Brabec et al., 2010) was reported in males, but not in females. In the present study, the location and orientation of the AG subnuclei corresponded to the classical definition of the AG ("V_{Class}") (Brabec et al., 2010). However, due to lack of visible landmarks on MRI for delineation of the anterior AG from the periamygdaloid cortices (Aghamohammadi-Sereshki et al., 2018; Allen et al., 2005), inclusion of some of the "V_{add}" (Brabec et al., 2010) tissue in our AG subnuclei segmentation method was inevitable. Therefore, our findings on age-related sexual dimorphism are partially in agreement with Brabec et al. (2010). Moreover, Giedd and colleagues (1997) reported sex differences in the AG maturation among 115 healthy children and adolescents with greater age-related volumetric increase in males than in females (Giedd et al., 1997).

The etiology of sexual dimorphism in neuroscience is not clear for two main reasons: first, the widespread use of male animals in preclinical studies; and second, a false conception that considers sex bias as minor and unimportant (Cahill and Aswad, 2015).

In general, the most plausible explanations for sexual differences are (1) estrogen and androgen-dependent mechanisms (Behl, 2002; Cosgrove et al., 2007), and (2) sexual regulatory mechanisms independent of sexual hormones (Jazin and Cahill, 2010; Cahill, 2006). Sex hormones have

considerable effect on the AG (Hamann et al., 2004). In human and non-human primate AG, the Ce nucleus is the only major nucleus without any report of estrogen receptor alpha (ERα) - immunoreactive neurons, mRNA expression of ERα and estrogen receptor beta (ERβ) in both sexes; and also, without any report of cytochrome P450 aromatase and androgen receptor mRNA expressions in males (Blurton-Jones et al., 1999; Österlund et al., 2000a, 2000b; Roselli et al., 2001). However, these sexual hormones markers are differentially distributed in the rest of the AG subnuclei (Blurton-Jones et al., 1999; Österlund et al., 2000a, 2000b; Roselli et al., 2001). Age-related decrease of the ERβ mRNA expression was reported in B nucleus and nucleus of the lateral olfactory tract [a part of the Co group (Sah et al., 2003)] of female rats (Yamaguchi-Shima and Yuri, 2007), while the La, anterior and posterior cortical, and Ce nuclei showed reduced ERβ mRNA expression in male rats (Yamaguchi and Yuri 2012), suggesting that these effects were sex-dependent (Yamaguchi and Yuri 2012).

Estrogen can also enhance neuron longevity via its neurotrophic and antioxidant roles or suppress apoptosis (Behl, 2002). Future studies would need to determine neuroprotective effects of estrogen on human AG in aging.

Imaging genetics of the AG

In the present study, we did not find any statistically significant effect of the BDNF and APOE polymorphisms on the AG and its subnuclei volumes.

The main objective of neuroimaging genetics is to identify genes that either precipitate or lessen deleterious age-related effects on brain structures and their functions (Fjell and Walhovd, 2010). Although lipoprotein transport and neuronal health are the two primary functions of APOE in the brain (Petrella et al., 2008), structural effects of APOE on brain regions are still poorly understood in healthy populations (Fjell and Walhovd, 2010). Most of the APOE studies have focused on the

hippocampus, though findings are contradictory. While some studies found negative effects of APOE ε4 alleles on the hippocampal volumes in the elderly, other studies did not report hippocampal volume differences between healthy APOE ε4 carriers vs. non-carriers in nondemented older adults (Fjell and Walhovd, 2010). However, the data about the AG and APOE genetic polymorphisms in healthy aging is scarce. One study, which used a manual segmentation procedure on 428 non-demented elderly individuals found that carriers of ε4 had significantly smaller bilateral AG than ε3ε3 genotype carriers. Furthermore, although ε2 carriers had more atrophy than those with the ε3ε3 genotype, the difference was not significant (den Heijer et al., 2002). A large neuroimaging-genetics study (30,717 individuals from 50 cohorts), which used automated segmentation tools (FSL-FIRST and FreeSurfer) did not find any association between the AG volume with either APOE or BDNF, and the AG showed the least heritability ($h^2 = 0.43$; confidence interval = 0.39, 0.48) amongst all the examined subcortical regions (Hibar et al., 2015). Finally, Soldan and colleagues (2015) demonstrated that the AG volume estimated using a semi-automated technique (n=245) did not depend on APOE-ε4 genotype.

BDNF is the most abundant neuronal growth factor (Sublette et al., 2008) which plays a key role in neuronal survival, synaptogenesis, proliferation and development (Petrella et al., 2008). Several studies showed that Val66Met genotype is associated with decreased volume in the hippocampus, prefrontal cortex, as well as temporal and occipital gray matter (Petrella et al., 2008; Sublette et al., 2008). Like APOE, the relationship between BDNF and AG has been less studied. In addition to Hibar and colleagues (2015), Sublette et al. (2008) explored the relationship between age, BDNF and AG volumes among 55 healthy right-handed volunteers using a manual tracing procedure. They found no difference in the raw and ICV-adjusted bilateral AG volumes between BDNF val66met allele carriers and non-carriers and reported an inverse correlation between the AG

volume and the age in BDNF val66met carriers but not in non-carriers. However, the authors suggested that these results should be interpreted with caution due to the small sample size, limited age range and inadequate statistical power to detect sex differences (Sublette et al., 2008).

Our findings are consistent with previous results reported by Hibar et al. (2015) and Sublette et al. (2008), which reported absence of a relationship between the AG volume and APOE or BDNF polymorphisms. Our results are also in partial agreement with those by Soldan and colleagues (2015) who demonstrated that the AG volume did not differ between APOE-ε4 carriers and non-carriers. However, the current study differs from previous research by den Heijer et al. (2002), which indicated ε4 carriers have more AG atrophy than ε3ε3 carriers.

Our result on relative preservation of AG subnuclei in ε2 carriers versus ε4 is in line with previous research, which indicated that the APOE ε2 allele can reduce the risk of developing Alzheimer's disease since it has positive survival and longevity effects in elderly individuals (Corder et al., 1996; Schächter et al., 1994; Wisdom et al., 2011), while homozygous APOE ε4 allele carriers are 10-12 times more likely to develop the late onset Alzheimer's disease (Farrer et al., 1997). However, volumes of the AG subnuclei in ε2 carriers were not statistically different form participants with the most common ε3 variant of APOE that is not associated with Alzheimer's disease (Corder et al., 1996; Lahiri et al., 2004; Wisdom et al., 2011). Although, in the present study ε3 carriers did not differ in any AG subnuclei volumes from ε4 carriers, and the age-related decline in AG volume was found in both groups, the larger effect size of AG volume decline with age in ε4 carriers could indicate that cognitively healthy participants with APOE ε4 allele were more vulnerable to aging then ε3 carriers and especially more than ε2 carriers. Since our sample size of ε2 and ε4 carriers in aging subgroups was relatively small, future studies with substantially

larger samples are needed in order to provide a conclusive evidence of neuroprotective effect of ε2 on the AG subnuclei.

It is important to mention that gene × environment interactions might also obscure effects of a specific gene on individual brain structures (Fjell and Walhovd, 2010). Finally, considerable differences in gene expression of various age cohort (e.g., old vs. young adults) further challenge our ability to detect the effect that a single gene has on each individual brain structure (Reinvang et al., 2010).

Limitations and future directions

This study was cross-sectional and therefore future longitudinal studies would have to address the nature and rate of the AG volume loss in healthy aging. Modest sample size for the genetic component of our study, particularly the number of ε2 carriers, could have prevented us from detecting any significant protective effects of this allele against aging. However, larger neuroimaging genetic studies might require the application of automated segmentation methods which might reduce the accuracy of the segmentation of the medial temporal lobe structures. The current manual segmentation protocol of the AG subnuclei is based on geometrical rules dependant on internal AG landmarks since the AG myelinated fibers are not visible even at 4.7 T FSE images (Aghamohammadi-Sereshki et al. 2018). Therefore, our macroscopically defined AG subnuclei are only an approximation of the individual microscopical subnuclei. Despite the fact that 4.7 T system is quite rare similar high-resolution MRI protocols have been successfully employed in aging studies of hippocampal subfields that used both lower (3T) and higher (7T) field strength magnets (see Malykhin e t al. 2017). Future volumetric MRI studies would also need to determine

whether the reported differences in aging patterns between the AG subnuclei are associated with differences in cognitive or affective functions.

Acknowledgements

Financial support for this study was provided by the Canadian Institutes of Health Research (CIHR) operating grant MOP115011 to Nikolai Malykhin. Scott Travis was supported by the CIHR Frederick Banting and Charles Best Canada Masters scholarship award and the Alberta Innovates Health Solutions (AIHS) Doctoral scholarship award. Stanislau Hrybouski was supported by Fredrick Banting and Charles Best CIHR Doctoral scholarship award. The authors have no conflicts of interest to disclose.

Chapter 6: Effects of childhood adversity on the volumes of the amygdala subnuclei and hippocampal subfields in major depressive disorder

Abstract

Background: Reductions in total hippocampus volume have frequently been reported in Magnetic Resonance Imaging (MRI) studies in major depressive disorder (MDD), while total amygdala volume differences have been inconsistent. Childhood maltreatment is an important risk factor for MDD in adulthood and may affect hippocampus and amygdala volumes. Here we compared the volumes of amygdala subnuclei and hippocampal subfields in MDD and controls and examined their relationship with childhood maltreatment.

Method: Thirty-five patients meeting DSM-IV criteria for MDD were recruited and also 35 healthy controls. MRI datasets were acquired on a 4.7T Varian Inova scanner. The amygdala subnuclei (lateral, basal, accessory basal nuclei, cortical and centromedial groups) and hippocampal subfields (cornu ammonis (CA1-3), subiculum and dentate gyrus) were manually delineated using reliable volumetric methods. Childhood maltreatment was assessed on the Childhood Trauma Questionnaire (CTQ) in MDD-participants.

Results: We did not find significant effects of MDD or antidepressant treatment on volumes of the amygdala and its subnuclei. However, history of childhood maltreatment was negatively associated with the anterior hippocampus bilaterally limited to CA1-3 subfield, while in the amygdala these effects were limited to basal, accessory basal, and cortical amygdala subnuclei

within the right hemisphere, implying that maltreatment might potentially lead to reduced development of these areas.

Limitations: This study was cross-sectional.

Conclusions: These results provide evidence of the negative associations between history of childhood maltreatment and the volumes of amygdala subnuclei and hippocampal subfields. This has implications for potential mechanisms for maltreatment to lead to subsequent clinical impacts.

Keywords: amygdala subnuclei, hippocampal subfields, depression, childhood maltreatment, stress, magnetic resonance imaging (MRI).

A version of this Chapter has been submitted to the Journal of Human Brain Mapping.

Arash Aghamohammadi-Sereshki, Nicholas J. Coupland, Peter H. Silverstone, Yushan Huang, Kathleen M. Hegadoren, Rawle Carter, Peter Seres, Nikolai V. Malykhin: Effects of depression and childhood adversity on the volumes of the amygdala subnuclei and hippocampal subfields.

6.1. Introduction

Major Depressive Disorder (MDD) causes worldwide disability (World Health Organization 2016), but the aetiology of MDD remains uncertain although changes in the hippocampus and amygdala have been suggested as potentially important (Schmaal et al., 2016). Volumetric reductions in the hippocampus have been often reported in Magnetic Resonance Imaging (MRI) studies of MDD (Koolschijn et al., 2009; Lorenzetti et al., 2009; Malykhin and Coupland, 2015; Schmaal et al. 2016). While the amygdala is an important structure in neuronal circuits of emotion, fear and stress (Davis and Whalen, 2001, LeDoux, 2007; Sah et al., 2003), the results of volumetric MRI studies of the amygdala in MDD have been inconsistent (Campbell et al., 2004; Hajek et al., 2009; Hamilton et al., 2008; Schmaal et al., 2016). The amygdala consists of several functionally different subnuclei groups (Price et al., 1987; Sah et al., 2003): (1) the basolateral complex (BLA), including lateral (La), basal (B) and accessory basal (AB) nuclei; (2) the cortical group (Co); and (3) the centromedial group (CeM), including the central and medial nuclei. Generally, the BLA amygdala is involved in learning and memory through its connections with prefrontal cortex and hippocampus (Roozendaal et al., 2009). Animal studies indicate that during chronic stress, the BLA amygdala undergoes adaptive plastic changes (McEwen et al., 2015; Qiao et al., 2016). In contrast, CeM amygdala is involved in the regulation of the behavioural, autonomic and hormonal responses to emotional stimuli, via its connections with the hypothalamus (Roozendaal et al., 2009); whilst Co group is involved in the olfactory-related responses (Yilmazer-Hanke, 2012). Until recently, MRI studies of the amygdala have studied amygdala at the level of its total volume (Schmaal et al., 2016). However, recent advances in MRI (Duyn, 2012) have enabled researchers to measure amygdala subnuclei in vivo (Aghamohammadi-Sereshki, 2018).

Childhood adversity, including trauma and maltreatment, has been recognized as an important risk factor for developing MDD in adulthood (Hammen et al., 2000; Hovens et al., 2010; Lindert et al., 2014). It can induce biological changes in stress-related brain structures, which may then become maladaptive in adult environments and make individuals more vulnerable to psychiatric disorders (McCrory and Viding, 2015). Previous MRI studies have found that childhood adversity was associated with smaller volumes of the anterior cingulate, dorsolateral prefrontal and orbitofrontal cortices, and hippocampus (Danese and McEwen, 2012; Teicher and Samson, 2016). The effects of childhood adversity might not be uniform across the entire structure of the hippocampus (Szeszko et al., 2006; Teicher et al., 2012). The hippocampus can be subdivided into subregions (head, body and tail) along its antero-posterior axis and into cellular subfields, including dentate gyrus (DG), cornu ammonis (CA1-3) and subiculum, along its cross-sectional axis (Duvernoy, 2005; Insausti et al., 2017). Animal models of adult chronic stress indicate that the CA3 subfield is most susceptible to cellular changes associated with prolonged stressors and glucocorticoid exposure (Conrad et al., 2017; Sapolsky, 2000). Additional changes include dendritic retraction and suppressed adult neurogenesis in the DG subfield (Leuner and Gould, 2010; Pittenger and Duman, 2008).

Previous human studies suggested that the adverse effects of psychological stress and childhood adversity were more pronounced in the anterior hippocampus (Szeszko et al., 2006; Vythilingam et al., 2002) and CA2-3, CA4-DG subfields (Teicher et al., 2012). The results of individual studies of the relationships of total amygdala volume to childhood adversity have been inconsistent (Andersen et al., 2008; Calem et al., 2017; Cohen et al., 2006; De Bellis et al., 2002; Lupien et al., 2011; Mehta et al., 2009; Tottenham et al., 2010). However, two meta-analyses showed that maltreated individuals regardless of the absence or presence of psychiatric disorders had

significantly smaller total amygdala volume than non-maltreated individuals (Lim et al., 2014; Paquola et al., 2016).

While most of the work on the impact of stress on the amygdala and hippocampal substructures has been conducted in animals (Conrad et al., 2017; Qiao et al., 2016), recent advances in high resolution MRI (Aghamohammadi-Sereshki, 2018; Duyn, 2012) allowed researchers to test the impact of the stressful events on these structures in humans.

In this study we aimed to (1) investigate volumetric differences in amygdala subnuclei between MDD and healthy participants and (2) determine the relationships between childhood maltreatment, as measured using Childhood Trauma Questionnaire (CTQ) and amygdala subnuclei and hippocampal subfield volumes, using ultra-high resolution 4.7T MRI methods developed by our group (Aghamohammadi-Sereshki, 2018; Malykhin et al., 2010a).

Considering findings from two previous meta-analyses on the total amygdala volumes in MDD (Hajek et al., 2009; Schmaal et al., 2016), which did not show any effects of MDD, we made no prior hypothesis in this regard. However, based on the previous animal (Conrad et al., 2017; McEwen et al., 2015; Qiao et al., 2016; Sapolsky, 2000; Vyas et al., 2002) and human studies (Lim et al., 2014; Paquola et al., 2016; Teicher and Samson, 2013, 2016), we hypothesized that childhood adversity would be associated with volumetric reductions in the BLA amygdala and in the CA1-3 and DG subfields, especially within the anterior hippocampus in the MDD participants. Furthermore, considering previous studies (Lim et al., 2014; Mehta et al., 2009; Paquola et al., 2016) that showed that the effects of childhood maltreatment were more pronounced on the right amygdala, we hypothesized that the effects of childhood adversity on the BLA amygdala would be more pronounced in the right hemisphere.

6.2. Material and methods

Participants

A total of 35 MDD participants were included in the study. These consisted of 12 males and 23 premenopausal females aged 18-49 who met DSM-IV criteria for MDD with moderate or severe episodes, based upon full clinical assessment and the Anxiety Disorders Interview Schedule for DSM-IV-Lifetime Version (ADIS-IV-L) (Brown et al., 1994). There were 35 age-, sex- and education-matched healthy controls (12 males, 23 premenopausal females). Written informed consent was obtained and the study was approved by the University of Alberta Health Research Ethics Board.

Among MDD participants, 25 reported continuous use of antidepressant treatments for more than 6 months and 10 were either antidepressant-naïve (7 MDD participants), or medication free ≥ 6 months (3 MDD participants). MDD exclusion criteria were mild depressive episodes, psychotic or atypical features, seasonal affective disorder, lifetime schizophrenia, bipolar disorder, alcohol or substance dependence, anorexia nervosa, predominant personality or anxiety disorders, antipsychotic or mood stabilizer treatment, corticosteroid use, significant medical or neurological diseases. Healthy controls did not have any lifetime psychiatric disorders, as assessed by the ADIS-IV-L, or reported psychosis or mood disorders in first-degree relatives.

The severity of depressive symptoms was assessed using the 17-item Hamilton Depression Rating Scale (HAM-D). Childhood maltreatment was assessed using the 28-item CTQ, which includes five 5-item subscales; emotional abuse (EA), physical abuse (PA), sexual abuse (SA), emotional neglect (EN) and physical neglect (PN) and 3 validity items (Bernstein and Fink, 1998; Bernstein et al., 2003).

MRI Data Acquisition and Analysis

Images were acquired using a 4.7 T MRI system (Varian, Palo Alto, CA). A T_2-weighted fast spin echo (FSE) MRI sequence (an echo time of 39 ms, repetition time of 11000 ms; FOV: 20×20 cm; native resolution: 0.52×0.68×1.0 mm^3) was used to obtain ninety contiguous slices perpendicular to the anterior–posterior commissure line (AC-PC) in a total acquisition time of 13.5 min. The original FSE datasets were interpolated in-plane by a factor of 2 to yield a final resolution of 0.26×0.34×1.0 mm^3 and voxel volume of .09 μl. In order to estimate intracranial volumes (ICV), a whole-brain T_1-weighted 3D Magnetization Prepared Rapid Gradient Echo (MPRAGE) sequence (axial, echo time/repetition time = 8.5 ms/4.5 ms; FOV: 256×200×180 mm^3; voxel size: 1×1×1 mm^3) was acquired. The program DISPLAY (Montreal Neurological Institute, QC, Canada) was used to manually trace ICVs on the T_1-weighted MPRAGE images and amygdala and hippocampus on the T_2-weighted FSE images. Raw volumetric measurements of the amygdala and hippocampus were then normalized to ICV by using a proportional method: *normalized volume: (raw volume (mm^3)/ICV (cm^3)) × sample average ICV (cm^3)*.

We have previously published detailed protocols for the manual delineation of the total amygdala (Malykhin et al., 2007), amygdala subnuclei (Aghamohammadi-Sereshki et al., 2018), hippocampal subregions (Malykhin et al., 2007), and hippocampal subfields (CA1-3, DG, and Sub (Malykhin et al., 2010a) (Figure 6.1). Two raters performed amygdala (A.A.S) and hippocampal measurements (Y.H). ICV was measured using the method of Eritaia et al. (2000). The volumetric results on hippocampal subfield volumes from this MDD cohort were previously reported elsewhere (Huang et al., 2013; Travis et al., 2015). The inter/intra-rater reliabilities and Dice Kappa coefficients for the total amygdala and its subnuclei, as well as the total hippocampus and its subfields are reported in Table 6.1.

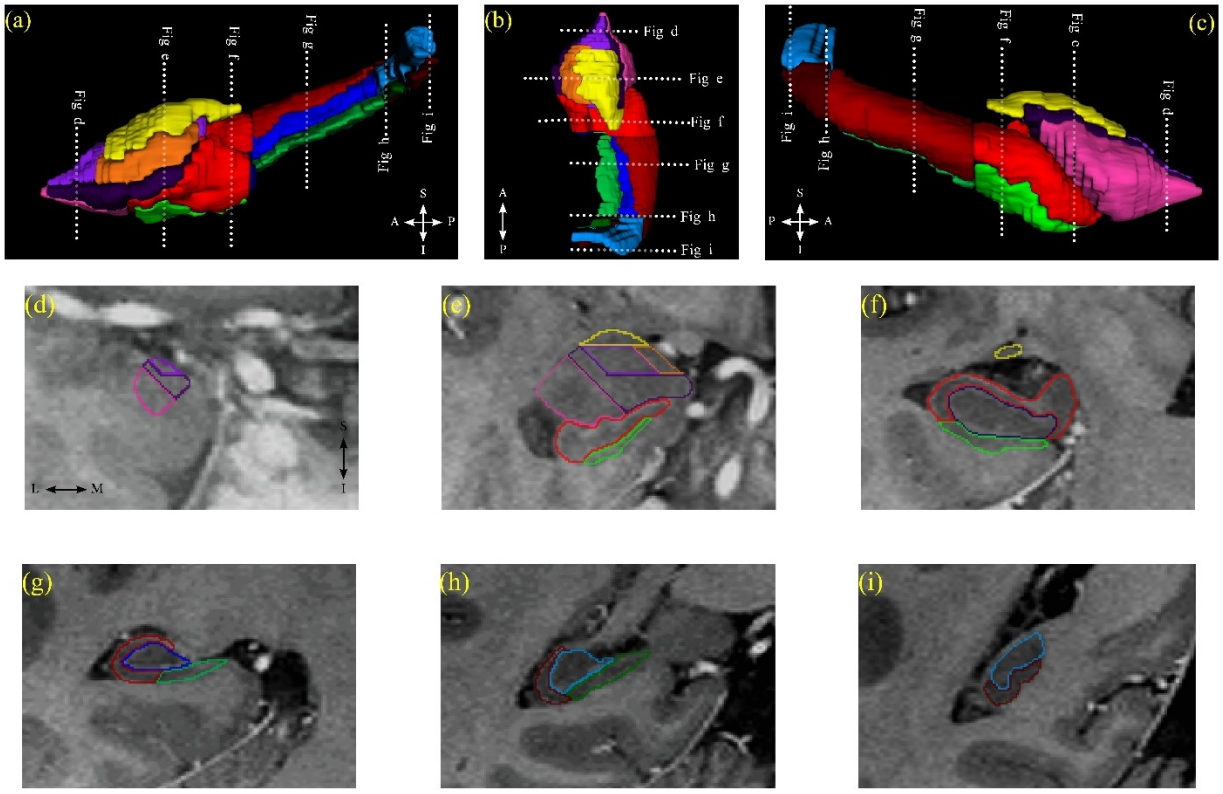

Figure 6.1. Three-dimensional reconstructions of the hippocampal subfields and subregions as well as the amygdala and its subnuclei from a healthy individual.

Key*:* 3-D images are shown from the medial (a), the superior (b), and the lateral (c) views were created using ITK-SNAP software (v. 3.8.0). Segmentation of the hippocampal subfields and subregions as well as the amygdala subnuclei on coronal (d-i) views is shown on T_2-weighted FSE images with inverted contrast. For the hippocampal subfields: the cornu ammonis (CA1-3) is outlined in red, dentate gyrus is outlined in blue, and subiculum is outlined in green. Hippocampal subfields along the antero-posterior axis of the hippocampus (head, body and tail) are shown with different colour intensity. For the amygdala subnuclei: lateral (La) nucleus is outlined in pink, basal (B) nucleus is outlined in dark purple, accessory basal (AB) nucleus is outlined in light purple, cortical (Co) group is outlined in orange and centromedial (CeM) group is outlined in yellow. Dotted lines indicate the locations of corresponding MRI slices.

Table 6.1. Reliability results.

ICCs and Dice's Kappa values				
	ICC		**Dice Kappa**	
	Intra-rater	**Inter-rater**	**Intra-rater**	**Inter-rater**
La	0.95	0.93	0.86	0.82
B	0.94	0.87	0.81	0.76
AB	0.96	0.95	0.77	0.71
Co	0.97	0.87	0.72	0.72
CeM	0.86	0.85	0.79	0.76
AG	0.93	0.95	0.93	0.91
HC head	0.92	0.95	0.90	0.89
HC body	0.93	0.83	0.87	0.86
HC tail	0.88	0.95	0.82	0.80
CA 1-3	0.92	0.92	0.75	0.73
DG	0.84	0.86	0.81	0.81
Sub	0.95	0.87	0.74	0.74
Total HC	0.97	0.95	0.90	0.89

Key: AB: Accessory Basal; AG: amygdala; B: basal; CA 1-3: Cornu Ammonis; CeM: centromedial; Co: cortical; DG: Dentate Gyrus; HC: hippocampus; La: lateral; Sub: subiculum.

Statistics

All analyses were carried out in IBM SPSS Statistics 25.0. One-way ANOVA was used to compare age, education, MDD characteristics and ICV in MDD and controls. We used analysis of covariance (ANCOVA) to compare amygdala volumes between MDD and healthy controls and between medicated and unmedicated MDD and control subjects. ANCOVAs included volume as

the dependent variable, diagnosis (or treatment) as a between-subject factor, hemisphere as a within- subject factor, the diagnosis (or treatment) hemisphere interaction and ICV as covariate. For the factor of diagnosis these were two-group analyses. For the factor of treatment, these were three-group analyses followed by pairwise ANCOVA of subgroups. Correlations between normalized volumetric measurements, CTQ scores, and clinical characteristics in MDD participants were tested using Pearson or Spearman correlations, as appropriate. Due to our priori hypotheses, for the amygdala, we examined effects of childhood adversity, first, on the total amygdala volume; and second, on the volumes of the BLA, Co and CeM groups. Similarly, for the hippocampus, we examined effects of childhood adversity, first, on the total hippocampal volume; and second, on the total subregion and subfield volumes. The Holm-Bonferroni correction for type I error inflation due to multiple hypothesis testing was used: for CeM, Co, and BLA groups (n=3), for the hippocampal subregions (n=3) and for the total subfield volumes (n=3). *P-values* survived Holm-Bonferroni correction were shown with a **bold asterisk** in the tables and the result section. The Levene's test was used to check the homogeneity of variance; and a significant level was *p-value* < 0.05 two-tailed test for all analyses, except for the associations between childhood adversity and the amygdala- and hippocampal-related volumes which was *p-value* < 0.05 one-tailed (e.g. negative correlations were hypothesized).

6.3. Results

Demographic and clinical characteristics

There were no significant differences in age, sex, education and ICV between MDD participants and healthy controls, or in demographic and clinical characteristics between unmedicated and medicated MDD participants (Table 6.2). ANOVA did not show significant effect of sex (all *ps* >

0.1) (Table 6.3) on CTQ measurements indicating that male and female MDD participants did not differ from each other.

Table 6.2. Demographic and clinical characteristics.

General demographic characteristics						
Demographic Characteristics	**Healthy controls (N=35)**	**MDD**			***P-values***	
		Total (N=35)	**Medicated (N=25)**	**Unmedicated (N=10)**	**Controls vs MDD**	**Three groups** †
Sex (Female/Male)	23/12	23/12	17/8	6/4	1.0	0.91
Age	32.3 ± 10.0	34.9 ± 8.7	36.1 ± 7.7	31.9 ± 10.8	0.25	0.25
Education (years)	15.7 ± 1.7	15.4 ± 1.8	15.7 ± 1.5	14.6 ± 2.2	0.55	0.19
ICV in cm^3	1599 ± 172	1561 ± 154	1537 ± 156	1622 ± 141	0.33	0.24

MDD clinical characteristics				
	Medicated (N=25)	**Unmedicated (N=10)**	***F***	***P-values***
HAM-D	17.0 ± 8.4	20.0 ± 2.6	3.04	0.09††
MDD duration (years)	4.6 ± 3.7	4.5 ± 4.7	0.004	0.95
Recurrent/non-recurrent	20/5	7/3	NA	0.66†††
Number of MDEs	2.5 ± 1.1	2.3 ± 1.1	0.30	0.59

Key: Values are mean ± standard deviation. MDD: major depressive disorder; MDE: major depressive episode; ICV: intracranial volume; † Three groups comparison between healthy controls, Medicated and Unmedicated MDD; ††Due to the violation of the homogeneity of variance, *P-value* is adjusted for Welch F test. †††Chi-square *P-value* is adjusted for the Fisher's exact test due to Pearson Chi-square assumption violation.

Table 6.3. Childhood Trauma Questionnaire (CTQ) scores.

CTQ factors *	MDD-patients			*P-values* †
	Total (n = 33)	**Male (n = 12)**	**Female (n = 21)**	
Total	50.1 ± 19.0	44.7 ± 17.8	53.2 ± 19.4	0.18
EA	11.7 ± 5.4	9.7 ± 5.8	12.9 ± 5.0	0.08
PA	8.3 ± 4.1	7.4 ± 3.3	8.8 ± 4.5	0.35
SA	8.4 ± 6.2	7.8 ± 5.8	8.8 ± 6.5	0.65
EN	13.5 ± 5.4	12.9 ± 4.9	13.8 ± 5.8	0.66
PN	8.2 ± 3.8	6.9 ± 3.3	9.0 ± 3.9	0.06

Key**:** CTQ: Childhood Trauma Questionnaire; EA: emotional abuse; PA: physical abuse; SA: sexual abuse; EN: emotional neglect; PN: physical neglect. † Since the total CTQ scores and all CTQ factors except for the EN were not normally distributed, males and females were compared using Mann-Whitney test.

Amygdala volumetric analyses

Diagnosis (MDD vs. control subjects) hemisphere, or treatment (unmedicated MDD vs. medicated MDD vs. control subjects) hemisphere interactions were not significant for any amygdala measurement (all *ps* > 0.23), indicating that any group differences were not lateralized. There were no main effects of diagnosis in the two-group analyses for total amygdala volume and the total volume of each subnuclei group (Table 6.4). Exploratory analysis or the BLA subnuclei also did not reveal significant effect of diagnosis or treatment (all *ps* > 0.16) on the total volume of each subnuclei. Correlational analyses did not reveal any significant relationships between the volumes of the amygdala or its subnuclei with HAM-D score, MDD duration, or number of major depressive episodes (all *ps* > 0.16).

Table 6.4. Analysis of covariance (ANCOVA) and descriptive statistics for the amygdala measurements.

ROIs	Healthy controls vs. MDD				Healthy controls vs. Unmedicated MDD vs. Medicated MDD											
	Healthy controls (N = 35)	MDD (N = 35)	$F_{2, 66}$	P † †	U-MDD (N =10)	M-MDD (N = 25)	$F_{2, 66}$	P † †	U-MDD vs. Healthy controls		M-MDD vs. Healthy controls		U-MDD vs. M-MDD	
									$F_{1, 42}$	P	$F_{1, 57}$	P	$F_{1, 32}$	P
Total AG	1994 ± 330	1880 ± 307	1.35	.24	1933 ± 285	1858 ± 319	0.67	.51	0.88	.35	1.10	.29	0.02	.90
CeM	287 ± 59	278 ± 71	0.06	.81	306 ± 101	267 ± 54	0.77	.46	0.45	.50	1.04	.31	0.81	.37
Co	157 ± 29	144 ± 33	1.03	.31	149 ± 38	142 ± 32	0.51	.60	0.69	.41	1.00	.32	0.02	.90
BLA	1552 ± 282	1457 ± 238	1.45	.23	1477 ± 205	1448 ± 253	0.78	.46	1.41	.24	0.83	.36	0.01	.94
La	642 ± 120	598 ± 94	2.02	.16	596 ± 90	599 ± 98	1.17	.31	2.22	.14	0.91	.34	0.01	.91
B	618 ± 122	581 ± 105	1.08	.30	597 ± 100	574 ± 108	0.54	.58	0.64	.42	0.84	.36	0.00	.95
AB	291 ± 57	277 ± 59	0.38	.53	283 ± 53	274 ± 62	0.23	.79	0.54	.46	0.24	.63	0.05	.83

Key: ANCOVA of volumes (mm^3) of the total amygdala (AG), basolateral (BLA), cortical (Co) and the centromedial (CeM) groups of the AG as well as the lateral (La), basal (B) and accessory basal (AB) nuclei of the BLA (covariate, intracranial volumes). Group (Diagnosis or Treatment) × hemisphere interactions

were not significant; volumes are mean ± SD of both hemispheres. † Diagnosis main effect in two-group comparison: Healthy controls and MDD. †† Treatment main effect in three-group comparison: Healthy controls, U-MDD and M-MDD.

Childhood adversity and amygdala volumes in MDD

The average total amygdala volume showed a trend towards significant negative relationship with the total CTQ-25 score ($p < 0.089$). Analyses within the left and right hemispheres showed that the aforementioned relationship was mainly driven by the right amygdala (r_s: -0.324, $p < 0.033$) and not the left amygdala ($p > 0.35$). The total CTQ-25 did not correlate with the average volumes of BLA, CeM and Co groups (all ps > 0.09), but analyses within the left and right hemispheres showed that the total CTQ-25 had a negative relationship with the right BLA (r_s: -0.311, $p < 0.040$) and not the left BLA ($p > 0.29$).

Exploratory analyses within BLA group showed that average volumes of the AB (r_s: -0.351, $p < 0.023$) and B (r_s: -0.297, $p < 0.047$) nuclei showed negative correlations with the total CTQ-25 score. Analyses within the left and right hemispheres showed that the total CTQ-25 had negative correlations with the right AB (r_s: -0.361, $p < 0.020$) and B (r_s: -0.288, $p < 0.052$) and not with the left nuclei (both ps > 0.11).

Exploratory analyses of the CTQ factors showed that only EA had negative correlations with the average volumes of the total amygdala (r_s: -0.278, $p < 0.059$), AB (r_s: -0.429, $p < 0.007$), B (r_s: -0.389, $p < 0.013$) and Co (r_s: -0.312, $p < 0.04$) nuclei. Analyses within the left and right hemispheres showed that the aforementioned correlations were mainly driven by the right amygdala ROIs (Table 6.5). However, none of the above-mentioned correlations remained significant after Holm-Bonferroni correction.

Childhood adversity and hippocampal volumes

Correlations between all CTQ-related scores and hippocampal measurements were present in both hemispheres. Therefore, we used average volumes for further analyses.

The total hippocampal volume showed a trend towards significant negative relationship with total CTQ-25 score (r_s: -0.286, $p < 0.054$). Amongst hippocampal subregions, only the head (r_s: -0.404, $p <$ **0.010***), but not the body or tail (both *p*s > 0.36) significantly correlated with total CTQ-25 score. Amongst hippocampal subfields, the total CA1-3 (r_s: -0.505, $p <$ **0.0014***), but not the total DG or subiculum (both *p*s > 0.27) showed a significant negative correlation with total CTQ-25 score.

Exploratory analyses amongst hippocampal subfields within the hippocampal head showed that only CA1-3 (r_s: -0.512, $p <$ **0.0012***), but not the total DG or subiculum (both *p*s > 0.17) showed a significant negative correlation with total CTQ-25 score (Table 6.5).

Exploratory analyses for the CTQ factors showed that EA, PA, EN and PN showed strong negative relationships with volumes of hippocampal head and CA1-3 in the hippocampal head. Weaker negative associations were found for the DG of the hippocampal head and body with PA and SA, but they did not survive the Holm-Bonferroni correction (Table 6.5).

Table 6.5. Summary of all p-values for relationships between CTQ factors scores and volumetric measurements in MDD participants.

CTQ factors (n = 33)	Amygdala		Hippocampus			Subfields within hippocampal subregions		
	Right	Left	Total	Subregions	Subfields	Head	Body	Tail
Emotional Abuse[1]	AG (r_s: -0.359, $p < 0.021$), BLA (r_s: -0.343, $p < 0.026$), AB (r_s: -0.448, $p < 0.0045$), B (r_s: -0.375, $p < 0.016$), Co (r_s: -0.383, $p < 0.015$).	B (r_s: -0.293, $p < 0.049$). The rest of the correlations were not significant.	r_s: -0.250, $p < 0.080$	Head (r_s: -0.305, $p < 0.043$)	CA1-3 (r_s: -0.418, $p < 0.008$)	CA1-3 (r_s: -0.459, $p < 0.004$)	NS	NS
Physical abuse[1]	NS	NS	r_s: -0.312, $p < 0.039$	Head (r_s: -0.428, $p < 0.007$)	CA1-3 (r_s: -0.430, $p < 0.007$)	CA1-3 (r_s: -0.417, $p < 0.008$) DG (r_s: -0.327, $p < 0.032$)	NS	NS
Sexual abuse[1]	NS	NS	r_s: -0.262, $p < 0.071$	Head (r_s: -0.256, $p < 0.076$)	CA1-3 (r_s: -0.232, $p < 0.098$)	DG (r_s: -0.254, $p < 0.077$)	DG (r_s: -0.299, $p < 0.046$)	NS
Emotional neglect[2]	NS	NS	r: -0.357, $p < 0.021$	Head (r: -0.394, $p < 0.012$)	CA1-3 (r: -0.467, ***p* < 0.0031***)	CA1-3 (r: -0.471, $p <$ 0.003)	CA1-3 (r: -0.250, $p < 0.081$)	NS
Physical neglect[1]	NS	NS	NS	Head (r_s: -0.390, $p < 0.013$)	CA1-3 (r_s: -0.496, ***p* < 0.002***)	CA1-3 (r_s: -0.534, ***p* < 0.0007***)	NS	NS

Key: AB: accessory basal; AG: total amygdala; B: basal; BLA: basolateral group; CA1-3: cornu ammonis, CeM: centromedial group; Co: cortical group; DG: dentate gyrus; La: lateral. NS: not significant, [1]

Spearman's correlation, [2] Pearson's correlation. *P-values* shown in **bold*** remained significant after Holm Bonferroni correction.

6.1. Discussion

This is the first structural *in vivo* MRI study that examined amygdala subnuclei in MDD and the effects of childhood adversity on both amygdala subnuclei and hippocampal subfield volumes. Although, we did not find any significant effect of MDD or long-term antidepressant treatment on amygdala subnuclei, we found that the childhood adversity was negatively associated with both hippocampal and amygdala volumes. The negative effects of childhood adversity measured by total CTQ-25 score were observed bilaterally within the anterior hippocampus (i.e. hippocampal head) and were limited to CA1-3 subfield, while in the amygdala these effects were limited to BLA amygdala within the right hemisphere.

Amygdala volume in MDD

Although previous meta-analyses did not find significant differences in the amygdala volume between MDD participants and controls (Campbell et al., 2004; Hajek et al., 2009; Hamilton et al., 2008; Koolschijn et al., 2009; Schmaal et al., 2016), individual studies reported increased (Frodl et al., 2002; Malykhin et al., 2012), decreased (Kronenberg et al., 2009), or no effect of MDD on the total amygdala volume (Frodl et al., 2008; Koolschijn et al., 2009; Zavorotnyy et al., 2018). Some of the confounding variables which might contribute to conflicting results include the age and sex of participants, age of onset of MDD, illness duration, medication status, and anatomical definition of the amygdala (Hajek et al., 2009; Hamilton et al., 2008; Koolschijn et al., 2009; Lorenzetti et al., 2009; Schmaal et al., 2016). In our previous study (Malykhin et al., 2012) we found larger amygdala in MDD participants. Although in the present study we employed

identical anatomical definition of the amygdala, differences in participant characteristics, field strength of MRI scanners between our studies (4.7T vs 1.5T), and higher resolution might have contributed to the discrepancies. Our results are in agreement with some previous studies (Hajek et al., 2009; Schmaal et al., 2016) that demonstrated similar amygdala volumes between MDD participants and healthy individuals.

Several previous postmortem studies investigated amygdala changes in MDD. Bowley et al. (2002) showed no significant volumetric and neuronal density difference in the amygdala between MDD participants and controls. However, MDD participants showed a significant reduction in the glial density and glial/neuron ratio in the left amygdala compared to controls (Bowley et al., 2002). Bielau et al. (2005) reported a trend towards amygdala volume reduction in MDD individuals, while Rubinow et al. (2016) reported a modest (11%) volumetric increase in the La nucleus with an increase in the number of neurovascular cells in the BLA group in MDD individuals without significant differences in the total number and densities of neurons and glia of the BLA group. The average age of MDD individuals in these postmortem studies was 10 to 40 years older compared to our study. This is an important issue since possible different neuronal and glial cell pathology has been suggested for young and old MDD participants (Khundakar et al., 2014).

Previous meta-analysis by Hamilton et al. (2008) reported larger amygdala volume in medicated MDD patients while reductions in the amygdala volumes were observed in unmedicated MDD patients. However, other meta-analyses (Hajek et al., 2009; Schmaal et al., 2016) and postmortem study (Rubinow et al., 2016) did not find either association between the medication status and the amygdala volume or effects of antidepressant treatment on BLA group, respectively. These findings agree with our current findings and also with our previous study (Malykhin et al., 2012).

Like previous studies (Frodl et al., 2003, 2008; Kronenberg et al., 2009; Saleh et al., 2012; Schmaal et al., 2016), we did not find any correlations between the amygdala and MDD duration/severity. However, Lorenzetti and colleagues (2009) indicated that the amygdala volume is increased during the early phase of MDD and then endures volumetric reduction during its late phase.

Effects of adverse childhood/adolescence experiences on amygdala and hippocampus

Both amygdala and hippocampus are regarded as targets of childhood adversity (Lupien et al., 2009; Teicher et al., 2003; Teicher and Samson, 2013, 2016) since they exhibit a protracted postnatal development, a high density of glucocorticoid receptors, and postnatal neurogenesis (Kempermann et al., 2018; Lupien et al., 2009, 2018; Patel et al., 2000; Teicher et al., 2003). The present study confirmed the negative effects of childhood adversity on both structures, and further emphasized the fact that these effects were limited to CA1-3 hippocampal subfield and BLA amygdala, structures shown to be affected by chronic stress in preclinical studies.

Amygdala functional MRI studies have consistently showed hyperactivity of the amygdala in response to threatening stimuli in maltreated individuals (Hein and Monk, 2017; McCrory et al., 2017; Teicher and Samson, 2016). In contrast, findings of structural studies of the amygdala in maltreated individuals are heterogenous. Some studies did not observe any significant effects of maltreatment on the amygdala volume either in healthy individuals (Calem et al., 2017; Cohen et al., 2006), or in psychiatric patients (Andersen et al., 2008; De Bellis et al., 2002). Others have reported either volumetric reduction (Lim et al., 2014; Paquola et al., 2016), or volumetric increase (Lupien et al., 2011; Mehta et al., 2009; Tottenham et al., 2010), although the timing and type of exposure to the early adverse environment may accounted for these heterogenous results (Teicher and Samson, 2016). The authors noted that volumetric enlargement was reported by studies that

investigated the effects of early maltreatment (mainly emotional and/or physical neglect) on the amygdala, while amygdala volumetric decrease was reported by studies with older adolescent or adults with more psychopathological symptoms exposed to different types of maltreatment across development (Teicher and Samson, 2016). Consequently, they hypothesized that early adverse environment might increase the amygdala volume during childhood, but further exposure to stressful environment during adulthood could cause volumetric reduction in the amygdala due to the biological embedding induced by early adverse environment exposure (Teicher and Samson, 2016).

Our finding on the negative relationship between the amygdala volume and childhood adversity is in line with our previous study (Malykhin et al., 2012), which showed that the amygdala volume in MDD participants with history of childhood sexual/physical abuse was smaller than in MDD participants without such history. Moreover, the current study provided first evidence on the underlying neuroanatomical sources of these changes within the amygdala structure and emphasized that history of EA was particularly detrimental. Our results demonstrated that the AB and B and Co nuclei are the main targets of the EA. Previous studies showed that childhood adversity induced abnormal changes in fronto-limbic regions (Hart and Rubia, 2012; Lim et al., 2014; Paquola et al., 2016). The majority of the amygdala reciprocal connections with other fronto-limbic regions including the CA1-3 hippocampal subfield, caudate, nucleus accumbens, orbitofrontal, medial prefrontal and anterior cingulate cortices run mainly through the AB and B nuclei and only to a lesser degree through the Co group (Freese and Amaral, 2009; Roozendaal et al., 2009; Yilmazer-Hanke, 2012). Finally, although the La nucleus has some common connectivity profile with B and AB nuclei, our findings did not show any significant effect of childhood adversity on this structure.

The negative associations between EA (and total abuse history) and the amygdala volumes were mainly observed in the right amygdala. Although, in agreement with our previous studies (Aghamohammadi-Sereshki et al., 2018, 2019) we did not find any hemispheric effects on the total amygdala and its subnuclei volumes in either group, while other studies have reported hemispheric asymmetries for emotional processing in the amygdala (Gainotti, 2018; McMenamin and Marsolek, 2013). It has been suggested that the right amygdala is involved in the rapid detection of threatening-related or early processing of affective stimuli via right hemisphere subcortical circuits, while the left amygdala is preferentially activated during decoding of cognitive-related emotional stimuli via left hemisphere's slower cortical feedback mechanisms (Gainotti, 2018). Moreover, in response to sad stimuli, activation of the right amygdala had positive correlations with CTQ factors, especially with PA (Grant et al., 2011). Furthermore, larger amygdala volume in adopted adolescents with severe early institutional deprivation was more pronounced on the right hemisphere than the left hemisphere compared to the non-institutionalized counterpart (Mehta et al., 2009). Recent meta-analysis demonstrated that the individuals with childhood maltreatment had smaller amygdala in both hemispheres, but the effect sizes for the right amygdala were larger in men (Paquola et al., 2016). Finally, our findings are consistent with the meta-analysis that showed that individuals with childhood maltreatment had significantly smaller right amygdala volume than individuals unexposed to childhood maltreatment (Lim et al., 2014). Therefore, we speculate that the observed negative relationships between the right amygdala volumes and specifically volumes of B and AB nuclei with the history of abuse that is considered as a threat (Humphreys and Zeanah, 2015; McLaughlin et al., 2014; Teicher and Samson, 2013) might be due to the critical role of the right amygdala in processing threat-related stimuli (Gainotti,

2018). Threatening stimuli sensitizes the right amygdala to stressful situations later in life consequently causing its volumetric reduction (Paquola et al., 2016; Teicher and Samson, 2016).

Animal models of chronic stress (Vyas et al., 2002, 2003, 2004) reported that while chronic immobilization stress induced dendritic hypertrophy in the BLA group, it did not change dendrites of the central amygdala. Chronic restraint stress showed both reduction (Bennur et al., 2007) and no significant change (Marcuzzo et al., 2007) in dendritic spine density in medial amygdala. While our findings of a negative correlation between the BLA group and CTQ scores differ from animal studies, most of these studies (Qiao et al., 2016) used rodents whose age are relevant to human adults (Dutta and Sengupta, 2016; Sengupta, 2013), but not to childhood. Therefore, future animal studies for comparison could investigate the effects of chronic stress in adult animals exposed to chronic stress during their weaning and adolescent periods. Although we did not segment central and medial nuclei separately, due to the larger volume of the central compared to the medial (García-Amado and Prensa, 2012), we believe that if the central nucleus had any associations with CTQ, the CeM group would also show such effect.

Hippocampus and adverse childhood/adolescence experiences

Our findings indicated that amongst all hippocampal subfields and subregions, the CA1-3 and the anterior hippocampus showed the strongest negative associations with childhood adversity. In contrast to our amygdala findings that were limited to history of emotional abuse, our findings on the effects of childhood adversity in relationship to hippocampus includes histories of both emotional and physical abuse and neglect.

It has been suggested that hippocampus might be the most vulnerable brain region to stress (Teicher and Samson, 2013). Previous studies have reported hippocampal volumetric reduction in

maltreated healthy individuals (Calem et al., 2017), MDD participants (Otte et al., 2016), and maltreated individuals regardless of the absence or presence of psychiatric disorders (Chaney et al., 2014; Opel et al., 2014; Paquola et al., 2016; Teicher and Samson, 2013, 2016; Vythilingam et al., 2002). Therefore, the hippocampal volume can be affected by childhood adversity, MDD itself, or both.

The results of our current study agree with previous studies in MDD participants (Vythilingam et al., 2002) and healthy controls (Szeszko et al., 2006) that suggested that childhood adversity affects anterior hippocampus (Malykhin et al., 2010b; Szeszko et al., 2006; Vythilingam et al., 2002). In addition, our previous study showed that cortisol levels negatively correlated with anterior hippocampus and CA1-3 volumes in both MDD and healthy participants (Travis et al., 2016).

Our results agree with previous findings on the negative relationships between childhood maltreatment and the CA2-3 subfield volumes (Teicher et al., 2012). Although we did not find statistically significant associations between DG and total CTQ-25 score, we think that these differences could be partially explained by different samples characteristics and the effects of antidepressant treatment on the DG in our current MDD cohort (Huang et al., 2013).

Animal models of chronic stress (Conrad et al., 2017) demonstrated that whilst chronic stress induced dendritic atrophy in both dorsal and ventral hippocampus, the CA3 was the most vulnerable hippocampal subfield. These agrees with our results. Dendritic retraction in CA1 and DG in animals occurred in response to more severe chronic stress (Conrad et al., 2017). Previously we demonstrated that the largest portion of the CA1-3 subfield is in the anterior hippocampus (Malykhin et al., 2010a, 2017) probably making this subregion a main target of chronic stress. In contrast, the largest portion of the DG is in the posterior hippocampus (i.e. body) that is particularly

affected by MDD (Huang et al., 2013) suggesting that impacts of MDD diagnosis and stress history may be distinct.

In contrast to the amygdala, our findings on hippocampal changes related to childhood adversity are in accordance with preclinical studies. The explanation might arise from the different vulnerability windows in postnatal development of these structures. While the hippocampus achieves dramatic growth in the first two years of life, the amygdala still develops until young adulthood (20s) (Lupien et al., 2009, 2018). Therefore, the childhood adversity exposure most likely does not correspond to hippocampal vulnerability postnatal window but could occur simultaneously with amygdala development.

In conclusion, this study provides the first *in vivo* evidence that childhood adversity has negative impacts on specific brain subregions, namely the BLA amygdala and CA1-3 hippocampal subfield.

Limitations

Our study sample was cross-sectional. Studies that incorporate a treatment-naïve group of MDD patients with/without history of childhood adversity are needed in order to separate the effects of MDD, history of abuse, and antidepressant treatment on hippocampal subfields and amygdala subnuclei. Future MRI studies would also need to combine cortisol measurements with childhood adversity assessment in both MDD patients and healthy subjects in order to evaluate if volumetric changes related to abuse history could be linked to cortisol overexposure.

Acknowledgements

The authors are thankful to all individuals who participated in this research.

Chapter 7: Healthy cognitive aging and limbic white matter tracts

Abstract

Cingulum and uncinate fasciculus are major limbic tracts involved in emotion, memory and cognition.

The goals of this diffusion tensor imaging (DTI) study were first, to investigate the relationship between age and the DTI-measurements of the uncinate fasciculus and the cingulum divided into the rostral, dorsal and parahippocampal cingulum in a large cohort of healthy individuals; and second, to determine effects of the catechol-O-methyl transferase gene (COMT) polymorphisms on the DTI-measurements of the uncinate fasciculus and cingulum.

One hundred and forty healthy participants (18–85 years old) were recruited and scanned on a 1.5 T system. Cingulum and the uncinate fasciculus were delineated using deterministic tractography to measure fractional anisotropy (FA), mean (MD), radial (RD) and axial (AD) diffusivities, tract volumes, linear (C_l), planar (C_p), and spherical (C_s) tensor shapes. The COMT (methionine homozygous and valine carriers) was obtained using single nucleotide polymorphisms.

We found that age was negatively associated with FA and C_l, but positively associated with MD, RD and C_s for the rostral cingulum, dorsal cingulum and uncinate fasciculus but not for the parahippocampal cingulum. Furthermore, individuals with the COMT methionine homozygous had higher FA and lower MD and RD values in the right rostral cingulum compared to the valine carriers across the entire life span.

Keywords: aging, cingulum, uncinate fasciculus, catechol-O-methyl transferase (COMT), Diffusion tensor imaging (DTI).

This Chapter is a manuscript prepared for submission.

Arash Aghamohammadi-Sereshki, Fraser Olsen, Richard Camicioli, Nikolai V. Malykhin: Healthy cognitive aging and limbic white matter tracts.

7.1. Introduction

The universal percentage of people at 65 years and older will be 16.7 % by 2050 (He et al., 2016). Therefore, it is imperative to broaden our understanding of healthy aging of the brain in order to have a better understanding of pathological age-related changes (Allen et al., 2005). Studies of age-related changes in brain white matter allow us to investigate the plausible underlying mechanisms of cognitive decline with aging, the differences between the aging trajectories of the white and grey matter; and compare it to pathological changes associated with different neuropsychiatric and neurological disorders (Yap et al., 2013). Overall, previous aging studies of white matter demonstrated a decrease in fractional anisotropy (FA) with an increase in mean (MD), radial (RD) and axial (AD) diffusivities from mid-adulthood to old age (Yap et al., 2013).

The limbic system is a group of cortical and subcortical structures interconnected by white matter tracts involved in memory, spatial orientation, emotion and motivation as well as goal-directed behaviours (Catani et al., 2013; Morgane et al., 2005; Rolls 2015). The cingulum and uncinate fasciculus are two major white matter tracts of the limbic system (Catani et al., 2013). The cingulum located all around the corpus callosum consisting of short and long association fibers as well as striatal, commissural, and subcortical fibers associated with emotional, attentional and memory-related mechanisms (Catani and Thiebaut de Schotten 2008; Schmahmann and Pandya 2006). All cingulate gyrus afferents and efferents move through the cingulum. Based on the connectivity profile, structural and functional properties, the cingulate cortex is divided into four subregions including the anterior cingulate, midcingulate, posterior cingulate and retrosplenial cortices (Vogt and Palomero-Gallagher 2012). Therefore, cingulum is also considered as a heterogenous tract since it carries white matter tracts from structurally and functionally distinct cingulate cortex subregions. However, most of the studies of healthy aging have analyzed the

cingulum either as a single structure that corresponds to (1) the dorsal cingulum (Lebel et al., 2012), (2) rostral + dorsal cingulum (Sala et al., 2012; Stadlbauer et al., 2008), (3) a whole cingulum bundle consisting of rostral + dorsal + parahippocampal cingulum (Voineskos et al., 2012) or as two separate structures that correspond to the rostral + dorsal cingulum and parahippocampal cingulum (Bennett et al., 2015; Cox et al., 2016; Westlye et al., 2010).

The second tract; uncinate fasciculus arises from the temporal pole, uncus, parahippocampal gyrus, and the amygdala (Catani et al., 2013). It connects the anterior portion of the temporal lobe to the inferior frontal gyrus and the orbital surface of the frontal lobe (Nieuwenhuys et al., 2008). It has been suggested that uncinate fasciculus might be involved in emotion, memory and language functions (Catani and Thiebaut de Schotten 2008).

Previous diffusion tensor imaging (DTI) studies of healthy aging generally reported that FA and MD of the uncinate fasciculus and cingulum follow curvilinear trajectory with age (Lebel et al., 2012; Westlye et al., 2010). For both uncinate fasciculus and cingulum, while FA and MD reach their maximum and minimum values respectively around 30s and 40s, FA decreases and MD increases during late adulthood (almost after 60 years of age) (Lebel et al., 2012; Westlye et al., 2010). However, other studies did not report any associations between age with either cingulum FA (Michielse et al., 2010; Stadlbauer et al., 2008) or MD (Stadlbauer et al., 2008).

Genetic studies of brain white matter tracts in healthy aging may help us to link white matter related changes in normal and pathological aging (Kanchibhotla et al., 2013). Budisavljevic et al. (2016) illustrated the genetic and familial factors had high effects on the FA and MD of the uncinate fasciculus and dorsal cingulum while these effects on the FA and MD of ventral cingulum (i.e. parahippocampal cingulum) were moderate. The catechol-O-methyl transferase gene (COMT) is involved in dopamine neurotransmission and degradation (Deary et al., 2004; Mier et al., 2009;

Petrella et al., 2008). Previously, dopamine protective effects on oligodendrocytes (Rosin et al., 2005) and its involvement in oligodendrocytes differentiation (Bongarzone et al., 1998) were suggested. The Val158Met polymorphism (rs4680) is a common COMT polymorphism in which the amino acid Valine (Val) is substituted with Methionine (Met) (Goldman et al., 2005). The Val allele has higher degrading activity than the Met allele which results in lower synaptic dopamine level. Since the presynaptic dopamine transporter in the prefrontal cortex is low, the COMT is major regulator of the dopamine level in the prefrontal cortex (Sambataro et al., 2012). It was showed that there is a dose-dependent fashion in COMT enzymatic activity so that Val/Val > Val/Met > Met/Met (Chen et al., 2004). Previous studies of Val158Met polymorphism focused on gray matter structures, found effects on volumes of the hippocampus, temporal and frontal lobes, as well as anterior cingulate and dorsolateral prefrontal cortices, thickness of the right inferior prefrontal and the right superior temporal sulci (for review see Sambataro et al., 2012; Witte and Flöel 2012).

Considering the aforementioned, the primary goal of the present study was to investigate if different anatomical subdivisions of cingulum bundle and the uncinate fasciculus follow similar relationship with age in a large sample of healthy individuals across the entire adult lifespan using DTI deterministic tractography method (Malykhin et al., 2008). We hypothesized that the parahippocampal cingulum would show relative preservation with age, compared to the rostral cingulum, dorsal cingulum and uncinate fasciculus. Our second goal was to determine whether COMT polymorphism is associated with the microstructural properties of the cingulum bundle and the uncinate fasciculus. Due to a limited knowledge about the effects of the COMT polymorphisms on brain white matter tracts, we made no prior hypothesis regarding this investigation.

7.2. Material and methods

Participants

140 healthy volunteers (62 men, 78 women), between 18 and 85 years of age (mean: 48.27, SD: 18.47) were recruited through online, poster and local advertisements. Of those, 106 participants were Caucasian (75.7%), 26 Asian (18.6%), 7 Latin American (5%) and 1 African (0.7%). An initial phone interview was conducted to screen candidates for existing neuropsychiatric disorders, as well as MRI contraindications. Participants were excluded if they or their first-degree relatives had any history of psychiatric disorders, as assessed by the Anxiety Disorders Interview Schedule—IV (Brown et al., 2001). The exclusion criteria were active and inactive medical conditions that may interfere with normal cognitive function (cerebrovascular pathology, tumors or congenital malformations of the nervous system, diabetes, multiple sclerosis, neurodegenerative diseases, epilepsy, dementia, and stroke) and use of psychotropics medications and non-prescribed substances that could affect brain function. Most of the individuals were right-handed (R: 124; L: 16). Handedness was assessed using a 20-item Edinburgh Handedness Inventory and individuals with laterality quotient ≥ +80 were determined as right-handed (Oldfield, 1971).

A face-to-face interview was conducted in order to verify that our older volunteers retained healthy cognitive function. Older subjects (>50 years of age) with Mild Cognitive Impairment and dementia were excluded from the study. For exclusion, dementia was defined according to the DSM-IV criteria. Mild Cognitive Impairment was defined based on presence of cognitive complaints (documented on the AD-8, Galvin et al., 2007) with documented impairment on the Montreal Cognitive Assessment Test (MOCA) (all included subjects had MOCA score ≥ 26) (Nasreddine et al., 2005). Furthermore, older participants (>50 years of age) were assessed for vascular dementia with the Hachinski Ischemic Scale (HIS) (Hachinski et al., 1975). A score above

7 out of 18 has 89% sensitivity (Moroney et al., 1997). All elderly participants included in this study received a HIS score of 3 or lower.

The Clinical Dementia Rating scale (CDR) was used as an assessment of dementia symptom severity (Hughes et al., 1982), where subjects are assessed for functional performance in six areas: memory, orientation, judgment and problem solving, community affairs, home and hobbies, and personal care. We employed CDR as an additional screening measure for dementia in older participants. A composite score from 0 to 3 was calculated. All of our subjects met the cutoff score of < 0.5 for total CDR score. In order to screen older participants for depression, the Geriatric Depression Scale (GDS) was used (Yesavage et al., 1982). Designed to rate depression in the elderly, a score of > 5 is suggestive of depression and a score > 10 is indicative of depression. Our subjects met the cutoff score of 4 and below.

Written, informed consent was obtained from each participant. The study was approved by the University of Alberta Health Research Ethics Board.

MRI acquisition and data analysis

Participants were scanned on a 1.5T Siemens Sonata MRI. A cradle and bilateral head supports were used to minimize subject motion in the MRI scanner. A whole brain T_1-weighted 3D MPRAGE sequence [TR: 2080 ms; TE: 4.38 ms; inversion time: 1100 ms; flip angle: 15°; bandwidth: 130 Hz/Px; FOV: 256×192×144 mm^3; voxel size: 1×1×1 mm^3; scan time: 5min 49sec] was acquired for intracranial volume (ICV) estimation (Eritaia et al., 2000). DISPLAY (Montreal Neurological Institute, QC, Canada) software was used to trace the ICV. DTI data sets were acquired using twice refocoused spin echo, echo planar imaging sequence (Reese et al., 2003) with the following parameters: TR=7700 ms, TE= 94 MS, 5 non-diffusion weighted (b = 0 s/mm^2) and

30 diffusion directions (b= 1,000 s/mm^2), FOV: 212×212×111 mm^3, voxel size: 2.2×2.2×2.2 mm^3, with full brain coverage without gap and a scan time of 4min 39sec. The diffusion tensor datasets were pre-processed by the rigid body co-registering to b0 image using Automatic Image Registration.

Detailed reliable protocols for the manual tracing of the uncinate fasciculus and cingulum bundle including rostral cingulum, dorsal cingulum and parahippocampal cingulum were previously reported (Malykhin et al., 2008) (Figure 7.1). The program DTI-studio V2.40 (Johns Hopkins University, Baltimore, MD) was utilized to quantify fractional anisotropy (FA), mean diffusivity (MD), axial diffusivity (AD), radial diffusivity (RD), and tract volume. In addition, linear (C_l = ($\lambda1 - \lambda2$) / $\lambda1$), planar (C_p = ($\lambda2 - \lambda3$) / $\lambda1$), and spherical (C_s = $\lambda3$ / $\lambda1$) measures were calculated as representations for geometrical shape of diffusion tensor (for more details, see Westin et al., 2002).

All measurements were performed by a single rater (A.S.S) who was blind to all demographic and genotype information. Raw tract volumetric measurements were adjusted to the ICV by using the following formula: *ICV-adjusted volume* = (*Raw tract volume (mm^3) / ICV of the same individual (cm^3)*) × *sample average ICV (cm ^{3})* (Aghamohammadi-Sereshki et al., 2019). Fiber tracking parameters were > 0.2 for FA threshold to initiate and continue tracking and the angular deviation of the propagating line > 60°. An FA threshold of 0.2 was chosen to prevent inclusion of grey matter and CSF voxels (Hecke and Emsell 2015). An FA threshold of 0.2 is generally regarded as optimal threshold while FA=0.1 or FA=0.3 may increase inclusion of nonwhite matter voxels or regarded as a strict threshold (Caan 2015; Tournier et al., 2011).

The inter-rater reliability was assessed by two raters (A.A.S and N.V.M), who independently traced the rostral cingulum, dorsal cingulum, parahippocampal cingulum and uncinate fasciculus in 5 subjects in both hemispheres. Intra-rater reliability for the aforementioned tracts was assessed by retracing the images from the same five subjects at 1–2 weeks interval by a single rater (A.A.S) who performed all DTI-measurements of the current study (Table 7.1). It is important to mention that the DTI images used to assess the intra/inter- rater reliability were different from the datasets used for training.

Genetic analysis

The genotypes for our genes of interest were obtained using single nucleotide polymorphisms (SNPs) derived from cheek swabs from our participants. Primer3PLUS was used to generate primers using sequence data from dbSNP. Primers were positioned to generate a clean single PCR product with the variant in a position near the centre of the read to avoid common technical artifacts that can occur during the sequencing step. All primers were purchased from Integrated DNA Technologies (Coralville, IA).

COMT polymorphisms were obtained using rs4680 (G; A), where the G allele encodes Val, and the A allele encodes Met. Due to the first, above mentioned dose-dependent COMT enzymatic activity; and second, the possible advantage of the Met allele over the Val allele in cognitive-related functions (Dixon et al., 2014; Mier et al., 2009; Petrella et al., 2008), the effects of COMT polymorphism on the DTI-measurements were studied between homozygous "Met/Met" vs. "Val/x" (i.e. Val/Val and Met/Val) individuals. All genotype frequencies are reported in the results section.

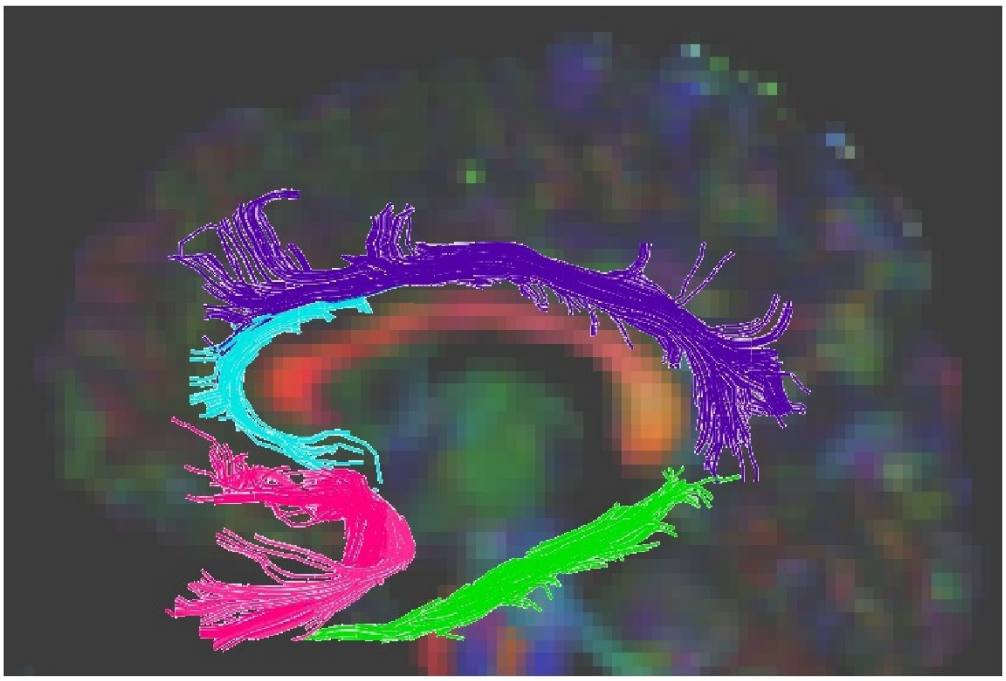

Figure 7.1. Three-dimensional reconstructions of the cingulum bundle and uncinate fasciculus.

Key*:* uncinate fasciculus is shown in pink, rostral cingulum is shown in cyan, dorsal cingulum is shown in purple and parahippocampal cingulum is shown in lime green.

Table 7.1. Inter/Intra-rater intra class correlation coefficients (ICC) and percent coefficient of variation (CV) for DTI-metrics.

Tracts	Fractional anisotropy				Mean Diffusivity				Axial diffusivity				Radial diffusivity				Number of voxels that fibers go			
	Inter-rater		Intra-rater		Inter-rater		Intra-rater		Inter-rater		Intra-rater		Inter-rater		Intra-rater		Inter-rater		Intra-rater	
	ICC	CV	ICC	CV	ICC	CV	ICC	CV	ICC	CV	ICC	CV	ICC	CV	ICC	CV	ICC	CV	ICC	CV
Uncinate Fasciculus	.98	.6	.96	.9	.97	.4	.95	.5	.98	.4	.91	1.2	.98	.6	.95	.9	.98	3.0	.98	7.2
Rostral Cingulum	.89	3.2	.97	1.5	.96	.6	.93	.8	.94	1.6	.97	1.1	.88	2.1	.96	1.3	.99	6.0	.96	8.6
Dorsal Cingulum	.96	.5	.91	1.1	.99	.3	.97	.5	.93	.6	.92	.6	.94	1.4	.96	1.2	.98	3.6	.95	6.3
Parahippo campal Cingulum	.99	.7	.99	.5	.97	.7	.98	.5	.94	.6	.96	.5	.98	1.0	.99	.7	.98	3.0	.99	2.3

Statistics

Demographic information

All inferential statistics other than regression models for age and COMT effects were carried out using IBM SPSS Statistics 25.0. Group characteristics such as age, education, and ICV were analyzed by a one-way analysis of variance (ANOVA) and with sex as the independent variable. Sex differences in DTI-measurements were tested using the independent sample T-test within 3 age groups including young (18-39 years old), middle age (40-59 years old) and old (60-85 years old) adults. Demographic characteristics between COMT (Met/Met vs. Val/x) polymorphisms was also analyzed using a one-way ANOVA. In addition, the chi-squared test was used to evaluate deviation from the Hardy–Weinberg equilibrium.

Hemisphere-related effects analysis

In order to investigate whether or not the left and right hemispheres age differently, first, we calculated asymmetry indices for each DTI parameter using following formula: [*({(Right measurement) / (Left measurement)} × 100) -100*]; and second, we tested the relationship between age and asymmetry indices using Pearson correlation coefficient. In addition, the inter-hemispheric differences in DTI-measurements were tested using the paired sampled T-test.

Modeling age and COMT relationships with the cingulum and Uncinate fasciculus

Lower order regression models (i.e. linear, quadratic, cubic) tend to impose severe shape restrictions to trendlines in regression analyses. Fjell et al. (2010) illustrated that studies utilizing quadratic models to estimate the parabolic appearing age trajectory of brain structures are significantly influenced by the age range of the subjects measured. Therefore, Fjell and colleagues (2010) recommended the use of non-parametric smoothing splines; however, since a smoothing

spline is a local non-parametric regression model, it is not well suited for inferential statistics. Also, using non-parametric smoothing splines on smaller sample sizes may produce higher-order functions, leading to overfitting and poor generalizability (Fjell et al., 2010; Royston and Sauerbrei 2008a). Considering the aforementioned limitations, we used multivariable fractional polynomial regression (MFP) modelling to assess the relationship between DTI-measurements and age (Royston and Sauerbrei 2008b).

To analyze the associations between age and COMT polymorphisms with the DTI-measurements of the cingulum bundle and uncinate fasciculus, DTI-measurements were selected as dependent variables and 'Age' (scaled), dummy-coded variables for the 'Sex' and COMT (Met/Met and Val/ *x*) as well as 'Age × Sex' and 'COMT × Age' interaction terms were selected as independent variables in MFP. MFP regression models were analyzed by STATA 15.

The MFP method consists of two simultaneous components, the *selection of independent variables* using the backward elimination (BE) method at α_1 levels (< 0.05 for 'Age', 'Sex' and 'COMT' terms; and < 0.01 for 'Age × Sex' and 'Age × COMT' interaction terms), and *selection of functions* for continuous independent variables using the function selection procedure (FSP) at the α_2 level (< 0.05) (Royston and Sauerbrei 2008b). Since interaction term might increase the risk of overfitting, it has been suggested to include them only if they have stronger effects (e.g. $p < 0.01$) (Royston and Sauerbrei 2008c).

The BE method was used for the variable selection (Royston and Sauerbrei 2008b). First, a linear model with all independent variables is fitted. The strongest and weakest independent variables are then determined by excluding each independent variable using BE. The strongest and weakest continuous independent variables are checked first and last for selecting the best power(s) respectively. However, if a variable is a binary (e.g. Sex or COMT), it does not undergo FSP,

instead the BE approach assesses whether or not including its dummy variable in the model is significant while other variables are in the models as adjustment terms.

The MFP method selects a functional form (i.e. power) for each continuous independent variable from a restricted set of powers S: {-2, -1, -0.5, 0, 0.5, 1, 2, 3} within $\beta_0 + \beta_1(x^P)$ regression framework (i.e. fractional polynomial degree 1 [FP1]). The best fitting model is chosen based on the maximum likelihood of all generated models using powers from S (Royston and Sauerbrei 2008d).

FP1 can be extended to the higher orders such as FP2, or FP3, etc. (Royston and Sauerbrei 2008b). For example, an FP2 regression framework is: if $P_1 \neq P_2$, then we have "$\beta_0 + \beta_1 (x^{P1}) + \beta_2 (x^{P2})$", or if $P_1 = P_2$, then we have "$\beta_0 + \beta_1 (x^{P1}) + \beta_2 (x^{P1}) \times (\log x)$". However, since using higher orders than FP2 (e.g. ≥ FP3) rarely improves the MFP model and reduces the generalizability (Royston and Sauerbrei 2008d), we restricted the MFP method to FP1 and FP2.

MPF method generates the best FP1 and FP2 models selecting the best power(s) from S. The FSP then selects the most suitable model (i.e. FP2, FP1, linear or null models) by approximate likelihood ratio chi-square (χ^2) tests measuring deviance (-2 log likelihood) differences between models. The analysis by FSP is as follow (Royston and Sauerbrei 2008d): (1). The *overall relationship* between DTI-measurements and independent variables are tested. To do so, the best FP2 model with 4 degrees of freedom is tested against the null model at the α level. If the test is not significant, the null model is selected, otherwise the analysis continues to the next step. (2) The best FP2 model with 3 degrees of freedom is tested against a straight line (P = 1) at the α level. This step statistically tests the *linearity vs. nonlinearity* nature of the relationship by comparing a linear model (with P = 1) against nonlinear models (with P ≠ 1). If the test is not significant, a straight line is selected as the final model, otherwise the analysis continues to the next step. (3).

The best FP2 model with 2 degrees of freedom is tested against the best FP1 model at the α level. If the test is not significant, the FP1 model is selected as the final model, otherwise FP2 model is selected. This step determines whether a more complicated nonlinear model (e.g. FP2) is *statistically* better than a simpler nonlinear model (e.g. FP1) in explaining the association between DTI-measurements and independent variables.

During FSP, the other independent variables are included in the model as adjustment terms; if an FP model with specific power is selected for the first examined independent variable, the independent variable is transformed (i.e. x_1^P) to the model for the subsequent analyses. This procedure runs for other continues variables.

The MFP procedure might follow more iteration(s) until the fractional polynomial models for continuous independent variables do not change, up to 4 cycles may be necessary (Royston and Sauerbrei 2008b). In the current study, the default cycle (n = 5) of STATA was adopted.

Finally, Holm-Bonferroni correction for type I error inflation due to multiple comparisons was used. Since previous published literature (Hasan et al., 2009; Lebel et al., 2012; Michielse et al., 2010; Sala et al., 2012; Yap et al., 2013) demonstrated the age-related effects on the DTI-measurements of the cingulum bundle and uncinate fasciculus, Holm-Bonferroni correction was used for the tensor shape- and genetic polymorphism-related analyses and not for the relationships between age and diffusion-related properties (e.g. FA, MD, RD and AD) and tracts' volumes. *P-values* survived Holm-Bonferroni correction were shown with a **bold asterisk** in the tables and the result section.

7.3. Results

Demographics

Participants' characteristics for the entire sample is shown in the Table 7.2. Males had larger ICVs [F (1, 138) = 118.6, $p < .0001$] than females whilst males and females did not differ in age, and education (both ps > .09) (Table 7.2). Furthermore, demographic characteristics were not different between carriers of the COMT genotypes ("Met/Met" vs "Val/x") (all ps > .19). Moreover, the chi-squared test showed that our sample for the COMT (χ^2: 0.38, p: .54) was in Hardy-Weinberg equilibrium.

Table 7.2. Demographic information (mean ± SD).

Variable	Male	Female	Total	F-Value	*p*-value
Number	62	78	140	-	-
Age in years	48.31 ± 19.51	48.24 ± 17.72	48.27 ± 18.47	0.000	0.98
Education in years	16.19 ± 2.44	15.50 ± 2.46	15.81 ± 2.46	2.722	0.10
ICV volume	1,739.75 ± 137.03	1,509.89 ± 112.74	1,611.68 ± 168.56	118.58	2.58E-20

Key: ICV: intracranial volume in cm^3.

Hemispheric differences and asymmetry analysis

Asymmetry for the rostral cingulum for the RD ($p <$ **.0004***) and MD ($p <$ **.008***) had significant relationships with age, whilst the rest of the asymmetry indices for all white matter tracts did not correlate with age (all corrected ps > .19). Therefore, we analyzed DTI-measurements of the left and right rostral cingulum separately in our regression analyses, whilst the averaged values of DTI-

measurements of the dorsal cingulum, parahippocampal cingulum and the uncinate fasciculus were used in the regression analyses.

The paired sampled T-test showed that first, for the uncinate fasciculus while the left FA was significantly higher than the right FA (p < **4.54E-12***), MD, RD, AD, volume and C_s were significantly higher in the right hemisphere compared to the left hemisphere (all ps < **8.22E-6***). There were no significant differences in the C_l and C_p between the left and right hemispheres (both ps > 0.058). Second, for the dorsal cingulum while the left hemisphere had significantly higher FA, volume and C_l than the right hemisphere (both ps < **3.29E-8***), the right hemisphere had significantly higher MD, RD, and C_s than the left hemisphere (all ps < **2.96E-20***). There were no significant differences in the AD and C_p between hemispheres (corrected p > 0.10). Third, for the parahippocampal cingulum, while the right hemisphere had significantly higher FA, volume and C_l than the left hemisphere (all ps < **8.05E-5***), the left hemisphere had significantly higher MD, RD, AD, and C_s than the right hemisphere (all ps < **1.53E-10***). However, there were no significant differences in the C_p between hemispheres (p > 0.29). Finally, due to the above-mentioned significant relationships between the age and asymmetry indices of the DTI parameters of the rostral cingulum, hemispheric differences of the rostral cingulum were analyzed separately for the young, middle-age and old adults. We found that across all three age groups while the left hemisphere had significantly higher FA than the right hemisphere (all ps < **6.81E-13***), the right hemisphere had significantly higher MD, RD, AD and C_s than the left hemisphere (all ps < **4.47E-9***).

Age-, Sex- and COMT-related effects on the DTI-measurements

FA

***Age effect*:** The effects of age were significant for the rostral cingulum in both hemispheres, dorsal cingulum and the uncinate fasciculus (all *p*s < 3.45E-5), but not for the parahippocampal cingulum. All the significant relationships were negative and linear (Figures 7.2, 7.4).

***Sex effect*:** While men showed higher FA in the left rostral cingulum and the dorsal cingulum (both *p*s < 1.93E-2), sex term was not significant for the right rostral cingulum, parahippocampal cingulum and uncinate fasciculus. However, neither cingulum bundle nor uncinate fasciculus showed significant sex difference for the FA in 3 age groups (all corrected-*p*s > .29).

COMT effects: Met/Met individuals had higher FA in the right rostral cingulum compared to the Val carriers (p < 2.17E-5). Group comparisons between two genotypes showed that Met/Met individuals had higher FA in the right rostral cingulum compared to the Val carriers (non-corrected p < .034) (Table III). However, COMT polymorphism effects were not present in other white matter tracts.

MD

***Age effect*:** The effects of age were significant for the left rostral cingulum, dorsal cingulum and the uncinate fasciculus (all *p*s < 3.52E-3), but not on the right rostral cingulum and parahippocampal cingulum. Furthermore, while age and MD of the dorsal cingulum and uncinate fasciculus showed positive nonlinear effects, the relationship for the left rostral cingulum was positive and linear (Figures 7.2, 7.4).

***Sex effect*:** Sex had effects only on the MD in the dorsal cingulum ($p < 4.94E-2$) in which women showed higher MD values. However, neither cingulum bundle nor uncinate fasciculus demonstrated significant sex difference for the MD in 3 age groups (all ps > .21).

COMT effects: Val carriers had higher MD in the right rostral cingulum compared to the Met/Met individuals ($p < 7.71E-5$). Group comparisons between two genotypes showed that Val carriers had significantly higher MD in the right rostral cingulum compared to the Met/Met individuals (p < **.0001***) (Table III). However, we did not find significant effects of the COMT polymorphism on the MD in other white matter tracts.

RD

***Age effect*:** The effects of age were significant for the left rostral cingulum, dorsal cingulum and the uncinate fasciculus (all ps < 1.63E-7), but not for the right rostral cingulum and parahippocampal cingulum. Furthermore, while age and RD of the dorsal cingulum and uncinate fasciculus showed positive nonlinear associations, the relationship for the RD in the left rostral cingulum was positive and linear Figures 7.2, 7.4).

***Sex effect*:** The sex term was not significant for the cingulum bundle and uncinate fasciculus.

COMT effects: Val carriers had higher RD in the right rostral cingulum compared to the Met/Met individuals ($p < 1.91E-4$). Group comparisons between two genotypes showed that Val carriers had significantly higher RD in the right rostral cingulum compared to the Met/Met individuals (p < **.0002***) (Table III). However, we did not find significant effects of the COMT polymorphism on the RD in other white matter tracts.

AD

***Age effect*:** The associations between age and AD were significant for the dorsal cingulum, parahippocampal cingulum and the uncinate fasciculus (all *p*s < 1.12E-2), but not for the rostral cingulum. Furthermore, while age and AD of the dorsal cingulum and uncinate fasciculus showed positive nonlinear associations correlation, the relationship for the parahippocampal cingulum was negative and linear (Figures 7.3, 7.4).

***Sex effect*:** The sex term was not significant for the cingulum bundle and uncinate fasciculus.

COMT effects: Val carriers had higher AD in the right rostral cingulum compared to the Met/Met individuals (p < 8.68E-3). Group comparisons between two genotypes showed that Val carriers had higher AD in the right rostral cingulum compared to the Met/Met individuals (non-corrected p < .0087) (Table 7.3). We did not find significant effects of the COMT polymorphism on the RD in other white matter tracts.

Tract volume

***Age effect*:** The effects of age were significant for the dorsal cingulum and the parahippocampal cingulum (all *p*s < 6.85E-3), but not for the uncinate fasciculus and the rostral cingulum. Furthermore, the tract volume of both dorsal cingulum and parahippocampal cingulum showed negative linear relationships with age (Figure 7.3).

***Sex effect*:** Sex had effects only on the rostral and dorsal cingulum (all *p*s < 1.51E-2) in which men had bigger tract volume. However, neither cingulum bundle nor uncinate fasciculus had significant sex difference for the volume in 3 age groups (all *p*s > .20).

COMT effects: We did not find significant effects of the COMT polymorphism on the tract volume of the cingulum bundle and uncinate fasciculus.

Linear geometry (C_l)

***Age effect*:** The effects of age were significant for the left rostral cingulum, the dorsal cingulum and uncinate fasciculus (all *p*s < 1.71E-3), but not on the right rostral cingulum and parahippocampal cingulum. Furthermore, the linear tensor shape of the left rostral cingulum, dorsal cingulum and uncinate fasciculus had negative linear relationships with age (Figures 7.3, 7.4).

***Sex effect*:** The sex term was not significant for the cingulum bundle and uncinate fasciculus.

COMT effects: We did not find significant effects of the COMT polymorphism on linear geometry of the white matter tracts.

Planar geometry (C_p)

We did not find any age-, sex- or COMT-related effects for the C_p in the studied tracts.

Spherical geometry (C_s)

***Age effect*:** The effects of age were significant for the rostral cingulum in both hemispheres, dorsal cingulum, and the uncinate fasciculus (all *p*s < 2.99E-3), but not for the parahippocampal cingulum. All the significant relationships were positive linear (Figures 7.3, 7.4).

***Sex effect*:** While women showed higher C_s in only the left rostral cingulum and the dorsal cingulum (both *p*s < 1.38E-2), sex term was not significant for the right rostral cingulum, parahippocampal cingulum and uncinate fasciculus. However, neither cingulum bundle nor uncinate fasciculus had significant sex difference for the C_s in 3 age groups (all corrected-*p*s > .16).

COMT effects: Val carriers had higher C_s in the right rostral cingulum compared to the Met/Met individuals (p < 2.52E-5). However, group comparisons between two genotypes showed that the C_s in the right rostral cingulum was marginally different between Met/Met individuals and the Val carriers (Val/+ > Met/Met, non-corrected p > .06) (Table 7.3).

We did not find any effects of 'Age × Sex' or 'Age × COMT' interactions on any of the DTI-measurements of the cingulum bundle and uncinate fasciculus. Finally, we did not find any effects of 'APOE', 'BDNF' 'Age × APOE', and 'Age × BDNF' interactions on any of the DTI-measurements of the cingulum bundle and uncinate fasciculus (results are not shown). All regression-related results of DTI-measurements are presented in Table 7.4.

Table 7.3. DTI-measurements of the cingulum bundle and uncinate fasciculus (mean ± SD) for the COMT Val/+ [Val/Val; Val/Met] and homozygous Met [Met/Met]) individuals.

Alleles' frequency in the total sample					
Met ≃ 0.464			**Val** ≃ 0.536		
Genotype comparisons					
Tract of Interest	**DTI-metrics**	**COMT genotypes**		***p*-value**	**Cohen's d**
		Met/Met (n = 32)	**Val/+ (n = 108)**		
Uncinate Fasciculus	FA	0.410 ± 0.025	0.410 ± 0.018	.97 [a]	0
	MD	0.809 ± 0.031	0.811 ± 0.028	.72	0.068
	RD	0.616 ± 0.035	0.617 ± 0.029	.82	0.031
	AD	1.194 ± 0.035	1.198 ± 0.035	.62	0.114
	Volume	2579 ± 774	2517 ± 712	.67	0.083
	C_l	0.412 ± 0.027	0.414 ± 0.030	.80	0.070
	C_p	0.144 ± 0.012	0.144 ± 0.029	.94	0
	C_s	0.444 ± 0.025	0.442 ± 0.025	.71	0.080
Right rostral cingulum	FA	0.358 ± 0.031	0.345 ± 0.028	.034	0.440
	MD	0.783 ± 0.060	0.822 ± 0.043	**.0001***	0.747

	RD	0.632 ± 0.052	0.668 ± 0.045	**.0002***	0.740
	AD	1.100 ± 0.073	1.131 ± 0.055	.0087	0.480
	Volume	863 ± 393	830 ± 389	.67	0.084
	C_l	0.354 ± 095	0.329 ± 0.063	.082	0.310
	C_p	0.167 ± 0.111	0.167 ± 0.062	1.00	0.090
	C_s	0.479 ± 0.073	0.504 ± 0.028	.064 [a]	0.452
Left rostral cingulum	FA	0.409 ± 0.032	0.405 ± 0.037	.58	0.116
	MD	0.702 ± 0.053	0.700 ± 0.042	.82	0.042
	RD	0.540 ± 0.051	0.540 ± 0.046	.98	0
	AD	1.026 ± 0.068	1.019 ± 0.054	.54	0.114
	Volume	989 ± 320	994 ± 451	.95	0.013
	C_l	0.383 ± 0.036	0.376 ± 0.043	.41	0.177
	C_p	0.182 ± 0.027	0.185 ± 0.027	.54	0.111
	C_s	0.435 ± 0.033	0.439 ± 0.038	.62	0.112
Dorsal cingulum	FA	0.459 ± 0.032	0.461 ± 0.027	.81	0.068
	MD	0.747 ± 0.038	0.745 ± 0.031	.72	0.058
	RD	0.541 ± 0.043	0.540 ± 0.036	.88	0.025
	AD	1.157 ± 0.038	1.156 ± 0.034	.88	0.028
	Volume	2854 ± 799	2970 ± 790	.48	0.146
	C_l	0.462 ± 0.047	0.457 ± 0.034	.57	0.122
	C_p	0.149 ± 0.037	0.153 ± 0.024	.50	0.128
	C_s	0.389 ± 0.041	0.389 ± 0.029	.93	0
Parahippocampal cingulum [b]	FA	0.374 ± 0.026	0.376 ± 0.022	.65	0.083
	MD	0.792 ± 0.041	0.782 ± 0.027	.20 [b]	0.288
	RD	0.623 ± 0.041	0.614 ± 0.029	.26 [b]	0.253
	AD	1.130 ± 0.052	1.118 ± 0.035	.25 [b]	0.271
	Volume	1280 ± 286	1219 ± 249	.26	0.227
	C_l	0.385 ± 0.032	0.387 ± 0.036	.76	0.059

	C_p	0.129 ± 0.018	0.131 ± 0.029	.78	0.083
	C_s	0.486 ± 0.025	0.483 ± 0.021	.41	0.130

Key: [a] *p-values* were adjusted for the violation of the equality variances. [b] The total number of Met/Met individuals were 31. ***** Significant corrected *p-values*.

Table 7.4. Regression models of the age-, sex- and COMT effects on the DTI-metrics of the cingulum bundle and uncinate fasciculus and their R^2, Adj-R^2, and Standardized *βs* (*P* values).

DTI metrics	Tracts		Significant Age terms	Sex [1]	COMT	R^2	Adj-R^2	*P*-value [2]	Regression model type
FA	RC	Right	Age [-0.338 (< *3.45E-5*)]	NS	0.183 (< *2.17E-2*)	0.147	0.134	< *1.91E-5*	Linear
		Left	Age [-0.506 (< *9.86E-11*)]	-0.171 (< *1.93E-2*)	NS	0.285	0.275	< *1.10E-10*	Linear
	DC		Age [-0.369 (< *5.46E-6*)]	-0.177 (< *2.46E-2*)	NS	0.167	0.155	< *3.57E-6*	Linear
	PHC		NS	NS	NS	0	0	NS	Null model
	UF		Age [-0.388 (< *2.14E-6*)]	NS	NS	0.151	0.145	< *2.14E-6*	Linear
MD	RC	Right	NS	NS	-0.328 (< *7.71E-5*)	0.107	0.101	< *7.71E-5*	Linear
		Left	Age [0.277 (< *9.32E-4*)]	NS	NS	0.077	0.070	< *9.32E-4*	Linear
	DC		Age [-1.677 (< *3.53E-4*)] + Age^2 [2.018 (< *2.10E-5*)]	0.010 (< *4.94E-2*)	NS	0.222	0.205	< *1.75E-7*	FP2 (Quadratic)
	PHC		NS	NS	NS	0	0	NS	Null model
	UF		Age^{-2} [0.302 (< *3.52E-3*)] + Age^3 [0.683 (< *4.65E-10*)]	NS	NS	0.270	0.260	< *4.29E-10*	FP2
RD	RC	Right	NS	NS	-0.31 (< *1.91E-4*)	0.096	0.090	< *1.91E-4*	Linear
		Left	Age [0.425 (< *1.63E-7*)]	NS	NS	0.181	0.175	< *1.63E-7*	Linear
	DC		Age^3 [0.435 (< *7.72E-8*)]	NS	NS	0.189	0.184	< *7.72E-8*	FP1
	PHC		NS	NS	NS	0	0	NS	Null model

	UF		Age^3 [0.496 (< *4.5E-10*)]	NS	NS	0.246	0.241	< *4.49E-10*	FP1
AD	**RC**	Right	NS	NS	-0.221 (< *8.68E-3*)	0.049	0.042	< *8.68E-3*	Linear
		Left	NS	NS	NS	0	0	NS	Null model
	DC		Age^2 [-1.728 (< *2.05E-3*)] + Age^3 [1.909 (< *6.91E-4*)]	NS	NS	0.104	0.091	< *5.24E-4*	FP2
	PHC		Age [-0.215 (<*1.12E-2*)]	NS	NS	0.046	0.039	< *1.12E-2*	Linear
	UF		Age^{-2} [0.437 (< *7.56E-5*)] + Age^3 [0.610 (< *7.04E-8*)]	NS	NS	0.192	0.180	< *4.61E-7*	FP2
Volume	**RC**	Right	NS	-0.181 (< *3.23E-2*)	NS	0.033	0.026	< *3.23E-2*	Linear
		Left	NS	-0.263 (<*1.67E-3*)	NS	0.069	0.063	< *1.67E-3*	Linear
	DC		Age [-0.224 (< *6.85E-3*)]	-0.201 (< *1.51E-2*)	NS	0.090	0.077	< *1.55E-3*	Linear
	PHC		Age [-0.412 (< *4.56E-7*)]	NS	NS	0.170	0.164	< *4.56E-7*	Linear
	UF		NS	NS	NS	0	0	NS	Null model
C_l	**RC**	Right	NS	NS	NS	0	0	NS	Null model
		Left	Age [-0.534 (< *1.07E-11*)]	NS	NS	0.285	0.280	***< 1.07E-11****	Linear
	DC		Age [-0.263 (<*1.71E-3*)]	NS	NS	0.069	0.062	***< 1.71E-3****	Linear
	PHC		NS	NS	NS	0	0	NS	Null model
	UF		Age [-0.374 (<*5.81E-6*)]	NS	NS	0.140	0.134	***< 5.81E-6****	Linear
C_p	**RC**	Right	NS	NS	NS	0	0	NS	Null model
		Left	NS	NS	NS	0	0	NS	Null model
	DC		NS	NS	NS	0	0	NS	Null model
	PHC		NS	NS	NS	0	0	NS	Null model
	UF		NS	NS	NS	0	0	NS	Null model

C_s	**RC**	Right	Age [0.242 (< *2.99E-3*)]	NS	-0.247 (< *2.52E-3*)	0.119	0.106	***< 1.76E-4****	Linear
		Left	Age [0.478 (< *1.26E-9*)]	0.183 (< *1.38E-2*)	NS	0.262	0.251	***< 9.09E-10****	Linear
	DC		Age [0.273 (< *9.46E-4*)]	0.181 (< *2.70E-2*)	NS	0.107	0.094	***< 4.40E-4****	Linear
	PHC		NS	NS	NS	0	0	NS	Null model
	UF		Age [0.389 (< *2.06E-6*)]	NS	NS	0.151	0.145	***< 2.05E-6****	Linear

Key: [1] negative standardized ***βs*** represent higher values in men and positive standardized ***βs*** represent higher values in women. In regression models, men and Val carriers were coded as 0 while women and Met/Met individuals were coded as 1. [2] Due to the previous studies, FA, MD, RD, AD and volume were not corrected for multiple comparisons, but the Holm-Bonferroni correction were applied to C_l, C_p, and C_s. NS: not significant. FP1: fractional polynomial regression degree 1, FP2: fractional polynomial regression degree 2. UF: uncinate fasciculus, RC: rostral cingulum, DC: dorsal cingulum, PHC: parahippocampal cingulum. Age × Sex and Age × COMT interaction terms were excluded from the table since they were not significant.

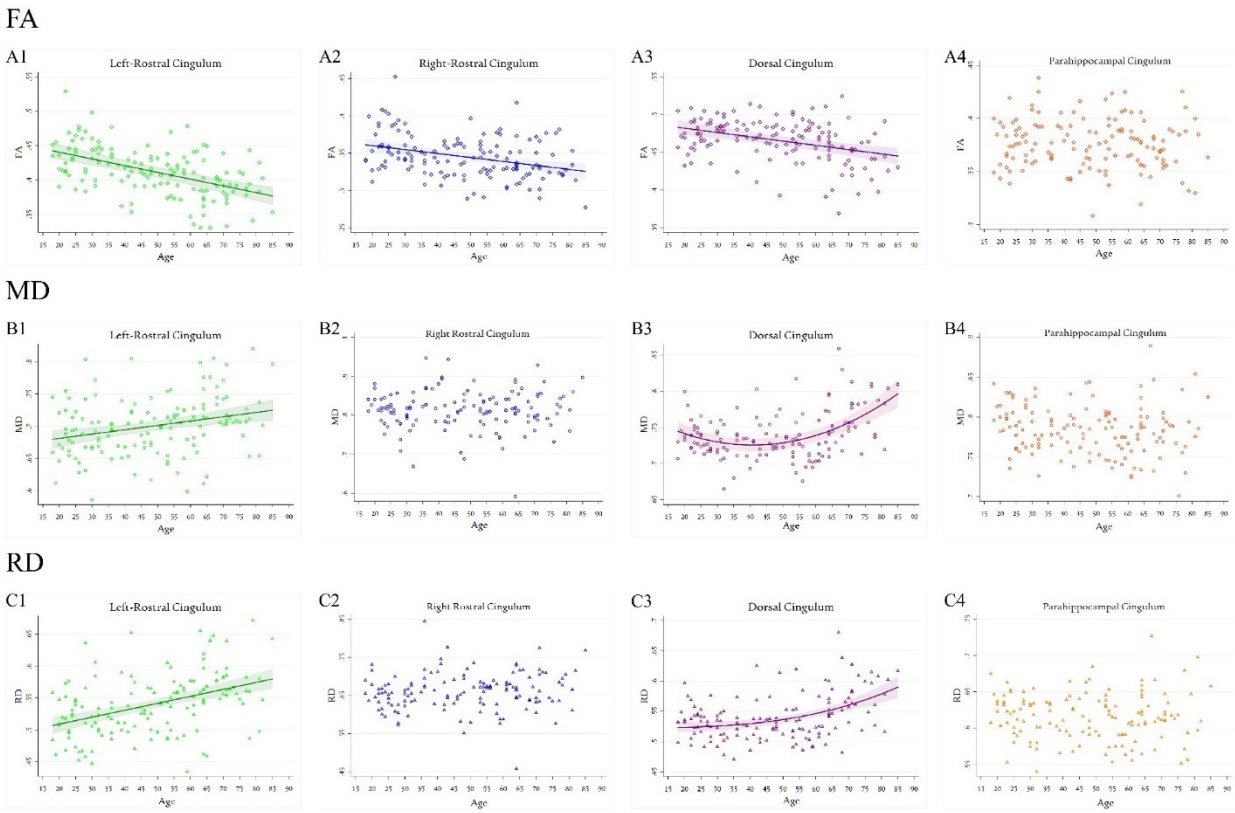

Figure 7.2. Regression plots showing the relationship between age and fractional anisotropy (FA), mean diffusivity (MD) and radial diffusivity (RD) in the cingulum bundle.

Key: A1-4: regression plots showing the relationship between FA and age in the left rostral cingulum, right rostral cingulum, dorsal cingulum and the parahippocampal cingulum (not significant); B1-3: regression plots showing the relationship between MD and age in the left rostral cingulum, right rostral cingulum (not significant), dorsal cingulum and the parahippocampal cingulum (not significant); C1-3: regression plots showing the relationship between RD and age in the left rostral cingulum, right rostral cingulum (not significant), dorsal cingulum and the parahippocampal cingulum (not significant).

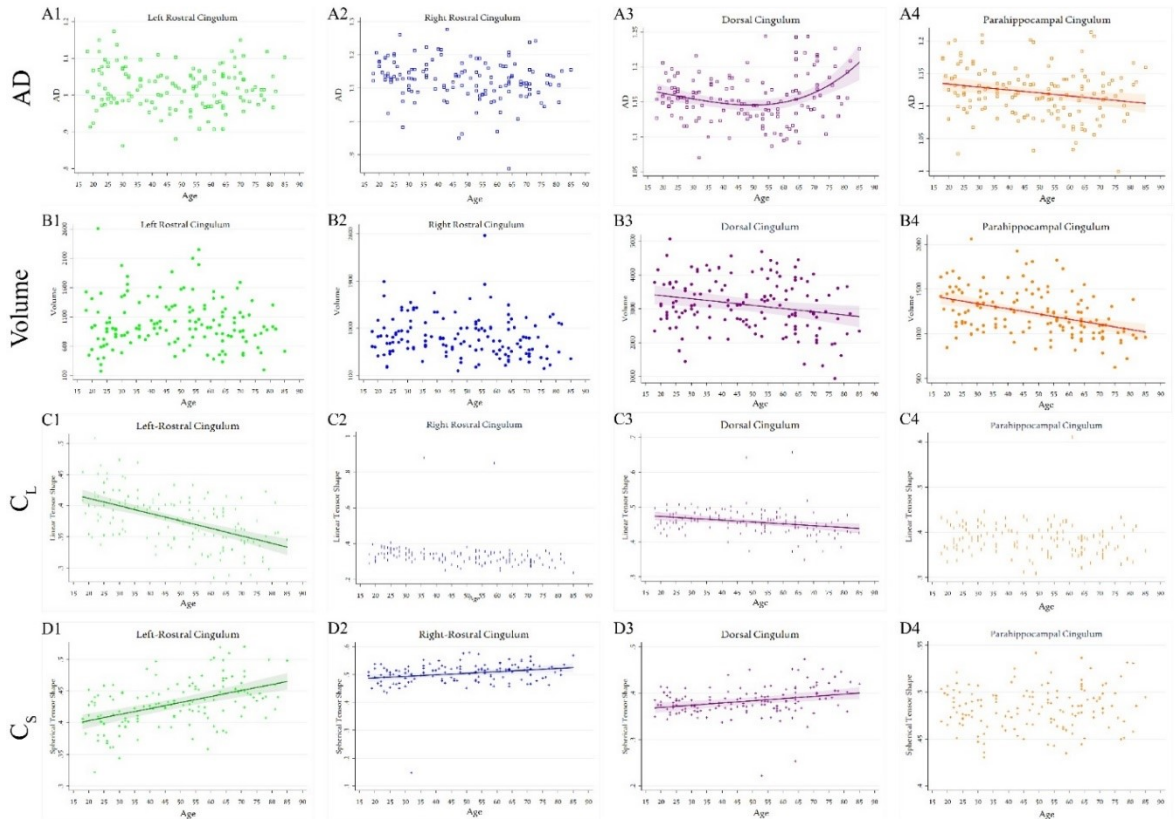

Figure 7.3. Regression plots showing the relationship between age and axial diffusivity (AD), volume, linear tensor shape (C_L) and spherical tensor shape (C_S) in the cingulum bundle.

Key: A1-3: regression plots showing the relationship between AD and age in the left rostral cingulum (not significant), right rostral cingulum (not significant), dorsal cingulum and the parahippocampal cingulum; B1-2: regression plots showing the relationship between the normalized volume and age in the left rostral cingulum (not significant), right rostral cingulum (not significant), dorsal cingulum and the parahippocampal cingulum; C1-2: regression plots showing the relationship between C_L and age in the left rostral cingulum, right rostral cingulum (not significant), dorsal cingulum and the parahippocampal cingulum (not significant). D1-4: regression plots showing the relationship between C_S and age in the left rostral cingulum, right rostral cingulum, dorsal cingulum and the parahippocampal cingulum (not significant).

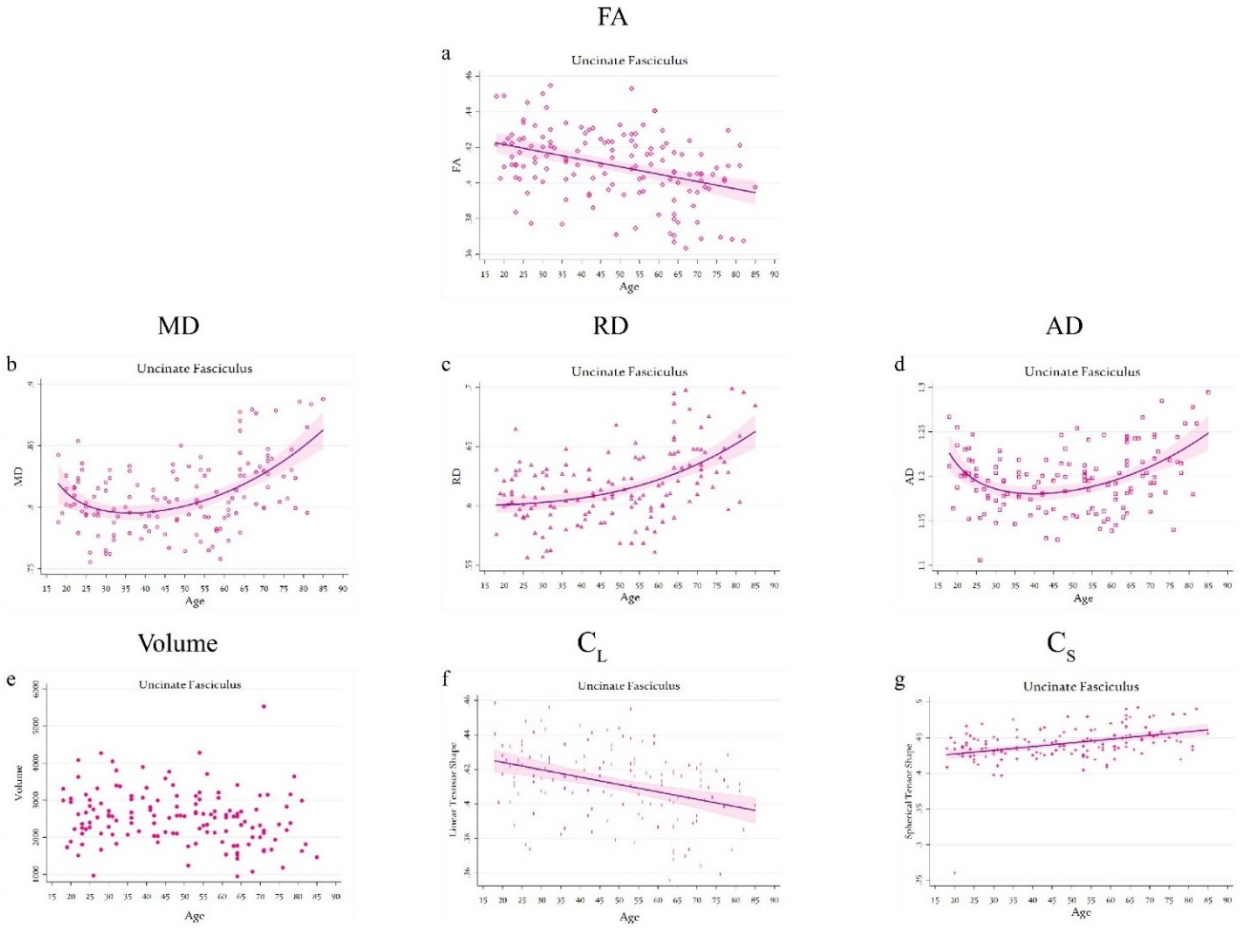

Figure 7.4. Regression plots showing the relationship between age and DTI-measurements in the uncinate fasciculus.

Key: regression plots showing the relationship between age and FA (a), MD (b), RD (c), AD (d), normalized volume (e) (not significant), C_L (f) and C_S (g) in the uncinate fasciculus.

7.4. Discussion

In the present study we used DTI tractography to examine the associations between age, sex, and COMT polymorphism with the microstructural properties of the cingulum bundle and uncinate fasciculus. Our results showed that aging was associated with lower microstructural integrity of the left rostral cingulum, dorsal cingulum and uncinate fasciculus, but it had less effects on the right rostral cingulum and the parahippocampal cingulum. Furthermore, while the FA, C_l and C_s were linearly associated with age, MD, RD and AD had mainly nonlinear relationships with age. We did not find any significant sex and the age × sex interaction effects on the DTI-measurements of the cingulum bundle and the uncinate fasciculus. Finally, we found that Met/Met individuals had better microstructural integrity for the right rostral cingulum compared to the Val carriers across life span.

Aging trajectories of the Cingulum bundle and the Uncinate Fasciculus

Previous studies of healthy aging demonstrated that the older age was associated with lower FA of the rostral cingulum (Jang et al., 2016), dorsal cingulum (Lebel et al., 2012), rostral + dorsal cingulum (Bennet et al., 2015; Cox et al., 2016; Sala et al., 2012; Westlye et al., 2010) and uncinate fasciculus (Bennet et al., 2015; Cox et al., 2016; Hasan et al., 2009; Lebel et al., 2012; Sala et al., 2012; Westlye et al., 2010), but not the FA of the parahippocampal cingulum (Bennet et al., 2015; Cox et al., 2016; Jang et al., 2016). Although Westlye et al. (2010) found an inverse U-shaped relationship between age and the FA in parahippocampal cingulum, they acknowledged that parahippocampal cingulum had a high degree of inter-individual variability which caused to have a “less clear-cut trajectory”. In contrast, Stadlbauer et al. (2008) did not find any associations

between age and the FA of rostral + dorsal cingulum. Our findings on the lower FA in the rostral cingulum, dorsal cingulum and uncinate fasciculus, but not in the parahippocampal cingulum are in accordance with most of the mentioned studies.

In contrast to FA, age demonstrated positive associations with the MD and/or RD of the dorsal cingulum, rostral + dorsal cingulum and uncinate fasciculus (Bennet et al., 2015; Cox et al., 2016; Hasan et al., 2009; Lebel et al., 2012; Sala et al., 2012; Westlye et al., 2010) which are in agreement with the current study. However, Stadlbauer et al. (2008) did not find any associations between age and the MD of rostral + dorsal cingulum. Our findings on the absence of the relationship between age and MD and RD of the parahippocampal cingulum is agreement with Bennet et al. (2015), but contradicts with Cox et al. (2016) and Westlye et al. (2010).

Compared to the MD and RD results, findings on the effects of healthy aging on the AD are less clear. Previously, no associations between the age and AD of the rostral + dorsal cingulum (Bennet et al., 2015; Cox et al., 2016; Stadlbauer et al., 2008) and uncinate fasciculus (Bennet et al., 2015; Hasan et al., 2009) were reported. In contrast, both lower AD (Sala et al., 2012) and higher AD (Cox et al., 2016) in uncinate fasciculus with older age were found. Our results suggest that age was associated with higher AD in both dorsal cingulum and uncinate fasciculus. Finally, although both the current study and Cox et al. (2016) indicate a significant relationship between age and AD of the parahippocampal cingulum, the former suggests a negative linear relationship, but the latter indicated a positive nonlinear correlation.

However, there were several factors amongst these studies that can contribute to observed differences including DTI acquisition protocols, FA threshold for fiber tractography, methods of DTI analyses (e.g. ROI-based vs. Tract-Based Spatial Statistics; deterministic vs. probabilistic), anatomical definition of tracts and the sample size of studies. Furthermore, most of the above-

mentioned studies tested only linear and quadratic models to explain the relationships between age and DTI-measurements which might not explain the nature of the relationship very well. As Fjell et al. (2010) noted first, in age-related studies, the quadratic trajectory shape is significantly affected by the age range sample. Therefore, while the quadratic regression might properly fit for studies including children and adolescents, it affects the maximum or minimum values for the adult studies. Second, quadratic model is one of the nonlinear models. Therefore, other nonlinear regression models should be tested to find out whether a more complicated model is statistically better for explaining a relationship. In the current study we used MPF method to test if a nonlinear model statistically better than a linear model. Furthermore, more complicated nonlinear models (FP2) were tested against the simpler nonlinear models (FP1) to test if a more complicated nonlinear model statistically better than the simple nonlinear models. Our analyses showed that amongst all 40 tests (5 tracts × 8 DTI-measurements), the age term was significant for 22 tests. Of these, 16 were linear, 1 quadratic, and 5 were other nonlinear models (3 of them were FP2, and 2 of them were FP1).

Our current findings are in agreement with our previous study that showed decrease in FA and increase in MD, RD and AD in the uncinate fasciculus after the age of 60s (Michielse et al., 2010). However, our current findings on the negative linear relationship between age and FA in the rostral and dorsal cingulum contradicts with our previous study although the absence of this relationship in the parahippocampal cingulum agrees with our previous result (Michielse et al., 2010). Furthermore, our current results are in general agreement with our previous findings on increasing MD, RD and AD and after 60s in the rostral and dorsal cingulum (Michielse et al., 2010). Also, the absence of the relationship between the MD and AD of the parahippocampal cingulum and age agrees with our previous study, current study indicates no association between age and the RD of

the parahippocampal cingulum which contradicts with our previous findings (Michielse et al., 2010). Finally, volumetric atrophy of the dorsal and parahippocampal cingulum is another replicated finding between our current and previous studies. Some of the confounding variables which might contribute to the inconsistent results between our previous and current studies are DTI acquisition and fiber tracking parameters as well as sample age structure and regression analytical methods. However, identical tractography methods were used for delineating UF and cingulum bundle in the current and our past study (Malykhin et al., 2008).

Finally, it was demonstrated that the direction of DTI eigenvectors (i.e. ν_1, ν_2, ν_3) may not have the same alignment as the underpinning structures which makes the biological-related interpretations of RD and AD equivocal (Wheeler-Kingshott and Cercignani 2009). Therefore, it was recommended to provide information about geometrical features besides RD and AD (Wheeler-Kingshott and Cercignani 2009). The C_l is high for the commissural (e.g. corpus callosum) and deep projection (e.g. internal capsule and corticospinal tract) fibers (Alexander et al., 2000) representing anisotropic diffusion parallel to the largest eigenvectors (ν_1) and a homogenous tract direction (Westin et al., 2002). The Cp is high in the arcuate fasciculus and peripheral radiation fibers (Alexander et al., 2000) representing confined diffusion by two eigenvectors (ν_1 and ν_2) (Westin et al., 2002). The C_s represents isotropic diffusion (Westin et al., 2002). In our study, the Cp did not correlate with age in any of the studied tracts. However, for the left rostral cingulum, dorsal cingulum and uncinate fasciculus C_l and C_s had negative linear and positive linear associations with age respectively. This might represent less restricted diffusion in aging. For the right rostral cingulum, the age-related association was only significant for the C_s (positive) and not for the C_l. Tensor shapes of the parahippocampal cingulum did not correlate with age.

Considering structural variability amongst different tracts (i.e. myelin thickness, the number of axons, axonal density, size and diameter as well as packing), crossing fibers-related issues and DTI acquisition parameters (Beaulieu 2014), it cannot clearly interpret diffusion data without examining the corresponding postmortem tissue (Beaulieu 2002). However, it was suggested that reduction in the FA in healthy aging might be concurrent with changes in other diffusivity parameters (i.e. MD, RD and AD) which have five specific tract-dependent patterns (for more details, see Burzynska et al., 2010). Each of these patterns might represent specific microstructural underlying for white matter age-related changes (Burzynska et al., 2010). In our present study, age-related alterations in the rostral cingulum, dorsal cingulum and the uncinate fasciculus follow the suggested pattern 1 displaying reduction in FA with increasing in RD and MD properties which might have increasing in AD too (Burzynska et al., 2010). These diffusivity properties might represent "chronic white matter degeneration" characterized by higher extracellular volume fraction and inter-axonal spacing as well as lower membrane density, lower relative volume of axons and reduction in the tortuosity of the extracellular space (for more details, see Burzynska et al., 2010).

Sex-related and hemispheric effects on the Cingulum bundle and the Uncinate Fasciculus

We did not find any sexual dimorphism in the age trajectories of the DTI-measurements of the cingulum bundle and the uncinate fasciculus which agrees with previous studies (Hasan et al., 2009; Lebel et al., 2012). However, Cox et al. (2016) who studied 27 tracts across the brain (including uncinate fasciculus, rostral + dorsal cingulum and parahippocampal cingulum) with a large sample size (N = 3,513, age range: 44.64 –77.12) reported that although there were some significant age × sex interactions, those were small and inconsistent. Furthermore, authors

concluded that power calculation analyses with sample size of 1,000 individuals indicated that the modest age × sex interactions would not be detected (Cox et al., 2016). Moreover, our results indicated the absence of significant sex differences in the DTI-measurements of the uncinate fasciculus and the cingulum bundle.

Finally, our findings demonstrated significant higher FA with lower MD, AD and RD in the left hemisphere compared to the right hemisphere throughout the adulthood in the rostral cingulum, dorsal cingulum and uncinate fasciculus. This in agreement with our previous study in which significantly higher FA in the rostral and dorsal cingulum in the left hemisphere compared to the right hemisphere was reported (Malykhin et al., 2008). Furthermore, our current results indicated significantly larger uncinate fasciculus in the right hemisphere compared to the left hemisphere which agrees with our previous results (Malykhin et al., 2008) and a postmortem study that showed the uncinate fasciculus in both men and women was 27% larger on the right hemisphere compared to the left hemisphere (Highley et al., 2002). However, for the parahippocampal cingulum, we found significant higher FA and lower MD, AD and RD in right hemisphere compared to the left hemisphere throughout the adulthood. Therefore, our results suggest better white matter integrity for the left rostral cingulum, dorsal cingulum and uncinate fasciculus and the right parahippocampal cingulum compared to their counterpart hemispheres.

COMT effects on the Cingulum bundle and uncinate fasciculus

Our findings suggest that for the COMT SNP, homozygous Met/Met has advantages over the Val/+ carriers which led to higher FA and lower MD, RD and AD in the right rostral cingulum. Also, the advantages have been preserved during the entire adulthood as indicated by the absence of the 'COMT × Age' interaction effects.

COMT is the catecholamines (e.g. dopamine, norepinephrine and epinephrine) metabolizing enzyme encoded by COMT gene (Goldman et al., 2005; Mammarella et al., 2016). Although the COMT enzyme is widely distributed in the brain, its enzyme and mRNA are mainly located in first, choroid plexus, second, frontal cortex; and third, cerebellum. However, its mRNA has low to moderate expression in the human amygdala and hippocampus (Myöhänen and Männisto 2010). Previous studies suggested that dopamine signaling might be involved in myelination (Bongarzone et al., 1998; Choi et al., 2017; Rosin et al., 2005). Bongarzone et al. (1998) suggested that dopamine D3 receptor might be involved in either oligodendrocytes differentiation and/or myelin formation by differentiated oligodendrocytes. Also, protective effects of the dopamine D2 and D3 agonists for oligodendrocytes against oxidative glutamate toxicity were shown (Rosin et al., 2005). Finally, the dopamine and dopamine D2 receptor involvement in the stress-induced myelin loss was reported (Choi et al., 2017).

Most of the healthy aging studies of COMT have been focused on cognition (for a review see Sambataro et al., 2012; Witte and Flöel 2012). Generally, the effects of COMT on brain structures (both grey and white matter) and not brain function have been less studied so far. To the best of our knowledge, Papenberg et al. (2015) has been the only age-related study that investigated the effects of COMT polymorphism on the brain white matter tracts. Papenberg and colleagues (2015) used TBSS method in older adults (60–87 years) and found higher FA and lower MD in cingulum of the Met homozygotes compared to Val carriers only in the oldest adult group (81-87 years old). Although our findings on the higher white matter integrity in Met homozygotes compared to the Val carriers are in accordance with those of Papenberg et al. (2015), there are some differences. First, the Met-related advantages were reported for the rostral + dorsal cingulum in both hemispheres in Papenberg et al. (2015). Second, Papenberg and colleagues (2015) found an age

group × COMT interaction which indicated that the Met-related advantages were confined to the oldest adults and not for the total sample. However, in the current study, the Met-related advantages first, were confined to the rostral cingulum in the right hemisphere; and second, it did not show any significant age × COMT interaction.

Future research is necessary to clarify whether COMT (rs4680) polymorphism affects the frontal white matter due to the above-mentioned importance of the dopamine signaling in myelination-related mechanisms.

In summary we found that limbic white matter tracts might be non-uniformly affected by healthy aging. Whilst uncinate fasciculus, rostral cingulum and dorsal cingulum showed strong associations with advanced age, the parahippocampal cingulum was relatively preserved. In addition, our findings indicate the COMT Met/Met genotype was associated with better microstructural integrity of the right rostral cingulum compared to the Val/+ genotype across life span.

Limitations

This study was a cross-sectional study and therefore all age-related findings should be interpreted as correlations with age.

Acknowledgements

Financial support for this study was provided by the Canadian Institutes of Health Research (CIHR) operating grant MOP115011 to Nikolai Malykhin. We would like to thank members of the Applied Genomics Core (TAGC, Faculty of Medicine and Dentistry, University of Alberta), Dr. Andrew L. Mason (Director), Dr. Georgina Macintyre and Ms Susan Kenney for their help with genetic data collection. The authors have no conflicts of interest to disclose.

III. Discussion

Chapter 8: Conclusion

The purpose of this chapter is to reflect on our findings in the context of current literature. This chapter is organized to explain the contribution that my research experiments has made to the knowledge in related research fields. For each experimental chapters (Chapters 4-7) I first presented a brief overview of literature in that field; then, I highlighted how our results contributed to advancing knowledge in the respective research areas.

8.1. *In vivo* study of the human amygdala (chapter 4)

Background and Knowledge Gaps

Most previous amygdala *in vivo* studies have analyzed this structure as a single homogenous brain region (Achten et al., 1998; Ancelin et al., 2019; Bickart et al., 2011; Bonilha et al., 2004; Convit et al., 1999; Makris et al., 1999; Makkinejad et al., 2019; Malykhin et al., 2007; Matsuoka et al., 2003; Pruessner et al., 2000; Siozopoulos et al., 2017; Watson et al., 1992; Zuo et al., 2019). Others, who published MRI methods and aimed to study amygdala subnuclei, were limited either by the accuracy of segmentation method or the number of studied subnuclei (Amunts et al., 2005; Bach et al., 2011; Bzdok et al., 2013; Entis et al., 2012; Prévost et al., 2011; Saygin et al., 2011; Solano-Castiella et al., 2010; 2011).

Contributions

For the first time, we used ultra-high resolution T_2-weighted FSE MRI images to develop a manual segmentation to study five major amygdala subnuclei including La, B, and AB nuclei, as well as Co and CeM groups. The protocol was established based on previous histological references (Brabec et al., 2010; García-Amado and Prensa, 2012; Mai et al., 2008; Schumann and Amaral,

2005) in order to segment amygdala subnuclei to approximately match the actual location and orientation of the individual amygdala subnuclei on coronal slices with submillimeter accuracy. Our volumetric results are comparable with a postmortem study of amygdala subnuclei (García-Amado and Prensa, 2012) demonstrating the validity of our method. Furthermore, computing ICC and Dice Kappa values proved that even our lowest reliability value (Dice kappa for the AB: 0.71) corresponds to the substantial agreement discussed by Landis and Koch (1977). Finally, our results showed no significant differences in the normalized volumes of the total amygdala and amygdala subnuclei between men and women, and also, between hemispheres.

We used two major landmarks for segmenting the amygdala subnuclei, including hippocampal head and the inferior amygdala border that are directly adjacent to the parahippocampal white matter. There are several reasons to choose these landmarks as the main ones: First, They are consistent landmarks that can be visualized across the entire length of the amygdala and have very little interindividual variability. Second, except for the first few MRI slices, these landmarks do not border CSF where usually first signs of atrophy are visible for both amygdala and hippocampus. Instead, this border is consistently attached to the hippocampal head and parahippocampal white matter both of which are preserved with age as previous (Malykhin et al., 2008a, 2017; Michielse et al., 2011) and current research have shown. Therefore, we believe that these landmarks are mostly preserved in healthy aging.

8.2. Healthy aging study of the human amygdala: Imaging-genetics (chapter 5)

Background and Knowledge Gaps

Overall, previous meta-analysis and review studies of the effects of healthy aging on the amygdala showed a modest volumetric reduction (Brierley et al., 2002; Fjell and Walhovd 2010; Mather 2016; Raz and Rodrigue 2006; Wright 2009). In contrast, a post-mortem study of the amygdala did not find a significant relationship between the amygdala volume and age (Brabec et al., 2010). However, none of the healthy aging studies of the amygdala analyzed the effects of healthy aging on the amygdala subnuclei to demonstrate the underlying neuroanatomical sources of the mentioned atrophy. Furthermore, despite the wide distribution of the sexual hormone markers in most of the amygdala subnuclei (Blurton-Jones et al., 1999; Osterlund et al., 2000a; 2000b; Roselli et al., 2001), suggesting a potential sexual dimorphism in the age trajectory of the amygdala, most of the previous studies did not analyze 'age × sex' interaction effects on the amygdala volume (Heckers et al., 1990; Laakso et al., 1995; Malykhin et al., 2008a; Mu et al., 1999; Sublette et al., 2008).

Also, regarding the effects of the APOE and BDNF polymorphisms on the amygdala volume, findings are scarce. Previously, no effects of APOE polymorphisms (Hibar et al., 2015), APOE-ε4 allele, or age × APOE-ε4 allele interaction (Soldan et al., 2015) on the total amygdala volume were reported. In contrast, den Heijer et al. (2002) found a smaller total amygdala volume in ε4 carriers, compared to ε3/ ε3 homozygote individuals. Furthermore, Hibar et al. (2015) found no effect of the BDNF polymorphism on the amygdala volume.

Contributions

For the first time, we found that age was associated with the amygdala subnuclei volumes in a different manner. We found significant negative relationship between age and the volume of the BLA group, but not with the volumes of the Co (showed a trend towards significant) and CeM groups. All of the BLA nuclei, including La, B and AB showed significant negative relationship with age. Our statistical analysis indicated that all the above-mentioned significant relationships were nonlinear. Furthermore, we found significant sexual dimorphism in the aging pattern of the total amygdala volume and volumes of its B and AB nuclei, as well as the Co group. The age trajectory of the La nucleus showed a trend towards significant sexual dimorphism. Therefore, our results suggest that: first, while BLA group (including La, B and AB nuclei) is more susceptible to age-related atrophy, CeM group is resilient to such changes. Second, our findings suggested that negative associations were present between age and volumes of the amygdala, and its BLA and Co groups, in men but not in women. Finally, our findings suggest that the rate of the volumetric atrophy is more deleterious with advanced age.

Our analyses did not reveal any significant differences in the volumes of the total amygdala and amygdala subnuclei between APOE (ε2/+ vs ε3/ ε3 vs ε4/+) and BDNF (Met/+ vs. Val/Val) genotypes. However, the amygdala volumetric comparisons within each genotype between young (individuals < 55 years old) and old (individuals ≥ 55 years old) groups suggested a potential protective effect for the APOE ε2 allele. This is explained by relatively smaller amygdala and amygdala subnuclei volumes in the older ε3/ε3 and ε4/+, but not in ε2/+ individuals compared to the younger individuals. We acknowledge that due to having a small sample size regarding genetic analysis, and especially for the number of ε2 carriers, these findings should be interpreted as preliminary results. However, this is an important finding for future studies, since most of the

previous APOE studies analyzed ε4 carriers vs non-carriers of ε4 without analyzing ε2 carriers as a separate group.

8.3. Effects of childhood adversity on the volumes of the amygdala subnuclei and hippocampal subfields in major depressive disorder (chapter 6)

Background and Knowledge Gaps

Volumetric reduction in the hippocampus, orbitofrontal and anterior cingulate cortices have been often reported in MRI studies of MDD (Koolschijn et al., 2009; Lorenzetti et al., 2009; Malykhin and Coupland 2015). However, despite the important role of the amygdala in neuronal circuits of emotion, fear and stress (Davis and Whalen 2001; LeDoux, 2007; Sah et al., 2003), volumetric *in vivo* studies of the total amygdala have been inconsistent (Campbell et al., 2004; Hajek et al. 2009; Hamilton et al., 2008; Schmaal et al., 2016). While some studies have demonstrated an increase in the amygdala volume (Frodl et al., 2002; Malykhin et al., 2012), others have reported either a volumetric reduction (Kronenberg et al., 2009) or no significant volumetric difference in MDD participants compared to healthy controls (Frodl et al., 2008; Koolschijn et al., 2009; Zavorotnyy et al., 2017). Furthermore, all previous MDD studies of the human amygdala analyzed this structure as a homogenous structure despite the fact that amygdala is a heterogeneous region in the medial temporal lobe which consists of functionally different subnuclei groups (Price et al., 1987; Sah et al., 2003).

Adverse childhood experiences have been recognized as an important risk factor for developing depression in adulthood (Hammen et al., 2000; Hovens et al., 2010; Lindert et al., 2014). The most

replicated findings on the adverse effects of childhood maltreatment on brain structures are volumetric reduction in the anterior cingulate, dorsolateral prefrontal and orbitofrontal cortices, and hippocampus (Danese and McEwen, 2012; Teicher and Samson, 2016), as well as the amygdala hyperactivity in response to threatening stimuli in maltreated individuals (Hein and Monk 2017; McCrory et al., 2017; Teicher and Samson 2016). However, there are some gaps in the literature: first, it has been shown that the adverse effects of childhood maltreatment or psychosocial stress might be different across the anteroposterior hippocampal axis and hippocampal subfields (Szeszko et al., 2006; Teicher et al., 2012). However, to date, there has been no structural MRI findings regarding the adverse effects of childhood maltreatment on the hippocampal subregions or subfields in MDD. Second, volumetric studies of the total human amygdala in maltreated individuals have been inconsistent (Andersen et al., 2008; Calem et al., 2017; Cohen et al., 2006; De Bellis et al., 2002; Lupien et al., 2011; Mehta et al., 2009; Tottenham et al., 2010). Finally, there has be no information regarding the effects of early life maltreatment on the volumes of the amygdala subnuclei.

Contributions

This was the first study that investigated the effects of MDD and childhood adversity on the amygdala subnuclei volumes. Our results did not show any significant differences in the volumes of the total amygdala or its subnuclei between healthy individuals and MDD participants or effects of long-term antidepressant treatment on amygdala volumes. However, we found negative relationships between the CTQ-25 score and the volume of the right amygdala in MDD participants, indicating the hemispheric difference of the effects of childhood abuse on the amygdala. Analyses of the amygdala subnuclei showed that the total CTQ-25 score had negative correlations with the volumes of the right AB and B nuclei in MDD participants. Also, amongst

all types of abuse and neglect, only emotional abuse showed negative associations with volumes of the B, AB and Co nuclei of the amygdala in the right hemisphere. However, none of the amygdala volumetric relationships with histories of childhood maltreatment survived correction for multiple comparisons.

Furthermore, we found significant negative associations between the total CTQ-25 score and volumes of the total hippocampal head, the total CA1-3, and the volume of the CA1-3 in the hippocampal head in MDD participants. Except for sexual abuse, all other types of abuse and neglect showed negative correlations with the volume of the CA1-3 in the hippocampal head in MDD participants. However, none of them survived correction for multiple comparisons, except for the relationship between the history of physical neglect and the volume of CA1-3 in the hippocampal head. These results further support the findings from preclinical studies of chronic stress and confirmed the vulnerability of the CA subfield to the impact of stress. Moreover, the volume of the DG in the hippocampal head and body showed non-significant negative associations with physical and sexual abuse in MDD participants, with possible impact on the hippocampal neurogenesis.

The current study provided first evidence on the underlying neuroanatomical sources of changes related to early adverse environment within the amygdala and hippocampus in MDD participants.

8.4. Healthy cognitive aging and limbic white matter tracts (chapter 7)

Background and Knowledge gaps

Overall, previous *in vivo* studies of the cingulum bundle and uncinate fasciculus in healthy aging showed that the FA and MD of these tracts decrease and increase respectively from mid-adulthood to older ages. However, most of previous age-related studies of the cingulum bundle analyzed this tract as either a homogenous single structure or two structures (the rostral + dorsal cingulum and parahippocampal cingulum [Bennett et al., 2015; Cox et al., 2016; Westlye et al., 2010]). Furthermore, the majority of previous studies used only linear and quadratic regression models to explain the age trajectory of DTI-metrics which might not explain the nature of the microstructural integrity associations with age in the cingulum bundle and uncinate fasciculus.

In contrast, the effects of the APOE polymorphism on the cingulum bundle and uncinate fasciculus were not consistent. Although some previous studies reported the negative effects of ε4 allele on the FA in cingulum (Heise et al., 2011; Smith et al., 2010) or fiber length in uncinate fasciculus (Salminen et al., 2013), others did not find a significant difference in FA or MD, when ε4 carriers were compared to the ε4 non-carriers (Laukka et al., 2015; Wang et al., 2017).

Furthermore, despite the important effects of dopamine on oligodendrocytes and myelin (Bongarzone et al., 1998; Choi et al., 2017; Rosin et al., 2005), there has been few studies that analyzed the effects of COMT polymorphism on the structural measurements of the brain white matter (for review see Witte and Flöel 2012; van Haren et al., 2008). To the best of our knowledge, there has been only one age-related study that has analyzed the effects of COMT polymorphism on brain white matter tracts (Papenberg et al., 2015).

Moreover, BDNF is a neurotrophic factor involved in neuronal survival, proliferation and differentiation, as well as synaptic growth (Papenberg et al., 2015; Petrella et al., 2008). BDNF is expressed in both neuron and glia throughout the brain and especially in the hippocampus and prefrontal cortex (Kanchibhotla et al., 2013; Papenberg et al., 2015; Petrella et al., 2008). Consequently, most imaging-genetics studies have focused on these two structures related to either functional or grey matter structural studies (for review see Papenberg et al., 2015; Petrella et al., 2008). However, some previous studies showed the effects of the BDNF polymorphism on the white matter integrity, despite some inconsistent findings (for review see Kanchibhotla et al., 2013).

The effects of SNPs on the white matter tracts in healthy aging have been less studied, compared to the grey matter and especially regarding the COMT. Finally, except for a few studies (e.g. Papenberg et al., 2015; n = 260), most of the previous DTI-genetics studies had a small sample size.

Contributions

In the present study we used manual deterministic DTI tractography to examine the association of age, sex, and APOE, COMT and BDNF polymorphisms with the microstructural properties of the cingulum bundle and uncinate fasciculus. Our findings showed that microstructural properties of most of the limbic tracts are deteriorated simultaneously in older ages. To be more specific, lower FA and the tensor shape linearity coincide with higher MD, RD and the tensor shape sphericity in the rostral cingulum, dorsal cingulum and the uncinate fasciculus, but not in the parahippocampal cingulum. These results suggest that limbic tracts might be affected differently by healthy aging. While the microstructural integrity of the rostral cingulum, dorsal cingulum and the uncinate fasciculus showed strong negative relationships with age, the parahippocampal cingulum

microstructural integrity showed a minor association with age (i.e. only negative correlation between age and AD). In addition, similar to most previous studies, we did not find sex differences in the aforementioned age-related trajectories as well.

Furthermore, in this study we used MFP procedure to depict the age-related associations. This analytical method is advantageous over linear and quadratic regression models used in previous adult studies. First, Fjell et al. (2010) indicated that studies utilizing quadratic models to estimate the parabolic appearing age trajectory of brain structures are significantly influenced by the age range of the subjects measured. The peak maxima of brain structure values, and consequently the observed age at which brain declines begin, is dependent on the bottom of the age range; as the floor of the age range decreases or increases, the age at which a measurement reaches its maximum changes respectively. Furthermore, while the age trajectory of the brain structure may be described as non-linear, this does not necessarily mean it is quadratic, and thus, more complex models need to properly define the relationship. The MFP procedure tests whether a nonlinear model is *statistically* better than a linear one. In addition to the quadratic model, MFP also tests other nonlinear models.

We did not find any effects of APOE (ε4 carriers vs ε4 non carriers) or BDNF (Val/Val vs Met carriers) polymorphisms as well as age × APOE or age × BDNF interactions on the DTI measurements of the cingulum bundle and uncinate fasciculus. However, we found COMT polymorphism effects on the FA and diffusivity parameters (i.e. MD, RD and AD) of the right rostral cingulum suggesting that Met/Met homozygous have better white matter integrity compared to the Val carriers across adult life span. To be more exact, the FA and AD were non-significantly higher in Met/Met homozygous and Val carriers compared to their counterparts respectively, and MD and RD were significantly higher in Val carriers compared to Met/Met

homozygous. However, longitudinal studies suggested age × COMT interaction effects indicating that Val homozygotes showed less cognitive deterioration compared to the Met homozygotes in aging (for review see Sambataro et al., 2012). In contrast, in the current study, we did not find any age × COMT interaction effects on the DTI-metrics of the cingulum bundle or uncinate fasciculus. Nevertheless, our findings on better microstructural integrity of the right rostral cingulum in Met homozygous are in agreement with other cross-sectional studies which showed "better cognitive profiles" in Met homozygous (for review see Sambataro et al., 2012). Future research is necessary to clarify the aforementioned potential of the age × COMT interaction effects on the frontal white matter.

8.5. Conclusion

Previous studies have reported atrophy in the CeM group of the amygdala in Alzheimer's disease patients (for a review see Wright 2009). Also, an *in vivo* study of the amygdala reported 20% to 30% atrophy in CeM group in Alzheimer's disease patients (Cavedo et al., 2011). Furthermore, although Harding et al. (2002) did not find a significant volumetric reduction in the BLA group of the amygdala, they reported a 30% volumetric reduction in the corticomedial group (i.e. Co, Me and Ce nuclei) of the amygdala in Parkinson's disease patients. However, our results suggest that the volume of the CeM group of the amygdala is almost resilient to both healthy cognitive aging and childhood maltreatment [i.e. early life stress (McLaughlin et al., 2014)]. Consequently, we suggest that an overt volumetric reduction in the CeM group of the amygdala might indicate pathological changes.

Our analysis showed that while the volume of the total amygdala and its subnuclei did not significantly differ between the left and the right hemisphere, DTI metrics of the uncinate

fasciculus were significantly different between hemispheres, suggesting more white matter integrity on the left hemisphere. Also, in contrast to the age trajectory of the uncinate fasciculus, that did not show sexual dimorphism, the age trajectory of the amygdala and most of its subnuclei was significantly different between men and women. A plausible explanation for these differences might be because besides the uncinate fasciculus, there are other white matter tracts that connect the amygdala to other brain structures, including the lateral olfactory stria, the stria terminalis and the ventral amygdalofugal pathway (Nieuwenhuys et al., 2008). However, another possibility might be an absence of correlation or some degree of independence between the white and grey matter structural properties.

Finally, our results suggest that, in contrast to the uncinate fasciculus, rostral and dorsal cingulum, FA, MD and RD of the parahippocampal cingulum were resilient to the normal aging. As we discussed in chapter 7, our findings on the absence of significant relationships between age and FA, MD and RD of the parahippocampal cingulum are in accordance with previous studies (see discussion in chapter 7). Therefore, we suggest that dramatic changes in the FA, MD and RD of the parahippocampal cingulum might indicate pathological changes.

References

Aan het Rot M, Mathew SJ, Charney DS, (2009): Neurobiological mechanisms in major depressive disorder. CMAJ 180(3):305-13. doi: 10.1503/cmaj.080697.

Abe O, Yamasue H, Yamada H, Masutani, Y, Kabasawa H, Sasaki H, Takei K, Suga M, Kasai K, Aoki S, Ohtomo K, (2010): Sex dimorphism in gray/white matter volume and diffusion tensor during normal aging. NMR Biomed. 23(5):446-458. doi: 10.1002/nbm.1479.

Achten E, Deblaere K, De Wagter C, Van Damme F, Boon P, De Reuck J, Kunnen M, (1998): Intra- and interobserver variability of MRI-based volume measurements of the hippocampus and amygdala using the manual ray-tracing method. Neuroradiology 40(9), 558–566.

Adolphs R, Tranel D, Damasio H, Damasio AR, (1995): Fear and the human amygdala. J Neurosci 15(9): 5879-5891.

Adolphs R, (2009): The social brain: neural basis of social knowledge. Annu. Rev. Psychol. 60, 693–716. doi: 10.1146/annurev.psych.60.110707.163514.

Adolphs R, (2010): What does the amygdala contribute to social cognition? Ann N Y Acad Sci 1191:42-61. doi: 10.1111/j.1749-6632.2010.05445.x.

Aghamohammadi-Sereshki A, Huang Y, Olsen F, Malykhin NV, (2018): In vivo quantification of amygdala subnuclei using 4.7 T fast spin echo imaging. Neuroimage. 170:151-163. doi: 10.1016/j.neuroimage.

Aghamohammadi-Sereshki A, Hrybouski S, Travis S, Huang Y, Olsen F, Carter R, Camicioli R, Malykhin NV, (2019): Amygdala subnuclei and healthy cognitive aging. Hum Brain Mapp. 40(1): 34-52. doi: 10.1002/hbm.24353.

Alexander AL, Hasan K, Kindlmann G, Parker DL, Tsuruda JS, (2000): A geometric analysis of diffusion tensor measurements of the human brain. Magn Reson Med. 44(2):283-91.

Allen JS, Bruss J, Brown CK, Damasio H, (2005): Normal neuroanatomical variation due to age: The major lobes and a parcellation of the temporal region. Neurobiology of Aging. 26(9): 1245–1260 discussion 1279-1282.

Amaral DG, Price J L, Pitkänen A, Carmichael ST, (1992): Anatomical organization of the primate amygdaloid complex. In: J. P. Aggleton (ed.). The amygdala. Wiley, New York, pp. 1–66.

Amaral RS, Park MTM, Devenyi GA, Lynn V, Pipitone J, Winterburn J, Chavez S, Schira M, Lobaugh NJ, Voineskos AN, Pruessner JC, Chakravarty M.M, the Alzheimer's Disease Neuroimaging Initiative, (2018): Manual segmentation of the fornix, fimbria, and alveus on high- resolution 3T MRI: Application via fully-automated mapping of the human memory circuit white and grey matter in healthy and pathological aging. NeuroImage. 170:132-150. doi: 10.1016/j.neuroimage.2016.10.027.

Amunts K Kedo O, Kindler M, Pieperhoff P, Mohlberg H, Shah NJ, Habel U, Schneider F, Zilles K, (2005): Cytoarchitectonic mapping of the human amygdala, hippocampal region and entorhinal cortex: intersubject variability and probability maps. Anat. Embryol. 210 (5–6), 343–352.

Ancelin ML, Carrière I, Artero S, Maller J, Meslin C, Ritchie K, Ryan J, Chaudieu I, (2019): Lifetime major depression and grey-matter volume. J Psychiatry Neurosci. 44(1):45-53.

Andersen SL, Tomada A, Vincow ES, Valente E, Polcari A, Teicher MH, (2008): Preliminary evidence for sensitive periods in the effect of childhood sexual abuse on regional brain

development. J Neuropsychiatry Clin Neurosci 20: 292-301. doi: 10.1176/appi.neuropsych.20.3.292.

Bach DR, Behrens TE, Garrido L, Weiskopf N, Dolan RJ, (2011): Deep and superficial amygdala nuclei projections revealed in vivo by probabilistic tractography. J. Neurosci. 31 (2), 618–623.

Barzilay R, Calkins ME, Moore TM, Wolf DH, Satterthwaite TD, Cobb Scott J, Jones JD2, Benton TD, Gur RC, Gur RE, (2019): Association between traumatic stress load, psychopathology, and cognition in the Philadelphia Neurodevelopmental Cohort. Psychol Med. 49(2):325-334. doi: 10.1017/S0033291718000880.

Basso M, Gelernter J, Yang J, MacAvoy MG, Varma P, Bronen RA, van Dyck CH, (2006): Apolipoprotein E epsilon4 is associated with atrophy of the amygdala in Alzheimer's disease. Neurobiol Aging. 27(10):1416-1424.

Beaulieu C, (2002): The basis of anisotropic water diffusion in the nervous system - a technical review. NMR Biomed. 15(7-8):435-55.

Beaulieu C, (2014): The Biological Basis of Diffusion Anisotropy. In: Johansen-Berg H, Behrens T.E.J, (eds.), Diffusion MRI: from quantitative measurement to In-vivo neuroanatomy 2nd ed. London: Elsevier Academic Press. Page: 155–183

Behl C, (2002): Oestrogen as a neuroprotective hormone. Nat Rev Neurosci. 3(6): 433-442.

Bennett IJ, Huffman DJ, Stark CE, (2015): Limbic Tract Integrity Contributes to Pattern Separation Performance Across the Lifespan. Cereb Cortex. 2015 Sep;25(9):2988-99. doi: 10.1093/cercor/bhu093.

Bennur S, Shankaranarayana Rao BS, Pawlak R, Strickland S, McEwen BS, Chattarji S, (2007): Stress-induced spine loss in the medial amygdala is mediated by tissue-plasminogen activator. Neuroscience 144: 8-16.

Bernstein DP, Fink L, (1998): Childhood Trauma Questionnaire: Retrospective Self-Report Manual. The Psychological Corporation., San Antonio, TX.

Bernstein DP, Stein JA, Newcomb MD, Walker E, Pogge D, Ahluvalia T, Stokes J, Handelsman L, Medrano M, Desmond D, Zule W, (2003): Development and validation of a brief screening version of the Childhood Trauma Questionnaire. Child Abuse Negl. 27(2): 169-90.

Berretta S, Pantazopoulos H, Lange N, (2007): Neuron Numbers and Volume of the Amygdala in Subjects Diagnosed with Bipolar Disorder or Schizophrenia. Biol Psychiatry 62: 884–893.

Bickart KC, Wright CI, Dautoff RJ, Dickerson BC, Barrett LF, (2011): Amygdala volume and social network size in humans. Nat Neurosci. 14(2):163-4. doi: 10.1038/nn.2724.

Bielau H, Trübner K, Krell D, Agelink MW, Bernstein HG, Stauch R, Mawrin C, Danos P, Gerhard L, Bogerts B, Baumann B, (2005): Volume deficits of subcortical nuclei in mood disorders A postmortem study. Eur Arch Psychiatry Clin Neurosci. 255(6): 401-12.

Blurton-Jones MM, Roberts JA, Tuszynski MH, (1999): Estrogen receptor immunoreactivity in the adult primate brain: neuronal distribution and association with p75, trkA, and choline acetyltransferase. J Comp Neurol. 405(4):529-42.

Bogerts B, Meertz E, Schonfeldt-Bausch R, (1985): Basal Ganglia and Limbic System Pathology in Schizophrenia. A morphometric study of brain volume and shrinkage. Arch Gen Psychiatry 42: 784-791.

Bogerts B, Lieberman JA, Ashtari M, Bilder RM, Degreef G, Lerner G, Johns C, Masiar S, (1993): Hippocampus-Amygdala Volumes and Psychopathology in Chronic Schizophrenia. Biol Psychiatry 33: 236-246.

Boll S, Gamer M, Gluth S, Finsterbusch J, Büchel C, (2013): Separate amygdala subregions signal surprise and predictiveness during associative fear learning in humans. Eur J Neurosci. 37(5): 758-767.

Bongarzone ER, Howard SG, Schonmann V, Campagnoni AT, (1998): Identification of the dopamine D3 receptor in oligodendrocyte precursors: potential role in regulating differentiation and myelin formation. J Neurosci. 1998 Jul 15;18(14):5344-53.

Bonilha L, Kobayashi E, Cendes F, Min Li L, (2004): Protocol for volumetric segmentation of medial temporal structures using high-resolution 3-D magnetic resonance imaging. Hum. Brain Mapp. 22 (2), 145–154.

Bonnici HM, Chadwick MJ, Kumaran D, Hassabis D, Weiskopf N, Maguire EA, (2012): Multi-voxel pattern analysis in human hippocampal subfields. Front Hum Neurosci 6:290.

Boutet C, Boutet M, Lehéricy S, Marrakchi-Kacem L, Epelbaum S, Poupon C, Wiggins C, Vignaud A, Hasboun D, Defontaines B, Hanon O, Dubois B, Sarazin M, Hertz-Pannie L, Colliot O, (2014): Detection of volume loss in hippocampal layers in Alzheimer's disease using 7 T MRI: A feasibility study. Neuroimage Clin, 5: 341-8.

Bowley MP, Drevets WC, Ongür D, Price JL, (2002): Low glial numbers in the amygdala in major depressive disorder. Biol Psychiatry. 52(5): 404-12.

Braak H, Braak E, Yilmazer D, de Vos RA, Jansen EN, Bohl J, Jellinger K, (1994): Amygdala pathology in Parkinson's disease. Acta Neuropathol. 88(6):493-500.

Brabec J, Rulseh A, Hoyt B, Vizek M, Horinek D, Hort J, Petrovicky P, (2010): Volumetry of the human amygdala—An anatomical study. Psychiatry Research, 182(1):67-72. doi: 10.1016/j.pscychresns.2009.11.005.

Brierley B, Shaw P, David AS, (2002): The human amygdala: A systematic review and meta-analysis of volumetric magnetic resonance imaging. Brain Research. Brain Research Reviews, 39(1): 84–105.

Broe GA, (2003). Population ageing, human lifespan and neurodegenerative disorders: A fifth epidemiologic transition. In: Sachdev P, (ed.), The ageing brain: The Neurobiology and Neuropsychiatry of Ageing. Publisher: Swets and Zeitlinger B, Lisse, The Netherlands. Page: 11-31.

Brown TA, DiNardo PA, Barlow DH, (1994): Anxiety Disorders Interview Schedule for DSM-IV: Adult and lifetime Version, Clinician Manual. Graywind publications., Albany, NY.

Brown TA, Di Nardo PA, Lehman CL, Campbell LA, (2001): Reliability of DSM-IV anxiety and mood disorders: implications for the classification of emotional disorders. J. Abnorm. Psychol. 110(1): 49–58.

Bubb EJ, Metzler-Baddeley C, Aggleton JP, (2018): The cingulum bundle: Anatomy, function, and dysfunction. Neurosci Biobehav Rev. 92:104-127. doi: 10.1016/j.neubiorev.2018.05.008.

Budisavljevic S, Kawadler JM, Dell'Acqua F, Rijsdijk FV, Kane F, Picchioni M, McGuire P, Toulopoulou T, Georgiades A, Kalidindi S, Kravariti E, Murray RM, Murphy DG, Craig MC, Catani M, (2016): Heritability of the limbic networks. Soc Cogn Affect Neurosci. 11(5):746-57. doi: 10.1093/scan/nsv156.

Burnham KP, Anderson DR, (2002): Model Selection and Multimodel Inference: A Practical Information-Theoretic Approach, 2nd ed. New York; Springer-Verlag.

Burzynska AZ, Preuschhof C, Bäckman L, Nyberg L, Li SC, Lindenberger U, Heekeren HR, (2010): Age-related differences in white matter microstructure: region- specific patterns of diffusivity. Neuroimage. 49(3):2104-12. doi: 10.1016/j.neuroimage.2009.09.041.

Bzdok D, Laird AR, Zilles K, Fox PT, Eickhoff SB, (2013): An Investigation of the Structural, Connectional, and Functional Subspecialization in the Human Amygdala. Human. Brain Mapp. 34(12): 3247–3266.

Caan M.W.A, (2015): DTI Analysis Methods: Fibre Tracking and Connectivity. In: Van Hecke, W., Emsell, L., Sunaert, S., (Eds.), Diffusion Tensor Imaging 1st ed. Springer, New York, 205–228.

Cahill L (2006): Why sex matters for neuroscience. Nat Rev Neurosci.7(6):477-484.

Cahill L, Aswad D, (2015): Sex Influences on the Brain: An Issue Whose Time Has Come. Neuron. 88(6):1084-1085. doi: 10.1016/j.neuron.2015.11.021.

Calem M, Bromis K, McGuire P, Morgan C, Kempton MJ, (2017): Meta-analysis of associations between childhood adversity and hippocampus and amygdala volume in non-

clinical and general population samples. Neuroimage Clin 14: 471-479. doi: 10.1016/j.nicl.2017.02.016. eCollection 2017.

Campbell S, Marriott M, Nahmias C, MacQueen GM, (2004): Lower hippocampal volume in patients suffering from depression: a meta-analysis. Am J Psychiatry 161: 598-607.

Casey G, (2013): Parkinson's disease: a long and difficult journey. Nurs N Z. 19(7): 20-4

Carlén M, (2017): What constitutes the prefrontal cortex? Science. 358(6362): 478-482. doi: 10.1126/science.aan8868.

Catani M, Howard RJ, Pajevic S, Jones DK, (2002): Virtual in vivo interactive dissection of white matter fasciculi in the human brain. Neuroimage. 17(1):77-94.

Catani M, Thiebaut de Schotten M, (2008): A diffusion tensor imaging tractography atlas for virtual in vivo dissections. Cortex. 44(8):1105-32. doi: 10.1016/j.cortex.2008.05.004.

Catani M, Dell'acqua F, Thiebaut de Schotten M, (2013): A revised limbic system model for memory, emotion and behaviour. Neurosci Biobehav Rev. 37(8):1724-37. doi: 10.1016/j.neubiorev.2013.07.001.

Cavedo E, Boccardi M, Ganzola R, Canu E, Beltramello A, Caltagirone C, Thompson PM, Frisoni GB, (2011): Local amygdala structural differences with 3T MRI in patients with Alzheimer disease. Neurology. 76(8):727-33. doi: 10.1212/WNL.0b013e31820d62d9.

Chance SA, Esiri MM, Crow TJ, (2002): Amygdala volume in schizophrenia: post-mortem study and review of magnetic resonance imaging findings. Br J Psychiatry 180: 331-338.

Chaney A, Carballedo A, Amico F, Fagan A, Skokauskas N, Meaney J, Frodl T, (2014): Effect of childhood maltreatment on brain structure in adult patients with major depressive disorder and healthy participants. J Psychiatry Neurosci. 39(1): 50-9. doi: 10.1503/jpn.120208.

Chareyron LJ, Banta Lavenex P, Amaral DG, Lavenex P, (2011): Stereological analysis of the rat and monkey amygdala. Journal of Comparative Neurology. 519(16): 3218–3239. doi: 10.1002/cne.22677.

Chen J, Lipska BK, Halim N, Ma QD, Matsumoto M, Melhem S, Kolachana BS, Hyde TM, Herman MM, Apud J, Egan MF, Kleinman JE, Weinberger DR, (2004): Functional analysis of genetic variation in catechol-O-methyltransferase (COMT): effects on mRNA, protein, and enzyme activity in postmortem human brain. Am J Hum Genet. 75(5):807-21.

Chen ST, Volle D, Jalil J, Wu P, Small GW, (2019): Health-Promoting Strategies for the Aging Brain. Am J Geriatr Psychiatry. 27(3):213-236. doi: 10.1016/j.jagp.2018.12.016.

Choi MH, Na JE, Yoon YR, Lee HJ, Yoon S, Rhyu IJ, Baik JH, (2017): Role of Dopamine D2 Receptor in Stress-Induced Myelin Loss. Sci Rep. 7(1):11654. doi: 10.1038/s41598-017-10173-9.

Coffey CE, Lucke JF, Saxton JA, Ratcliff G, Unitas LJ, Billig B, Bryan RN, (1998): Sex differences in brain aging: a quantitative magnetic resonance imaging study. Arch Neurol. 55(2):169-179.

Cohen RA, Grieve S, Hoth KF, Paul RH, Sweet L, Tate D, Gunstad J, Stroud L, McCaffery J, Hitsman B, Niaura R, Clark CR, McFarlane A, Bryant R, Gordon E, Williams LM, (2006): Early life stress and morphometry of the adult anterior cingulate cortex and caudate nuclei. Biol Psychiatry 59(10): 975-82.

Conrad CD, Ortiz JB, Judd JM, (2017): Chronic stress and hippocampal dendritic complexity: Methodological and functional considerations. Physiol Behav. 178: 66-81. doi: 10.1016/j.physbeh.2016.11.017.

Convit A, McHugh P, Wolf OT, de Leon MJ, Bobinski M, De Santi S, Roche A, Tsui W, (1999): MRI volume of the amygdala: a reliable method allowing separation from the hippocampal formation. Psychiatry Res. 90(2):113–123.

Corder EH, Lannfelt L, Viitanen M, Corder LS, Manton KG, Winblad B, Basun H, (1996): Apolipoprotein E genotype determines survival in the oldest old (85 years or older) who have good cognition. Arch Neurol. 53(5): 418-422.

Cosgrove KP, Mazure CM, Staley JK, (2007): Evolving knowledge of sex differences in brain structure, function, and chemistry. Biol Psychiatry. 62(8):847-855.

Cowell PE, Turetsky BI, Gur RC, Grossman RI, Shtasel DL, Gur RE, (1994): Sex differences in aging of the human frontal and temporal lobes. J Neurosci. 14(8):4748-4755.

Cox SR, Ritchie SJ, Tucker-Drob EM, Liewald DC, Hagenaars SP, Davies G, Wardlaw JM, Gale CR, Bastin ME, Deary IJ, (2016): Ageing and brain white matter structure in 3,513 UK Biobank participants. Nat Commun. 7:13629. doi: 10.1038/ncomms13629.

Danese A, McEwen BS, (2012): Adverse childhood experiences, allostasis, allostatic load, and age-related disease. Physiol Behav 106: 29-39. doi: 10.1016/j.physbeh.2011.08.019.

Davis M, Whalen PJ, (2001): The amygdala: vigilance and emotion. Mol Psychiatry. 6, 13-34.

Deary IJ, Wright AF, Harris SE, Whalley LJ, Starr JM, (2004): Searching for genetic influences on normal cognitive ageing. Trends in Cognitive Sciences. 8(4): 178–184.

De Bellis MD, Keshavan MS, Shifflett H, Iyengar S, Beers SR, Hall J, Moritz G, (2002): Brain structures in pediatric maltreatment-related posttraumatic stress disorder: a sociodemographically matched study. Biol Psychiatry 52(11): 1066-78.

den Heijer T, Oudkerk M, Launer LJ, van Duijn CM, Hofman A, Breteler MM, (2002): Hippocampal, amygdalar, and global brain atrophy in different apolipoprotein E genotypes. Neurology, 59(5): 746–748

Depression and Other Common Mental Disorders: Global Health Estimates. Geneva: World Health Organization; 2017. Licence: CC BY-NC-SA 3.0 IGO.

Despotović I, Goossens B, Philips W, (2015): MRI Segmentation of the Human Brain: Challenges, Methods, and Applications. Comput Math Methods Med. 2015:450341.

Dice LR, (1945): Measures of the amount of ecologic association between species. Ecology 26(3): 297–302.

Dixon RA, DeCarlo CA, MacDonald SW, Vergote D, Jhamandas J, Westaway D, (2014): APOE and COMT polymorphisms are complementary biomarkers of status, stability, and transitions in normal aging and early mild cognitive impairment. Front Aging Neurosci. 6:236. doi: 10.3389/fnagi.2014.00236.

Doraiswamy PM, Na C, Husain MM, Figiel GS, McDonald WM, Ellinwood EH Jr, Boyko OB, Krishnan KR, (1992): Morphometric changes of the human midbrain with normal aging: MR and stereologic findings. AJNR Am J Neuroradiol. 13(1):383-386.

Doty RL, (2012): Olfaction in Parkinson's disease and related disorders. Neurobiol Dis. 46(3):527-52. doi: 10.1016/j.nbd.2011.10.026.

Drevets WC, Price JL, Bardgett ME, Reich T, Todd RD, Raichle ME, (2002): Glucose metabolism in the amygdala in depression: relationship to diagnostic subtype and plasma cortisol levels. Pharmacol Biochem Behav. 71(3):431-47.

Drevets WC, (2003): Neuroimaging abnormalities in the amygdala in mood disorders. Ann N Y Acad Sci. 985:420-44.

Dutta S, Sengupta P, (2016): Men and mice: Relating their ages. Life Sci. 152, 244-8. doi: 10.1016/j.lfs.2015.10.025.

Duvernoy HM, (2005): The Human Hippocampus: Functional Anatomy, Vascularization, and Serial Sections with MRI, 3rd ed. Springer-Verlag., New York.

Duyn JH, (2012): The future of ultra-high field MRI and fMRI for study of the human brain. NeuroImage 62(2): 1241–1248. doi: 10.1016/j.neuroimage.2011.10.065.

Efron B, Tibshirani R, (1997): Improvements on cross-validation: the .632+ bootstrap method. J. Am. Stat. Assoc. 92(438):548-560.

Eickhoff SB, Thirion B, Varoquaux G, Bzdok D, (2015): Connectivity-Based Parcellation: Critique and Implications. Hum Brain Mapp. 36(12):4771-92.

Entis JJ, Doerga P, Barrett LF, Dickerson BC, (2012): A reliable protocol for the manual segmentation of the human amygdala and its subregions using ultra-high resolution MRI. Neuroimage. 60(2): 1226–1235.

Epel ES, Blackburn EH, Lin J, Dhabhar FS, Adler NE, Morrow JD, Cawthon RM, (2004): Accelerated telomere shortening in response to life stress. Proc Natl Acad Sci U S A. 101(49):17312-5.

Eritaia J, Wood SJ, Stuart GW, Bridle N, Dudgeon P, Maruff P, Velakoulis D, Pantelis C, (2000): An optimized method for estimating intracranial volume from magnetic resonance images. Magn. Reson. Med. 44(6): 973–977.

Espinoza S, Manago F, Leo D, Sotnikova TD, Gainetdinov RR, (2012): Role of catechol-O-methyltransferase (COMT)-dependent processes in Parkinson's disease and L-DOPA treatment. CNS Neurol Disord Drug Targets. 11(3):251-63.

Farrer LA, Cupples LA, Haines JL, Hyman B, Kukull WA, Mayeux R, Myers RH, Pericak-Vance MA, Risch N, van Duijn CM, (1997): Effects of age, sex, and ethnicity on the association between apolipoprotein E genotype and Alzheimer disease. A meta analysis. APOE and Alzheimer Disease Meta Analysis Consortium. JAMA. 278(16):1349-1356.

Fatterpekar GM, Naidich TP, Delman BN, Aguinaldo JG, Gultekin SH, Sherwood CC, Hof, PR, (2002): Cytoarchitecture of the Human Cerebral Cortex: MR Microscopy of Excised Specimens at 9.4 Tesla. AJNR Am J Neuroradiol. 23(8): 1313-21.

Filipek PA, Semrud-Clikeman M, Steingard RJ, Renshaw PF, Kennedy DN, Biederman J, (1997): Volumetric MRI analysis comparing subjects having attention-deficit disorder with normal controls. Neurology 48(3): 589–601.

Fjell AM, Westlye LT, Amlien I, Espeseth T, Reinvang I, Raz N, Agartz I, Salat DH, Greve DN, Fischl B, Dale AM, Walhovd KB, (2009): Minute effects of sex on the aging brain: A multisample magnetic resonance imaging study of healthy aging and Alzheimer's disease. The Journal of Neuroscience, 29(27): 8774–8783. doi: 10.1523/JNEUROSCI.0115-09.2009.

Fjell AM, Walhovd KB, Westlye LT, Østby Y, Tamnes CK, Jernigan TL, Gamst A, Dale AM, (2010): When does brain aging accelerate? Dangers of quadratic fits in cross-sectional studies. Neuroimage. 50(4):1376-83. doi: 10.1016/j.neuroimage.2010.01.061.

Fjell AM, Walhovd KB, (2010). Structural brain changes in aging: Courses, causes and cognitive consequences. Reviews in the Neurosciences. 21(3): 187–221.

Fjell AM, Westlye LT, Grydeland H, Amlien I, Espeseth T, Reinvang I, Raz N, Holland D, Dale AM, Walhovd KB, Alzheimer Disease Neuroimaging Initiative, (2013): Critical ages in the life course of the adult brain: nonlinear subcortical aging. Neurobiol Aging. 34(10):2239-2247. doi: 10.1016/j.neurobiolaging.2013.04.006.

Foley PB, (2019): Dopamine in psychiatry: a historical perspective. J Neural Transm (Vienna). 126(4):473-479. doi: 10.1007/s00702-019-01987-0.

Freese JL, Amaral DG, (2009): Neuroanatomy of the primate amygdala. In: Whalen PJ, Phelps EA, (Eds.), The human amygdala. New York: The Guilford Press. Page: 3-42.

Frodl T, Meisenzahl E, Zetzsche T, Bottlender R, Born C, Groll C, Jäger M, Leinsinger G, Hahn K, Möller HJ, (2002): Enlargement of the amygdala in patients with a first episode of major depression. Biol Psychiatry 51(9): 708-14.

Frodl T, Meisenzahl EM, Zetzsche T, Born C, Jäger M, Groll C, Bottlender R, Leinsinger G, Möller HJ, (2003): Larger amygdala volumes in first depressive episode as compared to recurrent major depression and healthy control subjects. Biol Psychiatry. 53(4) 338-44.

Frodl T, Jäger M, Smajstrlova I, Born C, Bottlender R, Palladino T, Reiser M, Möller HJ, Meisenzahl EM, (2008): Effect of hippocampal and amygdala volumes on clinical outcomes in

major depression: a 3-year prospective magnetic resonance imaging study. J Psychiatry Neurosci 33(5): 423-30.

Gainotti G, (2018): Emotions and the Right Hemisphere: Can New Data Clarify Old Models?. Neuroscientist. 25(3), 258-270. doi: 10.1177/1073858418785342.

Galvin JE, Roe CM, Coats MA, Morris JC, (2007): Patient's rating of cognitive ability: using the AD8, a brief informant interview, as a self-rating tool to detect dementia. Arch Neurol. 64(5):725-730.

García-Amado M, Prensa L, (2012): Stereological analysis of neuron, glial and endothelial cell numbers in the human amygdaloid complex. PLoS One 7 (6), e38692.

Giedd JN, Castellanos FX, Rajapakse J, Vaituzis CA, Rapoport J, (1997): Sexual dimorphism of the developing human brain. Prog.Neuro-Psychopharmacol and Biol Psychiatry. 21(8): 1185-201.

Goldman D, Oroszi G, Ducci F, (2005): The genetics of addictions: uncovering the genes. Nat Rev Genet. 6(7):521-32.

Goldstein JM, Seidman LJ, Horton NJ, Makris N, Kennedy DN, Caviness VS Jr, Faraone SV, Tsuang MT, (2001): Normal sexual dimorphism of the adult human brain assessed by in vivo magnetic resonance imaging. Cereb Cortex 11(6): 490-497.

Good CD, Johnsrude I, Ashburner J, Henson RN, Friston KJ, Frackowiak RS, (2001): Cerebral asymmetry and the effects of sex and handedness on brain structure: a voxel-based morphometric analysis of 465 normal adult human brains. NeuroImage. 14(3); 685–700.

Goubran M, Rudko DA, Santyr B, Gati J, Szekeres T, Peters TM, Khan AR, (2014): In vivo normative atlas of the hippocampal subfields using multi-echo susceptibility imaging at 7 T. Hum. Brain Mapp. 35(8): 3588–3601.

Grant MM, Cannistraci C, Hollon SD, Gore J, Shelton R, (2011): Childhood trauma history differentiates amygdala response to sad faces within MDD. J Psychiatr Res. 45(7): 886-95. doi: 10.1016/j.jpsychires.2010.12.004.

Grieve SM, Korgaonkar MS, Clark CR, Williams LM, (2011): Regional heterogeneity in limbic maturational changes: Evidence from integrating cortical thickness, volumetric and diffusion tensor imaging measures. NeuroImage. 55(3): 868–879.

Gur RC, Bockow T, Gur RE, (2010): Gender Differences in the Functional Organization of the Brain. In: Legato MJ, (Ed.). Principles of Gender-Specific Medicine 2nd ed. Elsevier Academic Press, San Diego. p 75-86.

Hachinski VC, Iliff LD, Zilhka E, Du Boulay GH, McAllister VL, Marshall J, Russell RW, Symon L, (1975): Cerebral blood flow in dementia. Arch Neurol. 32(9):632-637.

Hajek T, Kopecek M, Kozeny J, Gunde E, Alda M, Höschl C (2009): Amygdala volumes in mood disorders--meta-analysis of magnetic resonance volumetry studies. J Affect Disord 115(3): 395-410.

Hamann S, Herman RA, Nolan CL, Wallen K, (2004): Men and women differ in amygdala response to visual sexual stimuli. Nat Neurosci. 7(4):411-416.

Hamilton JP, Siemer M, Gotlib IH (2008): Amygdala volume in major depressive disorder: a meta-analysis of magnetic resonance imaging studies. Mol Psychiatry 13(11): 993-1000.

Hammen C, Henry R, Daley SE (2000): Depression and sensitization to stressors among young women as a function of childhood adversity. J Consult Clin Psychol 68(5): 782-7.

Hampton AN, Adolphs R, Tyszka MJ, O'Doherty JP, (2007): Contributions of the amygdala to reward expectancy and choice signals in human prefrontal cortex. Neuron. 55(4): 545–555.

Harding AJ, Stimson E, Henderson JM, Halliday GM, (2002): Clinical correlates of selective pathology in the amygdala of patients with Parkinson's disease. Brain. 125(Pt 11):2431-45.

Hart H, Rubia K, (2012): Neuroimaging of child abuse: a critical review. Front Hum Neurosci. 6:52. doi: 10.3389/fnhum.2012.00052. eCollection 2012.

Hasan KM, Iftikhar A, Kamali A, Kramer LA, Ashtari M, Cirino PT, Papanicolaou AC, Fletcher JM, Ewing-Cobbs L, (2009): Development and aging of the healthy human brain uncinate fasciculus across the lifespan using diffusion tensor tractography. Brain Res. 1276:67-76. doi: 10.1016/j.brainres.2009.04.025.

Hashimoto M, Yasuda M, Tanimukai S, Matsui M, Hirono N, Kazui H, Mori E (2001): Apolipoprotein E epsilon 4 and the pattern of regional brain atrophy in Alzheimer's disease. Neurology. 57(8):1461-1466.

He W, Goodkind D, Kowal P, U.S. Census Bureau, (2016): An Aging World: 2015. U.S. Government Publishing Office, Washington, DC.

Heckers S, Heinsen H, Heinsen YC, Beckmann H, (1990): Limbic structures and lateral ventricle in schizophrenia. A quantitative postmortem study. Archives of General Psychiatry. 47(11): 1016–1022.

Hein TC, Monk CS (2017): Research Review: Neural response to threat in children, adolescents, and adults after child maltreatment - a quantitative meta-analysis. J Child Psychol Psychiatry. 58(3): 222-230. doi: 10.1111/jcpp.12651.

Heise V, Filippini N, Ebmeier KP, Mackay CE, (2011): The APOE ε4 allele modulates brain white matter integrity in healthy adults. Mol Psychiatry. 16(9):908-16. doi: 10.1038/mp.2010.90.

Henry TR, Chupin M, Lehericy S, Strupp JP, Sikora MA, Sha ZY, Ugurbil K, Van de Moortele PF, (2011): Hippocampal sclerosis in temporal lobe epilepsy: findings at 7 T. Radiology 261 (1), 199–209.

Hesterberg T, Moore DS, Monagham S, Clipson A and Epstein R, (2009): Bootstrap Methods and Permutation Tests. In: Moore DS, McCabe GP, Craig BA, (Eds.). Introduction to the Practice of Statistics. 6th ed. New York: W.H. Freeman. p 16_1-16_60.

Hibar DP, Stein JL, Renteria ME, Arias-Vasquez A, Desrivières S, Jahanshad N, et al., (2015). Common genetic variants influence human subcortical brain structures. Nature, 520(7546): 224–229. doi: 10.1038/nature14101.

Highley JR, Walker MA, Esiri MM, Crow TJ, Harrison PJ, (2002): Asymmetry of the uncinate fasciculus: a post-mortem study of normal subjects and patients with schizophrenia. Cereb Cortex. 12(11):1218-24.

Honea RA, Vidoni E, Harsha A, Burns JM, (2009): Impact of APOE on the healthy aging brain: a voxel-based MRI and DTI study. J Alzheimers Dis. 18(3):553-64. doi: 10.3233/JAD-2009-1163.

Hovens JG, Wiersma JE, Giltay EJ, van Oppen P, Spinhoven P, Penninx BW, Zitman FG (2010): Childhood life events and childhood trauma in adult patients with depressive, anxiety and comorbid disorders vs. controls. Acta Psychiatr Scand 122(1): 66-74.

Hrybouski S, Aghamohammadi-Sereshki A, Madan CR, Shafer AT, Baron CA, Seres P, Beaulieu C, Olsen F, Malykhin NV, (2016): Amygdala subnuclei response and connectivity during emotional processing. Neuroimage. 133:98-110. doi: 10.1016/j.neuroimage.2016.02.056.

Huang Y, Coupland NJ, Lebel RM, Carter R, Seres P, Wilman AH, Malykhin NV, (2013): Structural changes in hippocampal subfields in major depressive disorder: a high-field magnetic resonance imaging study. Biol Psychiatry. 74(1): 62-8. doi: 10.1016/j.biopsych.2013.01.005.

Hughes CP, Berg L, Danziger WL, Coben LA, Martin RL, (1982): A new clinical scale for the staging of dementia. Br J Psychiatry.140:566-572.

Humphrey T, (1968): The development of the human amygdala during early embryonic life. J Comp Neurol. 132(1):135-165.

Humphreys KL, Zeanah CH, (2015): Deviations from the expectable environment in early childhood and emerging psychopathology. Neuropsychopharmacology. 40(1): 154-70. doi: 10.1038/npp.2014.165.

Insausti R, Marcos MP, Mohedano-Moriano A, Arroyo-Jiménez MM, Córcoles-Parada M, Artacho-Pérula E, Ubero-Martínez MM, Munoz-López M, (2017): The Nonhuman Primate Hippocampus: Neuroanatomy and Patterns of Cortical Connectivity. In: Hannula, D.E., Duff,

M.C. (Eds.), The Hippocampus from Cells to Systems. Springer International Publishing., Switzerland. Page: 3–36.

Jäncke L, Mérillat S, Liem F, Hänggi J, (2015): Brain size, sex, and the aging brain. Hum Brain Mapp. 36(1):150-69. doi: 10.1002/hbm.22619.

Jang SH, Kim SH, Kim OR, Byun WM, Kim MS, Seo JP, Chang MC, (2013): Cingulum injury in patients with diffuse axonal injury: a diffusion tensor imaging study. Neurosci Lett. 543:47-51. doi: 10.1016/j.neulet.2013.02.058.

Jang SH, Kwon YH, Lee MY, Kim JR, Seo JP, (2016): Aging of the cingulum in the human brain: Preliminary study of a diffusion tensor imaging study. Neurosci Lett. 610:213-7. doi: 10.1016/j.neulet.2015.11.018.

Jazin E, Cahill L, (2010): Sex differences in molecular neuroscience: from fruit flies to humans. Nat Rev Neurosci. 11(1): 9-17. doi: 10.1038/nrn2754.

Jernigan TL, Archibald SL, Fennema-Notestine C, Gamst AC, Stout JC, Bonner J, Hesselink JR, (2001): Effects of age on tissues and regions of the cerebrum and cerebellum. Neurobiology of Aging. 22(4): 581–594.

Johnston JB, (1923): Further contributions to the study of the evolution of the forebrain. J. Comp. Neurol. 35: 337–482.

Kanchibhotla SC, Mather KA, Wen W, Schofield PR, Kwok JB, Sachdev PS, (2013): Genetics of ageing-related changes in brain white matter integrity - a review. Ageing Res Rev. 12(1):391-401. doi: 10.1016/j.arr.2012.10.003.

Karchemskiy A, Garrett A, Howe M, Adleman N, Simeonova DI, Alegria D, Reiss A, Chang K, (2011): Amygdalar, hippocampal, and thalamic volumes in youth at high risk for development of bipolar disorder. Psychiatry Res. 194(3):319-325. doi: 10.1016/j.pscychresns.2011.03.006.

Kempermann G, Gage FH, Aigner L, Song H, Curtis MA, Thuret S, Kuhn HG, Jessberger S, Frankland PW, Cameron HA, Gould E, Hen R, Abrous DN, Toni N, Schinder AF, Zhao X, Lucassen PJ, Frisén J, (2018): Human Adult Neurogenesis: Evidence and Remaining Questions. Cell Stem Cell. 2391): 25-30. doi: 10.1016/j.stem.2018.04.004.

Kerchner GA, Deutsch GK, Zeineh M, Dougherty RF, Saranathan M, Rutt BK, (2012): Hippocampal CA1 apical neuropil atrophy and memory performance in Alzheimer's disease. Neuroimage 63(1):194-202.

Kessler RC, (1997): The effects of stressful life events on depression. Annu Rev Psychol. 48:191-214.

Khundakar AA, Thomas AJ, (2014): Cellular morphometry in late-life depression: a review of postmortem studies. Am J Geriatr Psychiatry. 22(2): 122-32. doi: 10.1016/j.jagp.2013.06.003.

Kim J, Basak JM, Holtzman DM, (2009): The role of apolipoprotein E in Alzheimer's disease. Neuron. 63(3):287-303. doi: 10.1016/j.neuron.2009.06.026.

Koolschijn PC, van Haren NE, Lensvelt-Mulders GJ, Hulshoff Pol HE, Kahn RS (2009): Brain volume abnormalities in major depressive disorder: a meta-analysis of magnetic resonance imaging studies. Hum Brain Mapp 30(11): 3719-35.

Krasuski JS, Alexander GE, Horwitz B, Daly EM, Murphy DG, Rapoport SI, Schapiro MB, (1998): Volumes of medial temporal lobe structures in patients with Alzheimer's disease and mild cognitive impairment (and in healthy controls). Biol Psychiatry. 43(1):60-8.

Kromer VLJ, Hyman BT, Van Hoesen GW, Damasio AR, (1990): Pathological alterations in the amygdala in Alzheimer's disease. Neuroscience 37(2): 377–385.

Kronenberg G, Tebartz van Elst L, Regen F, Deuschle M, Heuser I, Colla M, (2009): Reduced amygdala volume in newly admitted psychiatric in- patients with unipolar major depression. J Psychiatr Res 43(11): 1112-7. doi: 10.1016/j.jpsychires.2009.03.007.

Kurth F, Cherbuin N, Luders E, (2019): Age but no sex effects on subareas of the amygdala. Hum Brain Mapp. 40(6):1697-1704. doi: 10.1002/hbm.24481.

Laakso MP, Partanen K, Lehtovirta M, Hallikainen M, Hänninen T, Vainio P, Riekkinen P Sr, Soininen H, (1995): MRI of amygdala fails to diagnose early Alzheimer's disease. Neuroreport. 6(17):2414-8.

Lahiri DK, Sambamurti K, Bennett DA, (2004): Apolipoprotein gene and its interaction with the environmentally driven risk factors: molecular, genetic and epidemiological studies of Alzheimer's disease. Neurobiol Aging. 25(5):651-660.

La Joie R, Fouquet M, Mézenge F, Landeau B, Villain N, Mevel K, Pélerin A, Eustache F, Desgranges B, Chételat G, (2010): Differential effect of age on hippocampal subfields assessed using a new high resolution 3T MR sequence. NeuroImage. 53 (2), 506–514.

Landis JR, Koch GG, (1977): The measurement of observer agreement for categorical data. Biometrics. 33 (1), 159–174.

Laukka EJ, Lövdén M, Kalpouzos G, Papenberg G, Keller L, Graff C, Li TQ, Fratiglioni L, Bäckman L, (2015): Microstructural White Matter Properties Mediate the Association between APOE and Perceptual Speed in Very Old Persons without Dementia. PLoS One. 2015 Aug 7;10(8): e0134766. doi: 10.1371/journal.pone.0134766. eCollection 2015.

Lebel C, Gee M, Camicioli R, Wieler M, Martin W, Beaulieu C, (2012): Diffusion tensor imaging of white matter tract evolution over the lifespan. Neuroimage. 60(1):340-52. doi: 10.1016/j.neuroimage.2011.11.094.

LeDoux JE, (2007): The amygdala. Current Biology 17(20): R868-R874.

LeDoux JE, Schiller D, (2009): The human amygdala insight from other anmals. In: Whalen PJ, Phelps EA, (Eds.), The Human Amygdala. The Guilford Press, New York. Page: 43–60.

Lee JK, Johnson EG, Ghetti S, (2017): Hippocampal Development: Structure, Function and Implications. In: Hannula, D.E., Duff, M.C. (Eds.), The Hippocampus from Cells to Systems. Springer International Publishing., Switzerland. Page: 141–166.

Lehericy S, Baulac M, Chiras J, Pierot L, Martin N, Pillon B, Deweer B, Dubois B, Marsault C, (1994): Amygdalohippocampal MR volume measurements in the early stages of Alzheimer disease. AJNR Am. J. Neuroradiol 15(5): 929–937.

Leuner B, Gould E, (2010): Structural plasticity and hippocampal function. Annu Rev Psychol 61:111-140, C1-3. doi: 10.1146/annurev.psych.093008.100359.

Li W, van Tol MJ, Li M, Miao W, Jiao Y, Heinze HJ, Bogerts B, He H, Walter M, (2014): Regional specificity of sex effects on subcortical volumes across the lifespan in healthy aging. Hum Brain Mapp. 35(1):238-247. doi: 10.1002/hbm.22168.

Lim L, Radua J, Rubia K, (2014): Gray matter abnormalities in childhood maltreatment: a voxel- wise meta-analysis. Am J Psychiatry 171(8): 854-63. doi: 10.1176/appi.ajp.2014.13101427.

Lindert J, von Ehrenstein OS, Grashow R, Gal G, Braehler E, Weisskopf MG, (2014): Sexual and physical abuse in childhood is associated with depression and anxiety over the life course: systematic review and meta-analysis. Int J Public Health 59(2): 359-72.

Looi JCL, Sachdev PS, (2003): Structural neuroimaging of the ageing brain. In: Sachdev PS, (Ed.). The ageing brain: the neurobiology and neuropsychiatry of ageing. Netherlands: Swets and Zeitlinger PUBLISHERS. Page: 49-63.

Lorenzetti V, Allen NB, Fornito A, Yücel M (2009): Structural brain abnormalities in major depressive disorder: a selective review of recent MRI studies. J Affect Disord 117 (1-2): 1-17.

Luft AR, Skalej M, Schulz JB, Welte D, Kolb R, Bürk K, Klockgether T, Voight K, (1999): Patterns of age-related shrinkage in cerebellum and brainstem observed in vivo using three-dimensional MRI volumetry. Cereb Cortex. 9(7): 712-721.

Lupien SJ, McEwen BS, Gunnar MR, Heim C, (2009): Effects of stress throughout the lifespan on the brain, behaviour and cognition. Nat Rev Neurosci. 10(6): 434-45. doi: 10.1038/nrn2639.

Lupien SJ, Parent S, Evans AC, Tremblay RE, Zelazo PD, Corbo V, et al. (2011): Larger amygdala but no change in hippocampal volume in 10- year-old children exposed to maternal depressive symptomatology since birth. Proc Natl Acad Sci U S A 108(34): 14324-9. doi: 10.1073/pnas.1105371108.

Lupien SJ, Juster RP, Raymond C, Marin MF, (2018): The effects of chronic stress on the human brain: From neurotoxicity, to vulnerability, to opportunity. Front Neuroendocrinol. 49: 91-105. doi: 10.1016/j.yfrne.2018.02.001.

Mai JK, Paxinos G, Voss T, (2008): Atlas of the Human Brain 3rd ed. Elsevier Academic Press, New York. Page: 135–167.

Makkinejad N, Schneider JA, Yu J, Leurgans SE, Kotrotsou A, Evia AM, Bennett DA, Arfanakis K, (2019): Associations of amygdala volume and shape with transactive response DNA-binding protein 43 (TDP-43) pathology in a community cohort of older adults. Neurobiol Aging. 77:104-111. doi: 10.1016/j.neurobiolaging.2019.01.022.

Makris N, Meyer JW, Bates JF, Yeterian EH, Kennedy DN, Caviness VS, (1999): MRI-based topographic parcellation of human cerebral white matter and nuclei II. Rationale and applications with systematics of cerebral connectivity. Neuroimage. 9(1), 18–45.

Malhi GS, Mann JJ, (2018): Depression. Lancet. 392(10161):2299-2312. doi: 10.1016/S0140-6736(18)31948-2.

Malykhin NV, Bouchard TP, Ogilvie CJ, Coupland NJ, Seres P, Camicioli R, (2007): Three-dimensional volumetric analysis and reconstruction of amygdala and hippocampal head, body and tail. Psychiatry Res: Neuroimaging. 155(2): 155–165.

Malykhin NV, Bouchard TP, Camicioli R, Coupland NJ, (2008a): Aging hippocampus and amygdala. NeuroReport. 19(5): 543–547. doi: 10.1097/WNR.0b013e3282f8b18c.

Malykhin N, Concha L, Seres P, Beaulieu C, Coupland NJ, (2008b): Diffusion tensor imaging tractography and reliability analysis for limbic and paralimbic white matter tracts. Psychiatry Res. 164(2):132-42. doi: 10.1016/j.pscychresns.2007.11.007.

Malykhin NV, Lebel RM, Coupland NJ, Wilman AH, Carter R, (2010a): In vivo quantification of hippocampal subfields using 4.7 T fast spin echo imaging. Neuroimage. 49(2): 1224-30. doi: 10.1016/j.neuroimage.2009.09.042.

Malykhin NV, Carter R, Seres P, Coupland NJ, (2010b): Structural changes in the hippocampus in major depressive disorder: contributions of disease and treatment. J Psychiatry Neurosci. 35(5): 337-43. doi: 10.1503/jpn.100002.

Malykhin NV, Carter R, Hegadoren KM, Seres P, Coupland NJ (2012): Fronto-limbic volumetric changes in major depressive disorder. J Affect Disord 136(3): 1104-13. doi: 10.1016/j.jad.2011.10.038.

Malykhin NV, Coupland NJ, (2015): Hippocampal neuroplasticity in major depressive disorder. Neuroscience 309: 200-13.

Malykhin NV, Huang Y, Hrybouski S, Olsen F, (2017): Differential vulnerability of hippocampal subfields and anteroposterior hippocampal subregions in healthy cognitive aging. Neurobiol Aging. 59:121-134. doi: 10.1016/j.neurobiolaging.2017.08.001.

Mammarella N, Di Domenico A, Fairfield B, (2016): Aging and the genetic road towards the positivity effect in memory. Exp Gerontol. 82:120-4. doi: 10.1016/j.exger.2016.06.011.

Marcuzzo S, Dall'oglio A, Ribeiro MF, Achaval M, Rasia-Filho AA, (2007): Dendritic spines in the posterodorsal medial amygdala after restraint stress and ageing in rats. Neurosci Lett 424(1): 16-21.

Mather M, Knight MR, (2006): Angry faces get noticed quickly: threat detection is not impaired among older adults. J Gerontol B Psychol Sci Soc Sci. 61(1):54-57.

Mather M, (2016): The Affective Neuroscience of Aging. Annu Rev Psychol. 67:213-38. doi: 10.1146/annurev-psych-122414-033540.

Matsuoka Y, Mori E, Inagaki M, Kozaki, Y, Nakano T, Wenner M, Uchitomi Y, (2003): Manual tracing guideline for volumetry of hippocampus and amygdala with high-resolution MRI. No Shinkei 55 (8), 690–697.

McCrory EJ, Viding E, (2015): The theory of latent vulnerability: Reconceptualizing the link between childhood maltreatment and psychiatric disorder. Dev Psychopathol. 27(2): 493-505. doi: 10.1017/S0954579415000115.

McCrory EJ, Gerin MI, Viding E, (2017): Annual Research Review: Childhood maltreatment, latent vulnerability and the shift to preventative psychiatry – the contribution of functional brain imaging. J Child Psychol Psychiatry. 58(4): 338-357. doi: 10.1111/jcpp.12713.

McEwen BS, Bowles NP, Gray JD, Hill MN, Hunter RG, Karatsoreos IN, Nasca C, (2015): Mechanisms of stress in the brain. Nat Neurosci. 18(10): 1353-63. doi: 10.1038/nn.4086.

McGraw KO, Wong SP, (1996): Forming inferences about some intraclass correlation coefficients. Psychological Methods. 1: 30–46.

McLaughlin KA, Sheridan MA, Lambert HK, (2014): Childhood adversity and neural development: deprivation and threat as distinct dimensions of early experience. Neurosci Biobehav Rev. 47: 578-91.

McMenamin BW, Marsolek CJ, (2013): Can theories of visual representation help to explain asymmetries in amygdala function? Cogn Affect Behav Neurosci. 13(2): 211-24. doi: 10.3758/s13415-012-0139-1.

Mechelli A, Friston KJ, Frackowiak RS, Price CJ, (2005): Structural Covariance in the Human Cortex. J Neurosci 25(36): 8303– 8310.

Mehta MA, Golembo NI, Nosarti C, Colvert E, Mota A, Williams SC, et al. (2009): Amygdala, hippocampal and corpus callosum size following severe early institutional deprivation: the English and Romanian Adoptees study pilot. J Child Psychol Psychiatry. 50(8): 943-51. doi: 10.1111/j.1469-7610.2009.02084.x.

Michielse S, Coupland N, Camicioli R, Carter R, Seres P, Sabino J, Malykhin N, (2010): Selective effects of aging on brain white matter microstructure: a diffusion tensor imaging tractography study. Neuroimage. 52(4):1190-201. doi: 10.1016/j.neuroimage.2010.05.019.

Mier D, Kirsch P, Meyer-Lindenberg A, (2009): Neural substrates of pleiotropic action of genetic variation in COMT: a meta-analysis. Mol Psychiatry. 15(9):918-27. doi: 10.1038/mp.2009.36.

Mobley AS, Rodriguez-Gil DJ, Imamura F, Greer CA, (2014): Aging in the olfactory system. Trends Neurosci. 37(2):77-84. doi: 10.1016/j.tins.2013.11.004.

Moore DS, McCabe GP, Craig BA, (2009): Introduction to the Practice of Statistics. 6th ed. New York: W.H. Freeman. Page: 607- 636.

Moreno N, González A, (2007): Evolution of the amygdaloid complex in vertebrates, with special reference to the anamnio-amniotic transition. J Anat. 211(2):151-163.

Morgane PJ, Galler JR, Mokler DJ, (2005): A review of systems and networks of the limbic forebrain/limbic midbrain. Prog Neurobiol. 75(2):143-60.

Morey RA, Petty CM, Xu Y, Hayes JP, Wagner HR 2nd, Lewis DV, LaBar KS, Styner M, McCarthy G, (2009): A comparison of automated segmentation and manual tracing for quantifying hippocampal and amygdala volumes. Neuroimage. 45(3): 855-66.

Moroney JT, Bagiella E, Desmond DW, Hachinski VC, Mölsä PK, Gustafson L, Brun A, Fischer P, Erkinjuntti T, Rosen W, Paik MC, Tatemichi TK, (1997): Meta-analysis of the Hachinski Ischemic Score in pathologically verified dementias. Neurology. 49(4): 1096-1105.

Mori S, Kageyama Y, Hou Z, Aggarwal M, Patel J, Brown T, Miller MI, Wu D, Troncoso JC, (2017): Elucidation of White Matter Tracts of the Human Amygdala by Detailed Comparison between High-Resolution Postmortem Magnetic Resonance Imaging and Histology. Front Neuroanat. 11:16. doi: 10.3389/fnana.2017.00016. eCollection 2017.

Mu Q, Xie J, Wen Z, Weng Y, Shuyun Z, (1999): A quantitative MR study of the hippocampal formation, the amygdala, and the temporal horn of the lateral ventricle in healthy subjects 40 to 90 years of age. AJNR. American Journal of Neuroradiology. 20(2): 207–211.

Mueller SG, Stables L, Du AT, Schuff N, Truran D, Cashdollar N, Weiner MW, (2007): Measurement of hippocampal subfields and age-related changes with high resolution MRI at 4 T. Neurobiol Aging 28(5): 719-26.

Murphy DG, DeCarli C, McIntosh AR, Daly E, Mentis MJ, Pietrini P, Szczepanik J, Schapiro MB, Grady CL, Horwitz B, Rapoport SI, (1996): Sex differences in human brain morphometry and metabolism: An in vivo quantitative magnetic resonance imaging and positron emission tomography study on the effect of aging. Archives of General Psychiatry. 53(7): 585–594.

Murray EA, Wise SP, Drevets WC, (2011): Localization of dysfunction in major depressive disorder: prefrontal cortex and amygdala. Biol Psychiatry. 69(12): e43-54. doi: 10.1016/j.biopsych.2010.09.041.

Myöhänen TT, Männistö PT, (2010): Distribution and functions of catechol-O-methyltransferase proteins: do recent findings change the picture? Int Rev Neurobiol. 95:29-47. doi: 10.1016/B978-0-12-381326-8.00003-X.

Nasreddine ZS, Phillips NA, Bédirian V, Charbonneau S, Whitehead V, Collin I, Cummings JL, Chertkow H, (2005): The Montreal Cognitive Assessment, MoCA: a brief screening tool for mild cognitive impairment. J Am Geriatr Soc. 53(4): 695-699.

Nieuwenhuys R, Voogd J, van Huijzen CA, (2008): Greater Limbic System. In: The Human Central Nervous System. Berlin: Springer. Page: 401-426; 916–923.

Nordenskjöld R, Malmberg F, Larsson EM, Simmons A, Ahlström H, Johansson L, Kullberg J, (2015): Intracranial volume normalization methods: Considerations when investigating gender differences in regional brain volume. Psychiatry Research 231(3): 227-35. doi: 10.1016/j.pscychresns.2014.11.011.

Oldfield RC, (1971): The assessment and analysis of handedness: the Edinburgh inventory. Neuropsychologia. 9(1):97-113.

Oldfield RC, (1971): The assessment and analysis of handedness: the Edinburgh inventory. Neuropsychologia. 9(1): 97–113.

Opel N, Redlich R, Zwanzger P, Grotegerd D, Arolt V, Heindel W, Konrad C, Kugel H, Dannlowski U, (2014): Hippocampal atrophy in major depression: a function of childhood maltreatment rather than diagnosis? Neuropsychopharmacology. 39(12): 2723-31. doi: 10.1038/npp.2014.145.

Olson IR, Von Der Heide RJ, Alm KH, Vyas G, (2015): Development of the uncinate fasciculus: Implications for theory and developmental disorders. Dev Cogn Neurosci. 14:50-61. doi: 10.1016/j.dcn.2015.06.003.

Osterlund MK, Gustafsson JA, Keller E, Hurd YL, (2000a): Estrogen receptor beta (ERbeta) messenger ribonucleic acid (mRNA) expression within the human forebrain: distinct distribution pattern to ERalpha mRNA. J Clin Endocrinol Metab. 85(10):3840-6.

Osterlund MK, Keller E, Hurd YL, (2000b): The human forebrain has discrete estrogen receptor alpha messenger RNA expression: high levels in the amygdaloid complex. Neuroscience. 95(2):333-42.

Otte C, Gold SM, Penninx BW, Pariante CM, Etkin A, Fava M, Mohr DC, Schatzberg AF, (2016): Major depressive disorder. Nat Rev Dis Primers. 2:16065. doi: 10.1038/nrdp.2016.65.

Papenberg G, Lövdén M, Laukka EJ, Kalpouzos G, Keller L, Graff C, Köhncke Y, Li TQ, Fratiglioni L, Bäckman L, (2015): Magnified effects of the COMT gene on white-matter

microstructure in very old age. Brain Struct Funct. 220(5):2927-38. doi: 10.1007/s00429-014-0835-4.

Papenberg G, Salami A, Persson J, Lindenberger U, Bäckman L, (2015): Genetics and functional imaging: effects of APOE, BDNF, COMT, and KIBRA in aging. Neuropsychol Rev. 25(1):47-62. doi: 10.1007/s11065-015-9279-8.

Paquola C, Bennett MR, Lagopoulos J, (2016): Understanding heterogeneity in grey matter research of adults with childhood maltreatment-A meta-analysis and review. Neurosci Biobehav Rev 69: 299-312. doi: 10.1016/j.neubiorev.2016.08.011.

Parekh MB, Rutt BK, Purcell R, Chen Y, Zeineh MM, (2015): Ultra-high resolution in-vivo 7.0 T structural imaging of the human hippocampus reveals the endfolial pathway. Neuroimage. 15; 112: 1-6.

Patel PD, Lopez JF, Lyons DM, Burke S, Wallace M, Schatzberg AF, (2000): Glucocorticoid and mineralocorticoid receptor mRNA expression in squirrel monkey brain. J Psychiatr Res. 34(6): 383-92.

Paxinos G, Watson W, (2005): The Rat Brain in Stereotaxic Coordinates, 5th edn. Elsevier Academic Press, Amsterdam. Page: XXX.

Petrella JR, Mattay VS, Doraiswamy PM, (2008). Imaging genetics of brain longevity and mental wellness: The next frontier? Radiology. 246(1): 20–32.

Phelps EA, LeDoux JE, (2005): Contributions of the amygdala to emotion processing: from animal models to human behavior. Neuron 48(2): 175-187.

Pietzuch M, King AE, Ward DD, Vickers JC, (2019): The Influence of Genetic Factors and Cognitive Reserve on Structural and Functional Resting-State Brain Networks in Aging and Alzheimer's Disease. Front Aging Neurosci. 11:30. doi: 10.3389/fnagi.2019.00030.

Pitkänen A, Savander V, LeDoux JE, (1997): Organization of intra-amygdaloid circuitries in the rat: an emerging framework for understanding functions of the amygdala. Trends Neurosci, 20(11): 517–523.

Pittenger C, Duman RS, (2008): Stress, depression, and neuroplasticity: a convergence of mechanisms. Neuropsychopharmacology. 33(1): 88-109.

Prestia A, Boccardi M, Galluzzi S, Cavedo E, Adorni A, Soricelli A, Bonetti M, Geroldi C, Giannakopoulos P, Thompson P, Frisoni G, (2011): Hippocampal and amygdalar volume changes in elderly patients with Alzheimer's disease and schizophrenia. Psychiatry Research: Neuroimaging. 192(2): 77–83.

Prévost C, McCabe JA, Jessup RK, Bossaerts P, O'Doherty JP, (2011): Differentiable contributions of human amygdalar subregions in the computations underlying reward and avoidance learning. Eur. J. Neurosci. 34 (1), 134–145.

Price JL, Russchen FT, Amaral DG, (1987): The Limbic Region. II: The amygdaloid Complex. In: Bjorklund, A., Hökfelt, T., Swanson, L.W., (Eds.), Handbook of Chemical Neuroanatomy Integrated Systems of the CNS. Elsevier Science., Amsterdam. Page: 279-388.

Pruessner JC, Li LM, Serles W, Pruessner M, Collins DL, Kabani N, Lupien S, Evans AC, (2000): Volumetry of hippocampus and amygdala with high-resolution MRI and three-dimensional analysis software: minimizing the discrepancies between laboratories. Cereb. Cortex 10 (4), 433–442.

Pruessner JC, Collins DL, Pruessner M, Evans AC, (2001): Age and gender predict volume decline in the anterior and posterior hippocampus in early adulthood. J Neurosci. 21(1): 194-200.

Qiao H, Li MX, Xu C, Chen HB, An SC, Ma XM, (2016): Dendritic Spines in Depression: What We Learned from Animal Models. Neural Plast. 8056370. doi: 10.1155/2016/8056370.

Raz N, Gunning FM, Head D, Dupuis JH, McQuain J, Briggs SD, Loken WJ, Thornton AE, Acker JD, (1997): Selective aging of the human cerebral cortex observed in vivo: differential vulnerability of the prefrontal gray matter. Cereb Cortex. 7(3): 268-282.

Raz N (2000): Aging of the brain and its impact on cognitive performance: integration of structural and functional findings. In: Craik FIM, Salthouse TA, (Eds.). The handbook of Aging and Cognition, 2nd ed. Mahwah, NJ: Lawrence Erlbaum Associates. Page: 1–90.

Raz N, Gunning-Dixon F, Head D, Rodrigue KM, Williamson A, Acker JD, (2004): Aging, sexual dimorphism, and hemispheric asymmetry of the cerebral cortex: replicability of regional differences in volume. Neurobiol Aging. 25(3): 377-96.

Raz N, Lindenberger U, Rodrigue KM, Kennedy KM, Head D, Williamson A, Dahle C, Gerstorf D, Acker JD, (2005): Regional brain changes in aging healthy adults: general trends, individual differences and modifiers. Cereb Cortex. 15(11):1676-89.

Raz N, Rodrigue KM, (2006): Differential aging of the brain: patterns, cognitive correlates and modifiers. Neurosci Biobehav Rev. 30(6):730-48.

Raz N, Kennedy KM, (2009): A systems approach to the aging brain: neuroanatomic changes, their modifiers, and cognitive correlates. In: Jagust W, D'Esposito M, (Eds.). Imaging the Aging Brain. U S A: Oxford University Press. Page: 43-70.

Raz N, Ghisletta P, Rodrigue KM, Kennedy KM, Lindenberger U, (2010): Trajectories of brain aging in middle-aged and older adults: regional and individual differences. Neuroimage. 51(2): 501-511. doi: 10.1016/j.neuroimage.2010.03.020.

Raz N, Daugherty AM, Bender AR, Dahle CL, Land S, (2014): Volume of the hippocampal subfields in healthy adults: differential associations with age and a proinflammatory genetic variant. Brain Struct. Funct. 220 (5), 2663–2674.

Reardon PK, Clasen L, Giedd JN, Blumenthal J, Lerch JP, Chakravarty MM, Raznahan A, (2016): An Allometric Analysis of Sex and Sex Chromosome Dosage Effects on Subcortical Anatomy in Humans. J Neurosci. 36(8): 2438-48. doi: 10.1523/JNEUROSCI.3195-15.2016.

Reiman EM, Caselli RJ, Yun LS, Chen K, Bandy D, Minoshima S, Thibodeau SN, Osborne D, (1996): Preclinical evidence of Alzheimer's disease in persons homozygous for the epsilon 4 allele for apolipoprotein E. N Engl J Med. 334(12): 752-758.

Reiman EM, Chen K, Alexander GE, Caselli RJ, Bandy D, Osborne D, Saunders AM, Hardy J, (2004): Functional brain abnormalities in young adults at genetic risk for late-onset Alzheimer's dementia. Proc Natl Acad Sci U S A. 101(1): 284-289.

Reinvang I, Deary IJ, Fjel AM, Steen VM, Espeseth T, Parasuraman R, (2010): Neurogenetic effects on cognition in aging brains: a window of opportunity for intervention?. Front Aging Neurosci. 2:143. doi: 10.3389/fnagi.2010.00143. eCollection 2010.

Roberts DE, Killiany RJ, Rosene DL, (2012): Neuron numbers in the hypothalamus of the normal aging rhesus monkey: stability across the adult lifespan and between the sexes. J Comp Neurol. 520(6): 1181-1197. doi: 10.1002/cne.22761.

Rodrigue KM, Kennedy KM, (2011): The Cognitive Consequences of Structural Changes to the Aging Brain. In: Carstensen LL, Rando TG, (Eds.), The Handbooks of Aging 7th ed. Elsevier Academic Press, London. Page: 73–91.

Rogers MA, Yamasue H, Abe O, Yamada H, Ohtani T, Iwanami A, Aoki S, Kato N, Kasai K, (2009): Smaller amygdala volume and reduced anterior cingulate gray matter density associated with history of post-traumatic stress disorder. Psychiatry Research: Neuroimaging 174(3): 210–216.

Rolls ET, (2015): Limbic systems for emotion and for memory, but no single limbic system. Cortex. 62:119-57. doi: 10.1016/j.cortex.2013.12.005.

Roozendaal B, McEwen BS, Chattarji S, (2009): Stress, memory and the amygdala. Nat. Rev. Neurosci. 10 (6), 423–433. doi: 10.1038/nrn2651.

Roselli CE, Klosterman S, Resko JA, (2001): Anatomic relationships between aromatase and androgen receptor mRNA expression in the hypothalamus and amygdala of adult male cynomolgus monkeys. J Comp Neurol. 439(2):208-23.

Rosin C, Colombo S, Calver AA, Bates TE, Skaper SD, (2005): Dopamine D2 and D3 receptor agonists limit oligodendrocyte injury caused by glutamate oxidative stress and oxygen/glucose deprivation. Glia. 52(4):336-43.

Roxo MR, Franceschini PR, Zubaran C, Kleber FD, Sander JW, (2011): The limbic system conception and its historical evolution. ScientificWorldJournal. 11:2428-41. doi: 10.1100/2011/157150.

Royston P, Sauerbrei W, (2008a): Some Comparisons of MFP with Splines. In: Royston, P., Sauerbrei, W. (Eds.). Multivariable Model-Building A pragmatic approach to regression analysis based on fractional polynomials for modelling continuous variables. 1st. Chichester: Wiley. Chapter 9, Page: 201–222.

Royston P, Sauerbrei W, (2008b): MFP: Multivariable Model-Building with Fractional Polynomials. In: Royston P, Sauerbrei W, (Eds.). Multivariable Model-Building A pragmatic approach to regression analysis based on fractional polynomials for modelling continuous variables. 1st. Chichester: Wiley. Chapter 6, Page: 115–150.

Royston P, Sauerbrei W, (2008c): Interactions. In: Royston, P., Sauerbrei, W. (Eds.). Multivariable Model-Building A pragmatic approach to regression analysis based on fractional polynomials for modelling continuous variables. 1st. Chichester: Wiley. Chapter 7, Page: 151–182.

Royston P, Sauerbrei W, (2008d): MFP: Fractional Polynomials for One Variable. In: Royston, P., Sauerbrei, W. (Eds.). Multivariable Model-Building A pragmatic approach to regression analysis based on fractional polynomials for modelling continuous variables. 1st. Chichester: Wiley. Chapter 4, Page: 71–98.

Rubinow MJ, Mahajan G, May W, Overholser JC, Jurjus GJ, Dieter L, et al. (2016): Basolateral amygdala volume and cell numbers in major depressive disorder: a postmortem stereological study. Brain Struct Funct. 221(1): 171-84. doi: 10.1007/s00429-014-0900-z.

Sachdev P, Brodaty H, Cheang D, Cathcart S, (2000): Hippocampus and amygdala volumes in elderly schizophrenic patients as assessed by magnetic resonance imaging. Psychiatry Clin Neurosci.54(1):105–112.

Sah P, Faber ES, Lopez De Armentia, M, Power J, (2003): The amygdaloid complex: anatomy and physiology. Physiol. Rev. 83(3): 803–834.

Sala S, Agosta F, Pagani E, Copetti M, Comi G, Filippi M, (2012): Microstructural changes and atrophy in brain white matter tracts with aging. Neurobiol Aging. 33(3):488-498.e2. doi: 10.1016/j.neurobiolaging.2010.04.027.

Saleh K, Carballedo A, Lisiecka D, Fagan AJ, Connolly G, Boyle G, Frodl T, (2012): Impact of family history and depression on amygdala volume. Psychiatry Res. 203(1): 24-30. doi: 10.1016/j.pscychresns.2011.10.004.

Salminen LE, Schofield PR, Lane EM, Heaps JM, Pierce KD, Cabeen R, et al. (2013): Neuronal fiber bundle lengths in healthy adult carriers of the ApoE4 allele: a quantitative tractography DTI study. Brain Imaging Behav. 7(3):274-81. doi: 10.1007/s11682-013-9225-4.

Sambataro F, Pennuto M, Christian Wolf R, (2012): Catechol-o-methyl transferase modulates cognition in late life: evidence and implications for cognitive enhancement. CNS Neurol Disord Drug Targets. 11(3):195-208.

Sánchez-Benavides G, Gómez-Ansón B, Sainz A, Vives Y, Delfino M, Peña-Casanova J, (2010): Manual validation of FreeSurfer's automated hippocampal segmentation in normal aging, mild cognitive impairment, and Alzheimer Disease subjects. Psychiatry Res. 181(3): 219-225. doi: 10.1016/j.pscychresns.2009.10.011.

Sapolsky RM, (2000): Glucocorticoids and hippocampal atrophy in neuropsychiatric disorders. Arch Gen Psychiatry. 57(10): 925-35.

Saygin ZM, Osher DE, Augustinack J, Fischl B, Gabrieli JDE, (2011): Connectivity-based segmentation of human amygdala nuclei using probabilistic tractography. NeuroImage. 56(3), 1353–1361.

Saygin ZM, Kliemann D, Iglesias JE, van der Kouwe AJW, Boyd E, Reuter M, et al. (2017): High-resolution magnetic resonance imaging reveals nuclei of the human amygdala: manual segmentation to automatic atlas. Neuroimage. 155:370-382. doi: 10.1016/j.neuroimage.2017.04.046.

Schächter F, Faure-Delanef L, Guénot F, Rouger H, Froguel P, Lesueur-Ginot L, Cohen D, (1994): Genetic associations with human longevity at the APOE and ACE loci. Nat Genet. 6(1): 29-32.

Schmaal L, Veltman DJ, van Erp TG, Sämann PG, Frodl T, Jahanshad N, et al. (2016): Subcortical brain alterations in major depressive disorder: findings from the ENIGMA Major Depressive Disorder working group. Mol Psychiatry. 21(6): 806-12. doi: 10.1038/mp.2015.69.

Schmahmann, JD., Pandya, DN, (2006): Cingulum Bundle. In: Schmahmann, JD., Pandya, JD. (Eds.). Fiber Pathways of the Brain. Oxford University Press, Inc. Chapter 17. DOI:10.1093/acprof:oso/9780195104233.003.0017

Schoemaker D, Buss C, Head K, Sandman CA, Davis EP, Chakravarty MM, Gauthier S, Pruessner JC, (2016): Hippocampus and amygdala volumes from magnetic resonance images in children: Assessing accuracy of FreeSurfer and FSL against manual segmentation. NeuroImage. 129: 1–14. doi: 10.1016/j.neuroimage.2016.01.038.

Schumann CM, Amaral DG, (2005): Stereological estimation of the number of neurons in the human amygdaloid complex. J. Comp. Neurol. 491(4): 320–329.

Scott SA, DeKosky ST, Sparks DL, Knox CA, Scheff SW, (1992): Amygdala cell loss and atrophy in Alzheimer's disease. Ann Neurol. 32(4):555-63.

Sengupta P, (2013): The Laboratory Rat: Relating Its Age With Human's. Int J Prev Med. 4(6): 624-30.

Sims KS, Williams RS, (1990): The human amygdaloid complex: a cytologic and histochemical atlas using Nissl, myelin, acetylcholinesterase and nicotinamide adenine dinucleotide phosphate diaphorase staining. Neuroscience. 36(2):449-72.

Siozopoulos A, Thomaidis V, Prassopoulos P, Fiska A, (2017): In vivo estimation of normal amygdala volume from structural MRI scans with anatomical-based segmentation. Surg Radiol Anat. 40(2):145-157. doi: 10.1007/s00276-017-1915-y.

Smith CD, Chebrolu H, Andersen AH, Powell DA, Lovell MA, Xiong S, Gold BT, (2010): White matter diffusion alterations in normal women at risk of Alzheimer's disease. Neurobiol Aging. 31(7):1122-31. doi: 10.1016/j.neurobiolaging.2008.08.006.

Solano-Castiella E, Anwander A, Lohmann G, Weiss M, Docherty C, Geyer S, Reimer E, Friederici AD, Turner R, (2010): Diffusion tensor imaging segments the human amygdala in vivo. Neuroimage. 49(4): 2958–2965.

Solano-Castiella E, Schäfer A, Reimer A, Türke E, Pröger T, Lohmann G, Trampel R, Turner R, (2011): Parcellation of human amygdala in vivo using ultra high field structural MRI. NeuroImage. 58(3): 741–748. doi: 10.1016/j.neuroimage.2011.06.047.

Soldan A, Pettigrew C, Lu Y, Wang MC, Selnes O, Albert M, et al. (2015): Relationship of medial temporal lobe atrophy, APOE genotype, and cognitive reserve in preclinical Alzheimer's disease. Human Brain Mapping. 36(7): 2826–2841. doi: 10.1002/hbm.22810.

Spinney L, (2014): Alzheimer's disease: The forgetting gene. Nature. 510(7503): 26-8. doi: 10.1038/510026a.

Stadlbauer A, Salomonowitz E, Strunk G, Hammen T, Ganslandt O, (2008): Quantitative diffusion tensor fiber tracking of age-related changes in the limbic system. Eur Radiol. 18(1):130-7.

Sublette ME, Baca-Garcia E, Parsey RV, Oquendo MA, Rodrigues SM, Galfalvy H, Huang YY, Arango V, Mann JJ, (2008): Effect of BDNF val66met polymorphism on age-related amygdala volume changes in healthy subjects. Progress in Neuro-Psychopharmacology and Biological Psychiatry. 32(7): 1652–1655. doi: 10.1016/j.pnpbp.2008.06.009.

Swanson LW, Petrovich GD, (1998): What is the amygdala? Trends Neurosci. 21(8):323-31.

Szeszko PR, Robinson D, Alvir JM, Bilder RM, Lencz T, Ashtari M, Wu H, Bogerts B, (1999): Orbital frontal and amygdala volume reductions in obsessive–compulsive disorder. Arch Gen Psychiatry. 56(10): 913–919.

Szeszko PR, Betensky JD, Mentschel C, Gunduz-Bruce H, Lencz T, Ashtari M, Malhotra AK, Bilder RM, (2006): Increased stress and smaller anterior hippocampal volume. Neuroreport. 17(17): 1825-8.

Tan A, Ma W, Vira A, Marwha D, Eliot L, (2016): The human hippocampus is not sexually-dimorphic: Meta-analysis of structural MRI volumes. Neuroimage. 124 (Pt A):350-366. doi: 10.1016/j.neuroimage.2015.08.050.

Terburg D, Morgan BE, Montoya ER, Hooge IT, Thornton HB, Hariri AR, et al. (2012): Hypervigilance for fear after basolateral amygdala damage in humans. Transl Psychiatry. 2: e115.

Teicher MH, Andersen SL, Polcari A, Anderson CM, Navalta CP, Kim DM, (2003): The neurobiological consequences of early stress and childhood maltreatment. Neurosci Biobehav Rev. 27(1-2): 33-44.

Teicher MH, Anderson CM, Polcari A, (2012): Childhood maltreatment is associated with reduced volume in the hippocampal subfields CA3, dentate gyrus, and subiculum. Proc Natl Acad Sci U S A. 109(9): E563-72. doi: 10.1073/pnas.1115396109.

Teicher MH, Samson JA, (2013): Childhood maltreatment and psychopathology: A case for ecophenotypic variants as clinically and neurobiologically distinct subtypes. Am J Psychiatry. 170(10): 1114-33. doi: 10.1176/appi.ajp.2013.12070957.

Teicher MH, Samson JA, (2016): Annual Research Review: Enduring neurobiological effects of childhood abuse and neglect. J Child Psychol Psychiatry. 57(3): 241-66. doi: 10.1111/jcpp.12507.

Tottenham N, Hare TA, Casey BJ, (2009): A Developmental Perspective on Human Amygdala Function. In: Whalen PJ, Phelps EA, (Eds.), The human amygdala. The Guilford Press, New York. Page: 107-117.

Tottenham N, Hare TA, Quinn BT, McCarry TW, Nurse M, Gilhooly T, et al. (2010): Prolonged institutional rearing is associated with atypically large amygdala volume and difficulties in emotion regulation. Dev Sci. 13(1): 46-61. doi: 10.1111/j.1467-7687.2009.00852.x.

Tournier JD, Mori S, Leemans A, (2011): Diffusion tensor imaging and beyond. Magn Reson Med. 65(6):1532-56. doi: 10.1002/mrm.22924. Epub 2011 Apr 5.

Travis SG, Coupland NJ, Silverstone PH, Huang Y, Fujiwara E, Carter R, Seres P, Malykhin NV, (2015): Dentate gyrus volume and memory performance in major memory depressive disorder. J Affect Disord. 172, 159-64. doi: 10.1016/j.jad.2014.09.048.

Travis SG, Coupland NJ, Hegadoren K, Silverstone PH, Huang Y, Carter R, Fujiwara E, Seres P, Malykhin NV, (2016): Effects of cortisol on hippocampal subfields volumes and memory performance in healthy control subjects and patients with major depressive disorder. J Affect Disord. 201: 34-41. doi: 10.1016/j.jad.2016.04.049.

Tyszka JM, Pauli WM, (2016): In vivo delineation of subdivisions of the human amygdaloid complex in a high-resolution group template. Hum Brain Mapp. 37(11): 3979-3998. doi: 10.1002/hbm.23289.

van Haren NE, Bakker SC, Kahn RS., (2008): Genes and structural brain imaging in schizophrenia. Curr Opin Psychiatry. 21(2):161-7. doi: 10.1097/YCO.0b013e3282f4f25b.

Van Hecke W, Emsell L., 2015. Strategies and Challenges in DTI Analysis. In: Van Hecke, W., Emsell, L., Sunaert, S., (Eds.), Diffusion Tensor Imaging 1st ed. Springer, New York. Page: 153–173.

Vanni S, Colini Baldeschi A, Zattoni M, Legname G, (2019): Brain aging: A Ianus-faced player between health and neurodegeneration. J Neurosci Res. doi: 10.1002/jnr.24379.

Vassilopoulou K, Papathanasiou M, Michopoulos I, Boufidou F, Oulis P, Kelekis N, et al. (2013): A magnetic resonance imaging study of hippocampal, amygdala and subgenual prefrontal cortex volumes in major depression subtypes: melancholic versus psychotic depression. J Affect Disord. 146(2):197-204. doi: 10.1016/j.jad.2012.09.003.

Vogt BA, Palomero-Gallagher N, (2012). Cingulate Cortex. In J. K. Mai and G. Paxinos (Eds.), The human nervous system. 3rd ed. London: Elsevier Academic Press. Page: 943–987.

Voineskos AN, Lerch JP, Felsky D, Shaikh S, Rajji TK, Miranda D, et al. (2011): The brain-derived neurotrophic factor Val66Met polymorphism and prediction of neural risk for Alzheimer disease. Arch Gen Psychiatry. 68(2):198-206. doi: 10.1001/archgenpsychiatry.2010.194

Voineskos AN, Rajji TK, Lobaugh NJ, Miranda D, Shenton ME, Kennedy JL, et al. (2012): Age-related decline in white matter tract integrity and cognitive performance: a DTI tractography and structural equation modeling study. Neurobiol Aging. 33(1):21-34. doi: 10.1016/j.neurobiolaging.2010.02.009.

Von Der Heide RJ, Skipper LM, Klobusicky E, Olson IR, (2013): Dissecting the uncinate fasciculus: disorders, controversies and a hypothesis. Brain. 136(Pt 6):1692-707. doi: 10.1093/brain/awt094.

Vuilleumier P, (2009): The Role of the Human Amygdala in Perception and Attention. In: Whalen PJ, Phelps EA, (Eds.), The human amygdala. The Guilford Press, New York. Page: 220-249.

Vyas A, Mitra R, Shankaranarayana Rao BS, Chattarji S, (2002): Chronic stress induces contrasting patterns of dendritic remodeling in hippocampal and amygdaloid neurons. J Neurosci. 22(15): 6810-8.

Vyas A, Bernal S, Chattarji S, (2003): Effects of chronic stress on dendritic arborization in the central and extended amygdala. Brain Res 965 (1-2): 290-4.

Vyas A, Pillai AG, Chattarji S, (2004): Recovery after chronic stress fails to reverse amygdaloid neuronal hypertrophy and enhanced anxiety-like behavior. Neuroscience 128(4): 667-73.

Vythilingam M, Heim C, Newport J, Miller AH, Anderson E, Bronen R, et al. (2002): Childhood trauma associated with smaller hippocampal volume in women with major depression. Am J Psychiatry. 159(12): 2072-80.

Walhovd KB, Fjell AM, Reinvang I, Lundervold A, Dale AM, Eilertsen DE, et al. (2005): Effects of age on volumes of cortex, white matter and subcortical structures. Neurobiol Aging. 26(9): 1261-70; discussion 1275-8.

Wang Z, Dai Z, Shu H, Liu D, Guo Q, He Y, Zhang Z, (2017): Cortical Thickness and Microstructural White Matter Changes Detect Amnestic Mild Cognitive Impairment. J Alzheimers Dis. 56(1):415-428. doi: 10.3233/JAD-160724.

Watson C, Andermann F, Gloor P, Jones-Gotman M, Peters T, Evans A, et al. (1992): Anatomic basis of amygdaloid and hippocampal volume measurement by magnetic resonance imaging. Neurology 42 (9), 1743–1750.

Westin CF, Maier SE, Mamata H, Nabavi A, Jolesz FA, Kikinis R, (2002): Processing and visualization for diffusion tensor MRI. Med Image Anal. 6(2):93-108.

Westlye LT, Walhovd KB, Dale AM, Bjørnerud A, Due-Tønnessen P, Engvig A, et al. (2010): Life-span changes of the human brain white matter: diffusion tensor imaging (DTI) and volumetry. Cereb Cortex. 20(9):2055-68. doi: 10.1093/cercor/bhp280.

Wheeler-Kingshott CA, Cercignani M, (2009): About "axial" and "radial" diffusivities. Magn Reson Med. 61(5):1255-60. doi: 10.1002/mrm.21965.

Winterburn JL, Pruessner JC, Chavez S, Schira MM, Lobaugh NJ, Voineskos AN, Chakravarty MM, (2013): A novel in vivo atlas of human hippocampal subfields using high-resolution 3T magnetic resonance imaging. NeuroImage. 74: 254–265.

Wisdom NM, Callahan JL, Hawkins KA, (2011): The effects of apolipoprotein E on non-impaired cognitive functioning: a meta-analysis. Neurobiol Aging. 32(1):63-74. doi: 10.1016/j.neurobiolaging.2009.02.003.

Wisse LEM, Gerritsen L, Zwanenburg JJM, Kuijf HJ, Luijten PR, Biessels GJ, Geerlings MI, (2012): Subfields of the hippocampal formation at 7 T MRI: in vivo volumetric assessment. NeuroImage 61 (4), 1043–1049.

Wisse LE, Biessels GJ, Heringa SM, Kuijf HJ, Koek DH, Luijten PR, Geerlings MI, Utrecht Vascular Cognitive Impairment (VCI) Study Group, (2014): Hippocampal sub-field volumes at 7 T in early Alzheimer3s disease and normal aging. Neurobiology of Aging. 35(9): 2039–2045.

Witte AV, Flöel A, (2012): Effects of COMT polymorphisms on brain function and behavior in health and disease. Brain Res Bull. 88(5):418-28. doi: 10.1016/j.brainresbull.2011.11.012.

World Health Organization, (2016): Global Health Estimates 2015: Burden of disease by Cause, Age, Sex, by Country and by Region, 2000-2015. Geneva.

Wright CI, (2009). The human amygdala in normal aging and Alzheimer's disease. In: Whalen PJ, Phelps EA, (Eds.), The human amygdala. New York: The Guilford Press. Page: 382-405.

Yamaguchi-Shima N, Yuri K, (2007): Age-related changes in the expression of ER-beta mRNA in the female rat brain. Brain Res. 1155:34-41.

Yamaguchi N, Yuri K, (2012): Changes in oestrogen receptor-β mRNA expression in male rat brain with age. J Neuroendocrinol. 24(2): 310-318. doi: 10.1111/j.1365-2826.2011.02231.x.

Yang Z, Wen W, Jiang J, Crawford JD, Reppermund S, Levitan C, et al. (2016): Age-associated differences on structural brain MRI in nondemented individuals from 71 to 103 years. Neurobiol Aging. 40:86-97. doi: 10.1016/j.neurobiolaging.2016.01.006.

Yap QJ, Teh I, Fusar-Poli P, Sum MY, Kuswanto C, Sim K, (2013): Tracking cerebral white matter changes across the lifespan: insights from diffusion tensor imaging studies. J Neural Transm (Vienna). 120(9):1369-95. doi: 10.1007/s00702-013-0971-7.

Yesavage JA, Brink TL, Rose TL, Lum O, Huang V, Adey M, Leirer VO, (1982): Development and validation of a geriatric depression screening scale: a preliminary report. J Psychiatr Res. 17(10: 37-49.

Yilmazer-Hanke, DM, (2012): Amygdala. In: Mai JK, Paxinos G, (Eds.), The Human Nervous System3rd ed. Elsevier Academic Press, London. Page: 759–834.

Ystad MA, Lundervold AJ, Wehling E, Espeseth T, Rootwelt H, Westlye LT, et al. (2009): Hippocampal volumes are important predictors for memory function in elderly women. BMC Med Imaging. 22:9-17. doi: 10.1186/1471-2342-9-17.

Yushkevich PA, Piven J, Hazlett HC, Smith RG, Ho S, Gee JC, Gerig G, (2006): User-guided 3D active contour segmentation of anatomical structures: Significantly improved efficiency and reliability. NeuroImage. 31(3): 1116-1128.

Yushkevich PA, Avants BB, Pluta J, Das S, Minkoff D, Mechanic-Hamilton D, et al. (2009): A high-resolution computational atlas of the human hippocampus from postmortem magnetic resonance imaging at 9.4 T. NeuroImage 44 (2), 385–398.

Yushkevich PA, Amaral RS, Augustinack JC, Bender AR, Bernstein JD, Boccardi M, et al. (2015): Quantitative comparison of 21 protocols for labeling hippocampal subfields and parahippocampal subregions in in vivo MRI: towards a harmonized segmentation protocol. Neuroimage. 111:526-41. doi: 10.1016/j.neuroimage.2015.01.004.

Zavorotnyy M, Zöllner R, Schulte-Güstenberg LR, Wulff L, Schöning S, Dannlowski U, et al. (2017): Low left amygdala volume is associated with a longer duration of unipolar depression. J Neural Transm. 125(2): 229-238. doi: 10.1007/s00702-017-1811-y.

Ziegler G, Dahnke R, Gaser C, Alzheimer's Disease Neuroimaging Initiative, (2012): Models of the aging brain structure and individual decline. Front Neuroinform. 6:3. doi: 10.3389/fninf.2012.00003.

Zuo Z, Ran S, Wang Y, Li C, Han Q, Tang Q, et al. (2019): Asymmetry in cortical thickness and subcortical volume in treatment-naïve major depressive disorder. Neuroimage Clin. 21:101614. doi: 10.1016/j.nicl.2018.101614.